



Quantum kicked rotor and its variants: Chaos, localization and beyond



M.S. Santhanam ^{a,*}, Sanku Paul ^{b,c}, J. Bharathi Kannan ^a

^a Indian Institute of Science Education and Research, Dr. Homi Bhabha Road, Pune 411008, India

^b Department of Physics and Astronomy, Michigan State University, MI 48824, USA

^c Max Planck Institute for the Physics of Complex Systems, Dresden 01187, Germany

ARTICLE INFO

Article history:

Received 30 January 2021

Received in revised form 5 January 2022

Accepted 10 January 2022

Available online 18 February 2022

Editor: David Campbell

Keywords:

Chaos

Quantum chaos

Localization

Kicked rotor

Cold atoms

ABSTRACT

Kicked rotor is a paradigmatic model for classical and quantum chaos in time-dependent Hamiltonian systems. More than fifty years since the introduction of this model, there is an increase in the number of works that use kicked rotor model as a fundamental template to study a variety of questions in nonlinear dynamics, quantum chaos, condensed matter physics and quantum information. This is aided by the experimental approaches that have implemented many variants of the quantum kicked rotor model. The problems addressed using kicked rotor and its variants include the basic phenomenology of classical and quantum chaos, transport and localization in one- and higher dimensional kicked systems, effects of disorder and interactions, resonant dynamics and the relation between quantum correlations and chaos. This would also include a range of applications such as for constructing ratchet dynamics and for atom-optics based interferometry. This article reviews the current status of theoretical and experimental research devoted to exploring these ideas using the framework of kicked rotor model.

© 2022 Elsevier B.V. All rights reserved.

Contents

1. Introduction.....	2
1.1. Regularity to chaos: A historical background	2
2. Chaos in physical systems.....	4
2.1. Integrability and chaos in Hamiltonian systems.....	4
2.2. Chaos in time-independent Hamiltonian systems.....	5
2.3. Chaos in dissipative systems.....	7
2.4. Structure of this review	8
3. Kicked rotor model	8
3.1. Classical kicked rotor	8
3.2. Phase space geometry	9
4. Transition to chaos.....	9
4.1. Momentum and diffusive transport	13
4.2. Accelerator modes	14
5. Quantum kicked rotor.....	16
5.1. Timescales in quantum chaos and kicked rotor	17

* Corresponding author.

E-mail addresses: santh@iiserpune.ac.in (M.S. Santhanam), sankup005@gmail.com (S. Paul), bharathi.kannan@students.iiserpune.ac.in (J.B. Kannan).

URL: <http://sites.iiserpune.ac.in/~santh> (M.S. Santhanam).

5.2. Connection with Anderson localization	19
5.3. Quantum resonances	21
5.4. Localization and spectral statistics	23
5.5. Random band matrices and kicked rotor	27
6. Experimental realizations of quantum kicked rotor	29
6.1. Microwave ionization of hydrogen atoms	29
6.2. Cold atoms in flashing optical lattices	30
7. Variants of kicked rotor	33
7.1. Noisy kicked rotors	33
7.2. Non-KAM kicked rotors	34
7.3. Kicked Bose-Einstein condensates	35
7.4. Molecular kicked rotors	37
7.5. Spin-1/2 kicked rotor	38
8. Higher-dimensional kicked rotors	38
8.1. Arnold diffusion	38
8.2. N -dimensional kicked rotor	40
8.3. Quantum dynamics of N -dimensional kicked rotor	40
8.4. One-parameter scaling theory	42
8.5. Critical kick strength and exponent	44
9. Quasi-periodic kicked rotor	45
9.1. Classical dynamics of quasi-periodic rotor	46
9.2. Quantum quasi-periodic kicked rotor	46
9.3. Multifractality of wavefunctions at critical transition	49
9.4. Experimental realization of Anderson transition in quasi-periodic rotor	50
9.5. Other quasiperiodic systems: Aubry-André model and more	51
10. Quantum correlations and chaos	52
10.1. Coupled kicked rotors	52
10.2. Chaos and entanglement in coupled kicked rotors	55
10.3. Entanglement transition	58
10.4. Out-of-time-ordered correlator and kicked rotor	58
11. Applications	62
11.1. Quantum ratchets	62
11.2. Resonance ratchets	64
11.3. Atom interferometry with kicked rotor	66
11.4. Control of decoherence	68
11.5. Quantum computing the kicked rotor	70
12. Outlook	71
Declaration of competing interest	72
Acknowledgments	72
References	72

1. Introduction

1.1. Regularity to chaos: A historical background

In nature, almost everything changes with time. The air molecules that surround us change their positions and speeds, electrons and other sub-atomic particles are in a state of constant motion inside the atom, planets and galaxies never cease to move. In the last two millennia, the quantitative description of these dynamical processes is strongly influenced by the regularity displayed by the dynamical systems in nature. This is especially true for the apparent regularity and predictability associated with the large number of astronomical phenomena visible to the naked eye, namely the spectacular and regular occurrences of seasons, days and nights, phases of the moon and even the regular appearance of some of the comets. It is now known at least for the last 2000 years that due to the *saros* cycle, the relative positions of the sun, moon and the earth repeat with an approximate period of about 18 years and 11 days [1]. At any point on the earth, solar or lunar eclipses with identical geometry recur with this periodicity. Such recurring patterns in space and time have strengthened the faith in the idea of a predictable and clock-work-like universe.

In this context, of particular historical interest is the two-body problem and its periodic solutions that go back to the work of Johannes Kepler [2] and Isaac Newton [3]. The simplest two-body problem, for instance, the sun and the earth, is now routinely presented in the contemporary undergraduate text books of classical mechanics, and its solution provides an excellent example of regular orbits. These observations and mathematical solutions helped generate implicit faith in the idea of determinism – that dynamical systems can be quantitatively described in terms of deterministic equations whose solutions can be expected to be regular. This also meant that the future evolution is entirely predictable. Pierre Laplace eloquently expressed this idea in 1820 – “An intelligence which could comprehend all the forces by which nature

is animated and the respective situation of the beings who compose it – an intelligence sufficiently vast to submit these data to analysis ... for it, nothing would be uncertain and the future, as the past, would be present to its eyes” [4]. In this backdrop, it is not surprising at all that almost until the beginning of 20th century, irregular dynamics did not appear to be a realistic possibility in any natural phenomenon.

In contrast to the two-body problem, the search for a regular and closed form solutions to the three-body problem for well over two centuries beginning 1700s led to deeper insights and incisive mathematical tools but not the much sought-after solutions. The three-body problem could be either the sun–earth–moon system or the sun and two other planets or other variants. Much of the history of the three-body problem is inextricably intertwined with the development of tools and techniques of classical mechanics widely used today. The historical aspects of the three-body problem are recounted in a few recent articles [5,6].

Before the quantum revolution (during 1897–1925) relegated it to the back burner, the dynamics of three-body problem interacting through the gravitational potential was an outstanding unsolved problem in physics then and continues to be so to this day. It was considered so important that King of Sweden and Norway, Oscar II on the occasion of his 60th birthday announced a prize in 1885 to the mathematician who would solve any one of the four proposed problems. With the counsel of Mittag-Leffler, first among the four problems was the specific question related to N -body dynamics (of which 3-body problem is a special case); “Given a system of arbitrarily many mass points that attract each according to Newton’s law, under the assumption that no two points ever collide, try to find a representation of the coordinates of each point as a series in a variable that is some known function of time and for all of whose values the series converges uniformly”. Though Poincaré did not quite solve the stated problem, as one of the member of the jury the eminent mathematician Karl Weierstrass wrote, “it is nevertheless of such importance that its publication will inaugurate a new era in the history of celestial mechanics”. For the record, it is necessary to state that the N -body case, as strictly required by the problem statement, was first solved for $N = 3$ by Karl Sundman [7] in 1912, and much later by Quidong Wang in 1991 [8] for the general case of N -bodies. In both cases, the solutions exclude a certain class of initial conditions that lead to collisions among any of the N -bodies. Even so, the solutions were not helpful in practice. Hence, the statement of having “solved the N -body problem” requires further explanation and the interested reader is referred to Ref. [9] and its references.

The seminal importance of Poincaré’s work, published in an expanded form in 1892 [10], lies in the fact that it provided the first hint that even a three-body system can display astonishingly complex dynamics and it can be unpredictable as well. It was so complicated that Poincaré decided against sketching it explicitly. Today, we recognize this as deterministic chaos – seemingly irregular dynamics arising from deterministic equations of motion and exhibiting sensitive dependence on initial conditions. This makes their solution unpredictable beyond a short time horizon. It is worthwhile to recall the oft-repeated quotation from a paper by Sir James Lighthill [11]; “Here I have to pause, and to speak once again on behalf of the broad global fraternity of practitioners of mechanics. We are all deeply conscious today that the enthusiasm of our forebears for the marvelous achievements of Newtonian mechanics led them to make generalizations in this area of predictability which, indeed, we may have generally tended to believe before 1960, but which we now recognize were false. We collectively wish to apologize for having misled the general educated public by spreading ideas about the determinism of systems satisfying Newton’s laws of motion that, after 1960, were to be proved incorrect”. Clearly, it took another 60 years before this first hint of the failure of regular and predictable dynamics seen by Poincaré could be turned into a coherent theory of deterministic chaos standing on firm mathematical foundations. The subsequent research developments, from the 1960s onwards, took advantage of the arrival of digital computers which gave further impetus to chaotic dynamics becoming an active area of research.

In the light of Poincaré’s result, mathematically, it is reasonable to rule out the existence of solutions for the general three-body problem in terms of “some known function of time and for all of whose values the series converges uniformly”. The import of these ideas for physics was far reaching. At least since the time of Newton’s *Principia*, determinism and predictability were regarded as underlying principles governing the motion of material bodies. In the case of three-body problem, though the governing equations of motion are deterministic, the nonlinearity in the system plays a pivotal role and gives rise to chaotic dynamics with severe constraints on the predictability of its future evolution. Thanks to all these developments, by now, it is well understood that regular, and hence predictable, systems are exceptions rather than a rule. Since the 1960s, chaotic dynamics has been observed in a large number of simple one-dimensional difference equations called maps (logistic map being a prominent example), in dissipative systems such as the Lorenz model, and in a large class of conservative systems such as coupled oscillators in two and higher dimensions. This is not a figment of theoretical imagination. Experiments too have revealed chaos in Belousov–Zhabotinsky chemical reaction [12], hydrodynamic turbulence [13,14], and numerical simulations have shown evidence of chaos in spin-axis orientation of the planets [15]. On the other hand, one-dimensional Hamiltonian systems driven by an external field can display chaotic dynamics as well. This review article is focussed on one such remarkable model, the kicked rotor, introduced in 1969 [16]. It has turned out to be a paradigmatic model for chaos in time-dependent Hamiltonian systems, in both the classical and quantum versions.

2. Chaos in physical systems

2.1. Integrability and chaos in Hamiltonian systems

Before we plunge into details, a brief and minimal background is provided here to appreciate the kicked rotor in the broader scheme of chaotic systems. Regular dynamics in classical Hamiltonian systems is generally associated with the notion of integrability [17]. In particular, time-independent Hamiltonian systems in d degrees of freedom are characterized by the existence of a Hamiltonian function $H(q_1, q_2, \dots, q_d, p_1, p_2, \dots, p_d)$ that depends on generalized coordinates q_i and canonical momenta p_i , and it satisfies the Hamilton's equations of motion given by,

$$\dot{q}_i = \frac{\partial H}{\partial p_i}, \quad \dot{p}_i = -\frac{\partial H}{\partial q_i}, \quad i = 1, 2, \dots, d. \quad (1)$$

A d degree of freedom system is integrable if sufficient number of constants of motion exist such that the problem can be reduced to quadrature or performing an integral. In particular, if d independent constants of motion C_i exist, and if their Poisson brackets are such that $\{C_i, C_j\} = 0$ for all $i, j = 1, 2, \dots, d$, then the system represented by H is integrable. Physically, integrability implies that the trajectories are constrained to remain on a d -dimensional manifold in phase space, and the geometry of this manifold is equivalent to a d -dimensional invariant tori (a consequence of Poincaré–Hopf theorem). As the phase space geometry is a d -dimensional tori, the integrable systems can be exactly transformed in terms of action–angle variables such that actions are invariants of motion. The geometric constraints and uniqueness of solutions of the equations of motion ensure that two initial conditions starting in a small neighborhood will continue to stay near one another asymptotically in the course of time evolution. Hence, an ensemble of initial conditions starting from a small region of phase space cannot explore the entire phase space.

For the present purposes, it is convenient to write a general Hamiltonian as

$$H(\mathbf{q}, \mathbf{p}) = H_0(\mathbf{q}, \mathbf{p}) + \alpha V(\mathbf{q}), \quad (2)$$

where $H_0(\mathbf{q}, \mathbf{p})$ is the integrable part and $V(\mathbf{q})$ is the perturbing potential that breaks the integrability of the system and α is a parameter denoting the strength of perturbation. Clearly, if $\alpha = 0$, the system is integrable and the phase space is dominated by invariant tori. For simplicity, we will assume that the system is integrable only if $\alpha = 0$. In 2D systems, if the frequency of motion in the two dimensions is commensurable (incommensurable), then the dynamics is on a rational (irrational) tori. The fate of these invariant tori under the effect of the perturbing term $V(\mathbf{q})$ is the subject of two different theorems, namely, the Poincaré–Birkhoff theorem [17] that deals with rational tori and the Kolmogorov–Arnold–Moser (KAM) theorem that deals with the generic case of irrational tori (if some conditions are satisfied, see Section 4). For the moment, we will assume that $H(\mathbf{q}, \mathbf{p})$ satisfies the KAM theorem conditions. Since $\alpha \neq 0$ is the non-integrable regime, the rational (resonant) tori are destroyed but the irrational tori will continue to survive for sufficiently small α . Typically, the latter would be gradually destroyed as α increases. The genesis of chaos can be traced to the alternating sequence of elliptic and hyperbolic points created by the break-up of rational tori. The interaction of the stable and unstable manifolds of the same hyperbolic points leads to homoclinic orbits. If these manifolds arise from different hyperbolic points, heteroclinic orbits are obtained [18]. With the additional requirement that the orbits cannot intersect in phase space, the dynamics in the vicinity of these structures becomes incredibly complex. In the (translated) words of Poincaré [10], “When one tries to depict the figure formed by these two curves and their infinity of intersections, . . . these intersections form a kind of net, web, or infinitely tight mesh . . . One is struck by the complexity of this figure that I am not even attempting to draw. Nothing can give a better idea of the complexity of the 3-body problem and of all the problems of dynamics in general”. This complex mesh of trajectories called homoclinic and heteroclinic tangles cause chaotic trajectories. Typical dynamics of this scenario is captured by the Smale horseshoe map [19,20], a minimal model of chaos that maps a square onto itself. Even after the rational tori are destroyed, the irrational tori (in two-dimensional systems) continue to remain as dynamical barriers constraining the trajectories from exploring the energetically allowed phase space. In three- and higher dimensional systems, irrational tori would persist but they need not necessarily act as dynamical barriers constraining transport in phase space [17]. See Section 8.1 for more details.

Under certain assumptions about smoothness of the potential in $H(\mathbf{q}, \mathbf{p})$ and excluding the rational (or resonant) tori, KAM theorem guarantees that the invariant tori would survive for sufficiently small perturbations [17,21]. As the strength of perturbation α increases, the invariant tori are deformed and destroyed. Once all the tori are destroyed, the entire phase space becomes connected and is ultimately filled with chaotic trajectories. At this point, some remarks on the definition of classical chaos is in order. Due to lack of consensus, several definitions of chaos exist in the literature [22]. For instance, many model systems such as the logistic map can be shown to be chaotic in the sense of the definition given by Devaney [23]. However, for real physical systems it is almost impossible to exactly prove the existence of chaos. Though not realistic, dynamics of a free particle on a surface of constant negative curvature is one of the rare “physical” systems known to be chaotic [24,25].

In practice, commonly used devices to infer chaos in physical systems are the Poincaré section and other measures, prominent among them being the Lyapunov exponent. This was first studied by Oseledec [26] to characterize stochastic trajectories, as an extension of an earlier idea due to Lyapunov [27]. It defines the average rate at which two neighboring initial conditions diverge from one another in phase space under the action of Hamiltonian evolution. For an N degree of

freedom system, if $d(0)$ is the distance between two initial conditions at, say, time $t = 0$, then the Lyapunov exponent is defined as

$$\lambda = \lim_{t \rightarrow \infty} \lim_{d(0) \rightarrow 0} \frac{1}{t} \log \left(\frac{d(t)}{d(0)} \right), \quad (3)$$

where $d(t) = \sqrt{\sum_{i=1}^N \delta x_i^2(t)}$ and δx represents the first order variation with respect to some reference trajectory. With N degrees of freedom, there would be $2N$ orthogonal directions in phase space. With one Lyapunov exponent corresponding to each direction, there would be a total of $2N$ exponents: $\lambda_1, \lambda_2, \dots, \lambda_{2N}$. However, the structure of Hamiltonian dynamics imposes symmetry constraints on the Lyapunov exponents; $\lambda_i = -\lambda_{2N-i+1}$, $i = 1, 2, 3 \dots 2N$. Thus, for dynamics that preserves phase space volumes, the sum of Lyapunov exponents is zero. This can happen either because all the exponents are zero or due to stretching in one direction canceled by a contraction in another direction. The summation in Eq. (3) does converge and the exponents are independent of the metric used in Eq. (3) to measure distances in phase space [26]. Generally, if $\lambda > 0$ everywhere in phase space, it indicates that the system is chaotic, while $\lambda = 0$ implies regular dynamics if the system conserves phase space volumes. Numerically computing Lyapunov exponents is generally non-trivial, and requires specialized methods to determine all the exponents [28,29]. Note that Lyapunov exponent is a local measure, especially in mixed phase space, while Poincaré section provides a global picture of the nature of dynamics in phase space. Entropic measures are also popular characterizers of chaos. It can be shown that the Kolmogorov–Sinai entropy (distinct from the thermodynamic entropy) of a single connected stochastic region in phase space equals the sum of positive Lyapunov exponents [30].

It must be pointed out that real physical systems, generically, are neither integrable nor completely chaotic but display mixed type dynamics, *i.e.*, co-existence of regions of regularity and chaos in different parts of phase space. In this sense, Poincaré section lends itself as a useful tool to obtain a global portrait of phase space. It is not unusual to find minuscule regular regions in a large sea of chaos. Such mixed systems are both challenging and interesting to study because they give rise to interesting physics. For instance, recent studies of a three-body problem, namely, the three coupled rotor, have reported existence of periodic orbits with interesting stability properties in a regime dominated by the chaotic sea [31]. A variety of statistical measures associated with dynamics such as the Poincaré recurrence time distributions [32,33] are strongly influenced by small regular regions disproportionate to their size in the phase space. Physically, this arises due to the ‘sticky’ nature of the interface between the regular region and the surrounding chaotic sea. Trajectories originating in the chaotic sea are trapped by the interface region for a long time before being released back into the chaotic sea. Quite remarkably, as shown in Ref. [34], this influence extends to include energy correlation functions in the quantum domain as well.

2.2. Chaos in time-independent Hamiltonian systems

As the rest of this review is devoted to a time-dependent chaotic system, it is worthwhile to take this brief digression to discuss chaos in time-independent systems, firstly to provide a broader perspective and secondly because they are related to experimentally accessible situations of interest ranging from billiard and coupled oscillator models to atoms in strong external fields [35].

The billiard class of models encapsulate the dynamics of a free particle inside a confined region with a well defined boundary. Specular reflection takes place when the particle hits the boundary. The complexity of dynamics in this class of systems arises from the shape of its boundary, *e.g.*, rectangle and circle shaped billiards are integrable but stadium shaped billiards is chaotic. Thus, regularity to chaos transition can be induced simply by deforming the boundary, say, from circular to stadium shape. Billiards serve as idealized model for electronic transport inside quantum dots and superlattices [36], and can also be a source of lasing action [37,38]. Sinai billiard (also called Lorentz gas) is a square shaped region with a central circular disc scooped out. Stadium [39] and Sinai billiards [40] are rare examples of physical systems that have been analytically shown to display exponential divergence of trajectories everywhere.

Further surprises came from quantized version of the stadium billiards problem. Whether it is stadium or some other billiards, the quantum mechanical problem boils down to solving the Helmholtz equation with appropriate boundary conditions. For a detailed exposition of the numerical and computational aspects, the reader should consult Ref. [41]. Intuitively, generic quantum eigenstates of stadium billiards were expected to reflect the chaotic nature of the underlying classical dynamics. Hence, these eigenstates should be featureless, random superposition of plane waves, as a corollary of the semiclassical eigenfunction hypothesis [42]. However, a subset of states violated this intuitive expectation and displayed localization-like features in the form of selective concentration of probability density only in certain regions of configuration space. This was first noticed in the case of quantum stadium billiards [43]. Physically, such localized or scarred eigenstates [44], as Heller called them, were associated with isolated and least unstable classical periodic orbits. Fig. 1 shows $|\psi|^2$ in configuration space, one example of a generic (Fig. 1(a)) and a scarred state (Fig. 1(b)), for the chaotic cardioid billiard system. The generic state has approximately uniform density over the configuration space, whereas the scarred state displays selective density enhancement along a narrow vertical strip (Fig. 1(b)).

Remarkably, this effect survives in the semiclassical limit as $\hbar \rightarrow 0$. In general, asymptotic properties of quantum wavefunctions such as the scar intensity statistics and intensity correlations of eigenstates can be explained using short

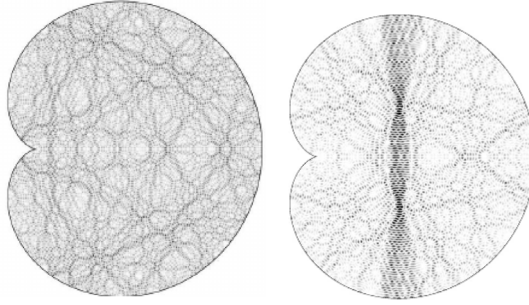


Fig. 1. Two of the eigenstates $|\psi|^2$ of Cardioid billiard. (left) a generic state, (right) a scarred state. The shape of the boundary of these highly excited eigenstates defines the cardioid billiard.

Source: Taken from Ref. [45].

time classical dynamics [46–48]. Strictly, scarring is a statistical property of a collection of eigenstates rather than of individual states. In the early 1990s, scars were experimentally observed in billiard shaped microwave cavities [49,50]. Scar effects are not specific to billiards alone, but were observed in a variety of time-independent Hamiltonians with chaotic classical limit such as the coupled quartic oscillator [51,52] and atoms in strong fields [53]. Interestingly, scar-like effects can also appear if the underlying periodic orbit is stable [51]. Semiclassical estimates of enhancements to scar intensity under the influence unstable periodic orbits, due to Bogomolny, provides theoretical basis for this phenomenon [54]. In the limit of highly excited states, the number of scarred states tend to zero, in a sense restoring the “ergodicity” in the wavefunctions. In the last few years, scars have witnessed a revival of interest since they were observed in the numerical simulations of interacting many-body systems such as variants of driven Bose–Hubbard model and Bose–Einstein condensates [55–58]. Though scarring is also a type of localization seen in chaotic quantum systems, it must be distinguished from the *dynamical* localization in temporally kicked systems to be encountered in the rest of this review. Dynamical localization is a purely quantum interference effect whereas scarring localization arises from classical remnants such as periodic orbits that leave a trail in the quantum regime.

For long, Henon–Heiles system [59], coupled anharmonic oscillators [60] and hydrogen atom in strong external magnetic fields [61] were prime examples of chaos in time-independent systems. It turns out that the latter problem, through use of a clever coordinate transformation that removes the singularity of the coulomb potential, can be modified into a coupled anharmonic oscillator system [61]. These systems were the testing grounds to study the boundary between the quantum and classical regimes [62]. The larger question of how the classical limit emerges from quantum regime as $\hbar \rightarrow 0$ is a fairly old one. It dates back to the question raised by Einstein in 1917 [63,64] about quantizing non-integrable systems, while proposing the now well-known Einstein–Brillouin–Keller (EBK) quantization scheme [65]. For a d degrees of freedom system, this scheme is given by

$$\oint p_i dq_i = \left(n_i + \frac{\mu_i}{4} \right) 2\pi\hbar, \quad i = 1, 2, \dots, d, \quad (4)$$

where $n_i \in \mathbb{Z}$ are the quantum numbers and μ_i is the Maslov index representing total phase loss in one period. It provides an estimate of the quantum eigenvalues in terms of the classical parameters only if the corresponding classical system is integrable. What happens in the case of chaotic systems? Periodic orbit theory, through a series of papers by Martin Gutzwiller in the late 1960s [66–69], answers this question with a formal relation connecting the quantum density of states $\rho(E)$ at energy E to the parameters like the stability and action of the classical periodic orbits. See Refs. [35,62] for a pedagogical introduction to periodic orbit theory. It is expressed as a sum over all the periodic orbits indexed by p , and it takes the form

$$\rho(E) = \frac{1}{\pi\hbar} \sum_p A_p \cos \left(\frac{S_p(E)}{\hbar} - \frac{\pi\mu_p}{2} \right). \quad (5)$$

In this, A_p is the pre-factor that depends on the period and stability of the orbit, S_p is its action. Since the 1970s, considerable amount of research effort has gone into understanding various aspects of periodic orbit theory, including applying it to physical systems. For a detailed discussion of these aspects, the reader is referred to Les Houches lectures [62]. In practice, the summation in Eq. (5) is difficult to perform due to exponential increase in the number of periodic orbits with the energy in chaotic system. However, by performing a Fourier transform on Eq. (5), it is possible to extract the contributions of the periodic orbits to the eigenlevels in the spectra. Fig. 2(a) shows the measured spectra for the chaotic diamagnetic hydrogen atom problem [61], and Fig. 2(b) shows peaks corresponding to scaled classical action, using which periodic orbit contribution has been identified [70].

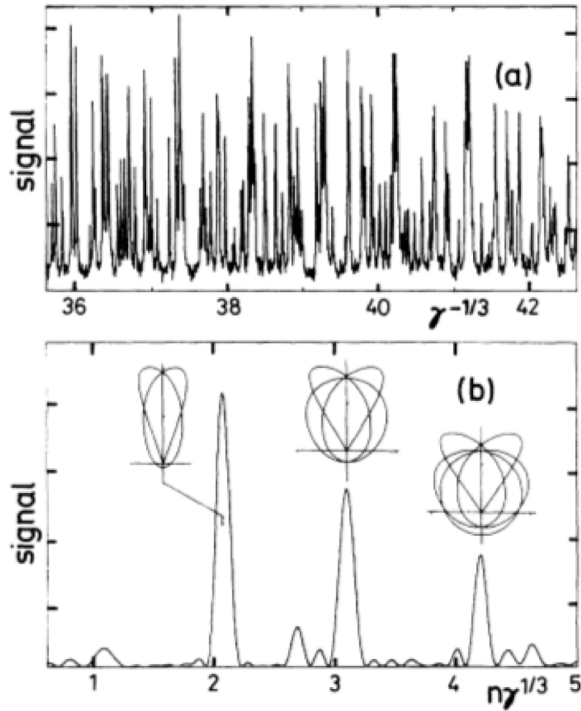


Fig. 2. (a) Measured (scaled) energy spectrum as a function of scaled (and dimensionless) external magnetic field for the hydrogen atom in strong magnetic field. (b) Fourier transform of the spectrum in (a). Note that the peaks in (b) correspond to contributions from closed orbits shown along side [70].

Source: Taken from Ref. [70].

2.3. Chaos in dissipative systems

All the systems discussed in Section 2.2 were conservative and their impact was felt largely within the domains of mathematics and physics. However, much of the excitement around the idea of chaos among the scientists and in popular culture is associated with such colorful terms as “butterfly effect” and even more unimaginable effects like “butterfly flapping its wings and creating a storm far away”. Butterfly effect has its origins in the strange attractor of the Lorenz model [71], which looks like a butterfly with two wings. Lorenz model is an example of a dissipative system, for which the volume defined by an ensemble of initial conditions contracts during time evolution. Lorenz model is a set of three coupled ordinary differential equations and is a simplified model for atmospheric convection [71]. Edward Lorenz was a meteorologist and his seminal paper in 1963 introducing this model gave impetus to much of further developments in nonlinear dynamics and chaos. In general, the equations of motion can be written as a coupled set of first order differential equations of the form $\dot{\mathbf{x}} = \mathbf{f}(\dot{\mathbf{x}})$, where \mathbf{f} is a nonlinear function. For dissipative systems $\nabla \cdot \mathbf{f} < 0$, whereas for conservative systems $\nabla \cdot \mathbf{f} = 0$. Other popular dissipative systems are the logistic map, Hénon map (with appropriate choice of parameters) and tent map. The logistic map is a one-dimensional difference equation or a map [72] and is even simpler than the Lorenz model. It was introduced by the population biologist Robert May in 1976 as a model for population evolution in ecosystem of prey and predators.

Since the 1960s, a large number of papers and books have been written on this subject, especially on the question of bifurcations and routes to chaos in these systems. We will not even attempt to summarize the main results here, but refer the reader to some of the books available on the subject [17,18,20,73–75]. Most striking aspect of dissipative systems is the existence of strange attractors, whose dimensionality is a non-integral number (fractal dimensions) and the dynamics on the attractor is chaotic. Asymptotically, any non-escaping trajectory, can be expected to settle down on the strange attractor. The Hamiltonian systems, on the other hand, cannot have attractors in phase space as they need to conserve “volumes”, a hierarchy of quantities called Poincaré invariants [21], in phase space. The presence of attractors in dissipative systems makes a marked difference in the qualitative geometry of phase space. It is also of interest to note that “dissipation” can be introduced in certain Hamiltonian systems by using absorbing ‘boundary conditions’ defined in certain regions of phase space. Any initial condition visiting this defined region, during the course of its evolution, is bound to get absorbed. This idea has been used to construct open models of kicked rotor [76–78].

2.4. Structure of this review

Broadly, this review is structured into two parts. The first part, in Sections 1 to 6, is the basic phenomenology of kicked rotor. Most of these results were obtained during the years from 1970s to 2000, and relate to the investigations on the basic phenomenology of classical and quantum chaos in which kicked rotor has played a central role. Some of these developments include the equivalence between kicked rotor and the Anderson impurity model, and first atom-optics experimental realizations. In Sections 1–6, the rich dynamical properties of classical and quantum dynamics of kicked rotor are described including a brief review of the experimental realizations of the kicked rotor.

The second part of the review, in Sections 7 to 11, covers the developments during the years 2000 to 2020. During this phase, kicked rotor model outgrew the contours of classical and quantum chaos and began to develop an overlap with wider spectrum of problems in condensed matter physics and other emerging areas such as the quantum information theory. Many variants of kicked rotor were also created to throw light on novel physical phenomena ranging from effects induced by non-KAM systems, localization to delocalization transitions and the effect of nonlinearity and interactions. Some of these were experimentally realized as well. In Sections 7 to 11, we describe some of the interesting variants of kicked rotor – higher dimensional and coupled kicked rotors, quasiperiodic kicked rotors – and novel physical insights obtained from them. In addition, significant parts of the review are devoted to the interface between chaos and quantum correlations, an area for which kicked rotor is one of the preferred models. This review concludes with a section on applications (Section 11) and a brief outlook for the future.

The volume of research output relating to kicked rotor and its variants is vast. We have attempted to focus on significant developments that also have overlaps with other areas of physics with the hope that it might interest scientists outside the community of quantum chaos. For the same reason, we have attempted to discuss various strands to ideas centered around kicked rotor rather than exclusively focus on a select few. Needless to say, this has meant cutting down on finer details for which sufficient pointers in the literature have been provided. As we have drawn from works of many scientists over the last five decades, it was challenging to maintain coherence in notation throughout the review. For example, symbols such as N stand for different entities throughout the review but represent the same quantity within any given section. In most places, quantum operators can be easily identified from the context and the traditional ‘hat’ symbol has not always been used to distinguish it.

3. Kicked rotor model

3.1. Classical kicked rotor

The time-dependent Hamiltonian of the classical kicked rotor model [16,17,79,80] is

$$H = \frac{p^2}{2I} + k \cos x \sum_{n=-\infty}^{\infty} \delta(t - nT), \quad (6)$$

where x and p are, respectively, angular displacement and angular momentum variables, and I is the moment of inertia. The dimensionless position-dependent potential function $\cos x$ with kick strength k is applied only at regular time intervals $T > 0$. Evidently, if $t \neq nT$, the system is essentially a free particle. The dynamics is that of a free particle interspersed with periodic kicks. Physically, this corresponds to a pendulum that receives energy through periodic external kicks. By setting $I = 1$ and performing the transformation $p \rightarrow pT$ and $t \rightarrow tT$, dimensionless Hamiltonian becomes

$$H = \frac{p^2}{2I} + K \cos x \sum_{n=-\infty}^{\infty} \delta(t - n), \quad (7)$$

where $K = kT$ is the (scaled) stochastic parameter that controls the qualitative nature of dynamics in the system. Since time-dependence enters in the form of δ -function, the Hamilton’s equation of motion corresponding to Eq. (7) can be exactly integrated. This results in a pair of difference equation given by

$$x_{n+1} = x_n + p_{n+1}, \quad (8)$$

$$p_{n+1} = p_n + K \sin x_n. \quad (9)$$

This celebrated map, known as the standard map or the Chirikov map, was introduced by Boris Chirikov [16,81]. Though kicked rotor is a physical system, standard map has also been studied independently as a mathematical object. In this article, we will often use the terms “standard map” and “kicked rotor system” interchangeably. The transformation $(x_n, p_n) \rightarrow (x_{n+1}, p_{n+1})$ is canonical and the associated Jacobian $|\partial(x_{n+1}, p_{n+1})/\partial(x_n, p_n)| = 1$ is unity. Hence, this is an area preserving transformation. If $K = 0$, this is simply the free particle system. Changes in the qualitative nature of dynamics take place as K is varied.

The map in Eqs. (8)–(9), at least locally in the p variable, captures the dynamical behavior displayed by several physical systems. One of the original physical motivation pointed out by Chirikov was the case of the magnetic bottle, a system for confining charged particles in mirror magnetic traps [81]. Another physical situation either reducible or closely related

to the standard map is the interaction of a single particle with a short bunched beam in a particle accelerator, in which case, the unperturbed part of the mapping is linear and nonlinearity is induced by the weak perturbation terms. This is often called a ‘nearly linear map’ to indicate this perturbative property [82]. Cometary or Kepler map describes the chaotic dynamics of comets orbiting the sun due to perturbative influence of Jupiter. The linearized dynamics around the fixed points of cometary map reduces to a standard map [83]. Another map similar to the cometary map was shown to model the chaotic dynamics of the Halley comet under the influence of Jupiter [84]. A recent work however points out that Halley comet’s chaotic dynamics has origins in its interaction with Venus, rather than with Jupiter [85]. A system realizable in the terrestrial laboratory is the highly excited hydrogen atom in a monochromatic microwave field. The classical version of this problem is chaotic for sufficiently strong field strength and can be reduced, firstly to the Kepler problem, and subsequently through a linearization to the standard map [86,87]. The dynamics of a charged particle between planar potential barriers, resonant tunneling diode, in externally applied electric and magnetic field can also be reduced to the standard map [88].

In conservative systems, stochasticity arises from the interaction of nonlinear resonances. Standard map contains infinite nonlinear resonances in phase space and, for $K < 1$, are arranged distant 2π apart along p -axis (Ref. 3(a)). The importance of standard map arises from its ability to be an effective local model for the origins of stochasticity in the vicinity of nonlinear resonance. It is precisely for this reason that many physical systems can be locally reduced to a standard map. When a large number of resonances overlap, the particle originating in one region of nonlinear resonance is able to break free and access phase space regions far from its starting point effectively leading to chaotic dynamics.

3.2. Phase space geometry

Depending on the physical problem, two different types of boundary conditions can be applied to kicked rotor in Eq. (7). By setting periodic boundary conditions in both the x and p variables, the geometry of phase space will take the form of a two-dimensional torus. This can be easily applied by taking modulo- 2π to the variables x and p in Eqs. (8)–(9). This is suitable to explore the details of classical phase space features such as cantori and KAM tori. On the other hand, by imposing periodicity only on x , and if $-\infty \leq p \leq \infty$, then phase space has the geometry of a cylinder. This version of the rotor is useful to study a host of transport and chaotic diffusion problems. One less commonly used possibility is the reflective boundary condition in x variable. This choice leads to a kicked rotor system that violates KAM theorem and displays distinctly different dynamical behaviors from the former cases. Explicit examples of this are considered in Section 7.2.

The integrable limit of kicked rotor corresponds to the choice of kick strength $K = 0$, representing the free particle problem. In this limit, the Hamiltonian can be transformed into action-angle variables such that the actions are the exact constants of motion. If the periodic boundary conditions are applied, and $0 \leq x, p \leq 2\pi$, then the action is given by, $I = p$ and $H = H_0 = I^2/2$. Since I is a constant of motion, H_0 is invariant as well. Explicit solution in action-angle variables can be written down as, $I(t) = p_0$ and $\theta(t) = \theta_0 + \omega t$, where (θ_0, p_0) are the initial conditions and $\omega = \partial H_0 / \partial I = 2\pi/T_0$ is the frequency of periodic motion. If we choose to look at the phase space stroboscopically at periods of τ , then phase space will display either a discrete set of points or flat curves parallel to x -axis depending on whether T_0/τ is a rational or irrational number. Though the integrable limit itself does not suggest a timescale for τ , to aid the analysis of the non-integrable kicked rotor further, it is useful to take τ as the kicking period T . For $K > 0$, kicked rotor becomes non-integrable and the flat curves in phase space would begin to deform. As K increases further, for $K \gg 1$, typically chaotic dynamics sets in and the entire phase space is dominated by chaotic solutions. This scenario will be described in some detail in the next section.

4. Transition to chaos

Fig. 3 displays the integrable to chaos transition in the stroboscopic map of the kicked rotor system. This figure is generated by numerically iterating Eqs. (8)–(9) starting from several initial conditions. Typically, each curve in Fig. 3(a) is generated from a different initial condition. To generate Fig. 3, about 20 initial conditions were used; $x = 0$ and 20 values of p within the range $(0, 2\pi)$. However, Fig. 3(f) is generated with just one initial condition for the entire chaotic layer, and three initial conditions to obtain the small regular regions embedded within the chaotic layer. For $K \ll 1$, broadly two kinds of structures are visible. (i) The elliptical structures indicate the existence of nonlinear resonances – when the ratio of external kick frequency ω_1 to the internal frequency of motion ω_2 is a *rational* number. Let us denote this ratio by $\mu = \omega_1/\omega_2$. If μ is a rational number, then nonlinear resonances satisfy the condition: $n_1\omega_1 + n_2\omega_2 = 0$ where n_1, n_2 are integers. For instance, in Fig. 3(a), $(x = \pi, p = 0)$ corresponds to a primary 1:1 resonance, whereas (π, π) and $(0, \pi)$ are part of the 1:2 resonance. The neighborhood surrounding these phase-space points are the nonlinear resonance regions. The latter is a higher order resonance and arises from the interaction of primary resonances. In the sense of classical perturbation theory (when parameter K is taken to be small), this 1:2 resonance emerges in the second order of perturbation, *i.e.*, in terms of order K^2 after a canonical transformation that removes perturbation terms of order K (see section 5.1 in Ref. [89] for details of perturbation theory calculations). (ii) The other visible structures are the irrational tori that are formed when μ is irrational. In this case, due to lack of commensurability between the two time periods, as the kicks are imparted the points on the section do not precisely repeat themselves, but instead fill a curve that effectively

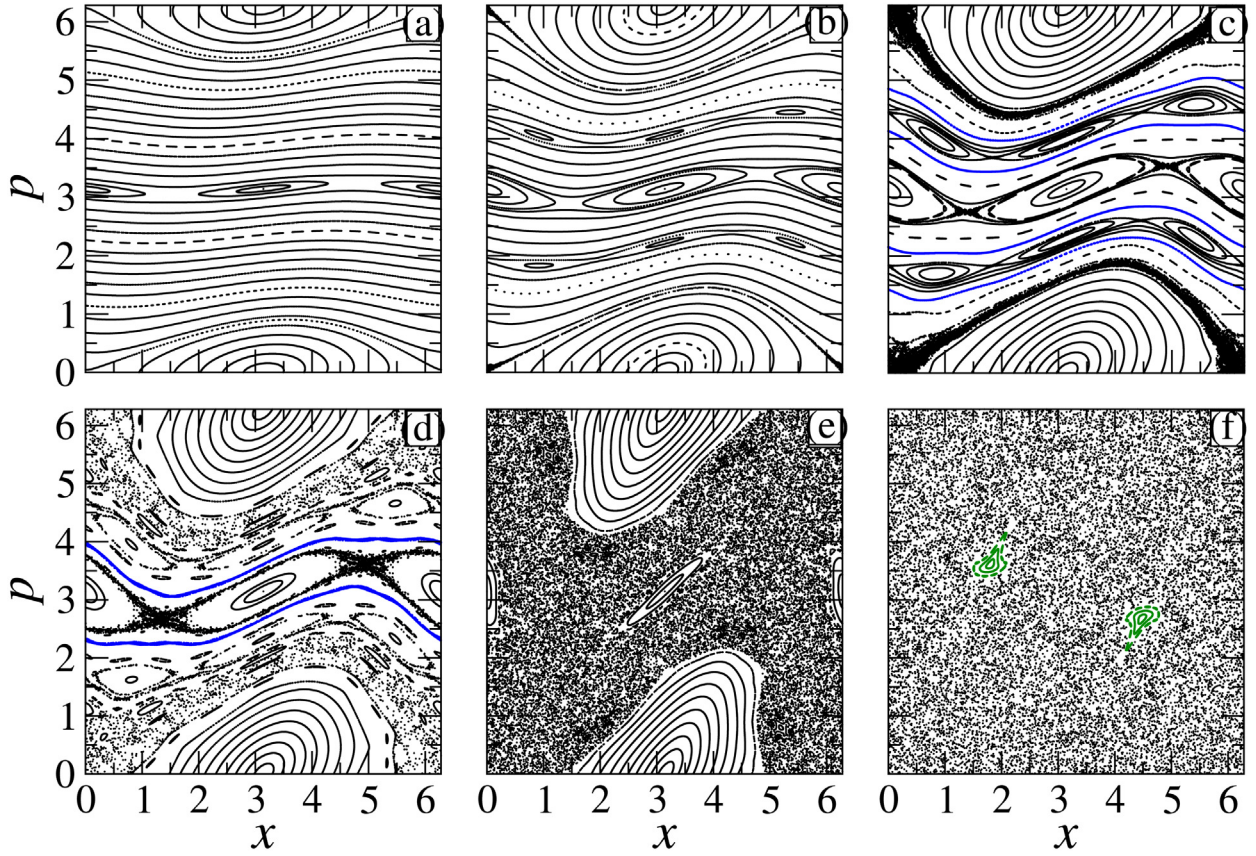


Fig. 3. Classical stroboscopic map for the kicked rotor obtained by evolving Eq. (9) with modulo- 2π . The kick strength is (a) $K = 0.2$, (b) $K = 0.5$, (c) $K = 0.8$, (d) $K = 0.971$, (e) $K = 1.8$ and (f) $K = 5.5$. Notice that as K increases the fraction of regular region in the phase space decreases on an average. In (c), the blue curves are among the many invariant tori in the system. In (d), the two blue curves are the two last invariant tori that survive as system becomes strongly nonlinear. In (f), two small regular regions are highlighted (in green color) in an otherwise chaotic sea.

becomes continuous as the number of kicks tend to infinity. On the other hand, for $K \gg 1$, the entire chaotic layer (except the two tiny islands shown in green) in Fig. 3(f) is generated starting from just one initial condition.

For kick strength $K = 0.2$ (Fig. 3(a)), the system is no more integrable and yet the phase space is dominated by the invariant curves as anticipated based on the Kolmogorov–Arnold–Moser (KAM) theorem [90–92]. For a more recent review of KAM theorem, see Ref. [93]. Under certain assumptions, the KAM theorem for autonomous two-dimensional systems guarantees the persistence of irrational tori under the application of mild perturbations [90–92]. Let a two-dimensional classical system of interest be denoted by $H = H_0(I_i) + \epsilon H_1(I_i, \omega_i)$, in which $i = 1, 2$ and H_0 represents its integrable part depending only on the action variables I_i , while the perturbation H_1 depends on both the actions and their associated frequencies ω_i . The tori whose frequency ratio $\mu = \omega_1/\omega_2$ is rational does not survive the perturbation and is subject to Poincaré–Birkhoff theorem [21]. The tori for which μ is irrational, called the irrational tori, do survive for small perturbations and fall within the ambit of KAM theorem. To apply KAM theorem, following conditions need to be met: (a) perturbation must be smooth, i.e., H_1 must be an analytic function (though later proofs of KAM theorem only require finite number of derivatives to exist [91]), (b) the frequencies of unperturbed motion must vary smoothly with action (non-degeneracy condition): $\det|\partial^2 H_0/\partial I_i \partial I_j| \neq 0$, and (c) the frequency ratios must not be well approximated by rational numbers. The condition (a) is to ensure fast convergence of the series solution, while (b) ensures that dense set of invariant tori exist in the unperturbed system, and condition (c) answers how far from rational should μ be to qualify as an irrational orbit. Assuming that these conditions are satisfied, if $T_0(\omega_1, \omega_2)$ represents an irrational tori of H_0 , then KAM theorem states that for very small perturbations, i.e., $\epsilon \ll 1$, an invariant tori $T(\omega_1, \omega_2)$ of H would persist “close to” $T_0(\omega_1, \omega_2)$ [90,92].

To apply KAM theorem to maps, it is important to realize that mappings (such as the standard map) can be thought of as rotations about (possibly deformed) circles which intersect a notional section or a plane in phase space. The dynamics on this section is then seen to be generated by a canonical generating function $S = S_0 + \epsilon S_1$, where S_0 leads to an integrable map, and S_1 to non-integrable map for $\epsilon \ll 1$. For details on how to construct the generating function, see Refs. [17,21]. Hence, the conditions given above must be applied on S_0 and S as the generator of dynamics. In 1962, Moser proved

a version of KAM theorem valid for mappings and it requires H_0 to have only a finite, rather than infinite, number of derivatives [91]. Further refinements since the 1970s have brought down the number of derivatives required to single digits [94,95].

The map in Eqs. (8)–(9) for the kicked rotor system satisfies the requirements of the KAM theorem. The perturbation in Eq. (9) is a sine function and it is analytic. The integrable part, being a free particle system with $H_0 = I^2/2$, is non-degenerate. Then, it follows from KAM theorem that for sufficiently small perturbations, $K \ll 1$, the invariant tori would survive the perturbations. Indeed, as seen Figs. 3(a–d), some of the invariant tori survive well until $K \approx 1$. Nonlinear resonances (chains of island-like structures) are clearly visible in the phase space in Figs. 3(a–d), and are replaced by chaotic layer as K increases. In Fig. 3(a–e), a large primary resonance region around the elliptic fixed point at $(\pi, 0)$ is visible, and also the 1:2 resonances that form a chain two islands with stable fixed points at $(0, \pi)$ and (π, π) . In the regime $2 \leq K \leq 4$, this 1:2 island chain is unstable. First symptoms of chaos arise in the vicinity of hyperbolic fixed points. As K is increased, this manifests on the stroboscopic map as a resonance layer, surrounding the island chains in which the dynamics is irregular. Three contiguous resonance layers enclosed within the invariant tori or KAM tori (drawn in blue color) are shown in Fig. 3(c). The invariant tori act as barriers to global diffusion of particles and energy, and prohibit transport from one resonance layer to the other. As K increases, the area of the resonance layers increases, the invariant tori are destroyed and some of the resonance layers merge. Such mergers (or, overlap) of nonlinear resonances are the basic mechanism through which KAM tori are destroyed and chaos ensues [17]. The last surviving invariant tori at $K = 0.971$, often called the golden KAM tori since it has a winding number $w_g = \frac{\sqrt{5}-1}{2}$, is shown in Fig. 3(d) and inhibits global transport. If w_g is represented as a continued fraction

$$w_g = 0 + \cfrac{1}{1 + \cfrac{1}{1 + \cfrac{1}{1 + \dots}}} = [0, 1, 1, 1, \dots], \quad (10)$$

then the golden KAM tori has the most irrational winding number and is the last one to break up under the impact of increasing strength of perturbations. If K_c represents the critical kick strength at which the last invariant tori is destroyed, then for $K > K_c$, a large and connected chaotic region emerges as seen in Fig. 3(e). As nonlinearity is further increased and when $K \gg K_c$, remaining regular regions shrink and the phase space is predominantly occupied by chaotic trajectories. One such case is displayed in Fig. 3(f), in which chaos dominates everywhere barring two tiny island structures. This also serves to highlight a general feature of kicked rotor as a mixed system. Irrespective of kick strength K , kicked rotor is not known to be a C-system, i.e., trajectories are unstable everywhere in phase space with positive Lyapunov exponent. For all practical purposes, dynamics of kicked rotor is essentially chaotic for $K \gg 1$.

Considerable effort had been expended on determining the critical value K_c . Numerical results indicate that $K_c = 0.971635\dots$ [96,97]. The analytical underpinnings for determining K_c with sufficient accuracy are due to the work of Greene [96], and Shenker and Kadanoff [98]. The main idea is based on examining the stability of successive cycles of continued fraction approximation to the winding number w_g of the last invariant tori. For instance, the approximation to w_g at i th cycle would be $w_i \approx n_i/m_i = [0, 1, 1, \dots, a_i]$, where $a_i = 1$ such that n_i, m_i are integers and this is unique except in the last term. Clearly, $w_g = \lim_{i \rightarrow \infty} w_i$. The golden tori is destroyed when all the successive rational approximants to the invariant tori become unstable. For the golden KAM tori, many more terms of the continued fraction are needed for convergence to w_g when compared to the case of any other KAM tori. In terms of dynamics, on the stroboscopic section, this would imply that the associated n_i/m_i resonances are of higher order and the elliptic island chains are small. Consequently, the golden tori become much harder to destroy. These arguments have led to further significant insights. The scaling theory of KAM tori based renormalization mapping techniques developed in Ref. [97] help to quantitatively understand that the phase space structure in the vicinity of a golden KAM tori is universal for the entire class of nonintegrable twist maps, of which standard map derived from kicked rotor Hamiltonian is one specific example.

Another approach to determine K_c is through the so-called 'converse KAM theorem' and this is an attempt to show that invariant tori cannot exist for any value of $K > K_c$. Using interval arithmetic and computations, MacKay and Percival [99] show the non-existence of invariant tori for $K \geq 63/64 = 0.984375$. A less accurate but physically appealing technique is the celebrated method of overlapping resonances introduced by Chirikov [16,81]. The basic premise is that a system that displays many resonances in phase space can become chaotic when these resonance layers begin to merge. In the context of kicked rotor, this idea can be implemented by rewriting the Hamiltonian in Eq. (7) in the form

$$H = \frac{p^2}{2} + K \sum_{n=-\infty}^{\infty} \cos(x - 2\pi nt), \quad (11)$$

where the Poisson sum formula has been used to represent the series of delta kicks in terms of a cosine function. In this form, it represents a series of resonances whenever $p = 2\pi n$. Thus, the distance between any two successive resonance regions is $\Delta p_{\text{res}} = 2\pi$. Each of these resonances labeled by n , considered individually, can be thought of as a pendulum

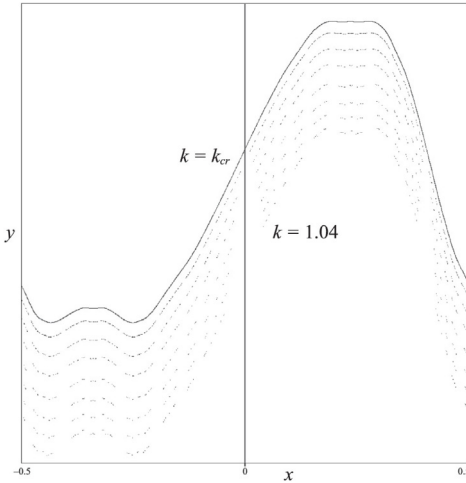


Fig. 4. Cantori for the standard map. The y -axis is the momentum p and x -axis is position. Top most curve is the golden KAM invariant tori at $K_c = 0.971635$. For the next curve just below $K = 0.98$ and so on until for the lower most curve $K = 1.04$. Note that all the invariant curves have large gaps in them and particles can pass through them. Successive cantori have been shifted vertically for clarity.

Source: Taken from Ref. [108].

system with Hamiltonian given by, $p^2/2 + K \cos \theta_n$, where $\theta_n = x - 2\pi nt$. Then, the half-width $\Delta\omega$ of the region enclosed by the separatrices is $2\sqrt{K}$. Resonances labeled n and $n + 1$ will begin to overlap if

$$\frac{2\Delta\omega}{\Delta p_{\text{res}}} > 1, \quad (12)$$

effectively allowing transport between these two regions. This criterion predicts that chaos will set in when $2\sqrt{K}/\pi > 1$, or equivalently, when $K = K_c = \pi^2/4 \approx 2.46$. As discussed earlier, $K_c \approx 0.97$, and it is also evident from Fig. 3(d). This criterion of overlapping resonances overestimates K_c and this can be attributed to a series of approximations that have gone into it including the assumption that resonances do not interact with one another. More accurate estimates [100] based on overlap criteria have taken into account overlap of resonances taking place at smaller scales. It might be pointed out that analogues of nonlinear resonances also exist in quantum systems as first reported by Berman and Zaslavsky [101], and further confirmed by later studies in a variety of chaotic quantum systems [102–107].

When the golden KAM tori has been destroyed, the remnants of this break-up leave a visible trail of structures in the phase space. Such structures called *cantorus* are essentially broken KAM invariant tori. Consequently, they have leaky segments (see Fig. 4) as kick strength increases beyond K_c . As seen in Fig. 4, this set of points has interleaving gaps arising due to overlap of surrounding elliptic islands and is a geometric object with non-integral dimension called cantor set [109–113]. Physically, the net effect on dynamics is that now the particles can diffuse through the gaps in cantori and access rest of the connected phase space. Thus, cantori form partial barriers and serve to regulate, rather than entirely prohibit, transport. As $K \gg K_c$, the cantori disappear and phase space is dominated by chaotic trajectories. Even in a phase space with a large chaotic component, presence of small regular islands tends to lend stickiness to the dynamics. Chaotic trajectories exploring the phase space can get stuck in the vicinity of these regular regions for long times before being released back into the surrounding chaotic sea. This happens due to the presence of cantori which regulates the trajectories at the interface between regular islands and the chaotic sea. This effect leads to power-law decay of survival probability, as opposed to exponential decay in completely chaotic systems [114–116]. A recent survey of transport properties in Hamiltonian systems, especially focused on cantori describes the progress made in understanding the effects of cantori [108]. It is worth pointing out that the effects of cantori show up as pinning transition in an entirely different system, namely, the Frank–Kontorowa model of atoms interacting through harmonic springs in a periodic potential [117]. Remarkably, the presence of cantori affects quantum dynamics of kicked rotor [118,119], as well as the cold atom realizations of kicked rotor system [120], and inhibits quantum transport far more effectively than it does in the classical regime. For a systematics of how partial barriers such as cantori affect quantum dynamics, see Refs. [121,122].

For $K \gg K_c$, kicked rotor is mostly chaotic as seen from plots of Poincaré sections (not shown here). At these parameters, the Lyapunov exponents are positive as well. In the chaotic regime of $K \gg 1$, the Lyapunov exponent can be analytically estimated. The idea is to consider the time evolution of a small excursion from a reference phase space point, from which growth rate can be extracted. To do this, the standard map in Eq. (9) is linearized about some (\tilde{x}, \tilde{p}) resulting in a tangent mapping: $u_{n+1} = u_n + v_{n+1}$ and $v_{n+1} = v_n + Ku_n \cos x_n$, where $u = x - \tilde{x}$ and $v = p - \tilde{p}$. To solve the tangent

map, x_n is needed, which is equivalent to solving the standard map in the first place. The way out is to consider a linear map of the form

$$x_{n+1} = \{x_n + p_{n+1}\}, \quad p_{n+1} = p_n + kx_n, \quad (13)$$

where $\{\cdot\}$ represents the fractional part and makes this a non-linear mapping. However, the tangent map corresponding to this is linear: $u_{n+1} = u_n + v_{n+1}$ and $v_{n+1} = v_n + Ku_n$. The eigenvalues of this map are: $L_{\pm} = 1 + k/2 \pm \sqrt{k(1+k/4)}$. For $k \in [-4, 0]$ the eigenvalues are complex numbers, and $|L_+| = |L_-| = 1$. Any small initial variation does not grow, but instead displays bounded oscillations. However, if $k \notin [-4, 0]$, then the eigenvalues satisfy $|L_+| > 1$ and $|L_-| < 1$ and local instability ensues. Comparing Eq. (13) to the tangent map, $k = K \cos x$, or equivalently the linear map is valid in the region of phase space points at which $k = \pm K$. Then, Lyapunov exponent can be written down as

$$\lambda \approx \frac{1}{2\pi} \int_{-\pi}^{\pi} dx \ln |L_+(x)| = \frac{1}{2\pi} \int_{-\pi}^{\pi} dx \ln \left| 1 + \frac{K \cos x}{2} + \sqrt{K \cos x \left(1 + \frac{K \cos x}{4} \right)} \right|. \quad (14)$$

For $K \gg 0$, well into the chaotic regime, a good agreement with numerically computed Lyapunov exponent is seen. In particular, for large K , the asymptotic result is [81,123,124]

$$\lambda \approx \ln(K/2). \quad (15)$$

4.1. Momentum and diffusive transport

In this section, the discussion will pertain to evolution of momentum and energy of the standard map defined on a cylinder. Starting from Eq. (9) and iterating it up to time N , the change in momentum Δp_N can be written as

$$\Delta p_N = p_N - p_0 = K \sum_{n=0}^N \sin x_n. \quad (16)$$

From the stroboscopic maps such as Fig. 3(f), it is clear that in the chaotic regime of $K \gg 1$, the successive iterates of x_n are uncorrelated. Further, as chaotic dynamics emerges for $K \gg 1$, the position variable x_n can be assumed to be ergodic on the interval $0 \leq x \leq 2\pi$, though strictly ergodicity has not been proven yet. This is equivalent to assuming that the position (or momentum) evolution is similar to a random process. Hence, for $N \gg 1$, the summation in Eq. (16) can be replaced by an integral over x (time average replaced by phase space average) and the mean value becomes $\langle \Delta p_N \rangle = 0$. An expression for variance $\langle (\Delta p)_N^2 \rangle$ can be obtained as

$$\langle (\Delta p)_N^2 \rangle = K^2 \sum_{n=0}^N \sum_{n'=0}^N \langle \sin x_n \sin x_{n'} \rangle. \quad (17)$$

As argued before, successive x_n are uncorrelated and the double summation can be evaluated as

$$\sum_{n=0}^N \sum_{n'=0}^N \langle \sin x_n \sin x_{n'} \rangle \approx \sum_{n=0}^N \sum_{n'=0}^N \langle \sin x_n \sin x_{n'} \rangle \delta_{n,n'} = \sum_{n=0}^N \langle \sin^2 x_n \rangle = \frac{N}{2}. \quad (18)$$

Using this in Eq. (17), the variance becomes

$$\langle (\Delta p)_N^2 \rangle = \frac{1}{2} K^2 N = D_0(K)N, \quad (19)$$

where $D_0(K) = K^2/2$ is diffusion coefficient. The variance is proportional to time N , and this is a signature of diffusive processes, e.g., random walk. In the chaotic regime, an ensemble of kicked rotor trajectories displays unbounded diffusion in the momentum direction, much like a random walker on an infinite lattice.

Even in the chaotic regime, the successive iterates of standard map are never strictly uncorrelated. In chaotic systems, correlations decay exponentially fast and hence short time correlations can exist. From this perspective, the result in Eq. (19) represents a zeroth order or quasi-linear approximation that neglects correlations in the dynamics. The programme of not ignoring the correlations was carried out by Rechester and White [125,126] by applying a probabilistic approach to solve Vlasov equation for an ensemble of initial conditions for the standard map. For $K \gg 1$, typically if $K > 4.5$, the diffusion coefficient becomes

$$D(K) = D_0(K) (1 - 2J_2(K) (1 - J_2(K))), \quad (20)$$

where $J_2(\cdot)$ is the Bessel function of order-2. As $K \rightarrow \infty$, $J_2(K) \rightarrow 0$. Hence, for sufficiently large K , $D(K) \approx D_0(K) = K^2/2$. The effect of correlation is seen in the last two terms of Eq. (20) which appear with negative sign and tend to decrease the diffusion coefficient from its quasi-linear value D_0 . With these results in place, the energy growth for the kicked rotor systems is

$$\Delta E(N) = \frac{\langle \Delta p^2(t) \rangle}{2} = \frac{D(K)}{2}. \quad (21)$$

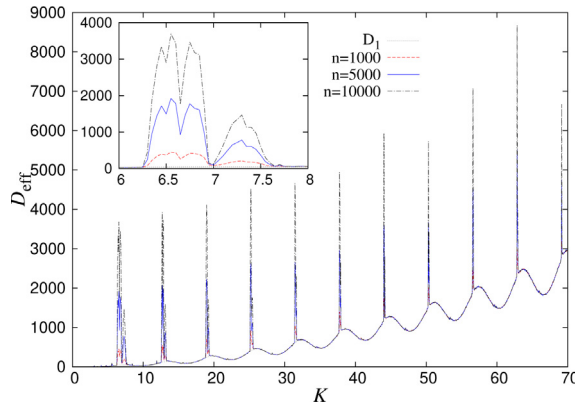


Fig. 5. Effective diffusion coefficient D_{eff} as a function of K . D_{eff} is calculated based on data from $n = 1000, 5000$ and 10000 iterations. The quasi-linear approximation is denoted by D_1 and is shown as gray line. Note the large spikes in diffusion coefficients for large K . First of these spikes (magnified in inset) correspond to the accelerator mode in the interval $6.283 \leq K \leq 7.448$ obtained by setting $M = 1$ in Eq. (27).

Source: Taken from Ref. [127].

In the quasi-linear approximation relevant in the chaotic limit of $K \gg 1$, the energy growth becomes $\Delta E(N) = K^2 N / 4$. Notwithstanding this result based on assuming statistical properties of chaotic dynamics, it must be emphasized that even in the limit $K \gg 1$, there could be pronounced deviations from diffusion and energy growth predicted, respectively, by Eqs. (20) and (21) due to presence of tiny stable island chains in phase space. In the next section, one such case of accelerator modes will be discussed.

The momentum distribution after N kicks can be obtained as follows. Formally, the probability that after N kicks momentum lies between p and $p + \Delta p$ is

$$g_N(\Delta p) = \langle \delta(\Delta p - (p_N - p_0)) \rangle = \left\langle \frac{1}{2\pi} \int_{-\infty}^{\infty} dt \exp[i(\Delta p - (p_N - p_0))t] \right\rangle \quad (22)$$

where $\langle \cdot \rangle$ represents an average taken over many realizations with different initial conditions. The last form is obtained by using the Fourier integral representation for δ -function. After simple manipulations as done before, we assume that successive positions are uncorrelated in the chaotic regime. When the long time limit $N \rightarrow \infty$ is taken, the momentum distribution becomes

$$g(\Delta p) = \frac{1}{K\sqrt{\pi N}} \exp\left(-\frac{\Delta p^2}{K^2 N}\right). \quad (23)$$

As would be expected of a diffusion process consistent with Eq. (19), the momentum distribution is a Gaussian distribution with its time-dependent standard deviation. Note that $\Delta p = p_N - p_0 = \sum_{n=0}^{N-1} p_{n+1} - p_n$ could be thought of as a random variable (due to chaotic dynamics) representing a sum over change in momenta for $N \gg 1$. Hence, in the spirit of central limit theorem, it is natural to expect that momentum would be Gaussian distributed as shown in Eq. (23).

4.2. Accelerator modes

Accelerator modes [89,128,129] are solutions corresponding to special choice of initial conditions in certain small intervals of kick strength K at which acceleration is possible. In the accelerator mode, the position variable grows ballistically as $x_n \sim n^2$ and momentum variable displays linear growth, i.e., $p_n \sim n$. Thus, successive iterates of momentum differ by integral multiple of a basic unit, 2π in the present case. These initial conditions are special because, for certain intervals in K , they are part of stable elliptic islands and solutions starting from these islands also undergo acceleration. Typically, accelerator modes display anomalous diffusion of the form $\langle(p_n - p_0)^2\rangle \sim n^\gamma$, where $\gamma \approx 2$. In practice, the exponent γ can be in the range $1 < \gamma < 2$, depending on the presence of other stable islands [89,130–132]. This is in contrast to the normal diffusion, i.e., $\gamma = 1$ predicted by the analysis in the previous section for $K \gg 1$.

Now, let us consider a choice of initial conditions

$$x_0 = \pi - \sin^{-1}(2M\pi/K), \quad p_0 = 0, \quad (24)$$

in which $M \geq 0$ is any integer. In this case, the successive iterates in time n will be

$$x_n = ((n^2 + n)M + 1)\pi - \sin^{-1}\left(\frac{2M\pi}{K}\right), \quad p_n = (2M\pi)n. \quad (25)$$

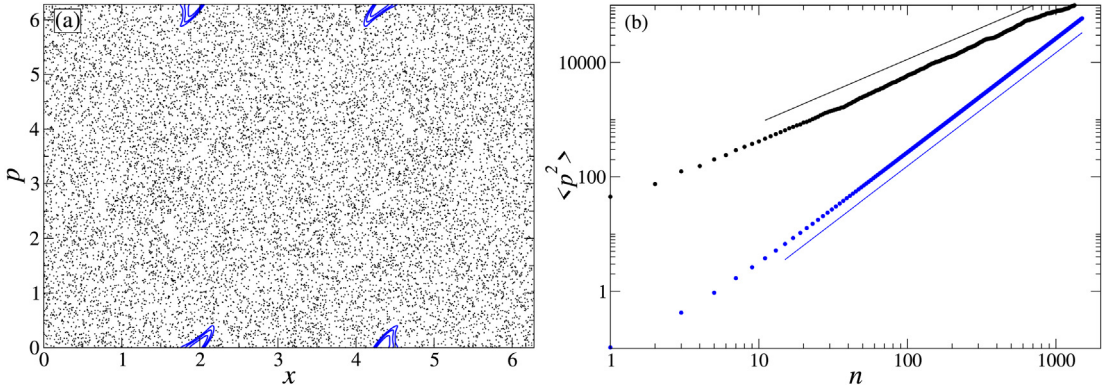


Fig. 6. (a) Stroboscopic map for standard map at $K = 6.8$. Accelerator modes are visible as small elliptic islands (shown in blue). (b) $\langle p^2 \rangle$ as a function of time n in log-log plot. The blue symbols had its initial conditions located in the accelerator modes shown in (a). The black symbols had initial conditions located in the chaotic sea shown in (a). The blue and black solid lines are best fit lines to the data with slopes 1.978 and 1.088 respectively.

By linearizing the standard map about (x_0, p_0) , the so-called tangent map T can be obtained as

$$T = \begin{pmatrix} 1 & K \cos x_0 \\ 1 & 1 + K \cos x_0 \end{pmatrix}. \quad (26)$$

If the eigenvalues of the tangent map T are of the form $e^{\pm i\alpha}$ (α is some real number), then it guarantees existence of elliptic stable region locally in phase space in the vicinity of (x_0, p_0) . This is satisfied if $|\text{Tr } T| \leq 2$. This condition restricts the possible values of kick strength K that will support accelerator modes. In this case, the range of K to realize accelerator modes turns out to be [89,130]

$$2\pi M \leq K \leq \sqrt{(2\pi M)^2 + 16}. \quad (27)$$

It can also be verified that the intervals of K are approximately $9/K$, though due to the bifurcations of accelerator modes the effective interval is $\approx 8/K$. Fig. 5 displays the effective diffusion coefficient defined as $D_{\text{eff}}(K) = \langle (p_n - p_0)^2 \rangle / n$ as a function of K . In certain windows of K , the accelerator modes induce strong deviations from diffusion coefficient obtained through quasi-linear approximation. For instance, using the initial conditions given above, if $M = 1$ is inserted in Eq. (27), the range of kick strength for accelerator mode turns out to be $6.28 \leq K \leq 7.45$. As is evident in Fig. 5 and in the inset, this is precisely the range of K over which D_{eff} deviates strongly from quasi-linear D_0 . An explicit numerical simulation of stroboscopic map for $K = 6.8$ shown in Fig. 6(a) reveals the presence of small elliptic regions (responsible for accelerator mode) in a pre-dominantly chaotic phase space. The elliptic fixed point is located precisely at the initial conditions given in Eq. (24) with $M = 1$. If an ensemble of trajectories are started from these initial conditions, then the temporal growth of $\langle p^2 \rangle$ is quadratic in time n (see Fig. 6(b)). This is an instance of ballistic growth in energy. On the other hand, if an ensemble of initial conditions is chosen from the chaotic sea, ballistic growth is replaced by almost linear growth of $\langle p^2 \rangle$ with n (black symbols and line in Fig. 6(b)). Even if an accelerator mode is present, time taken to converge towards $\gamma = 2$ is far longer than the time taken to converge to $\gamma = 1$ in the chaotic limit [133], depending on how close the initial conditions are to the accelerator mode and the sticky regions in its vicinity. Further, these modes induce long range temporal correlations of power-law form $C(\tau) = \langle u(t) u(t + \tau) \rangle = \tau^\alpha$, where $u(t)$ could be either x or p variable and α is the exponent. The momentum distributions also display interesting temporal scaling properties [134].

The anomalous diffusion in the presence of accelerator modes or elliptic islands (even if they are not accelerator modes) embedded in a sea of chaos is rather complex [133] and a comprehensive theory of these effects does not exist as yet, though major advances have been made by application of fractional kinetics to anomalous diffusion problems [135]. Physically, accelerator modes act as sticky regions in a largely chaotic phase space. A typical chaotic trajectory might get trapped in its vicinity for long times before escaping into the chaotic part. Such dynamics are examples of Levy flights [136], well studied in the context of anomalous diffusion [80,135,137]. The effects of anomalous diffusion are also visible in the quantum regime in the form of non-exponential wavefunction profiles and quantum accelerator modes [138–140]. Anomalous diffusion and accelerator modes are not special to kicked rotor and arise in a variety of mixed classical systems [80,141–144]. The diffusion effects in non-KAM systems can be even more richer with the formation of stochastic web structures in phase space as in the case of kicked rotor in a harmonic oscillator potential [80]. However, these will take us far outside the focus of this review. It must be remarked that the diffusion story in chaotic systems is far from over. How the diffusion effects play out in higher dimensional systems is yet to be systematically investigated [145]. Recently, it was shown that a combination of linear diffusion generated by a chaotic system and localizing dynamics of a non-chaotic system can, surprisingly, produce anomalous diffusion [146].

5. Quantum kicked rotor

The quantum kicked rotor model was first introduced in Ref. [147]. Starting from Eq. (6), the time-dependent Schrödinger equation for this model is

$$i\hbar \frac{\partial}{\partial t} \psi(x, t) = -\frac{\hbar^2}{2I} \frac{\partial^2}{\partial x^2} \psi(x, t) + V(x) \sum_n \delta(t - nT) \psi(x, t), \quad V(x) = k \cos x. \quad (28)$$

By transforming the time variable $t \rightarrow tT$ and dividing both sides by I , two quantum mechanical parameters can be identified, namely, the scaled Planck's constant $\hbar_s = \hbar T/I$ and kick strength, $\kappa = k/\hbar$, both of which in combination give a pure quantum parameter, similar to the classical one, $K = \kappa \hbar_s = kT/I$. As is often done, we will set $I = 1$, except when specified otherwise. This defines the commutator relation as $[\hat{p}, \hat{x}] = -i\hbar_s$. The classical limit can be approached by taking the limit $\hbar_s \rightarrow 0$ and $\kappa \rightarrow \infty$ such that K remains constant. Unlike its classical counterpart, the dynamics of quantized kicked rotor is governed by two parameters: κ and \hbar_s . The kicked rotor potential is periodic in time and its quantized version can be described by the Floquet theory [79,148]. Further, since the time-dependent potential in Eq. (7) appears as a δ -function, the period-1 Floquet operator takes a relatively simple form as a product of kick operator and a free evolution part, namely,

$$\hat{U} = \hat{U}_{\text{kick}} \hat{U}_{\text{free}} = \exp\left(-\frac{i}{\hbar_s} K \cos \hat{x}\right) \exp\left(-\frac{i}{2\hbar_s} \hat{p}^2\right). \quad (29)$$

This operator maps an arbitrary initial state at integer time n , $\psi(x, n)$, just after n th kick to $\psi(x, n+1) = \hat{U} \psi(x, n)$ just after the next kick. In scaled units, the time period between kicks is unity. It is convenient to write down the Floquet operator \hat{U} in the basis of angular momentum eigenstates

$$\langle x|m\rangle = \frac{1}{\sqrt{2\pi}} e^{imx}, \quad m = 0, \pm 1, \pm 2, \dots \dots \quad (30)$$

Then, the explicit form of Floquet operator will be

$$\hat{U}_{m_1, m_2} = \frac{1}{2\pi} \int_0^{2\pi} e^{-im_1 x} \exp\left(-\frac{i}{\hbar_s} K \cos \hat{x}\right) \exp\left(-\frac{i}{2\hbar_s} \hat{p}^2\right) e^{im_2 x} dx. \quad (31)$$

At this point, an identity involving the Bessel function $J_p(\cdot)$,

$$e^{iz \cos \theta} = \sum_{p=-\infty}^{\infty} (-i)^p J_p(z) e^{ip\theta}, \quad (32)$$

can be used to write down a compact expression for the matrix elements \hat{U}_{m_1, m_2} as

$$\hat{U}_{m_1, m_2} = \exp\left(-\frac{i}{2} \hbar_s m_2^2\right) i^{m_2 - m_1} J_{m_2 - m_1}\left(\frac{K}{\hbar_s}\right). \quad (33)$$

Note that \hat{U}_{m_1, m_2} is a diagonally dominant matrix since $J_{m_2 - m_1}(\cdot) \rightarrow 0$ for $|m_2 - m_1| \gg 1$. This property makes \hat{U} an effectively banded matrix. The eigenvectors of such a matrix can be expected to get significant contributions only from a narrow band of basis states, implying localized excitations. This is the first clue that localization in momentum basis might result in course of time evolution. This deviation from the classical dynamics was first observed in [147,149]. The localization effect can be verified by computing the quantum mean energy $\langle \hat{p}^2 \rangle$ as a function of time for irrational values of $\hbar_s/4\pi$. In this and the next section, we will assume $\hbar_s/4\pi$ to be an irrational number. Formally, $\langle \hat{p}^2 \rangle$ can be obtained by performing the integral

$$\left\langle \frac{\hat{p}^2}{2} \right\rangle_N = \frac{1}{2} \left\langle \psi(x, 0) \left| \hat{U}^{\dagger N} \hat{p}^2 \hat{U}^N \right| \psi(x, 0) \right\rangle, \quad (34)$$

where the initial state is generally taken to be $\psi(x, 0) = 1/\sqrt{2\pi}$. It was expected that in the semi-classical regime of $\hbar_s \ll 1$ such that $K \gg 1$, the quantum energy should display diffusive growth closely following the classical energy growth. But surprisingly, it was found that the quantum energy grows as anticipated only until a timescale t_b , to be called break time, after which it shows pronounced deviation from the classical mean energy growth (Eq. (19)) [147]. The computed mean energy is shown in Fig. 7(a) in both the quantum and classical regimes. Remarkably, the classical and quantum time evolutions display similar trend only for a short time beyond which the quantized kicked rotor localizes in momentum basis [147,149,150]. This is evident in the saturation of mean energy (blue curve) in Fig. 7(a) while its classical counterpart, shown as black curve in the same figure, continues to remain diffusive and maintains an approximately linear growth in time. While the classical momentum distributions evolve in time according to Eq. (23), the spread of quantum momentum distribution is strongly attenuated. This can be equivalently seen in the eigenstates of the Floquet operator \hat{U} . Let the eigenvalue equation for \hat{U} be

$$\hat{U} |\phi\rangle = e^{-i\beta} |\phi\rangle, \quad (35)$$

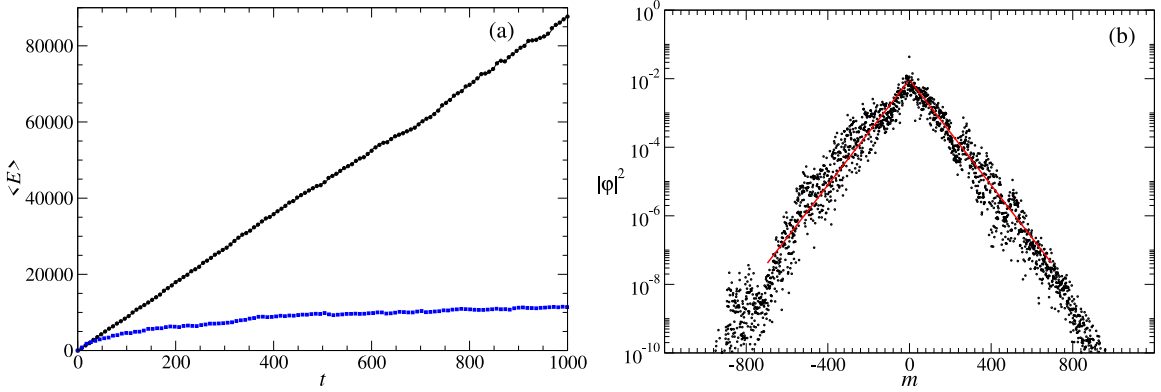


Fig. 7. (a) The temporal evolution of classical (black) and quantum (blue) mean energy for kicked rotor with $K = 12.0$ and $\hbar_s = 0.7$. Beyond break time, quantum effects strongly arrest the spread of wavefunction over the momentum basis, and quantum mean energy saturates. (b) Average $|\phi|_m^2$ is shown. Averaging over several eigenstates of \hat{U} is performed after shifting each eigenstate to a common center, $m = 0$ in this case. The solid (red) line is obtained through regression and the magnitude of slope is 0.0176 ± 0.0002 .

in which β represents the Floquet eigenphase or *quasi-energy*. All the eigenstates $\{|\phi\rangle\}$ are localized in the momentum basis, and even more striking is the fact that they display exponential profile representing a compact spread over this basis. This can be inferred from the linear decay profiles of $|\phi|^2$ in the semi-log plot shown in Fig. 7(b). The leading behavior, centered around some m_0 , is well described by a functional form given by

$$|\langle m | \phi \rangle|^2 = |\phi|_m^2 \sim e^{-2|m - m_0|/m_L}, \quad m = 0, \pm 1, \pm 2, \dots, \quad (36)$$

where m_L represents the localization length, a measure for the effective number of basis states over which a state localizes. In Fig. 7(b), several eigenstates are averaged over (after shifting them to a common center $m = 0$) and the averaged $|\phi|_m^2$ is displayed. The exponential decay profile is now clearly evident (solid red line shows the best-fit curve obtained by regression) and its slope is a measure of localization length m_L . The next few sections will be devoted to exploring this localization, taking place in the semiclassical regime and $K \gg 1$, in some detail.

5.1. Timescales in quantum chaos and kicked rotor

Before the focus shifts to other aspects of kicked rotor, a brief mention must be made about the two important timescales in quantum chaos. To analyze the timescales, we will work with scaled (dimensionless) Planck constant \hbar_s which will be the ratio \hbar/\mathcal{I} in which \mathcal{I} has dimensions of action. Further, in this section, it is assumed that the ratio $\hbar_s/4\pi$ is an irrational number to avoid the quantum resonance effects discussed in Section 5.3.

First of the characteristic timescales is the random or Ehrenfest timescale. According to the Ehrenfest theorem [151], quantum averages evolve close to the classical averages for sufficiently localized wavepackets. The Ehrenfest timescale t_E is the one for which quantum dynamics mimics the classical evolution. Equivalently, beyond $t > t_E$, the crucial assumption of a localized wavepacket breaks down due to wavepacket spreading and therefore Ehrenfest theorem does not hold good any more. In this limit $\hbar_s \rightarrow 0$, it is to be anticipated that the spreading of an initially compact wavepacket will reflect the spread of a bundle of underlying classical trajectories. Since the nature of spread of classical trajectories is different for integrable and chaotic systems, Ehrenfest time scale will be different as well. For the classical integrable systems, the evolution of small perturbations is at most polynomial in time. Based on this, an estimate of Ehrenfest time will be some power of \hbar_s^{-1} so that the order of magnitude result is $t_E \sim 1/\hbar_s$. For instance, in the case of free evolution of a coherent wavepacket it will be $t_E \sim 1/\sqrt{\hbar_s}$. This timescale is rather long since the effective Planck constant $\hbar_s \rightarrow 0$.

This timescale was first obtained for a chaotic system – a periodically kicked nonlinear oscillator – by Berman and Zaslavsky [152] who showed that quantum corrections to the classical averages grow exponentially with time. This work did not quite invoke the connections with Ehrenfest theorem. This connection was made in Ref. [149] and the timescale was named after the Austrian–Dutch physicist Paul Ehrenfest in Ref. [153], even though Ehrenfest did not discuss the timescales associated with chaotic dynamics in his original paper [151]. The Ehrenfest timescale for chaotic systems was also estimated for the first time in Ref. [149]. If largest Lyapunov exponent is $\lambda > 0$ for a classically chaotic system, then the Ehrenfest timescale can be estimated from the condition $\hbar_s \exp(\lambda t_E) \sim 1$. This leads to a much shorter timescale (than for integrable systems): $t_E \sim (1/\lambda) \ln(1/\hbar_s)$. For the kicked rotor, if we take the quantum parameters to be $T = \hbar_s$ and $K = \kappa$, and using Eq. (15) for its largest Lyapunov exponent, t_E can be explicitly estimated as [149]

$$t_E \sim \frac{|\ln T|}{\ln(K/2)}. \quad (37)$$

In the kicked rotor context, this timescale is significant because quantum chaos (as an analogue of classical chaos in terms of local instability etc.) persists only up to a finite timescale t_E . For $t < t_E$, quantum wavepacket evolution reflects the stochasticity of the underlying classical dynamics. Note that in the semiclassical limit as $\hbar_s \rightarrow 0$, t_E can become extremely long. Classical chaos is strictly defined in the limit of $t \rightarrow \infty$. Though t_E can be made arbitrarily long, infinite time limit is not reachable in quantum systems.

The second important timescale is the relaxation timescale or the break-time t_b related to the time taken for a typical wavepacket to resolve the discreteness of quantum spectrum. In the kicked rotor context, spectrum refers to the quasienergy values or eigenphases β of the time evolution operator (see Eq. (35)). Based on Heisenberg's uncertainty principle, it can be estimated to be $t_b \sim \rho_0$ [149], where the density of states $\rho_0 = \langle \Delta\beta \rangle^{-1}$ is for the set of states $\{|m\rangle\}$ that have overlap with the initial quantum state, and $\langle \Delta\beta \rangle$ is mean quasienergy level spacing. The quantum dynamics is effectively controlled by $\{|m\rangle\}$ and demarcates the timescale t_b . For $t \ll t_b$, the quantum evolution does not “feel” the discreteness of the spectrum, and it is possible for quantum diffusion to take place. For the kicked rotor, it is remarkable that break-time is simply proportional to the classical diffusion rate: $t_b \propto D_0$ (see Eq. (40)). For $t > t_b$, quantum effects begin to dominate leading to suppression of classical diffusion effects. In the semiclassical limit as $\hbar_s \rightarrow 0$, as would be anticipated, break-time diverges and classical effects continue to dominate the dynamics.

Now, assembling all this information, the relation between the two timescales is

$$t_E \ll t_b. \quad (38)$$

Both these timescales diverge as $\hbar_s \rightarrow 0$. For a detailed and engaging discussion on the ramifications of these timescales, see Refs. [154,155]. In summary, two relevant time-scales can be identified for the kicked rotor: (i) Ehrenfest timescale $t < t_E$ in which quantum–classical correspondence holds, quantum dynamics mimics the chaotic dynamics [149], and (ii) Relaxation timescale $t_E < t < t_b$ in which diffusion in momentum space and statistical relaxation occurs. In this regime, quantum diffusion (in some coarse sense) can still be observed. For $t > t_b$, quantum interference effects become stronger leading to a suppression of diffusion.

In the kicked rotor with $\hbar_s/4\pi$ set to an irrational number (the relevant parameter setting for the present discussions), quantum effects begin to dominate when discreteness in the spectrum cannot be ignored any more implying that until this happens the quantum evolution might be, qualitatively if not quantitatively, similar to the classical case. The case of rational \hbar_s leads to qualitatively different dynamics – namely to continuous quantum spectrum and yet strong quantum resonance effects discussed in Section 5.3. When breaktime is sufficiently large, $t_b \gg 1$, as shown in Fig. 7(a), the classical and quantum evolution of $\langle E \rangle$ approximately mimic each other for $t < t_b$, though they need not exactly follow one another. Strictly, though, the quantum and classical evolutions will follow one another only in the semiclassical limit.

This connection between the break-time and the mean level spacing for the kicked rotor can be made quantitative to estimate the localization length. Since the break time t_b is the timescale at which quantum evolution of mean energy departs from the classical evolution and settles down to quasi-periodic behavior, this could be represented in terms of localization length m_L as

$$\langle \Delta\hat{p}^2 \rangle \sim m_L^2 \hbar_s^2 \sim D_0 t_b, \quad (39)$$

where D_0 is the quasi-linear diffusion coefficient. This essentially states that in the timescale of t_b , the quantum evolution has significant excitations only over m_L momentum basis states. The last two terms in Eq. (39) effectively connect the classical evolution with the quantum. The localization length m_L can also be independently estimated as follows; if $\rho_0(\beta)$ is the mean level density over the relevant spectral range in which evolution takes place, then the break-time is also equal to $1/\rho_0(\beta)$. Since the Floquet phases β defined in Eq. (35) are uniformly distributed over $[0, 2\pi]$, we get for the mean level density $\rho_0(\beta) = m_L$. Using this, break time turns out to be $t_b \sim m_L$. This can be used to obtain important order-of-magnitude estimates. By eliminating m_L in Eq. (39), the estimated break time is

$$t_b \approx \alpha \frac{D_0}{\hbar_s^2} = \frac{K^2}{4\hbar_s^2}, \quad (40)$$

where α was determined from numerical results to be $1/2$ [156]. Thus, the quantum–classical break time is proportional to D_0 that describes classical diffusion and inversely related to \hbar_s^2 . For the parameters used in Fig. 7(a), Eq. (40) predicts $t_b \sim 73$ and this approximately corresponds with the trend seen in this figure. It must be remarked that the \hbar -scaling of break time in Eq. (40) appears to hold even if the classical dynamics shows anomalous diffusion [157] arising due to the presence of regular regions in a largely chaotic phase space. It might be remarked that in the semiclassical limit, as $\hbar_s \rightarrow 0$, the break time diverges signifying that the quantum evolution would follow the classical for extremely long times.

Even more remarkable result can be obtained if the relation $t_b \sim m_L$ is used to eliminate t_b from Eq. (39). This leads to an important order-of-magnitude result [149,153]:

$$\hbar_s^2 m_L \sim D_0. \quad (41)$$

Localization length is inherently quantum mechanical in origin, and yet it is determined by the diffusion rate D_0 that originates in the classical dynamics. This is an example in which quantum behavior is determined by a classical measure.

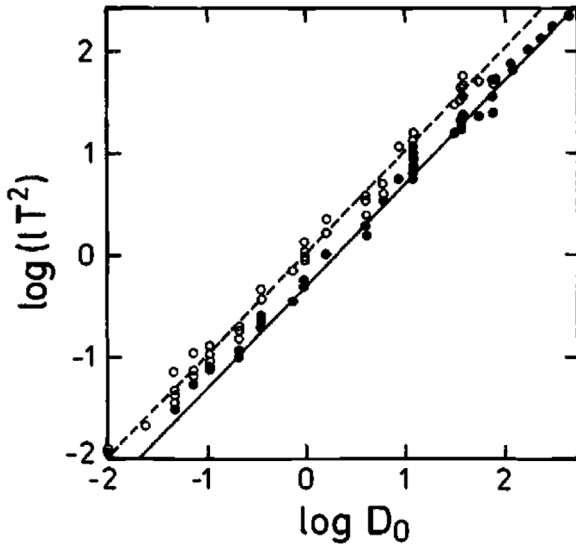


Fig. 8. Localization length (scaled by T^2) plotted as a function of diffusion rate D_0 . The circles are obtained from kicked rotor simulations with localization length estimated by two different approaches. The two quantities display a linear relation as predicted by Eq. (41). The simulation data suggests $\hbar_s^2 m_L = D_0/2$ rather than $\hbar_s^2 m_L = D_0$. See Ref. [156] for more details.

Source: Taken from Ref. [156].

Shepelyanski [156] explicitly verified this result through extensive numerical simulations of the kicked rotor. Fig. 8 reveals a good linear relation between $\hbar_s^2 m_L$ (if $\hbar = 1$, then $\hbar_s = T$) and D_0 . In particular, note that $T^2 m_L \sim \alpha D_0/2$, the factor $\alpha = 1/2$ is inferred from numerical simulations [156]. Interestingly, for the Lloyd model [158], a model for electronic mobility in a nearest-neighbor coupled lattice with Lorentzian distributed on-site energies, the value of α can be exactly calculated and it turns out to be $1/2$ [156]. For the eigenstates shown in Fig. 7(b), we get $m_L \sim 56.8$, while this order-of-magnitude estimate in Eq. (41) gives ~ 73.4 . The estimate in Eq. (41) holds good provided the number of basis states occupied by the initial state is smaller than m_L . The work done in the last two decades has shown that quantum entanglement is strongly correlated with classical phase space structures (see Section 10.2), but Eq. (41) is an early indication of such surprising quantum-classical connections and one for which an order-of-magnitude relation between the two could be explicitly shown.

5.2. Connection with Anderson localization

The emergence of localized states and their exponential decay profile points to a strong resemblance with another phenomena in condensed matter physics – localization of electronic states in a disordered crystalline lattice. This is the case of the celebrated Anderson localization [159]. In the absence of disorder, this situation results in Bloch states in allowed bands and none in the forbidden bands. Grempel, Fishman and Prange [160] were the first to establish that the localization in kicked rotor is similar to that in the Anderson model. In this section, we assume that $\hbar_s/4\pi$ is an irrational number. If it were rational, it leads to a fundamentally different quantum dynamics discussed in Section 5.3.

Starting from the Floquet operator for the kicked rotor in Eq. (29), the corresponding eigenvalue equation can be explicitly written down in two different ways as

$$e^{-iV(x)} e^{-iH_0(p)} \phi^+ = e^{-i\beta} \phi^+, \quad \text{and} \quad e^{-iH_0(p)} e^{-iV(x)} \phi^- = e^{-i\beta} \phi^-, \quad (42)$$

in which $H_0(p)$ is the kinetic energy operator and ϕ^\pm represents the Floquet states with eigenphase β . The central piece of the trick is to perform a transformation by defining a Hermitian operator

$$W(x) = -\tan\left(\frac{V(x)}{2}\right) \quad (43)$$

and writing the unitary kick operator in terms of $W(x)$ as

$$e^{-iV(x)} = \frac{1 + iW(x)}{1 - iW(x)}. \quad (44)$$

The two eigenvectors, associated with the same eigenphase β in Eq. (42), in position representation are related through

$$\phi^-(x) = e^{iV(x)} \phi^+(x) = e^{i(\beta-H_0)} \phi^+(x), \quad (45)$$

the last form obtained by using Eq. (42). Now, the eigenvector ϕ is written as a linear combination

$$|\phi\rangle = \frac{1}{2}[|\phi^+\rangle + |\phi^-\rangle]. \quad (46)$$

If this expression is taken in position representation and by using Eq. (45), after simple manipulations, equation for $\phi(x)$ becomes

$$(1 - iW(x))\phi(x) = e^{i(\beta-H_0)}(1 + iW(x))\phi(x). \quad (47)$$

Upon expressing this in the momentum representation, we get

$$T_m\phi_m + \sum_{r(\neq 0)} W_r \phi_{m+r} = E \phi_m, \quad (48)$$

where W_r is the Fourier representation of $W(x)$, E is the mean of Fourier expansion of $W(x)$ and further we have designated

$$T_m = i \frac{1 - e^{i(\beta - \hbar m^2/2)}}{1 - e^{i(\beta + \hbar m^2/2)}} = \tan\left(\frac{\beta - \hbar m^2/2}{2}\right), \quad \text{and} \quad E = -W_0. \quad (49)$$

The structure of Eq. (48) is reminiscent of the Anderson model [159] for electronic transport in a disordered lattice, given by

$$\tilde{T}_m u_m + \tilde{W}(u_{m+1} + u_{m-1}) = \varepsilon u_m. \quad (50)$$

In this, \tilde{T}_m is the random on-site potential and \tilde{W} is the hopping amplitude of the particle, and ε is the energy of the particle. In the mapped model in Eq. (48), T_m plays the role of on-site potential \tilde{T}_m , and W_r is equivalent to the hopping amplitude \tilde{W} . Though, the quantum kicked rotor in the momentum basis (48) has some similarity with the one-dimensional Anderson model in the position basis (50), this analogy does not quite constitute a proof of localization of eigenstates for the kicked rotor model. This statement must be explained further with some caveats, and we discuss this below.

There are some significant differences between the two models. The on-site potential in the Anderson model (50) is random. However, the on-site potential T_m in Eq. (48) is only pseudo-random, though numerical evidence has shown that pseudo-randomness also results in localization [161,162] provided the hopping is short-ranged. The mapped model in Eq. (48) implies long range coupling, though localization in Anderson model has been rigorously shown only for short-range hopping [163–166]. Further, an infinite number of quantum resonances (to be discussed in Section 5.3) exist in the kicked rotor and they lead to *non-localized* wavefunctions. This aspect could not yet be confirmed in the 1D Anderson model. The mapping points to the analogy between the eigenstates in both the problems, and does not apply to the time evolution of arbitrary initial states. For instance, the initial diffusive phase observed in kicked rotor is absent in the standard 1D Anderson problem of Eq. (50) with nearest neighbor coupling. However, this phase is present in the mapped model of Eq. (48) which couples r nearest neighboring “sites”. In spite of similarities between Eqs. (48) and (50), the reduction of the kicked rotor problem to Eq. (48) does not strictly constitute a proof that the kicked rotor system displays localized states. The presence of quantum resonance effects (see Section 5.3) does not make it easier to prove localization. In spite of these gray areas [167], it must also be noted that the hopping amplitude W_r , the Fourier transform of $W(x)$, is indeed short ranged and decays exponentially with r . As shown previously, it is sufficient that hopping amplitude decays faster than $1/|m - r|$ to sustain exponential localization [168]. A significant outcome of this mapping exercise is that random on-site potential is only a necessary and not a sufficient condition for localization in the Anderson model. In the case of $V(x) = K \cos x$, the matrix elements of \hat{U} decay faster than exponential beyond a band of width b about the diagonal, making it effectively a banded matrix. Within the band, the elements are pseudo-random provided the classical dynamics is chaotic, *i.e.*, $K \gg 1$. This band property has led to explorations of the localization in banded random matrices [168,169], discussed in some detail in Section 5.5. In general, localization is displayed by kicked rotor for any size of the band if $\hbar_s/4\pi$ is set to be an irrational number. However, delocalization can be expected if the matrix elements decay slowly (say, as a power law) outside the band [168]. Thus, the two crucial ingredients – pseudo random disorder and sufficiently fast decay of hopping amplitudes (as discussed above) – ensure that quantum kicked rotor for $K \gg 1$ displays localization. This is often called *dynamical localization* to indicate its dynamical origins, *i.e.*, localization emerges as a function of time rather than system parameter. Even so, dynamical localization is related to the localization of eigenstates in the kicked rotor, and can also be thought of as originating due to Anderson-type localization.

Quantum localization in kicked rotor and Anderson model is a delicate quantum coherence effect arising from destructive quantum interferences of wavefunctions. Much of the variants of kicked rotor and its applications are, in some sense, based on exploiting the quantum coherences built up by the localized states. Strictly, localization has no classical analogue though classical dynamics of certain piecewise linear kicking potentials mimic features of dynamical localization [170]. However, localization as a phenomenon of “absence of diffusion”, as Anderson called in his landmark paper [159], can occasionally be observed in integrable and near-integrable systems. In all these cases, localization arises due to the influence of classical phase space structures and is not a quantum phenomenon.

Notwithstanding the analogy with Anderson model, as yet, there is no known rigorous analytical proof for localization in kicked rotor or for the exponential profile of its eigenstates. This continues to remain an outstanding problem. However, if the hopping is assumed to be only among nearest neighbor lattice sites and the on-site potential is drawn from an uncorrelated random sequence having a Lorentzian distribution

$$\mathcal{P}(T_m) = \frac{1}{\pi(1+T_m^2)}, \quad (51)$$

then the localization length, averaged over an appropriate ensemble, can be shown to depend only on the energy E and the strength of hopping to nearest neighbor sites [171–173]. This exactly solvable model is referred to as the Lloyd's model [158]. It is one rare instance for which exponential localization has been rigorously established.

Kicked dynamical systems come in various hues and display a variety of properties ranging from localization to diffusion. Another prominent example is the Fermi accelerator model, a simple model of classical chaos and displays quantum localization [174]. In Section 7, we will explore more of this variety. For now, it is sufficient to remark that not all kicked systems display localization. For instance, another popular quantum chaotic model, namely, the kicked top [148,175] does not show localization effects. However, a particular limiting case of kicked top becomes the kicked rotor model itself and this displays localization [176].

5.3. Quantum resonances

In strong contrast to localization discussed in the last section, another special type of dynamical evolution in the quantum kicked rotor happens when the conditions for quantum resonance are met. This was first reported in Ref. [147]. See also Refs. [177,178] for a detailed theoretical analysis. Considering the period-1 Floquet operator in Eq. (29), the choice $\hbar_s = 4\pi$ corresponds to primary quantum resonance, in which case the unitary operator for the free evolution part \hat{U}_{free} becomes unity. Then, any initial state in the position representation $\psi(x, 0)$ will acquire a phase imparted by the kick operator \hat{U}_{kick} (see Eq. (29)) at every time step. Physically, this ensures that all the kicks add up in a coherent manner for quantum resonance to take place. This also implies that the eigenvalue of the Floquet operator \hat{U} is $e^{iK \cos x}$ and the quasi-energy spectrum $\beta = K \cos x$ is continuous (see Ref. [179] for more discussions). This can be seen as a consequence of translational invariance of \hat{U} in momentum representation. Specializing to the case of kicked rotor periodic in position, the momentum is quantized as integer multiple of Planck constant. In this case, the general case of primary quantum resonance condition reads as

$$\hbar_s = 4\pi l, \quad l = 1, 2, \dots \quad (52)$$

In the analogue of tight-binding model, this condition corresponds to a free propagation of Bloch waves in a periodic lattice. The condition in Eq. (52) can be physically understood as arising from the following argument. The energy of the unperturbed rotor is $E_m = m^2\hbar^2/2$, where m is the quantum number. Thus, transitions between any two unperturbed levels can take place if energy $\Delta E_m = E_{m+1} - E_m = l'\hbar^2/2$ ($l' = 2m + 1$ is an integer) is supplied from an external source. External kicking field supplies photon energy $2\pi\hbar/T$, where T is the period of kick. If the energy supplied by l photons matches ΔE_m , then the quantum resonance condition

$$\hbar_s = \hbar T = 4\pi \frac{l}{l'} \quad (53)$$

is satisfied assuming that no common integer factor exists between l and l' . This is the general condition for quantum resonance, of which Eq. (52) is a special case for primary resonance if $l' = 1$. Higher order quantum resonances occur if $l' \geq 2$. When Eq. (53) holds good, it leads to remarkable implications. It can be rigorously shown [177,178] that the Floquet operator \hat{U} in Eq. (29), written in position representation, becomes a finite size matrix $\hat{\mathcal{U}}$ of order l' . This effectively implies that, in x space, only l' discrete points, equally spaced in $(0, 2\pi)$ and depending on initial position $0 < x_0 < 2\pi$, are involved in the time evolution at resonance (for odd l'). Then, the eigenfunctions of the Floquet operator (in position representation) are the eigenvectors of finite matrix $\hat{\mathcal{U}}$. If taken in momentum representation, it is interesting to note that the eigenfunctions are Bloch states with a periodicity of l' . Then, the quasienergy spectrum has l' bands depending on continuous values of $0 \leq x_0 < 2\pi/l'$ and can be thought of as a periodic crystal with l' atoms. This continuous spectrum leads to unbounded increase in energy with time and has been exactly obtained only for a few low-order resonances [177,178]. See Ref. [177,178] for a treatment of even l' case and also for detailed calculations that lead to these results. In contrast, for irrational values of $\hbar_s/4\pi$, the Floquet matrix is of infinite order and results in dynamical localization.

Eq. (52) also points out the explicit T dependence that was implicit in Eq. (52). In practice, quantum resonance condition can be satisfied either by tuning the Planck constant or by tuning kick period T . Typically, experiments on quantum resonances are performed by tuning the kick period. Since any irrational number can be approximated to arbitrary precision by a rational number, it might appear that, in practice, satisfying and realizing resonance condition can be hard (say, on a computer due to its finite precision representation of numbers). However, it is known that even for $l' \gg 1$

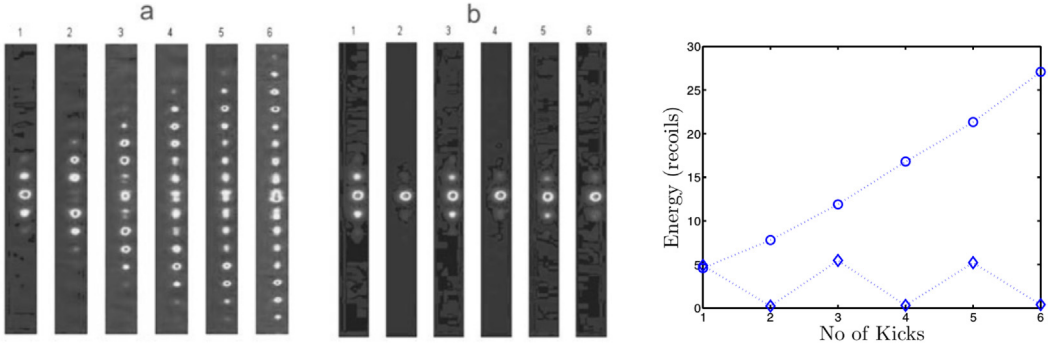


Fig. 9. Absorption images as a function of kick number obtained from atom-optics experiment using Bose-Einstein condensate with parameters set for (a) quantum resonance and (b) anti-resonance conditions. Also shown in right extreme is the mean energy as a function of number of kicks. Notice that the mean energy grows (open circles) for resonance and oscillates for (open diamonds) anti-resonance.
Source: Taken from Ref. [181].

resonant dynamics ultimately sets in after a long time spent in executing non-resonant dynamics [177,178,180]. For the primary or the first order quantum resonance ($\hbar_s = 4\pi l$), an initial state $\psi(x, 0)$ evolves as

$$\psi(x, n) = \exp\left(-\frac{i}{\hbar_s} Kn \cos \hat{x}\right) \psi(x, 0). \quad (54)$$

In this case, quantum resonance is simply a case of quantum revivals – wavefunction rebuilds at revival periods with phase imprinted on it – when unperturbed and driving frequencies match. If the initial state is taken to be $\psi(x, 0) = \exp(-im_0x)/\sqrt{2\pi}$, then the mean energy grows quadratically in time as $K^2 n^2/4 + m_0^2/2$. For any other arbitrary choice of initial states, energy growth is still quadratic as $n \rightarrow \infty$, though in addition a term linear in time would also appear. A quadratic growth in energy is also observed in the *classical* accelerator modes only for certain values of kick strengths K (Eq. (25)). As a purely quantum phenomenon, quantum resonance is unrelated to this classical feature, and occurs for any arbitrary value of K provided Eq. (52) is satisfied. Quantum resonance clearly disregards the classical dynamical features. Higher order quantum resonances can occur if $l' \geq 2$, and these are similar to fractional revivals. The initial wavefunction rebuilds itself in several diminished copies of itself. For detailed theoretical treatment of higher order resonances, see Refs. [177,178]. Higher order resonances also have continuous quasienergy bands, though the width of the bands decays exponentially for most part as $l \rightarrow \infty$ and $l' \rightarrow \infty$ such that \hbar_s is approximately held constant [124,177,178]. In this limit, the quasienergy spectrum would tend to become discrete as in a non-resonant case. Hence, the higher order resonances are notoriously difficult to observe in experiments.

On the other hand, if $\hbar_s = (2l + 1)2\pi$, then an unusual dynamical behavior called quantum anti-resonance can be observed. In this case, if m_0 is an odd integer, then the time-evolving wavefunction $\psi(x, t)$ acquires a phase which is canceled at a subsequent step. The initial wavefunction is re-created at intervals of one time step. The effect of a kick is negated exactly by the next kick. Under this condition, the mean energy oscillates instead of displaying any growth in time. Fig. 9(c) shows the two contrasting dynamical evolution – quadratic mean energy growth at resonance and oscillatory mean energy at anti-resonance. Fig. 9(a,b) displays experimental evidence from an atom-optics set-up using Bose-Einstein condensates. The typical behavior of the condensate kicked by optical lattices is shown as absorption images. The quadratic mean energy growth for resonance, and oscillations in case of anti-resonance are clearly observed in the experiment. However, if the initial state is taken to be a thermal state of Gaussian form instead of a zero momentum state, then at resonance and anti-resonance the growth of energy is linear and the growth rate is nearly same as the classical diffusion rate [182]. In the light of Eq. (53), we might state that dynamical localization occurs if \hbar_s is an irrational multiple of 4π . Physically, it is indeed intuitive to note that dynamical localization occurs if the kick period and Talbot time are incommensurate with one another.

The quantum resonance effect can be thought of as the matter-wave analogue of optical Talbot effect [183], in which diffracted image due to a plane wave incident on a grating is recreated at a characteristic length scale called Talbot length. In a similar spirit, quantum resonances are its temporal analogue and the relevant characteristic timescale is the Talbot time. In time domain, quantum resonance manifests in the form of local maxima in the energy absorbed at the resonant values of (scaled) kick period T (see Fig. 10). This is observed, for instance, in experiments of cold Cesium atomic cloud evolving under the effects of a flashing standing wave [184], and locally maximal energy absorption by the atomic cloud marks the resonance regime. Some higher order resonances have also been observed in atom-optics experiments [185–187]. The resonances discussed here through Eq. (52) can be generalized to kicked particle (without periodic boundary conditions in x). These extensions had been extensively studied in theory [188,189], and have also been observed in atom-optics experiments [185–187]. For some of the applications of the quantum dynamics at resonance, the reader is referred to Refs. [190,191].

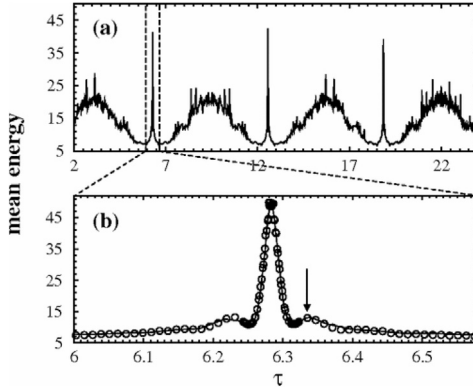


Fig. 10. (a) Mean energy at 30th kick for an ensemble of Gaussian distributed atomic cloud, shown as a function of effective Planck constant. Peaks in the mean energy correspond to quantum resonances. (b) Shows enlarged portion of a quantum resonance peak (solid line) along with data from ϵ -classical map (circles).

Source: Taken from Ref. [192].

Though quantum resonance has no analogue in the classical kicked rotor dynamics in the usual semiclassical sense, yet the experiments [184,193] and theoretical developments [188,194] during the early 2000s led to identification of its unusual classical underpinnings. If we consider the kicked rotor defined on a cylinder, due to its spatial periodicity, it can be transformed into a rotor problem for a fixed value of fractional part of momentum, also known as quasi-momentum β . This latter model, to be referred as β -kicked rotor model, shows resonances for $\hbar_s = 4\pi l$ ($l > 0$ is an integer) but only for finite number of special values of β . If tuned away from resonances, dynamical localization is realized. Now, if the β -kicked rotor is analyzed in the vicinity of a resonance by setting $\hbar_s = 2\pi l + \epsilon$, such that $\epsilon \ll 2\pi$, then (after some simplification) the Floquet operator can be written as

$$\hat{U}_\beta = e^{-i\tilde{k}\cos\tilde{\theta}/|\epsilon|} e^{-i\tilde{\mathcal{H}}_\beta/|\epsilon|}, \quad (55)$$

where \tilde{k} is the scaled kick strength and $\tilde{\mathcal{H}}_\beta$ depends only on the angular momentum operator [194]. Eq. (55) is quite suggestive in that $|\epsilon|$ might be regarded as Planck's constant, and its corresponding "classical" map can be written down. The term "classical" does not denote $\hbar_s \rightarrow 0$ limit, but rather $|\epsilon| \rightarrow 0$ limit. Ref. [194] calls it ϵ -classical since it does not require Planck's constant to be small. The ϵ -classical map corresponding to Eq. (55) remarkably reproduces the structure of resonances obtained from full quantum calculations, as seen in Fig. 10(b). Significantly, quantum resonances are associated with the integrable nature of ϵ -classical map, while the resonances of β -kicked rotor model have correspondence with classical resonances of the near-integrable ϵ -classical map. This theoretical framework [194] was used to explain the experimental results for kicked rotor under the influence of gravity displaying quantum accelerator modes [184,193], and also derive a scaling in the widths of the resonance peaks in the kicked rotor model [188,192]. These results lead one to ask a general question – can purely classical dynamics mimic quantum phenomena? By incorporating the idea that only finite number of phase points map into each other by the unitary operator of kicked rotor at quantum resonance, a *classical* map was written down that displayed quantum localization beyond break-time or quantum resonance effects [195] depending on the parameters chosen. See also Ref. [149] for a classical map that shows localization effects. Another classical map displaying "quantum" behaviors was obtained in 2014. A class of classical maps with piecewise linear potentials display quasi-localization or quantum resonance type behavior depending on whether a constant (related to momentum) is rational or irrational multiple of 2π [170].

Finally, it might be remarked that quantum resonances have as yet unexploited applications in quantum walk analogues [196–198], resonance ratchets and atomic interferometers, among other things. Some of these are discussed in detail in Sections 11.2 and 11.3.

5.4. Localization and spectral statistics

Fig. 7(b) shows the signature of localization in the eigenstates of the Floquet operator. How does dynamical localization appear from the perspective of eigenvalues of Floquet matrix? A more general form of this question pertains to the statistical properties of the eigenvalues of quantum operators subject to broad symmetry constraints. The non-trivial answer to this forms the subject matter of spectral statistics and random matrix theory. It is impossible to do justice in a short introduction to this remarkable area of mathematics extensively applied in many areas of physics. The application of random matrix theory in many-body problems of nuclear physics began in the 1950s [199] with the Wigner surmise that the local fluctuations in a pure sequence of nuclear level spectra has statistical properties similar to that of an appropriately chosen random matrix ensemble [200,201]. For three decades following that, random matrix theory was put

on a firm mathematical footing and was extensively applied to many-body quantum physics, especially nuclear physics, problems [202].

Consider a pure sequence of spectra $\lambda_i, i = 1, 2, \dots, N$ for a Hermitian operator. Then, the scaled spacings are defined to be

$$s_i = \frac{\lambda_{i+1} - \lambda_i}{\langle s \rangle_{\text{loc}}}, \quad (56)$$

where $\langle s \rangle_{\text{loc}}$ represents the local mean spacing averaged over a suitable spectral scale. The process of determining $\langle s \rangle_{\text{loc}}$ is equivalent to unfolding the spectrum [148] which locally rescales the levels and effectively removes system-specific features from the spectrum. If the density of states $\rho(E)$ at any energy E can be expressed as a sum of an average part and an oscillatory part, $\rho(E) = \rho_{\text{avg}}(E) + \rho_{\text{osc}}(E)$, then the unfolded spectrum retains only the oscillatory part that contributes to level fluctuations. For a quantum system with sufficiently complex interactions (e.g., nuclear or atomic levels with high atomic number), level fluctuations defined in terms of the spacings between consecutive levels follows the celebrated Wigner distribution given by

$$P(s) = A_\beta s^\beta e^{-B_\beta s^2}, \quad (57)$$

in which $\beta = 1, 2, 4$ are indicative of the symmetry class in which the quantum system under consideration falls. The constants A_β and B_β are determined from the normalization requirement that $\int_0^\infty P(s) ds = 1$ and $\langle s \rangle = 1$. The values of β correspond to the three standard Gaussian ensembles (introduced by Dyson [203]): orthogonal ensemble ($\beta = 1$) of RMT corresponds to systems with time-reversal symmetry but without spin- $\frac{1}{2}$ interactions, unitary ensemble ($\beta = 2$) for systems without time-reversal symmetry and symplectic ensemble ($\beta = 4$) for systems with time-reversal symmetry and spin- $\frac{1}{2}$ interactions [201,203–206]. See Ref. [207] for new symmetry classes beyond these three. In practice, β also indicates the degree of repulsion between consecutive levels for small spacings, $s \rightarrow 0$. Thus, random matrix spectra and those from complex quantum systems exhibit “level repulsion” as their main characteristic and hence the levels are correlated. For the orthogonal ensemble ($\beta = 1$), $A_\beta = \pi/2$ and $B_\beta = \pi/4$.

As far as quantum chaos is concerned, numerically computed spectral statistics for the chaotic billiards was first reported in 1980 [208], and next year Sinai billiards spectra was analyzed as well [209]. Strong classical chaos properties have been proved for both these billiard models [39,40,210]. The former work [208] displayed a spacing distribution, though with poor statistics, that did reveal a quantitative correspondence with RMT distribution. The latter work [209] did discuss the relevance of random matrix theory but suffered from insufficient levels for reliable statistical analysis. Yet, these early results hinted at possible connections between spectral statistics of classically chaotic systems and random matrix theory. Based on thorough numerical evidence from Sinai billiard model, it was the Bohigas–Giannoni–Schmidt (BGS) conjecture in 1984 [211] that made this connection formal and led to forays of random matrix theory into one- and few body problems in quantum chaos, and later in condensed matter physics. According to this conjecture, “Spectra of time reversal-invariant systems whose classical analogues are K systems show the same fluctuation properties as predicted by Gaussian Orthogonal Ensemble (GOE)” of random matrix theory. The term K -systems indicate dynamical systems with positive Kolmogorov–Sinai (KS) entropy [212–214] or, equivalently, systems which display average exponential divergence of nearby trajectories [17]. Thus, even one- or few-body systems can display random matrix type spectral fluctuations provided the classical limit of the system is chaotic. This has been amply demonstrated in a large number of chaotic systems [204], and even though a rigorous and complete proof of the BGS conjecture is still awaited, partial attempts already provide us a deeper insight into dynamics and RMT connections [215–218]. The rapid developments in the theory and applications of random matrices since the 1980s have been summarized in several review articles and monographs [204,205,219,220].

In practice, when RMT is applied to a physical system, the analysis of spectral fluctuations must be carried out in the semiclassical regime. This implies that spectra must be drawn from a regime of large excitations in energy. It is also in this regime that justifications of BGS conjecture have been worked out based on periodic orbit theory of Gutzwiller [35], which shows that spectral fluctuations arise from closed orbits in the classical system. It is worth mentioning that semiclassical limit implies that the ratio $\hbar_s = \hbar/\mathcal{I} \rightarrow 0$, where \mathcal{I} is some typical quantity with dimensions of classical action. Often, for convenience, this correct limiting procedure is replaced with the shorthand form $\hbar \rightarrow 0$. The actual value of effective \hbar_s suggests a natural timescale through mean level spacing. By itself, the limit of $\hbar_s \rightarrow 0$ alone is non-trivial [221]. In general, the two limits $\hbar_s \rightarrow 0$ and timescale $t \rightarrow \infty$ do not commute and this constitutes one of the central problems of quantum chaos. Care must be taken while applying these limits since $t \rightarrow \infty$ followed by $\hbar_s \rightarrow 0$ preserves the quantum–classical correspondence, but taking the limit in the reverse order breaks this correspondence [222]. With this background information, we now look at the kicked rotor system in the semiclassical limit.

While dealing with time-dependent systems with Hamiltonian $\hat{H}(t)$, the object of interest is the unitary time evolution operator of the form $e^{i\hat{H}t}$ and the corresponding eigenvalues $e^{i\theta}$, where θ are the eigenphases. Application of random matrix theory in this scenario requires a different ensemble introduced by Dyson, the circular orthogonal ($\beta = 1$), unitary ($\beta = 2$) and symplectic ($\beta = 4$) ensembles [223,224]. The Wigner distribution in Eq. (57) also describes the fluctuation properties of eigenphases from the circular ensembles as well.

For the kicked rotor spectra, the eigenphases $\beta_i, i = 1, 2, \dots, N$ associated with Floquet operator \hat{U} (see Eq. (35)) can be analyzed. In this, N is the number of angular momentum basis states used to construct the Floquet matrix. The

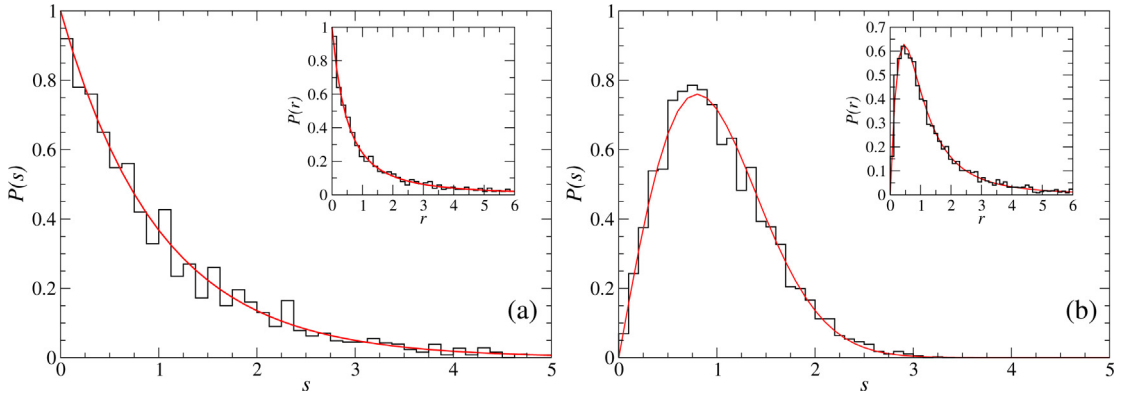


Fig. 11. Spacing distribution (histogram) for the eigenphases of kicked rotor obtained through simulations. (a) the quantum kicked rotor defined on cylinder with $K = 12.0$, $h_s = 0.7$ and $A \approx 0.027$. Solid red line is the Poisson distribution. (Inset) shows the spacing ratio distribution $P(r)$ for the same data. The solid red line is the theoretical result $P_P(r) = (1 + r^2)^{-1}$. (b) the quantum kicked rotor defined on a torus with $K = 20000.0$ and $N = 99$. Solid red line is the Wigner distribution in Eq. (57) with $\beta = 1$. (Inset) shows $P(r)$ for the same data along with the theoretical result (solid red line) given in Eq. (62) with $\beta = 1$.

scaled nearest neighbor level spacing is $s_i = (\beta_{i+1} - \beta_i)/\langle s \rangle_{\text{loc}}$. Since the eigenphases β are ergodic on the unit circle, the level density is uniform over the entire spectral range and consequently $\langle s \rangle_{\text{loc}}$ is a constant over the entire spectrum. This simplifies an otherwise elaborate and even ambiguous unfolding procedure that will be required at this point. The kicked rotor under consideration is defined on a cylinder, bounded in position and unbounded in momentum direction. For large kick strength, this kicked rotor displays chaotic dynamics. A naive expectation based on BGS conjecture would be that the spacing distribution would coincide with the Wigner distribution in Eq. (57). However, the emergence of dynamical localization on timescales longer than the localization length effectively arrests the effects of classical chaos and precludes such a possibility. As discussed in the previous section, eigenphases are in fact pseudo-random and uncorrelated. Exponential localization would also imply negligible overlap between the eigenstates in the momentum representation. These qualitative arguments can be distilled into a quantitative criteria by considering the ratio of localization length m_L in an infinite sample size system to the total number of momentum basis states N used in solving the eigenvalue problem: $\Lambda = m_L/N$ [225]. In terms of Λ , one can expect uncorrelated spacings if the centers (or, the peaks) of eigenstates are well separated in momentum space. This would be the case if $\kappa \gg 1$ and

$$\Lambda = \frac{m_L}{N} \ll 1. \quad (58)$$

Under these conditions, the spacings are well described by Poisson distribution of the form

$$P(s) = e^{-s}. \quad (59)$$

As seen in Fig. 11(a), a reasonably good agreement with this $P(s)$ is observed in the case of a kicked rotor with $K = 12$ and $h_s = 0.7$. The spectra is numerically computed by truncating the basis at $N = 2048$ unperturbed states, and the localization length was numerically estimated to be ≈ 56 . In this case, $\Lambda = 56/2048 \approx 0.027$ and $\kappa = 17.14$. As shown by Berry and Tabor [226], this is precisely the distribution expected for quantum systems that are integrable in the classical limit. Though the classical rotor is chaotic for large kick strengths, quantum dynamics is governed by quantum interference effects for timescales beyond break-time t_b and this manifests in the spectral fluctuations as well, in what appears, at first sight, to be a violation of BGS conjecture [227]. It must be emphasized that Poisson statistics can be expected strictly in the limit of infinite system size $N \rightarrow \infty$. For Anderson model of infinite sample size, it was rigorously shown that Poisson spacings must be expected [228], but such a result for the kicked rotor still remains an open problem. In general, if the eigenfunctions of Floquet operators are sufficiently well separated in momentum basis, then the spacing distribution is seen to approach the Poisson limit [161,227].

To explore the $\Lambda \gg 1$ limit, we need the kicked rotor to reside in finite dimensional Hilbert space. This is achieved by enforcing periodic boundary conditions in both position and momentum variables. The corresponding classical kicked rotor with bounded phase space restricts the unbounded diffusion for strong kick strengths. If $\Lambda \gg 1$, then localization length is so large as to occupy all the basis states. The parameter Λ can be estimated using the diffusion coefficient in Eq. (20). In this limit, localization loses its putative meaning, and properties expected of strong chaos and BGS conjecture can be realized if $\kappa \gg 1$. Indeed, numerical results do show that for $\Lambda \gg 1$, histogram of spacings are consistent with Wigner distribution [153,229,230]. Kicked rotor on a torus were quantized in the late 1980s and we follow this recipe here [153,229,231]. Focussing on the kicked rotor Hamiltonian in Eq. (6), the periodicity of momentum is $2\pi/T$. If the basic periodicity is assumed to be $p_0 = 2\pi m_0/T$, where $m_0 > 0$ is an integer, then the number of discrete momentum states supported is $N = 2\pi m_0/T\hbar$, from which one can infer the scaled periodicity to be $T\hbar = 4\pi(m_0/2N)$. This, as it

turns out, is just the scaled Planck's constant $\hbar_s = T\hbar$ meeting the condition $\hbar_s = 4\pi r/q$, ($r, q \in \mathbb{Z}$), required for quantum resonance [124]. As rigorously shown in Ref. [178] in the context of quantum resonance, not just the momentum, the position variable is discrete as well and takes q equally spaced values in $[0, 2\pi]$, if q is odd integer. For a detailed discussion for even q and other subtleties, the reader must consult Ref. [124,178]. Consequently, dimensionality of the Hilbert space is finite for this problem and the Planck's constant is inversely related to the Hilbert space dimension. In this case, the Floquet operator in Eq. (29) in momentum representation becomes [229]

$$U_{nm} = e^{i\hbar_s n^2/2} e^{-i\theta_0(n-m)} \frac{1}{N} \sum_{l=-(N-1)/2}^{(N-1)/2} e^{-ik \cos(2\pi l/N + \theta_0)} e^{-2\pi i l(n-m)/N}, \quad m, n = -\frac{N-1}{2}, \dots, \frac{N-1}{2}. \quad (60)$$

The classical limit is obtained by taking the limits $k \rightarrow \infty$ and $\hbar_s \rightarrow 0$, such that $K = k\hbar_s$ remains constant. In addition, $N\hbar_s$ must remain constant as $N \rightarrow \infty$. The eigenphases of the operator U_{nm} can be obtained by numerical diagonalization of an ensemble of 40 Floquet matrices each of order $N = 99$ and K varying from 19990 to 20010 in steps of 0.5. In U_{nm} , θ_0 is the Bloch number, and the corresponding model preserves parity only if $\theta_0 = 0$ or π/N . For the level spacing distribution shown in Fig. 11(b), $\theta_0 = \pi/2$ and parity is explicitly not conserved. The eigenphases obtained by diagonalizing U_{nm} are used to construct the histogram in Fig. 11(b). It displays a good agreement with the Wigner distribution, in the spirit of the BGS conjecture.

In summary, the value of Λ plays a central role in distinguishing the correct limiting spectral statistics for the kicked rotor. An exhaustive review of spectral statistics as applied to kicked rotor can be found in Ref. [124], while for general considerations about the relation between spectral statistics and quantum chaos the reader is directed to Refs. [148,204,232].

If the Floquet matrix is truncated due to finite basis size, deviation from Poisson statistics is observed even if $\kappa \gg 1$ [161,233–236]. In such cases, the classical system is chaotic, and the quantum system shows restricted statistical properties as opposed to that of maximal chaos. Then, the spacing distribution is intermediate between the Poisson limit and the GOE limit, and this is termed “intermediate statistics”. This is often modeled using phenomenological distributions such as the Brody distribution [202,237] or the Izrailev distribution [231], both of which, at some level, provide an interpolating function between the Poisson and GOE functional forms. The Berry-Robnik form [238] for intermediate statistics is useful when such deviations can be attributed to the presence of stable classical structures in phase space. In kicked rotor, we are dealing with $K \gg 1$ for which quantum effects dominate and classical structures are insignificant to play any role.

This is a good place to digress a bit and point out that spectral unfolding (though not required for Floquet spectra) is often a numerical procedure fraught with ambiguity and prone to errors. Increasingly, the widely popular analysis of spacings is being replaced by spacing ratios defined as

$$r_i = \min\left(\tilde{r}_i, \frac{1}{\tilde{r}_i}\right), \quad \text{with} \quad \tilde{r}_i = \frac{s_i}{s_{i-1}}. \quad (61)$$

Since this ratio has constant density over the spectrum, unfolding the spectrum is unnecessary. It was introduced in Ref. [239], and random matrix averages for spacing ratio distribution is [240]

$$P(r) = C_\beta \frac{(r+r^2)^\beta}{(1+r+r^2)^{1+3\beta/2}}, \quad (62)$$

where $\beta = 1, 2, 4$ and C_β is the normalization constant; $C_1 = 27/8$, $C_2 = 81\sqrt{3}/4\pi$ and $C_4 = 729\sqrt{3}/4\pi$ [240]. For the quantum systems whose classical limit is integrable, the spacing ratio distribution is $P_P(r) = 1/(1+r)^2$. The insets in Fig. 11(a,b) show the spacing ratio distribution for the spectra displayed in the corresponding main figure. In both the cases, a good agreement with RMT based averages is observed. Recently, higher order spacings, i.e., level spacings beyond the nearest neighbor were studied [241]. In this, it was shown that the distribution of higher order spacing ratios display scaling relations with the standard spacing ratio distribution $P(r)$ evaluated at a modified index β' . These scaling relations can be exploited to infer symmetries in complex quantum systems [242]. Spacing ratios are now extensively used to characterize phase transitions such as the metal-insulator and localization-delocalization transitions [243–246]. In Fig. 11(a) the spacing distribution (histogram) for the simulated quantum kicked rotor on a cylinder with $K = 12.0$ and $\hbar_s = 0.7$ is shown. A good agreement with the Poisson distribution (red line) is observed. The inset in this figure shows the spacing ratio distribution, which also demonstrates a good agreement. In Fig. 11(b) the histogram is numerically computed distribution for kicked rotor on a torus with $K = 20000$ and $\hbar_s = 1/99$ and displays a good agreement with Wigner distribution (red line). A similar scenario results for the spacing ratio shown in the inset of this figure.

Until this point, the spectral statistics was entirely about the analysis of eigenvalues of the Floquet operator. It is also possible to analyze its eigenfunctions in terms of random matrix theory results [230]. We will only make brief remarks here. For $\Lambda \ll 1$, the eigenstates are localized over the angular momentum basis, while in the opposite limit $\Lambda \gg 1$ they are delocalized and in this case the eigenfunctions will display statistical properties consistent with maximal chaos and random matrix theory. Let ϕ represent an eigenstate of the Floquet operator \hat{U} (see Eq. (35)) such that $\phi_{n,i}$, ($i = 1, 2, \dots, N$) is the i th component of the n th eigenvector, and N is the dimension of \hat{U} matrix. For our present purposes we will

suppress the index n , so that $\phi_{n,i} = \phi_i$. For a delocalized state, which could be regarded as a random state, the theoretical expectation is that the components ϕ_i are distributed as [202]

$$f(\phi) = \frac{\Gamma(N/2)}{\sqrt{\pi}\Gamma(N-1/2)} (1-\phi^2)^{\frac{N-3}{2}}, \quad (63)$$

which in the limit of $N \rightarrow \infty$ tends to a Gaussian distribution. This was verified for the kicked rotor floquet states [230]. For localized states, strong deviations from Gaussian form are observed. These statistical features of the eigenfunctions as a marker of maximal quantum chaos are not confined to kicked rotor model alone. They are also observed in a variety of systems including the kicked top [175] and other conservative chaotic systems [247]. In Izrailev's work [225,231], a different measure of localization l_H based on information entropy (rather than localization length) of the eigenstate ϕ was introduced to accommodate finite Hilbert space dimension of the system. Using the definition of information entropy, an eigenstate has an associated entropy (not to be confused with thermodynamic entropy) given by

$$\mathcal{H}_N = - \sum_{i=1}^N (\text{Re } \phi_i)^2 \ln(\text{Re } \phi_i)^2, \quad (64)$$

constrained by the normalization $\sum_i (\text{Re } \phi_i)^2 = 1$. Note that, in this definition real part of ϕ_i is used since parity and time-reversal invariance symmetries lead to $\text{Re } \phi_i = \text{Im } \phi_i$. Physically, \mathcal{H}_N is a measure of logarithm of number of basis states that carry significant probability density. Then, entropy-based localization measure is defined as

$$l_H = N \exp(\mathcal{H}_N - \mathcal{H}_N^{\text{GOE}}), \quad (65)$$

where the random matrix average of information entropy is $\mathcal{H}_N^{\text{GOE}} \approx \ln(N/2) + O(1/N)$ if $N \gg 1$ [248]. The advantage of this measure is that, in an average sense, for a chaotic (extended) state, $l_H = N$. This is in contrast with localization length m_L which can tend to infinity for extended states. Thus, we might regard l_H also as representing the effective number of basis states over which the state ϕ is localized, normalized with respect to a random state. In analogy with Λ , a parameter $\beta = \langle l_H \rangle / N$ can be introduced in which $\langle l_H \rangle$ is averaged over all the eigenstates of \widehat{U} . Note that $0 \leq \beta \leq 1$, though these bounds on β can be somewhat violated due to fluctuations about $\langle l_H \rangle$. In general, small values of β is a characteristic of localized states and large β corresponds to extended states. It was also shown that β is proportional to the degree of level repulsion in the quasi-energy spectrum. Thus, β is useful to explore the regime of intermediate statistics as well. All the arguments presented above in terms of Λ can be re-phrased in terms of β with no qualitative change in results. The real utility of β is seen in the remarkable scaling relation [249]

$$\beta = \frac{\langle l_H \rangle}{N} \approx g(\kappa^2/N), \quad (66)$$

where $g(\cdot)$ is the scaling function. This is reminiscent of a similar scaling relation in solid state physics between localization length in finite samples and residual conductance [250,251]. This scaling relation for kicked rotor, plotted for a range of kick strengths, is illustrated in the left panel of Fig. 12. For detailed discussions on the caveats and validity of this scaling, see [124,249]. In summary, the eigenvectors carry more fine-grained information and their analysis using RMT methods forms an important diagnostic tool for the dynamical phases exhibited by the system.

5.5. Random band matrices and kicked rotor

It was pointed out earlier that the matrix elements of Floquet operator for the kicked rotor \widehat{U} (in angular momentum basis) is effectively a banded matrix. This can be traced back to the Bessel function in the expression for the matrix element in Eq. (33). The matrix elements of \widehat{U} , beyond distance b from diagonal, decay faster than exponential. In the spirit of random matrix theory, it is then natural to study the predictions of banded matrix with random entries drawn from suitable distribution, called random banded matrices (RBM). This line of research led to significant developments in the study of random banded matrices. We will only briefly review these developments, redirecting an interested reader to recent reviews [252,253]. RBMs are also relevant in many other physics problems ranging from one-dimensional Anderson model to atomic spectra of rare earth elements such as Ce [254].

An ensemble of matrices \mathbf{H} would be called RBM if its matrix elements are random variables of the form

$$H_{ij} = G_{ij} a(|i-j|) \quad (67)$$

where G_{ij} are elements drawn from Gaussian Orthogonal Ensemble (GOE), $r = |i-j|$ is the “distance” from the diagonal, and $a(r)$ is a suitable function that imposes the bandedness condition: $\lim_{r \rightarrow \infty} a(r) = 0$. It is convenient to define an effective bandwidth b such that $a(r) = 0$ for $r > b$. Accounting for symmetries, the number of independent matrix elements in RBM is $b(2N-b+1)/2$. Such RBMs were first introduced in 1985 as a RMT based model for the transitional regime from integrability to chaos [255], though Wigner himself had studied a different version of RBM model called “bordered matrices” in 1955 [256]. The relevance of RBM models for kicked rotor stems from the banded nature of Floquet operator \widehat{U} (in angular momentum basis) with approximate bandwidth $\sim \kappa = K/\hbar_s$. This is clear from the structure of Eq. (33) as the matrix elements are modulated by a Bessel function that decays away from the diagonal. For large κ , the

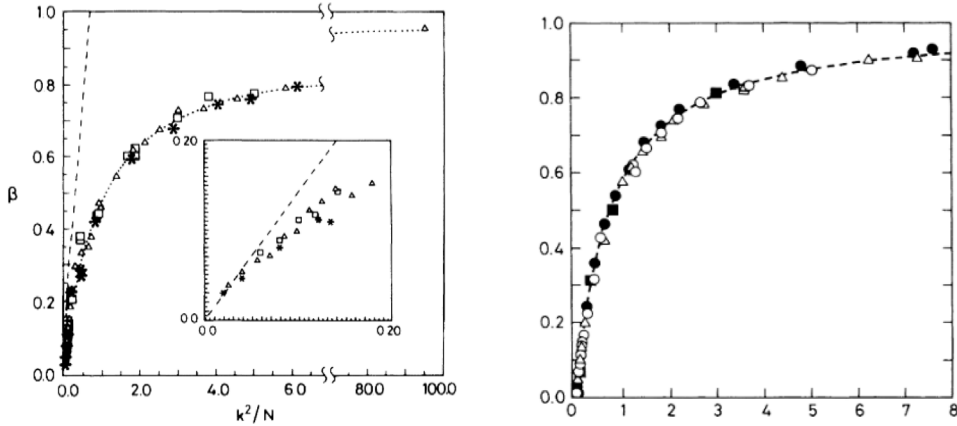


Fig. 12. Scaling of localized states in kicked rotor and RBM. (left) Scaling in kicked rotor. Average localization length plotted as a function of effective parameter k^2/N . (right) Scaling in random banded matrices. Average localization length of eigenvectors plotted as a function of b^2/N .
Source: Figures taken from Ref. [249,257].

underlying classical dynamics is chaotic, and the matrix elements of \hat{U} behave like pseudo random numbers and thus suitable for analysis within the framework of random matrix theory.

The spectral statistics of RBMs, for eigenvalues and eigenvectors, are different from that of the standard Gaussian ensembles. For an ensemble of random banded matrices of order $N \rightarrow \infty$ and bandwidth $b \gg 1$, the eigenvalues are uncorrelated and spacings are Poisson distributed. A typical eigenvector has b^2 non-zero components (out of possible N), and the rest are exponentially small. For an ensemble of RBMs of finite order N , the spectral statistics depends only on an effective scaling parameter $x = b^2/N$, rather than individually on b or N . As x changes from zero to infinity, spectral statistics change from nearly Poissonian type to Wigner–Dyson distribution in Eq. (57) [257]. One of the significant findings was the existence of scaling of localized states with the number of basis states N (“sample size”) for the kicked rotor defined on a torus [249]. This was just discussed at the end of the previous section. This scaling is demonstrated through numerical simulations in Fig. 12(a). Interestingly, a similar scaling also exists in the spectrum of RBMs [257]. In the RBM setting, the bandwidth b plays the role of κ . As shown in Fig. 12(b), an excellent scaling is observed if κ in Eq. (66) is replaced by b . Another measure of localization, namely the participation ratio, also scales with b^2/N [258]. An analytical proof of the scaling in RBM was obtained through reduction to a nonlinear, supersymmetric σ -model [169].

Physically, this scaling can be understood in terms of a quantum particle in tight-binding representation. In this case, the Hamiltonian diagonal matrix elements represent random on-site energy and off-diagonal elements represent hoppings. The RBMs can be thought of as particle in a one-dimensional lattice with random on-site energies and long range hopping. The particle has a non-zero probability for hopping up to b sites. Then, it is known from studies of Anderson model that as system size $N \rightarrow \infty$, eigenstates are localized with some localization length ξ . For finite system size, scaling hypothesis describes the situation – that ξ is the only operative parameter at a given disorder and the ratio ξ/N effectively determines other statistical properties associated with the system. Remarkably, this broad scenario carries over to the RBMs and to the kicked rotor system as well. Fig. 12 represents a demonstration of these ideas.

Recently, it was shown that finite range Coulomb gas models provide an alternative theoretical framework to study the properties of RBMs and the kicked rotor spectra. This model is a generalization of the Dyson’s Coulomb gas approach [259]. In Dyson’s picture, the eigenvalues of random matrix ensemble are identified with the positions of Coulomb particles (on a lattice) with infinite range of interaction. If finite range of interactions are considered, it turns to be an appropriate framework for RBMs [260]. This approach was recently applied to kicked rotor system [261,262]. Finite range Coulomb gas models were earlier studied in the context of intermediate statistics straddling Poisson and Wigner limits [263]. There are other interesting extensions of RBMs to the case in which matrix elements of time evolution operator decay in a power-law fashion (rather than exponential) as we move away from the diagonal. If the potential function $V(x)$ in Eq. (28) has discontinuities, then the resulting \hat{U} displays power-law decay of its matrix elements: $a(r) \sim r^{-\alpha}$ as $r \rightarrow \infty$ and α is the exponent. A specific example of a dynamical system that shows this trend is the quantum Fermi accelerator model representing the dynamics of a particle between two walls such that one wall is fixed in position and the other has periodic oscillations. The classical version of this model was originally introduced by Enrico Fermi [264] in the context of acceleration of charged particles in interstellar space due to collisions with varying magnetic fields. Another example is the tight-binding Anderson models with long-range (slowly decaying) hopping terms. The evolution operators in such problems can be modeled as an ensemble of power-law random banded matrices (PRBM). Its important features are the existence of a transition from localized to delocalized states at a critical value of α , and multifractality of the eigenstates at criticality [168,265,266]. These novel results have led to enormous interest from condensed matter physics. For a detailed review of these considerations, see Ref. [267]. Interestingly, PRBM has applications to classical problems of underwater sound propagation [268,269]. Recently, the case of sparse PRBM had been studied as well [270].

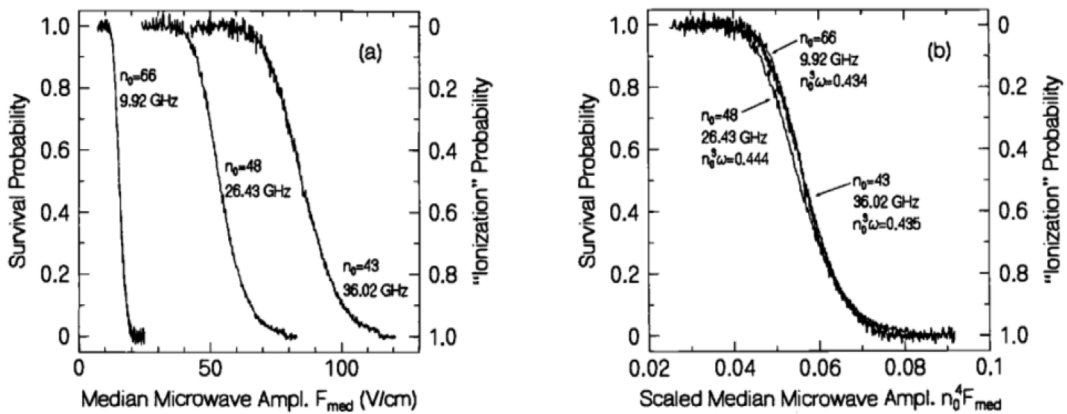


Fig. 13. (left) Survival probability of the hydrogen atoms plotted as a function of field strength F . Three curves correspond to atoms prepared with three different principal quantum numbers n . The scaled microwave frequencies in all the three cases is 0.439. (right) Survival probability as a function of scaled field strength $n^4 F$.
Source: Figure taken from [274].

6. Experimental realizations of quantum kicked rotor

6.1. Microwave ionization of hydrogen atoms

The ionization of excited hydrogen atoms by microwave fields is a remarkable set of experiments performed during the 1970s and 80s and was first reported by Bayfield and Koch [271,272]. In fact, the original experiment was not really planned as a realization of chaotic kicked rotor model. It was the unexpected results that led to the suspicion that chaos might be playing a role. It is well understood based on Einstein's theory for photo-electric effect that if the atoms are bombarded with electromagnetic radiation of frequency ν , then ionization would appear only if $\nu > \nu_0$, where ν_0 is a threshold frequency, irrespective of the intensity of radiation. The experiments by Bayfield and Koch found that, rather than threshold frequency, a critical strength of microwave field is required for ionization to kick in. For instance, with hydrogen atoms excited to principal quantum number ~ 65 , they could be ionized by using photons whose energy is only about one percent of the ionization energy. This counter-intuitive experimental result led to a flurry of activity. Since the excited states involved in the experiments had principal quantum numbers in the range 60–70, and it was expected that correspondence principle might operate at these excitations. It led to a suggestion that classical mechanics might be able to explain the experimental results [273]. Indeed, the results show that over a large range of principal quantum numbers of hydrogen atom, a good correspondence existed between the observed ionization threshold and the onset of chaos (based on Chirikov resonance overlap criteria) in one-dimensional classical model similar to the standard map.

The schematic of the experimental apparatus is discussed in sufficient detail in many publications [275,276]. The experiment was carried out by preparing the hydrogen atoms in highly excited states. A beam of hydrogen atoms with 14 Kev energy are made to pass through regions with static field of 10^4 V cm $^{-1}$ in which CO₂ laser is used to excite the atoms to principal quantum numbers $n = 63$ – 69 . The atoms were prepared in states labeled by $(n, 0, n - 1, 0)$ and this makes it quasi one-dimensional since electronic density is strongly elongated along one direction. These atoms enter a microwave cavity with oscillating electric fields whose frequencies are about 8–36 GHz and field strengths up to 100 V cm $^{-1}$. The atoms are ionized by the microwave radiation and ionization is pronounced for field strengths exceeding a critical value. Finally, the fraction of surviving atoms are measured or, equivalently, the ions and electrons produced can be measured as well.

This interaction of hydrogen atom with the microwave field of strength F and frequency ω should be studied by solving the corresponding 3-dimensional Schrödinger equation. This being a scaling system, following scaled variables (relevant for present discussions) can be extracted:

$$\tilde{F} = n^4 F, \quad \text{and} \quad \tilde{\omega} = n^3 \omega, \quad (68)$$

and n being the principal quantum number. Fig. 13(a) shows the fraction of atoms that survive without ionization and for three different choices of n , the field strength required to create widespread ionization is different. Quite remarkably, if the scaled variables are used, as shown in Fig. 13(b), all the three curves collapse on one another indicating two things – naive expectation based on photoelectric effect does not hold, and approach to ionization threshold has a common physical process depending on both field strength and quantum number n .

As shown in [273,277], it turns out that classical equations of motion can account for many features of the experimental results, in particular, the ionization threshold. The one-dimensional Hamiltonian for the hydrogen atom in monochromatic

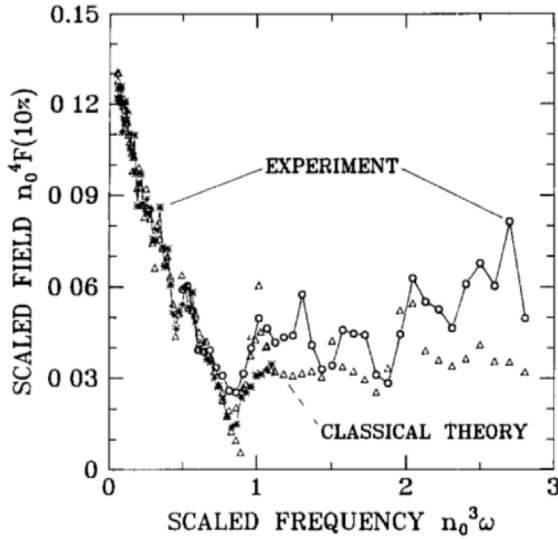


Fig. 14. For $\tilde{\omega} < 1$, experimental verification of $\tilde{F} \propto \tilde{\omega}^{-1/3}$ predicted through an analogy with classical standard map. The scaled amplitude required to ionize 10% of the atoms is shown as a function of scaled frequency. The deviation from classical theory for $\tilde{\omega} > 1$ is a signature of dynamical localization.

Source: Taken from [274].

time-varying field of amplitude F with frequency ω can be written as,

$$H = \frac{p^2}{2} + V(x) + xF \cos(\omega t), \text{ where } V(x) = \begin{cases} -1/x, & x > 0, \\ \infty, & x \leq 0. \end{cases} \quad (69)$$

For further analysis, the position and momentum are replaced by phase of the oscillating field Φ and energy E as the phase space variables. The equations of motion can be reduced, in the limit that the electron motion is not strongly influenced by the microwave radiation over one cycle, to the Kepler map [277,278]

$$\begin{aligned} \Phi_{n+1} &= \Phi_n + 2\pi\omega(2|E_{n+1}|)^{-3/2} \\ E_{n+1} &= E_n + \omega k \sin \Phi_n, \end{aligned} \quad (70)$$

where $k = 2.58\omega^{-5/3}F$. If this map is linearized around a reference energy, it reduces to a standard map with kick strength $K = 48.6\tilde{\omega}^{1/3}\tilde{F}$. With this analogy, the ionization threshold can be identified with kick strength at which global chaos sets in, namely, $K \approx 1.0$. This sets the critical field strength for widespread ionization to be at $\tilde{F} \approx 0.027$, while in the experiment it is nearly 0.04. The discrepancy arises from the approximations employed in arriving at Eq. (70).

Far more instructive is to plot the scaled field strength and the scaled frequency at ionization threshold. The analogy with the classical standard map predicts that $\tilde{F} \propto \tilde{\omega}^{-1/3}$. This is amply verified in Fig. 14 which displays the critical field needed for ionizing 10% of the atoms. An agreement with classical simulations is observed for $\tilde{\omega} < 1$. Physically, at low values of $0.1 \lesssim \tilde{\omega} \lesssim 1$, a strong driving field couples many excited states resulting in higher density of states and hence a good agreement with classical theory can be expected. Thus, in a classical picture, we can imagine electron's dynamics to be trapped by invariant curves and it finally breaks out when scaled kick strength $K \approx 1$. Similar physical scenario occurs in non-hydrogenic alkali Rydberg atoms interacting with microwave fields [279]. For $\tilde{\omega} > 1$, there is a clear deviation from classical theory and stronger field strength must be applied to create 10% ionization. The enhanced stability (higher ionization thresholds) results from quantum localization effects and requires solution to the time-dependent Schrödinger equation. This provides the first experimental evidence for effects arising due to dynamical localization [280], and an improved experiment presents a clearer evidence for suppression of ionization due to localization [281]. By tuning the ionization potential of the atomic state, it is also possible to transition from dynamical localization to photoelectric effect regime [282].

6.2. Cold atoms in flashing optical lattices

Another testing ground for quantum chaos is the cold atomic cloud in optical lattices. Unlike the microwave ionization of hydrogen atoms, the cold atoms and optical lattice set up allows one to tune many parameters to study not just the dynamical localization but also effects such as effects of noise on the parameters associated with kicked rotor system. Not surprisingly, cold atoms in optical lattices have emerged as a popular test bed by early 2000s [283,284]. In the

context of kicked rotor, suggestion for employing cold atoms on optical lattices was put forth in 1992 [285] and dynamical localization was achieved in experiment two years later [286]. In these experiments, atomic cloud is cooled down to a temperature of almost $15\mu K$ and trapped in a magneto-optical trap. The trapped atoms are then released from the trap and interact with the standing radiation field that is flashed periodically.

The physical setting is that the two-level atoms are traversing along z -direction and interacting with standing wave created by light field along x -direction. The two relevant levels in the atom, labeled $|g\rangle$ and $|e\rangle$ with $\hbar\omega_0$ being energy difference between the levels. The light field can be represented by $\mathbf{E}(x, t) = \hat{\mathbf{y}}E_0 \cos(k_L x)e^{i\omega_L t} + c.c.$, where $\hat{\mathbf{y}}$ is the unit vector along y -direction, E_0 is the amplitude, ω_L is the angular frequency. It is assumed that the nodes of the standing wave oscillate induced by the oscillations in one of the mirrors. Hence, light field becomes $\mathbf{E}(x - \Delta L \sin \omega t, t)$. Within the electric dipole and rotating wave approximations, the effective Hamiltonian can be written down as

$$H = \frac{p^2}{2M} + \hbar\omega_0|e\rangle\langle e| - dE_0 \cos(k_L(x - \Delta L \sin \omega t)) e^{i\omega_L t} \sigma_+ + h.c. \quad (71)$$

In this, M is the mass of the atom, d is the dipole moment, p is the momentum of its center-of-mass, and σ_{\pm} are the Pauli operators. If we go to a reference frame moving with the atom in z -direction, then the equation for the motion of the center-of-mass along x -axis is the only one that matters for the problem. The general state of the atom can be represented as a superposition

$$|\psi_{\text{atom}}\rangle = \psi_g(x, t)|g\rangle + \psi_e(x, t)e^{i\omega_L t}|e\rangle, \quad (72)$$

in which ψ_g and ψ_e are the amplitudes in ground and excited states. At this point, two coupled time-dependent Schrödinger equations will be obtained corresponding to ψ_g and ψ_e . Further, if detuning $\delta_L = \omega_0 - \omega_L$ is assumed to be large compared to Rabi frequency $\Omega = 2dE_0/\hbar$ then it allows for adiabatic elimination of excited state amplitude. Secondly, spontaneous emission from state $|e\rangle$ is largely suppressed. The effective equation of motion is

$$i\hbar \frac{\partial \psi_g}{\partial t} = -\frac{\hbar^2}{2M} \frac{\partial^2 \psi_g}{\partial x^2} - \frac{\hbar\Omega_{\text{eff}}}{4} \cos^2(k_L(x - \Delta L \sin \omega t)) \psi_g, \quad (73)$$

where $\Omega_{\text{eff}} = \Omega^2/\delta_L$. The ground state is governed by the Hamiltonian

$$H = \frac{p_x^2}{2M} - \frac{\hbar\Omega_{\text{eff}}}{8} \cos(2k_L(x - \Delta L \sin \omega t)) \quad (74)$$

in which energy shift of $\hbar\Omega_{\text{eff}}/8$ has been effected to cancel a constant term. By rescaling the variables $t' = \omega t$, $X = 2k_L x$, $P = (2k_L/M\omega)p_x$ and the Hamiltonian $H' = (4k_L^2/M\omega^2)H$, the dimensionless Hamiltonian describing the ground state dynamics turns out to be

$$H = \frac{P^2}{2} - K \cos(X - \lambda \sin t), \quad \text{where } K = \frac{\hbar k_L^2 \Omega_{\text{eff}}}{2M\delta_L\omega^2}, \quad (75)$$

and $\lambda = 2k_L \Delta L$. This Hamiltonian resembles that for a driven pendulum. Note that the kick strength K can also be written in terms of the recoil frequency $\omega_r = \hbar k_L^2/2M$. From this point onwards, the approach to deriving the classical map is somewhat similar to the route taken for the microwave ionization problem in the previous section. The essential physics is as follows; the pendulum passes by the primary resonance zone twice during every time period. We restrict only to the case when this process is sufficiently fast such that the rate of change in pendulum frequency is negligible compared to rate of change in the position of primary resonance. If the pendulum is not in the vicinity of the resonance, it is effectively a free rotor. Thus, the ingredients of a kicked rotor – free motion and a kick part – can be identified here. Going through the mathematical manipulations, the equivalent kicked rotor problem can be described by the map

$$\begin{aligned} X_{n+1} &= X_n + 2\pi P_{n+1}, \\ P_{n+1} &= P_n - 2\sqrt{\pi} \frac{K}{\sqrt{\lambda}} \sin(X_n). \end{aligned} \quad (76)$$

This is identical to the standard map in Eq. (9), provided the second equation is multiplied by 2π such that the momentum variable is $L_n = 2\pi P_n$. Then, it is straightforward to identify the last KAM barrier would break at $4\pi^2 K / \sqrt{\lambda\pi} > 1$. This implies that $K > \sqrt{\lambda\pi}/4\pi^2$. The resonance crossing takes place only if $|P| < \lambda$, i.e., until atomic speed is less than the that of standing wave, and this restricts the chaotic layer in the classical phase space and the regime of chaotic diffusion. In the quantum regime, the Planck's constant $\hbar_s = 8\omega_r/\omega$ becomes a parameter as well such that $[P, X] = i\hbar_s$.

It must be emphasized that our starting point, the Hamiltonian in Eq. (74), is a system for which time-dependence arises from spatial modulation of the standing waves. In that sense, even though this Hamiltonian reduces to a standard map under several layers of approximation, it cannot be taken to be a direct experimental realization of the kicked rotor system. A direct realization of kicked rotor is possible by dispensing the spatial modulation term $\Delta L \sin \omega t$, and instead considering a train of pulses $f(t)$ that will modulate the space-dependent potential. The Hamiltonian with this provision for the ground state dynamics will be a modified form of Eq. (75):

$$H = \frac{P^2}{2} - K \cos(X) f(t), \quad \text{where } f(t) = \sum_{n=0}^N e^{-(t-n)^2/2\sigma^2}. \quad (77)$$

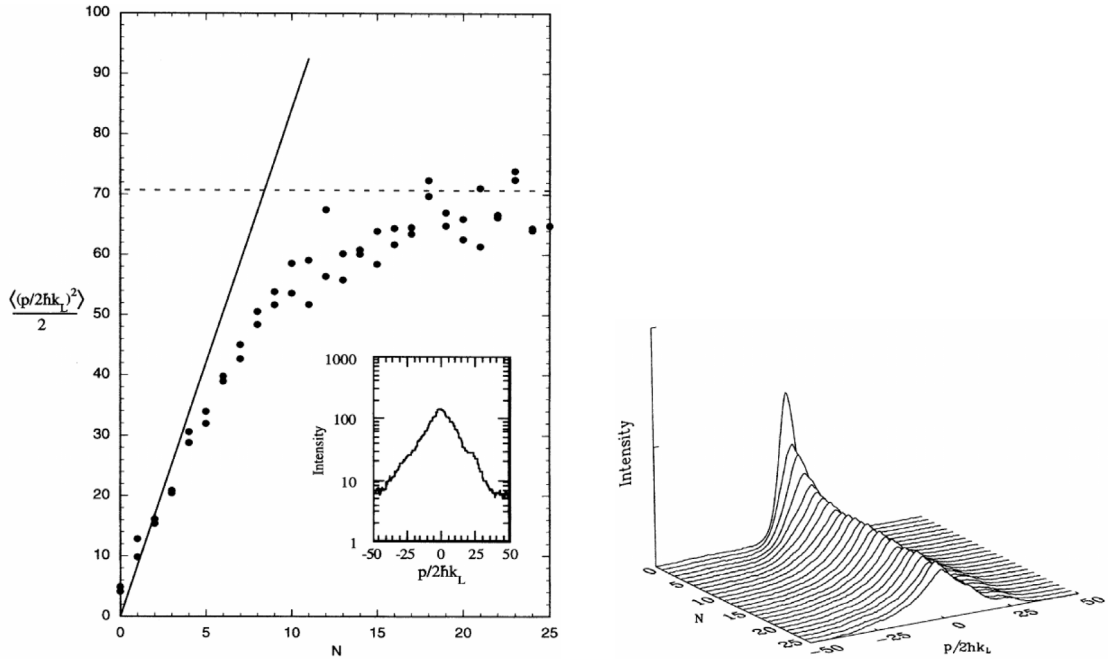


Fig. 15. Experimental observation of dynamical localization. (left) Solid symbols show the saturation of mean energy as a function of time N . Dashed line is the expected saturation energy. Solid line is the classical quasi-linear diffusion. (inset) shows the exponential momentum distribution after localization is achieved. (right) The momentum distribution at various times. The initial distribution at $N = 0$ is close to Gaussian while at $N = 25$ the distribution has evolved to nearly an exponential form.

Source: Taken from Ref. [287].

In this example, a train of Gaussian pulses of width σ is considered, as was done in the first experimental realization [287]. Note, however, that other forms for $f(t)$ such as rectangular sinc functions can also be implemented [288]. If σ is smaller, it will provide a better approximation to $f(t)$ as a train of delta kicks. The potential can be written in Fourier basis, and gives

$$H = \frac{P^2}{2} - \sqrt{2\pi}\alpha K \sum_{r=-\infty}^{\infty} e^{-2\pi^2\alpha^2 r^2} \cos(X - 2\pi rt), \quad (78)$$

and the effective kick strength is $\sqrt{2\pi}\alpha K$. This is in a suggestive form, especially to simply read out the resonances located at $P = 2\pi r$. Successive resonance widths are weighted by the Gaussian factor controlled by σ and decay quickly. This sets the bounds on maximum value of momenta $|p_{\max}|$ in phase space for which dynamics will be chaotic and exhibit diffusion. This implies that in experiments, to realize dynamical localization, the energies reached by the atomic cloud should be less than $|p_{\max}^2|/2$. As a consistency check, it is straightforward to see that if the limit of narrow pulse width is taken, $\alpha \rightarrow 0$, we also require $K \rightarrow \infty$ such that the effective kick strength $\sqrt{2\pi}\alpha K$ remains constant. In this limit, the Fourier coefficients in Eq. (78) are all equal to 1, and by use of Poisson sum formula the potential term in Eq. (78) recovers the δ -kick form.

The detailed experimental procedure is given Ref. [286,287]. Neutral sodium atoms were trapped and cooled using a magneto-optical trap (MOT). Then, the atoms were released from the MOT and they interact with the spatially modulated standing wave [286] or a train of Gaussian pulses [287]. The diffusion in momentum takes place during this time. At this point, the standing wave is turned off and the atomic cloud is allowed to expand freely. The evolved positions of the atoms are frozen turning on the cooling beams to form optical molasses. Finally, atomic fluorescence imaging is done that captures the extent of diffusion. From this information and by deconvolution of the initial momentum distribution, the final momentum spread can be extracted from the time of flight. From the measured momentum spread, mean energy can be estimated. First experimental observation of dynamical localization was reported using modulated standing waves [286] and a more direct evidence using a train of Gaussian waves was obtained later [286]. The quantum suppression of classical diffusion using Gaussian train of pulses, in Fig. 15(a), shows the expected mean energy saturation as a function of time and inset shows the exponential profile of momentum distribution for the evolved cold atomic cloud. Fig. 15(b) depicts the temporal progression from an initial Gaussian momentum distribution to almost exponential profile beyond the break-time.

It might be remarked that dynamical localization, like the Anderson localization, is a general emergent phenomena of wave dynamics in the presence of disorder and its analogues can be observed in many physical situations. It is not

surprising that it has been experimentally observed in the spatial frequency domain of kicked optical system [289] and in frequency domain of mode-locked lasers with dispersion [290].

7. Variants of kicked rotor

7.1. Noisy kicked rotors

The experiments with cold atoms in optical lattices have led to many other insights as well, primarily arising from several variants of the standard kicked rotor. In this section some of them will be briefly discussed. An important question of interest relates to how robust is the dynamical localization. Secondly, since the kicked rotor does not show quantum diffusion beyond the break-time, the question is if noise can induce asymptotic quantum diffusion. In the context of experiments, spontaneous emission induces decoherence and can enhance the tendency to behave like a classical system. This is indeed borne out by the theoretical and experimental results [288]. In atom-optics experiments spontaneous emission can be tuned using detuning parameter δ , this experiment [288] shows that smaller detuning δ (compared to natural line width), corresponding to higher spontaneous emission probabilities per kick, leads to decoherence and a loss of dynamical localization. Theoretically, this scenario is represented as a noisy kicked rotor [291] obtained by adding a noise term

$$\nu \phi(x, t) \sum_n \delta(t - n), \quad \text{where,} \quad \phi(x, t) = \sqrt{2} \Delta_n \cos(x + \alpha_n), \quad (79)$$

to the kicked rotor Hamiltonian in Eq. (7). In this, ν is the noise strength and Δ_n is Gaussian noise with zero mean and unit variance, while α_n is white noise in $[0, 2\pi]$. For reasonably large kick strength $K > 1$, classical diffusion coefficient becomes $D_{cl} = K^2/4 + \nu^2/2$ [291]. Thus, D_{cl} is nearly the same as for the noiseless case provided $K^2 \gg \nu^2$. For $\nu \gg K$, the noise is anyway expected to dominate both in the classical and quantum regimes. Naturally, the interest is focussed in the regime of low noise strength. In the quantum regime, the effect of noise is probed in terms of the quantum diffusion coefficient defined as [288,292]

$$D_q = \lim_{t \rightarrow \infty} \frac{\langle (\hat{p}(t) - \hat{p}(0))^2 \rangle}{t}, \quad (80)$$

and $\langle . \rangle$ represents an average taken over noise realizations. If $\nu = 0$, then $D_q = 0$ in the regime of dynamical localization. In this case, the coherence time is inversely related to noise strength and this gives

$$t_c \sim \frac{\hbar^2}{\nu^2}, \quad (81)$$

the regime of low noise strength $\nu \rightarrow 0$ is the one for which break-time t_b is much smaller than coherence time, and quantum localization is sustained. If $\nu \gg 0$, then $D_q \approx D_{cl}$ and typically quantum diffusion dominates over localization effects (an exception occurs for quantum kicked particle model [292]). Rigorous theoretical results show that even a small amount of noise is sufficient to induce loss of coherence, though $D_q \sim D_{cl}$ only in the semiclassical limit of small \hbar . In broad agreement with these expectations, the cold atoms experiment [288] with controlled spontaneous scattering probability η per kick agrees with $D_q = \eta t_b D_{cl}/(1 + \eta t_b)$. Quantum diffusion increases as with η but tends to saturate. As $\hbar \rightarrow 0$, the break-time becomes large, $t_b \gg 1$, and $D_q \rightarrow D_{cl}$. On the other hand, correlated noise tends to exert non-trivial influence on the quantum kicked rotor as both diffusion and coherence depend on long lived auto-correlations in the quantum regime [293], though in the classical regime the effect is negligible due to chaotic dynamics in phase space. It turns out that the manifestations of noisy kicked rotor are not too different from the effects induced by physical dissipation mechanism such as spontaneous scattering events. In general, it is not easy to distinguish between them, especially if we are only monitoring the diffusion induced by these processes [294].

If either the time period of kick or the amplitude of kick is made noisy, experiments show that localized state makes a transition to classical diffusive rate [295,296]. However, 'phase noise' works a little differently. Consider the dimensionless Hamiltonian with an explicit phase degree of freedom and it has the form [297]

$$H = \frac{p^2}{2} + K \cos(x + \alpha \cos(\omega_p t)) \sum_{n=0}^{N-1} \delta(t - n), \quad (82)$$

where ω_p and α are, respectively, the phase modulation frequency and amplitude. As a physical undriven pendulum problem (without the train of δ -pulses), phase modulation of this form would imply that gravity has a direction that rotates with frequency ω_p . In this problem, there are two possible time-scales, represented by kick frequency ω_k and ω_p . Dramatic behavior is seen if the kick period ω_k^{-1} is set to $\tau_T/2$, i.e., half the Talbot time. Without the phase modulation, the kicked rotor would display quantum anti-resonance, an effect due to phase addition from successive kicks adding up destructively. Oscillations in energy as a function of time is an explicit manifestation of anti-resonance. Remarkably, as experiments show, if $\omega_k = 2\omega_p$, then anti-resonance is converted into a resonance or vice-versa [297]. The 'noise' part comes into play when the ratio ω_k/ω_p is incommensurate and hence the phase of the kicking field becomes quasi-random. In general, dynamical localization is more sensitive to phase noise than quantum resonance effects.

In the results discussed above, a variable or parameter of the kicked rotor is contaminated by *stationary* noise process, and the net outcome is decoherence of the localized mode. The decoherence factor decays exponentially in time, e^{-t/t_c} , where t_c is the coherence time. On the other hand, if *non-stationary* noise process is superimposed on a suitably modified kicked rotor, a remarkable result is that the temporal decay of coherence can be slowed down considerably. If the periodic kick sequence is manipulated such that kick amplitude is subjected to random noise, and this noise is superposed on the kicks at time instants separated by interval τ drawn from Lévy distribution $f(\tau) \sim \tau^{-(1+\alpha)}$, where $0 < \alpha < 1$ is the Lévy exponent. Effectively, the kicks imparted to a standard kicked rotor are occasionally made noisy after random intervals of time. Remarkably, the non-stationarity of Levy distribution in the range $0 < \alpha < 1$ ensures that the mean coherence time diverges and the decoherence is strongly attenuated [298]. A modified version of this idea was experimentally achieved in the cold atoms test bed [299]. Further details about decoherence will be discussed in Section 11.4.

7.2. Non-KAM kicked rotors

Kicked rotor is not just a paradigm for Hamiltonian chaos, but also for a system that obeys the assumptions of Kolmogorov–Arnold–Moser (KAM) theorem (discussed in detail in Section 4). If the Hamiltonian in action J_i and θ_i coordinates ($i = 1, 2, \dots, N$) is of the form

$$H(J_1, J_2, \dots, J_N; \theta_1, \theta_2, \dots, \theta_N, t) = H_0(J_1, J_2, \dots, J_N) + \epsilon V(J_1, J_2, \dots, J_N; \theta_1, \theta_2, \dots, \theta_N, t), \quad (83)$$

where H_0 is the integrable part and the perturbation is assumed to be sufficiently small, i.e., $\epsilon V(.) \ll 1$. The phase space of the unperturbed system is covered with either rational or irrational tori. If H_0 is analytic and the corresponding unperturbed motion is non-degenerate, then KAM theorem guarantees that most of the irrational tori (of the unperturbed system) survive under the effect of perturbation (see Section 4 and references therein). Effectively, KAM theorem tells us that the change from order to chaos will be gradual and not abrupt, if the conditions of the theorem are met. For precise statement of KAM theorem and recent developments, readers might consult Ref. [300]. With an increasing interest in the physics of quantum many-body localization, there are also initial attempts underway towards formulating a quantum version of KAM theorem [301].

An interesting question is to ask what happens if the assumptions that underlie the KAM theorem are violated. This aspect of Hamiltonian dynamics has received far less attention compared to its KAM-compliant counterparts. Once again, variants of kicked rotors have provided the lead results here and we will briefly highlight them here. The kicked harmonic oscillator, introduced by Zaslavsky, is a prominent example of this class with the dimensionless Hamiltonian given by [302,303]

$$H_{\text{kho}} = \frac{1}{2} (p^2 + \omega_0^2 x^2) - \omega_0 K V(x) \sum_{n=-\infty}^{\infty} \delta(t-n), \quad V(x) = \cos x. \quad (84)$$

The parameters are ω_0 and perturbation strength K . Physically, this corresponds to the dynamics of a particle placed in a uniform magnetic field and interacting with an electrostatic wavepacket propagating perpendicular to the field. In this case too, the classical dynamics can be reduced to difference equations often called the web map [303].

For the present purposes, an important feature is that the unperturbed part of the problem is the simple harmonic oscillator, $H_0 = (p^2 + \omega_0^2 x^2)/2$, is degenerate. This is because in action-angle coordinates, $H_0 = I\omega_0$ and $d^2 H_0/dI^2 = 0$, and this violates one of the assumptions of the KAM theorem. As a consequence, Eq. (84) is fundamentally different from the standard kicked rotor. In particular, the quasi-periodic orbits are *not* guaranteed to exist even for arbitrarily small K and Chirikov's resonance overlap criteria would not be applicable. Unbounded global diffusion and chaos is indeed a possibility even for $K \ll 1$. Whenever there is a resonance between the oscillator frequency and kick frequency, $\omega_0 T = 2\pi/q$, ($q \in \mathbb{Z}$), then the phase space is tiled with inter-connected channels through which global transport is possible. Diffusion takes place through these intricate connected set of channels often called "stochastic web" in phase space for any $K > 0$ and $\omega_0 = 2\pi l_1/l_2$ (l_1, l_2 are co-primes). Visually striking images of stochastic web show crystalline symmetry for $l_1 = 3, 4, 6$ and $l_1 = 5$ shows quasi-crystalline symmetry [303]. A generalized version of the Hamiltonian in Eq. (84) is the well studied kicked Harper model given by,

$$H_{\text{khm}} = L' \cos p - K' \cos x \sum_{n=-\infty}^{\infty} \delta(t-n). \quad (85)$$

Both H_{kho} and H_{khm} are exactly related to one another [304]. The quantized models support dynamical localization, quantum resonances and anomalous quantum diffusion (delocalization) in different parametric windows of L' and K' and depending on the form of $V(x)$ [305–310]. In fact, quantum transport through stochastic webs is enhanced near avoided crossings due to closer interaction between the eigenstates localized on island structures and extended web eigenstates. This can be achieved by tuning ω_0 and the wave vector of the kicking field [311]. Experiments have found that stochastic webs (induced by non-KAM dynamics) enhance the current flow through semiconductor superlattices [312], though they have been contested recently [313]. However, experimental realization of kicked harmonic oscillator using light beams has been achieved [314], though a proposal based on ion-traps [315], to the best of our knowledge, does not seem to have been implemented yet.

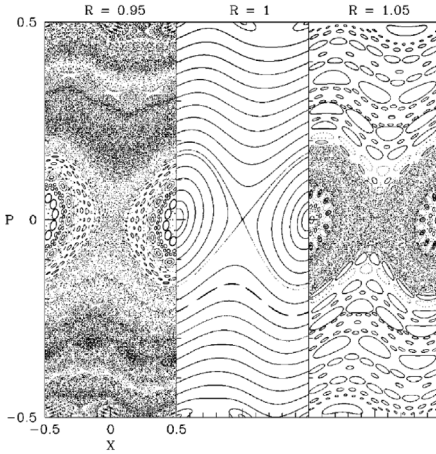


Fig. 16. Poincaré section for the kicked rotor in infinite well system. This is a non-KAM system. Yet for $R = 1$ this reduces to standard kicked rotor and invariant tori as dynamical barriers are visible in the middle panel. However, if $R \neq 1$, it is a non-KAM system and is characterized by the absence of dynamical barriers to transport.

Source: Taken from Ref. [316].

Of the two central assumptions of KAM theorem, kicked oscillator in Eq. (84) violates one of them related to classical degeneracy. Is it possible to violate the other assumption related to smoothness of potential? It turns out that if the kicked rotor is placed ‘inside’ a confining potential with hard walls such as the finite or infinite square well potential, then it is a non-KAM system [316–321]. The Hamiltonian in this case would take the form,

$$H_w = \frac{p^2}{2M} + V_w(x; L) + K \cos(2\pi x/\lambda) \sum_{n=-\infty}^{\infty} \delta(t-n), \quad (86)$$

and its dynamics can be written down in terms of a map [318]. In this, $V_w(x)$ is either a infinite square well or finite well potential and λ is the wavelength of the external field. Note that the problem has another spatial scale defined by the width L of the potential well. Hence, dynamics is governed, apart from kick strength K , by the ratio $R = L/\lambda$. For $R \neq 1$, as would be expected for a non-KAM system, the phase space is devoid of invariant tori that prevent global transport. If $R = 1$, this simply reduces to standard kicked rotor despite the singularity in the potential, and a general condition for this to happen is obtained in Ref. [319]. Fig. 16 shows these distinguishing features arising in a non-KAM system. If $V_w(x; L)$ is a finite potential well, the classical dynamics is more richer and, quite unusually, the potential barriers induce subdiffusive growth of energy. The standard kicked rotor exhibits regular to super-diffusion, but not subdiffusion. Taken together, the singularity in the potential (or, equivalently its non-KAM character) and classical subdiffusive energy growth have a strong influence in the quantum dynamical localization. In particular, the eigenstates tend to display localization with power-law, as opposed to, exponential profiles [322]. This appears to be a generic result in case of kicked systems with singular potentials [323,324], though a rigorous result to this effect is probably missing. Further, this is one of the cases where non-integral \hbar -scaling is seen and the non-integral exponent is related to classical subdiffusive exponents [319].

7.3. Kicked Bose-Einstein condensates

The quantum kicked rotor variants discussed until this point are effectively the dynamics of a single kicked particle. It is natural to investigate if interactions modify our understanding of transport and localization in chaotic systems. In particular, it is of interest to study the far-from equilibrium dynamics of interacting many-body systems, such as the Bose-Einstein condensates (BEC), both for exploring new physics and due to the central role they are expected to play in the emerging area of quantum technologies.

A best starting point for this pursuit, both from theoretical and experimental perspective of kicked systems, is to study the effect of periodic kicks on the Bose-Einstein condensates. The condensates encapsulate many-body interactions and, within the mean-field approximation, are described by an additional nonlinear term in the Schrödinger equation [325]. Now, the governing equation for BECs is a nonlinear partial differential equation, as opposed to the linear Schrödinger equation for kicked rotor. Much of the machinery of classical nonlinear dynamics – instability, bifurcations, chaos – can be applied here. Importantly, the missing ingredient in the quantum kicked rotor, namely, the instability of the wavefunction now has become a realistic possibility that can have experimental consequences as well. In contrast, the quantum kicked rotor, governed by the linear Schrödinger equation, does not display instability or chaos. In general, the central theme in the study of kicked BECs is to understand the stability properties, including transition to instability and chaos, under a

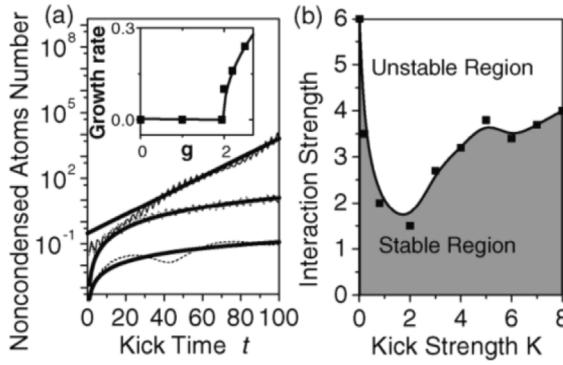


Fig. 17. (a) Number of non-condensed atoms versus time with $K = 0.8$ and, for curves from bottom to top, $g = 0.1, 1.5$ and 2.0 . Note the near exponential increase for $g = 2.0$. The inset shows the growth rate of non-condensed atoms as a function of g . (b) Phase diagram in the space of g and K that shows the stable and unstable regimes.

Source: Taken from Ref. [326].

variety of conditions and potentials. Not the least important is the question about the survival of the dynamically localized modes in the presence of interactions.

The governing equation of motion, the Gross–Pitaveskii (GP) equation, for condensate of N atoms in a toroidal trap is

$$i \frac{\partial}{\partial t} \psi(\theta, t) = \left(-\frac{1}{2} \frac{\partial^2}{\partial \theta^2} + g|\psi|^2 + K \cos \theta \sum_{n=-\infty}^{\infty} \delta(t - nT) \right) \psi(\theta, t), \quad (87)$$

where θ is the azimuthal angle and periodic boundary conditions $\psi(\theta, t) = \psi(\theta + 2\pi, t)$ are applied. Further, it is assumed that the radius R of the trap is far greater than its thickness r that the dynamics is effectively one-dimensional. In this, K is the kick strength, $g = 8NaR/r^2$ is the interaction strength and it depends s -wave scattering length a . Experiments with BECs afford an excellent control due to the tunability of g through Feshbach resonances from attractive to repulsive interactions. Gross–Pitaveskii equation in Eq. (87) is nonlinear unlike the Schrödinger equation which is linear. We must then expect to see nonlinear effects. To understand the disintegration of BECs into non-condensed atoms, GP equation requires to be supplemented with correction through Bogoliubov–de Gennes theory [327] which describes non-condensed atoms in terms of Bosonic quasiparticles or “excitations”. This is typically the framework – GP equation and Bogoliubov excitations through Castin and Dum approach [328] – in which most of the results described below have been obtained.

To see the effect of nonlinearity and interactions, let us consider BEC in a toroidal trap given in Eq. (87) and the baseline can be taken to be the kicked rotor ($g = 0$). If the parameters are set to quantum anti-resonance ($T = 2\pi$) and the initial state is $\langle \theta | 0 \rangle = 1/\sqrt{2\pi}$, then the mean energy $\langle E \rangle$ (at $g = 0$) will oscillate and remain bounded as a function of time t . Another possibility is to start from a dynamically localized state with appropriate choice of K . In both cases, the emerging scenario is nearly the same. In general, for small kick strengths and weak interactions, $K < 1$ and $g \lesssim 1$, quasiperiodic motion ensures that the condensates are preserved by and large, *i.e.*, the growth in the number of non-condensed atoms is slow – polynomial in time (see Fig. 17(a)). This must be compared with the case of large kick strengths $K \gg 1$ and stronger interactions $g \gg 1$. In this regime, quasiperiodic motion gives way to diffusive increase of energy though weaker than the quasi-linear diffusion of standard classical kicked rotor. As seen in Fig. 17(a), even for $K = 0.8$ and $g = 2$, this is accompanied by an exponential increase in the number of non-condensed atoms, an indicator of instability in the Bose–Einstein condensates. The boundary between the regimes of stability and instability depend on both g and K [326]. The onset of instability might appear to suggest onset of chaos as well. However, other evidences point towards resonances in the low-lying modes giving rise to exponential proliferation of non-condensed atoms rather than chaos in the mean-field limit [329]. Another theoretical approach to this problem based on an analysis of nonlinear Schrödinger equation argues against chaotic dynamics due to existence of Lax pair (a signature of integrability) and countable infinite set of conserved quantities [330], though if the interaction strength is made time-dependent, $g \rightarrow g(t)$, then Lax pair does not exist implying possibility non-integrability including chaos [331]. Indeed, numerical results do exhibit chaos. Another perspective is to go beyond the mean-field approximation through explicit conservation of the total number of atoms, and this suggests damping of non-condensate fraction resulting in coherence in the system rather than unbounded exponential increase [332,333]. Experiments of kicked BECs in toroidal trap are yet to give definite results, though for δ -kicked BECs in harmonic trap chaotic dynamics has not been observed and this is attributed to finite width of condensate’s momentum distribution at initial time [334]. In any case, the question of chaotic dynamics of BECs in toroidal trap remains not yet satisfactorily settled, though the fraction of non-condensed atoms appears to grow, and in some cases, exponentially.

Do interactions sustain the dynamical localization in the standard kicked rotor? An early work that addressed this question, due to Dima Shepelyansky, shows that by applying Chirikov’s overlapping resonance criteria a critical strength

of nonlinear interaction $g = g_c$ exists above which localization is destroyed [335]. For $g > g_c$, a power-law diffusion over unperturbed states of the form

$$(\Delta n)^2 \propto g^{4/5} t^{2/5} \quad (88)$$

is predicted. This is in a regime of weak nonlinearity. The expectation is that this could be valid for nonlinear lattice models as well, in view of the connection of the kicked rotor model with Anderson lattice model. However, more recent works have argued that the universality of the results might require revision [336,337]. Numerical simulations within the GP framework for the nonlinear disordered systems have shown that dynamical localization is indeed replaced by subdiffusive spreading of the form $E \sim t^\alpha$. Two regimes of spreading can be identified; first is a transient strong-chaos regime with $\alpha = 1/2$, and an asymptotic weak-chaos regime with $\alpha = 1/3$. For an explanation and reconciliation with 2/5 subdiffusive growth, see Ref. [337]. The existence of two regimes can be explained via mode interaction as follows. If the solution of $g = 0$ case can be written in angular momentum basis, $\psi(\theta, t) = (2\pi)^{-1} \sum_n A_n(t) e^{in\theta}$, and if the nonlinear term is treated as a perturbation, then an approximate map [335]

$$A_n(t+1) = \sum_m (-i)^{n-m} J_{n-m}(K) A_m(t) e^{-i\frac{\hbar T}{2} m^2 + ig|A_m|^2} \quad (89)$$

can be obtained. The key factor is the nonlinear quasienergy shift $\Delta\phi_m = g|A_m|^2$. These two regimes depend on the relative values of the mean frequency spacing $\Delta\omega$ between interacting modes and $\Delta\phi_m$. If $\Delta\phi_m > \Delta\omega$, then resonant interaction among eigenmodes leads to strong-chaos. If mean frequency spacing dominates, then minimal resonant interaction leads to weak-chaos. Though it must be emphasized that even in the strong-chaos case, the wavepacket spreading is subdiffusive, rather than normal diffusion. Going beyond one-dimension, localization is also destroyed in higher dimensional kicked nonlinear rotors [338], as well as in the relative momentum space of two rotors coupled through contact interactions [339]. In the nonlinear versions of kicked rotor and Anderson lattice models, destruction of localization through subdiffusive spreading appears as a generic feature [340] and the associated subdiffusive exponents depend on the dimension of the problem and the exponent of the nonlinear term in the wave equation [337,341]. Quasiperiodic kicked rotors are analogous to higher dimensional Anderson models, and this will be discussed in Section 9.2. Recently, this equivalence has been exploited to study the dynamics of BEC through GP equation and subdiffusive regime was not observed. In this, for small nonlinearity, a quasi-insulator to metal transition, analogous to the metal-insulator transition in Anderson model, has been observed [342]. Going beyond localization, interesting quantum resonance effects exist in quantum nonlinear kicked rotors [343,344], and has been experimentally observed as well [185].

7.4. Molecular kicked rotors

The idea of quantum rotor, in its textbook sense, applies to linear molecules, and some good examples are N₂, CO₂ and ICl. It is then natural to excite molecular rotations through application of external pulses of suitable frequency [345]. The standard quantum rotor is a two-dimensional system with one rotational degree of freedom with angular momentum $-\infty \leq J \leq \infty$. In contrast, the three-dimensional (3D) rotors have two angular degrees of freedom, polar and azimuthal. An important distinction between the two rotors is that negative angular momentum, $J < 0$, is not allowed for 3D rotors and it has consequences, such as the edge states that populates the vicinity of angular momentum quantum number $J = 0$. The edge states are similar to the surface states in crystalline solids and arise in 3D rotors, but not in 2D rotors, under some conditions. The system of interest is modeled as a periodically kicked 3D rotor, whose Hamiltonian is

$$H = \frac{\hat{J}^2}{2} - K \cos^2 \theta \sum_{n=1}^N \delta(t - (n - 1/2)T). \quad (90)$$

In this, K is the kick strength and the potential has been chosen to be $\cos^2 \theta$ to match with experiments. The possibility of observing dynamical localization was proposed [346,347] and more recently it was observed in an experiment in which N₂ molecules were kicked with femtosecond pulses [348]. Other molecular kicked rotor experiments have observed resonance effects [349] and rotational Bloch oscillations [350], the latter being a solid state phenomenon in which electronic motion in a lattice oscillates when subject to constant directional force. The existence of edge localized states [351] sets the molecular rotors apart from the other experimental quantum kicked rotor test beds. In this case, an initial state in $J = 0$ angular momentum state continues to be localized predominantly at $J = 0$ in spite of the kicks being imparted to the system with kick periods of $T = (p/q)t_{rev}$ (p, q mutual co-primes), a rational multiple of revival period t_{rev} for the molecular kicked rotor. Edge states can also exist in 3D kicked rotor with the kicking potential function $V(\theta) = \cos \theta$ [352]. The idea of molecular rotors opens up possibilities for studying condensed matter phenomena beyond quantum localization within the framework of kicked rotors. One drawback at the present time is that experiments cannot be sustained for more than about 20 kicks.

7.5. Spin-1/2 kicked rotor

Another interesting extension of kicked rotor is to couple it with an internal spin degree of freedom [353]. The simplest choice is to couple the standard kicked rotor to a spin in the Pauli basis. Then, the symmetric form of unitary operator for this problem becomes [353]

$$\hat{U} = \exp\left(-i\frac{p^2}{4\hbar}\right) \exp\left(-i\frac{K}{\hbar} \sum_{l=0}^3 V_l(\theta) \sigma_l\right) \exp\left(-i\frac{p^2}{4\hbar}\right), \quad l = 0, 1, 2, 3, \quad (91)$$

where σ_0 and σ_l are, respectively, the identity matrix and standard Pauli matrices. Further, K is the kick strength and the kicking potential is given by 2π -periodic function $V_l(\theta)$. This can be mapped to a tight binding model [354] and hence the eigenfunctions are localized with localization length not too different from that of the standard kicked rotor. In fact, this model in an external magnetic field is also equivalent to the Anderson model [354]. By appropriate choice of potential function $V_l(\theta)$ in Eq. (91), it is possible to tune the anti-unitary symmetries such that, in the sense of random matrix theory, the suitable symmetry classes would correspond to Dyson index $\beta = 1, 2, 4$. The transition between the symmetry classes is smooth. It is shown that the localization length λ depends on symmetry class, i.e., $\lambda(\beta) = \beta\lambda_0$ for a fixed classical diffusion constant [355], with λ_0 being the localization length for the standard ($\beta = 1$) kicked rotor. Generally, it is of interest to explore how kicked systems (at least those that exhibit dynamical localization) respond to symmetries and changes in the symmetries of the system. A recent experiment shows that the kicked rotor, supplemented with artificial gauge fields in time, is able to distinguish between parity and time-reversal symmetry classes [356].

As would be expected, kicked rotor coupled to a spin-1/2 particle expands the gamut of possibilities including realization of quantum Hall effect in effectively a one-dimensional system (by using an incommensurate frequency) [357,358]. Kicked rotor based system is computationally efficient to study quantum Hall effect than the many-body spin models. In particular, it becomes experimentally feasible in cold atoms in optical lattice systems. In a broader context, kicked rotor variants are increasingly employed as quantum simulator for much more complex condensed matter systems — some recent works include Floquet topological phases in double kicked rotor coupled to spin-1/2 particle [359] and a far more involved kicked model dubbed the “kicked Hall system” [360,361].

8. Higher-dimensional kicked rotors

The discussions in Section 3 were centered on one-dimensional kicked rotor and its variants. In the next sections, focus will be on higher dimensional kicked rotors. Primary motivations to explore higher dimensional rotors are the following — firstly, from the classical dynamics point of view, Arnold diffusion is expected in autonomous classical dynamical systems with degrees of freedom $d \geq 3$ or in time-dependent systems with $d = 2$. Coupled kicked rotor would fall in the latter class. Secondly, given the analogy between the one-dimensional quantum kicked rotor and the Anderson localization discussed in Section 5.2, it is natural to explore if this analogy carries over to the higher dimensions as well. Since metal-insulator transitions shows up in Anderson model in dimension $d > 2$, it is of interest to explore occurrence of equivalent localization-delocalization transitions in higher dimensional kicked rotors.

8.1. Arnold diffusion

Physically, Arnold diffusion arises because the dynamical barriers (KAM curves) for $d < 3$, which prevent trajectories from wandering everywhere in phase space, are not barriers for $d \geq 3$. To make the discussion concrete, let us consider a $d = 2$ nonlinear system with Hamiltonian in action-angle variables: $H(I_i, \theta_i) = H_0(I_i) + \epsilon V(I_i, \theta_i)$, with $i = 1, 2$ and $\epsilon \ll 1$ is a parameter. If $\epsilon = 0$, H_0 is integrable, and nonlinear resonances between the two degrees of freedom exist if the condition $m_1\omega_1 + m_2\omega_2 = 0$ is satisfied, where $m_{1,2}$ are integers and $\omega_{1,2}$ are frequencies of motion dependent on actions. The phase space regions in the vicinity of such resonances constitute a dense resonance layer enclosed between irrational tori. The dynamics within each layer can have stochastic component as well, though a trajectory cannot move from one layer to another. This is because in case of $d = 2$, phase space has four dimensions, and dynamics takes place on a three dimensional energy shell due to energy conservation, and irrational tori are two dimensional. Then, irrational tori are hard barriers through which no transport is possible. If a mild perturbation is applied, resonance layers continue to remain enclosed between KAM invariant surfaces (which are deformed from irrational tori) as guaranteed by the KAM theorem (see Section 4). The KAM surfaces inhibit transport of trajectories from one layer to another.

This scenario is modified in systems for which $d > 2$ because KAM surfaces cannot act as barriers between resonance layers. In d degree of freedom system, dimension of tori is d and hence it cannot divide the $2d - 1$ dimensional energy shell into an “inside” and “outside”. This allows large variations in action (in action space) for a trajectory along a resonance layer. Secondly, the nonlinear resonances can actually intersect and form a dense network in phase space. As argued by Arnold, this is a generic feature for $d > 2$ systems [362], and a rigorous proof of this provided by Holmes and Marsden [363]. Any stochastic trajectory in a separatrix region of a nonlinear resonance can now wander through the network of resonances to other parts of phase space. For $d > 2$, the combination of large variations in action along a resonance layer and the dense web created by intersecting resonance layers allows trajectories to reach almost any part

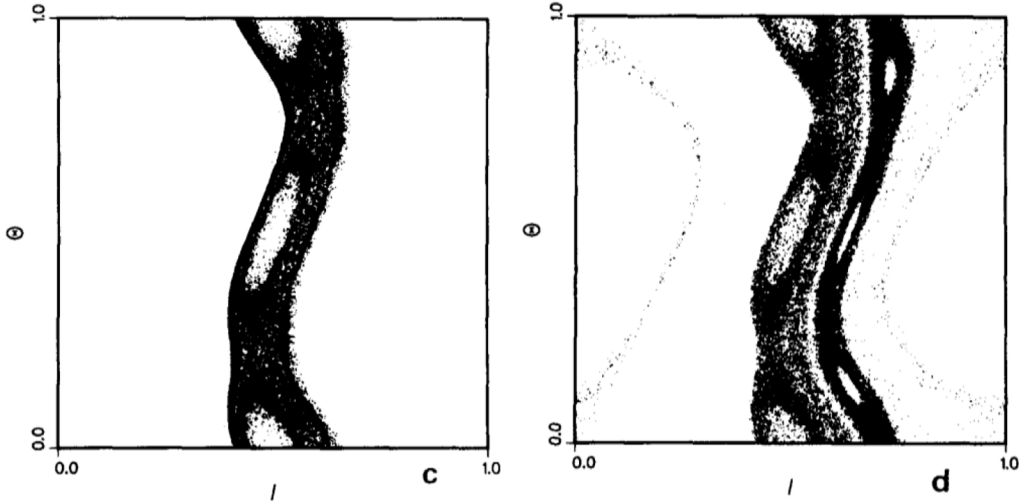


Fig. 18. Arnold diffusion in coupled kicked rotor with $K_1 = K_2 = 0.8$ and $b = 0.02$. (left) Phase space for up to $n = 5 \times 10^4$ iterations starting from just one initial condition. A trajectory starting from inside a resonance layer stays in it for long time. (right) phase space drawn with n from 1.5×10^5 to 2×10^5 . Note that another resonance layer is now populated by a rather slow process of Arnold diffusion.
Source: Taken from Ref. [370].

of phase space. This type of unstable motion was first theoretically shown by V. I. Arnold [362] (English reprint available in Ref. [364]) and is now called the Arnold diffusion. This diffusion does not require a minimal perturbation strength. This must be contrasted with the KAM scenario which requires a minimum perturbation strength for transition to chaos. A detailed phenomenology of Arnold diffusion and associated theoretical developments are treated in monographs [17,79], and for a physically motivated presentation see Ref. [365]. Arnold diffusion rates were first theoretically obtained by Chirikov for a many-dimensional oscillator [89,123], and also for a time-dependent quartic oscillator [366]. First numerical results on coupled standard map were obtained by Froeschlé [367]. Theoretical estimates based on a local model of three resonances show that the resonance layers are exponentially thin in the perturbation parameter ϵ and the local rate of diffusion through these layers is generally small. For many resonances, a rigorous upper bound for diffusion rate was obtained by Nekhoroshev [368], though it is typically much larger than computed rates. In general, if $d \geq 3$, Arnold diffusion takes place even before the last KAM tori breaks at some critical perturbation strength $\epsilon = \epsilon_c$, which is approximately unity in the case of 1D kicked rotor. A simple tractable example of Arnold diffusion is studied in Ref. [81], and recently a more realistic example (not based on a kicked system) relevant for vibrational states of molecules is presented in Ref. [369].

As the one-dimensional standard mapping in Eq. (9) is sufficiently well understood, its natural extensions in higher dimensions come in handy to explore the occurrence of Arnold diffusion. In a straightforward extension to higher dimensions, a standard mapping in four-dimensional phase space can be constructed as [370],

$$\begin{aligned} I_{n+1} &= I_n + K_1 \sin \theta_n + b \sin (\theta_n + \phi_n), \\ \theta_{n+1} &= \theta_n + I_{n+1}, \\ J_{n+1} &= J_n + K_2 \sin \phi_n + b \sin (\theta_n + \phi_n), \\ \phi_{n+1} &= \phi_n + J_{n+1}. \end{aligned} \tag{92}$$

In this, (I, θ) and (J, ϕ) are the action and angle variables in each degree of freedom, $b \ll 1$ is the parameter that couples them, and $K_{1,2} < 1$ are the kick strengths. Fig. 18(a) shows numerical simulation of Eq. (92) for up to 5×10^4 iterations. One single initial condition is seen to fill the entire resonance layer. For longer times, shown in 18(b), the same trajectory invades a second resonance layer due to Arnold diffusion [370]. For this model, it has been shown that while the local diffusion rates are consistent with a theoretical model of three resonances [370,371], global diffusion rates depend on local diffusion rates and the volumes occupied by the stochastic layers [372].

Beyond kicked rotor, direct evidence of Arnold diffusion has been numerically demonstrated in a quasi-integrable system [373], and for a Hydrogen atom in crossed electric and magnetic fields [374]. Quite interestingly, Arnold diffusion leaves its trail in quantum regime too in somewhat weaker form than its classical counterpart – quantum diffusion rate being slower than the classical. This happens in weakly coupled oscillators in external fields [375–377], in $d = 3$ open billiards problem [378] and in atoms in driven two-dimensional optical lattices [379]. These effects arise if the quantum wavefunctions are influenced by classical resonance networks provided the width of resonance layers is larger than the effective Planck constant in the problem. Arnold diffusion might see a revival of interest [380–382] in the context of higher dimensional and many-body problems that have gained traction in quantum chaos [375,383] and condensed matter physics [384–387].

8.2. N-dimensional kicked rotor

There are several inequivalent approaches to constructing higher dimensional kicked rotors, each one useful in a specific scenario. The case of $N = 2$ [388] and $N = 3$ [389] were studied earlier. More recently, N -dimensional kicked rotor [390,391] as a generalization of one-dimensional case to N spatial dimensions has attracted attention. In this case, the scaled Hamiltonian is given by

$$H(t) = \sum_{i=1}^N \frac{\tau_i p_i^2}{2} + K \prod_{i=1}^N \cos x_i \sum_n \delta(t - n), \quad i = 1, 2, \dots, N, \quad (93)$$

where $\{x_i\}$ are the position coordinates and $\{p_i\}$ are the corresponding conjugate momenta along the i -th direction. The stochastic parameter K that also acts as the coupling parameter in this case and $\{\tau_i\}$ determine the global dynamics of the system, and τ_i are chosen to be irrational numbers which are not too close to any rational multiple of π . Ensuring that $\tau_i, i = 1, 2, \dots, N$ is incommensurate with one another makes it a higher dimensional system. In general, a quantitative understanding of the role of τ_i in the emergence of localization effects remains an open number theoretic problem.

The Hamilton's equations of motion can be reduced to a set of $2N$ difference equations or maps:

$$p_i^{n+1} = p_i^n + K \left(\prod_{j=1, j \neq i}^N \cos x_j^n \right) \sin x_i^n \quad (94)$$

$$x_i^{n+1} = x_i^n + \tau_i p_i^{n+1} \quad (95)$$

In these, the superscript $n = 0, 1, 2, \dots$, represents kick number (in units of kick period) and subscript $i = 1, 2, \dots, N$ represents the direction. As anticipated, for $K > K_c$ the “area” of regular regions in the phase space becomes very small and there are no transporting trajectories. For sufficiently strong kick strengths, the position variable becomes uncorrelated and leads to the usual quasi-linear approximation. In general, it is non-trivial to visualize the dynamics of higher dimensional kicked rotors in phase space [392,393]. Then, the dynamics represented by Eqs. (94)–(95) is equivalent to a random walk in the momentum variable. The diffusion constant in the i th direction is,

$$D^{(i)} = \left(\frac{1}{2\pi} \right)^N \iiint \dots \int_0^{2\pi} \tau_i \left(K \left(\prod_{j=1, j \neq i}^N \cos x_n^{(j)} \right) \sin x_n^{(i)} \right)^2 dx^1 dx^2 \dots dx^N. \quad (96)$$

For sufficiently large K and long time evolution, the diffusion constant in any direction depends on the value of τ in that direction and is given by,

$$D^{(i)} \approx \tau_i \frac{K^2}{2^N}. \quad (97)$$

For $K \ll 1$, a perturbative approach helps in computing D^i . Following the standard KAM scenario, as K increases, the invariant tori are gradually destroyed. Global phase space transport begins when kick strength crosses chaos border at $K = K_c$. In general, K_c decreases as system dimensionality increases. For any value of dimension N , the diffusion coefficient D (as a function of K) oscillates about its quasi-linear value D_0 [125,126], though its amplitude decreases as the number of dimensions increase. The correlation between different directions i and j is $C(x^i, x^j) = \langle x_t^i x_{t+T}^j \rangle \rightarrow 0$. As in the case of one-dimensional kicked rotor, diffusive dynamics is dominant in $K \gg K_c$ limit. This is evident in Fig. 19 which shows the mean energy as a function of time (in units of kick period) in each dimension for two- and three-dimensional kicked rotor for $K = 5$, and $\tau_1 = \sigma\alpha$, $\tau_2 = \alpha$ and $\tau_3 = \alpha/\sigma$, where $\sigma \approx 1.618$ (the golden mean) and α is a random number from uniform distribution.

8.3. Quantum dynamics of N -dimensional kicked rotor

The potential function being periodic in time, the time-dependent Schrödinger equation is a straightforward generalization of the 1D case in Eq. (28). Then, the quantum dynamics can be conveniently studied by considering the unitary time evolution operator,

$$\widehat{U} = \widehat{U}_{\text{kick}} \widehat{U}_{\text{free}} = \exp \left(-\frac{i}{\hbar_s} \widehat{V}(\mathbf{x}) \right) \exp \left(-\frac{\widehat{T}(\mathbf{p})}{\hbar_s} \right), \quad (98)$$

in which

$$V(\mathbf{x}) = K \prod_{i=1}^N \cos \widehat{x}_i, \quad T(\mathbf{p}) = \sum_{i=1}^N \frac{\tau_i \widehat{p}_i^2}{2}, \quad \text{and} \quad \widehat{p}_i = -i\hbar_s \frac{\partial}{\partial x_i}. \quad (99)$$

The scaled Planck's constant is \hbar_s . The operator \widehat{U} can be written in the momentum basis $|\mathbf{n}\rangle = |n_1, n_2, \dots, n_N\rangle$. In this, the state $|n_i\rangle$ is the solution of the eigenvalue problem $\widehat{p}_i |n_i\rangle = n_i \hbar_s |n_i\rangle$, $i = 1, 2, \dots, N$. By following the recipe applied

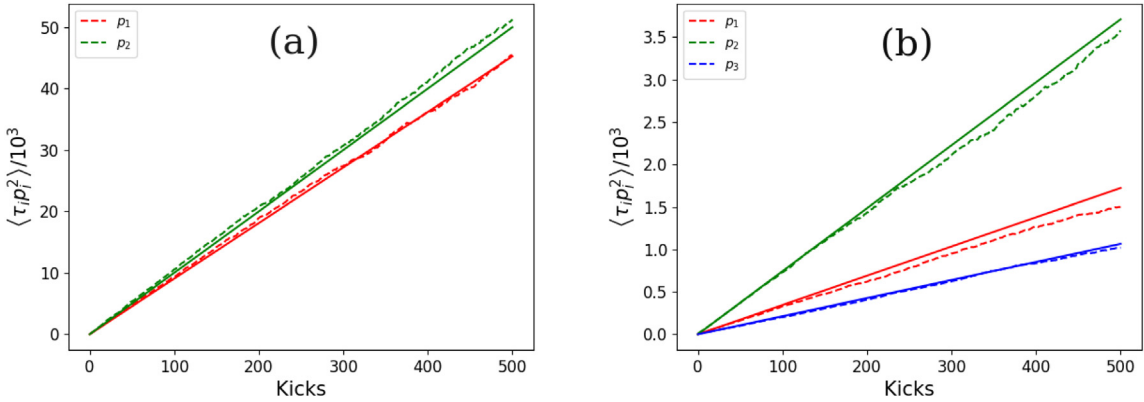


Fig. 19. Plots of average classical energy ($\langle \tau_i p_i^2 \rangle$) vs kick number for (a) 2D kicked rotor, and (b) 3D kicked rotor at $K = 5$, and $\tau_1 = \sigma\alpha$, $\tau_2 = \alpha$ and $\tau_3 = \alpha/\sigma$, where $\sigma \approx 1.618$ (the golden mean) and α is a random number from uniform distribution in $[0, 1]$. Dashed lines are from numerical simulations and solid lines from theory.

in the case of 1D kicked rotor in Section 5.2, it is possible to map this system to N -dimensional Anderson model. The main ingredient is the transformation (equivalent to Eq. (43) for 1D),

$$W(\mathbf{m} - \mathbf{n}) = \frac{-1}{(2\pi)^N} \int_{-\pi}^{\pi} d\mathbf{x} \tan\left(\frac{V(\mathbf{x})}{2}\right) e^{-i\mathbf{x} \cdot (\mathbf{m} - \mathbf{n})} \propto \exp(-B|\mathbf{m} - \mathbf{n}|), \quad (100)$$

where B is typically a decreasing function of K . This integral cannot be evaluated analytically for $N > 1$ and must be numerically performed. In Ref. [390], this is systematically done for $N = 2, 3$ for a different coupled kicked rotor. Let ψ be an eigenstate of \hat{U} such that $\hat{U}\psi = e^{-i\omega}\psi$, where ω is the quasi-energy. The kick operator \hat{U}_{kick} is written in terms of $W(\mathbf{m} - \mathbf{n})$ and going through similar set of algebra as in Section 5.2, we obtain the following lattice model:

$$E \psi_{\mathbf{n}} = \epsilon_{\mathbf{n}} \psi_{\mathbf{n}} + \sum_{\mathbf{m}} W(\mathbf{m} - \mathbf{n}) \psi_{\mathbf{m}} \quad (101)$$

where E is the energy and the onsite potential is

$$\epsilon_{\mathbf{n}} = \tan\left(\frac{\omega}{2} - \frac{1}{4} \sum_{i=1}^N \hbar_s \tau_i n_i^2\right). \quad (102)$$

Thus, Eq. (101) has the same form as the Anderson model in N -dimensions, with $W(\mathbf{m} - \mathbf{n})$ playing the role of hopping amplitude. The short range hopping in Eq. (100) and pseudo-randomness of the onsite potential together points to an equivalence of kicked rotor with the Anderson model. This mapping has been discussed in Ref. [389] and also explicitly shown for the case $N = 2$ in Ref. [388].

In higher dimensions, existence of a mapping to Anderson model does not necessarily guarantee the existence of localized states at arbitrary kick strengths. In fact, a major prediction of the localization theory [394] is that the two-dimensional version of Eq. (101) has localized states for any disorder and energy, though the localization length can become arbitrarily large. However, it also predicts a metal-insulator (or, equivalently, delocalization-localization) transition in systems of dimension $d > 2$ at a critical value of disorder. The critical disorder increases with the spatial dimensionality of the system. An interesting question is to verify if the predictions of the localization theory for a lattice model holds good in the context of an “equivalent” kicked rotor. On the other hand, we now have an Anderson model in Eq. (101) that is different in the sense that its onsite potential is *pseudo-random* and not random, and hopping is not just to nearest-neighbor sites. Then, it is equally important to decide if localization theory predictions are respected by a pseudo-random model with somewhat long range hopping amplitudes. As will be seen in the next sections, the global behavior of the 3-dimensional kicked rotors is similar to the N -dimensional Anderson model.

Before any comparison with localization theory can be made, let us first look at the simulation results from $N = 2$ and $N = 3$ quantum kicked rotors. We compute the mean energy along the i th direction defined as,

$$\langle E_i \rangle = \left\langle \frac{\tau_i p_i^2}{2} \right\rangle = \left\langle \Psi(t) \left| \frac{\tau_i p_i^2}{2} \right| \Psi(t) \right\rangle, \quad (103)$$

and the momentum density given by

$$f(p_i) = |\langle p_i | \Psi(t) \rangle|^2. \quad (104)$$

Fig. 20 displays both $\langle E_i \rangle$ and $f(p_i)$ for $N = 2$ and 3 cases of kicked rotor. In the $N = 2$ rotor (Fig. 20a, b), evolution of $\langle E_i \rangle$ mean energy shows saturation for two different kick strengths, a signature of localization. For $K = 4$ in Fig. 20(b),

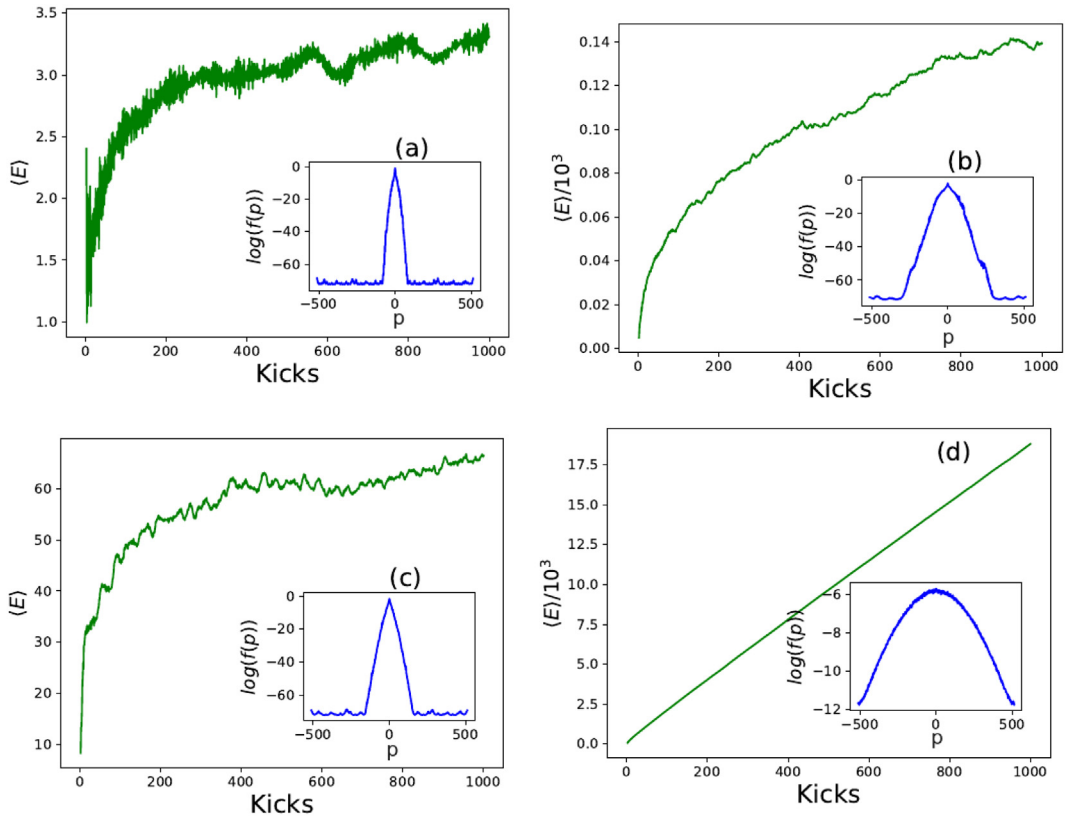


Fig. 20. Mean energy $\langle E \rangle$ plotted against kick number (time) for quantum kicked rotor in 2- and 3-dimensions. The inset shows the momentum distribution $f(p)$ at kick number 1000. (a) $N = 2, K = 1$, (b) $N = 2, K = 4$, (c) $N = 3, K = 1$, (d) $N = 3, K = 4$.

$\langle E \rangle$ would localize as $t \rightarrow \infty$. of $f(p_i)$ (shown as inset) reveals exponential profile of its localized eigenstates. It is evident that the localization length is larger for $K = 4$ than for $K = 1$. Indeed, in 2D, the localization length ξ is an exponential function of kick strength: $\xi(K) \sim \exp(K)$ [388], and is confirmed by atom-optics based experiment as well [395] (an earlier experiment appears to suggest that 2D quasi-periodic kicked rotor may also witness a loss of localization [396]). However, for $N = 3$, localization occurs only for $K < K_c$, where K_c is the kick strength at the localization-to-delocalization transition point. For $K = 1$, the mean energy growth appears to saturate and the wavefunction has an approximate exponential profile (see inset of Fig. 20(c)). For $K = 4$, the mean energy $\langle E_i \rangle$ is diffusive, and the wavefunction has Gaussian profile (as shown in the inset). From Fig. 20, it is clear that there is a transition from localized (insulator) to diffusive (metal) phase upon increasing the kicking strength K for the kicked rotor in 3-dimensions, but this transition is absent in 2-dimensions.

Another corroborative evidence can be obtained through spectral statistics. It can tell us if a transition exists at all. In Section 5.4, it was argued that the localized (insulator) regime corresponds to Poisson spectral fluctuations as shown in Fig. 11(a). On the other hand, in the delocalized (metallic) regime the fluctuations have the Wigner-Dyson form as seen in Fig. 11(b). The spectral statistics of 3D kicked rotor in Fig. 21 reveals a Poisson type fluctuations at $K = 1.6$ and Wigner-Dyson type fluctuations at $K = 3.6$ (see Ref. [389] for values of τ_i used in generating this figure). This implies that a spectral transition must exist somewhere in the range $1.6 \ll K \ll 3.6$. It is generally cumbersome to track a critical transition through spectral statistics. Based only on the diagnostic probes such as the energy growth, momentum distribution or spectral statistics, it is difficult to accurately determine the parameter $K = K_c$ for the metal-insulator transition. The critical parameters are accurately calculated in the next sections through an analogy with the elegant theory of one-parameter scaling and finite-size scaling.

8.4. One-parameter scaling theory

In the backdrop of equivalence between N -dimensional kicked rotor and Anderson problem, further insight into localization properties of kicked rotor can be gleaned from progress made in understanding metal-insulator behavior in Anderson model. In this pursuit, the results obtained from the celebrated one-parameter scaling theory (OPT) for

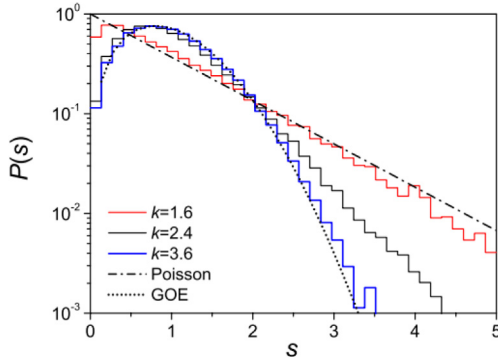


Fig. 21. The level spacing distribution $P(s)$ for three different kicking strengths. A transition from Poisson to Wigner–Dyson statistics must happen in the range $1.6 \ll K \ll 3.6$.

Source: Taken from Ref. [389].

localization [251,394] shall be our guide. For rigorous theoretical calculations of OPT, the readers are directed to Ref. [394]. Here, the broad ideas are indicated using dimensional and scaling arguments. The main premise of the OPT is that macroscopic quantity like the dimensionless conductance $g(L) = G/(e^2/h)$ (G is conductance, e is electronic charge and h is Planck's constant) in a disordered lattice is essentially a scale-dependent quantity. In particular, g at a higher length scale depends on g at a lower length scale, rather than on L itself. Hence, the behavior of g , as a function of size L of the system, determines if the eigenstates are localized or not. The dimensionless conductance is the ratio of two energy scales and is given by

$$g = \frac{E_T}{\Delta}, \quad (105)$$

in which Δ is the mean level spacing, and Thouless energy E_T is defined in terms of the diffusion time-scale τ_D and the classical diffusion coefficient D as $E_T = h/\tau_D$. In this, $\tau_D = L^2/D$ is the time taken to diffuse through the sample. We can make quick estimates as follows. For a d -dimensional system, if n_0 is the number of states in unit interval of energy in unit volume, then the mean energy spacing is $\Delta \propto (n_0 L^d)^{-1}$. In the diffusive limit (or equivalently, when the conductance is large), we have $E_T \propto 1/L^2$. Using these length dependent estimates in Eq. (105), we get $g \propto L^{d-2}$. In case of insulator or small g , the wavefunctions are exponentially localized and conductance is $g \propto e^{-L/l}$, where l is the localization length.

To proceed further, a scale-independent quantity is defined as follows;

$$\beta(g) = \frac{L}{g} \frac{dg(L)}{dL} = \frac{d \log g}{d \log L}. \quad (106)$$

Now, in one dimension $d = 1$, for weak disorder the conductance is $g \propto L^{d-2}$ and consequently $\beta < 0$ and hence we should expect $g \rightarrow 0$ for $L \gg 1$. For strong disorder, $g \propto e^{-L/l}$ and hence, once again $g \rightarrow 0$. Thus, in one-dimension, the states are always localized. In 2D too, for weak disorder $g \gg 1$, $\beta \rightarrow 0$ and implies that g has weak dependence on L . For $g \gg 1$, the states are indeed localized, though the localization lengths can be large. If $g \ll 1$ as in strong disorder, the states are exponentially localized though better estimates will require quantum corrections originating from weak localization effects to be applied. Thus, in 2D, all the states are localized. In 3D, a different scenario emerges. The limiting cases can be examined first. In the regimes of weak disorder ($g \gg 1$) and strong disorder ($g \ll 1$), respectively, we get

$$\lim_{L \rightarrow \infty} g(L) \rightarrow \infty, \quad \text{and} \quad \lim_{L \rightarrow \infty} g(L) \rightarrow 0. \quad (107)$$

As $g(L)$ is a monotonic and smooth function of L , a metal–insulator transition is expected at a critical value of $g = g_c$ independent of L . This scale-invariance is characteristic of the transition. In three dimensions, retaining only the L dependence, the mean level spacing is $\Delta \propto L^{-3}$. The conditions for scale-invariance of conductance at $g = g_c$ will be satisfied if Thouless energy is $E_T \propto L^{-3}$. Using the classical diffusion picture, this is possible only if the mean square of displacement takes the form

$$\sigma_r^2(t) \sim t^{2/3}. \quad (108)$$

Thus, anomalous diffusion, subdiffusion in this case, is expected at the critical transition in three dimensions. With these results from Anderson model, now we are in a position to verify the validity of OPT for a 3D kicked rotor, despite the differences between Anderson model and kicked rotor. The scale-invariance is the main feature to look for at the critical transition, and one possible way to probe this is to construct scale dependent quantities which would converge to a scale-independent value at the transition. This is the idea behind the finite-size scaling theory usually implemented to

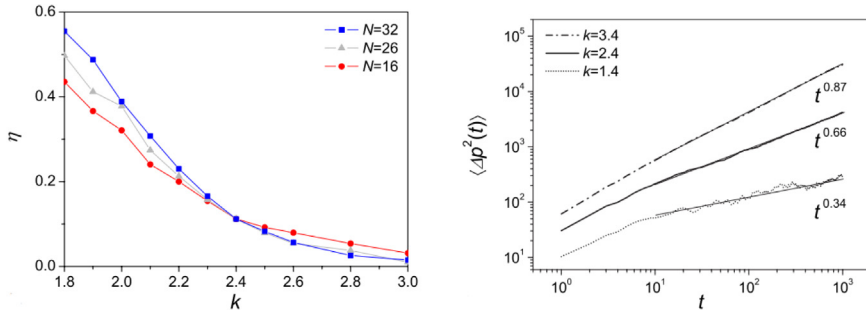


Fig. 22. (left) Scaling function η as a function of K for different system sizes N_b of 3D kicked rotor with $\alpha \approx 17.213$. The critical value of kick strength $K_c \approx 2.35$. Note that all the three curves meet at this point. (right) Quantum diffusion for different kick strengths. Note that near the critical point, $K \approx 2.4$, the diffusion is indeed anomalous with exponent $\approx 2/3$ in agreement with one-parameter scaling theory. Source: Taken from Ref. [389].

determine the parameter at critical transition. In the 3D kicked rotor, the relevant parameter is the kick strength K and critical transition happens at $K = K_c$. In the vicinity of the transition, correlation length diverges as,

$$\xi(k) = \xi_0 |K - K_c|^{-\nu} \quad (109)$$

where ξ_0 is a constant and ν is the exponent characteristic of the transition.

8.5. Critical kick strength and exponent

In this section, focussing on 3D kicked rotor, the critical kick strength K_c and ν will be determined [389]. Finite-size scaling theory is used to evaluate K_c [389]. The main idea behind the finite-size scaling theory is to construct a spectral-correlator as a function of system size L and K . If OPT is the right description, the spectral-correlator becomes size-independent at the point of transition $K = K_c$. The spectral-correlator used in Ref. [389] is a modified and size-dependent level spacing distribution.

In 3D kicked rotor, the levels to be used for analysis are the eigenphases obtained by numerical diagonalization of the operator $\langle \mathbf{m} | \hat{U} | \mathbf{n} \rangle$ (Eqs. (98)–(99) with $N = 3$) in momentum basis. If the number of single particle basis states used is N_b , then the Hilbert space dimension is N_b^3 , and for the present purpose N_b serves as a measure for the size L of the system. Then, one possible choice is to employ spacing distributions and construct $\eta(N_b, K)$ given by [397]

$$\eta(N_b, K) = \frac{\text{var}(s) - \text{var}_{WD}}{\text{var}_p - \text{var}_{WD}} \quad (110)$$

where $\text{var}(s) = \langle s^2 \rangle - \langle s \rangle^2$ is the variance of the numerically computed spacing distribution for the 3D kicked rotor with kick strength K and system size N_b is used to solve for the eigensolutions. The critical transition can be located as $K = K_c$ at which $\eta(N_b, K)$ becomes independent of N_b . In this, $\langle \dots \rangle$ denotes spectral averaging over a single set of $\{\tau_i\}$. From the spacing distributions in Eq. (59), it is easy to get the variance of Poisson distribution (applicable for the insulator phase) as $\text{var}_p = 1$. Similarly, using Eq. (57), the variance of Wigner distribution (for metallic phase) is evaluated as $\text{var}_{WD} \approx 0.286$. It is clear from Eq. (110) that $\eta \rightarrow 0$ will imply that $\text{var}(s) \rightarrow \text{var}_{WD}$, and $\eta \rightarrow 1$ will imply $\text{var}(s) \rightarrow \text{var}_p$.

In Fig. 22, the function η is plotted against K for different system sizes. The critical kicking strength $K = K_c$ at which η is scale-invariant can be clearly identified as the point at which all the three curves meet. For $K > K_c$, η tends to zero, indicating the metallic phase. The dynamics is localized for $K < K_c$ as $\eta \rightarrow 1$. Unlike the Anderson model in 3D in which there is metal-insulator transition upon increasing the disorder strength, in the case of 3D kicked rotor there is an insulator-metal transition as K increases. Both K_c and the critical exponent ν can be numerically calculated by expressing η in terms of correlation length as $\eta(N_b, K) = f(N_b/\xi(K))$. By Taylor expanding about $K = K_c$, we have the explicit form

$$\eta(N_b, K) = \eta_c + \sum_n C_n (K - K_c)^n N_b^{n/\nu} \quad (111)$$

suitable to apply regression. In Ref. [389], keeping up to two terms in this expansion, and by using regression the critical values are found to be $K_c = 2.35 \pm 0.1$ with $\nu = 1.67 \pm 0.27$ for the given set of $\{\tau_i\}$. For the 3D Anderson model, $\nu = 1.5$. The numerical value of ν for kicked rotor is close this value but slightly higher. As expected the localization effects are weaker in a non-random potential of rotor problem compared to the random potential of Anderson model [389]. This is because destructive interference will be less effective in arresting the quantum motion in non-random potential.

It might be remarked that near the critical transition, the spectral fluctuations display the characteristics of both metallic and insulating phases. In the limit of small spacings, $s \ll 1$, the spacing distribution behaves as $P(s) \sim s$, a typical feature of metallic phase. For $s \gg 1$, the spacing distribution follows an exponential decay just like an insulator.

The spectral fluctuations of 3D kicked rotor with $K = 2.4$ display these characteristics in Fig. 21. Nearest neighbor level spacings measure fluctuations on a spectral scale of unit mean spacing. In comparison, other measures such as spectral rigidity or Σ_2 statistics are useful in this context to probe longer range spectral correlations, and these reported in Refs. [398–400].

Finally, the prediction of OPT for the quantum diffusion can also be verified in 3D kicked rotor. The mean energy growth near the insulator–metal transition point is examined. As shown previously the classical motion is diffusive $\langle \Delta p^2(t) \rangle \propto t$ if the classical phase space is fully chaotic. The quantum diffusion depends on K . According to the OPT, for $K \approx K_c$, the quantum diffusion must be anomalous as predicted in Eq. (108). In Fig. 22(b), the quantum $\langle \Delta p^2(t) \rangle$ is shown as a function of K . Clearly, a good agreement is observed with the predictions of OPT. Dynamical localization is avoided for $K > K_c$ and, for $K \approx K_c$ diffusion is anomalous with $\langle \Delta p^2(t) \rangle \propto t^\beta$, $\beta \approx 0.66$. The foregoing results imply that equivalent systems, namely, a disordered system and a quasi-random system, exhibit nearly similar behavior in the close vicinity of the critical transition, and are well described by the one-parameter scaling theory. Though 3D kicked rotor given by Eq. (98) ($N = 3$) provided deeper insight into the connections between the kicked rotor and the Anderson impurity model, as yet, there are no experiments that could verify the results discussed above. Now, we will discuss an alternative model of kicked rotor that provides a test-bed to compare with OPT with the experiments.

9. Quasi-periodic kicked rotor

The kick sequence in a quasiperiodic kicked rotor is deterministic and *aperiodic*. Aperiodicity is introduced by combining several incommensurate periodicities. It turns out that a one-dimensional rotor kicked by N *incommensurable* frequencies is equivalent to a N -dimensional kicked rotor [401]. This idea has important implications, both for theoretical and experimental approaches to localization in quantum systems. By implication, with relative ease, it is possible to work with an 1D system and look for signatures of metal–insulator transition, which otherwise is observable only in 3D (or higher dimensional) Anderson models. Secondly, with straightforward tweaks, 1D cold atoms experiments can be modified to make it “three-dimensional”. This is an especially useful shortcut since genuine 3D kicked rotor is much harder to realize in experiments.

Quasi-periodic kicked rotor (QPKR) is obtained by introducing additional frequencies (or, time-scales) in the temporal domain, such that the kicking potential is modulated by these frequencies along with delta kicks. Thus, QPKR can have more temporal dimensions along with a pre-existing spatial dimension. In general, a quasi-periodic kicked rotor with N incommensurable frequencies is equivalent to a N dimensional Anderson model [401–403]. The Hamiltonian of a quasi-periodic kicked rotor with three incommensurate frequencies is given by

$$H_{\text{qp}} = \frac{p^2}{2} + K \cos x \left[1 + \varepsilon \prod_{i=2}^3 \cos(\omega_i t) \right] \sum_n \delta(t - n). \quad (112)$$

The frequencies present in the system are \hbar_s (through the Talbot timescale) and additional frequencies $\{\omega_i\}$. Here, ε is the strength for the quasi-periodic modulation of the kicking strength K , and $\{\omega_i\}$ represents a set of frequencies. In order to see a true 3-dimensional behavior, all these frequencies must be incommensurate with one another and with π . Stated explicitly, \hbar_s , $\{\omega_i\}$, and π must be incommensurate with each other. Though Eq. (112) is one-dimensional, it is these 3 frequencies, \hbar_s and 2 incommensurate frequencies, that makes it “3-dimensional” in an extended phase space.

The standard 1D kicked rotor in Eq. (7) has time-independent potential $V(x) = K \cos x$, and this supports mapping to the 1D Anderson model (see Section 5.2). In particular, the kick operator U_{kick} in Eq. (29) is time-independent. The quasi-periodic rotor in Eq. (112), on the other hand, has time-dependent potential since kick strength K is modulated by two time-scales. This property does not lend itself to performing the mapping to Anderson model since the unitary kick operator is now time-dependent. However, a different version of the 3D kicked rotor, often dubbed *pseudo* 3D kicked rotor to imply that it has terms linear in momentum, given by

$$H_{3D} = \frac{p_1^2}{2} + \sum_{i=2}^3 \omega_i p_i + K \cos x_1 \left[1 + \varepsilon \prod_{i=2}^3 \cos x_i \right] \sum_n \delta(t - n). \quad (113)$$

can be reduced to the Anderson model [401]. Then, the question is to figure out the relation between these two models. In particular, do they represent qualitatively similar dynamics at equivalent parameter values? It can be shown that the Hamiltonians in Eqs. (112) and (113) display the same transport properties. Let $\psi_{\text{qp}}(x_1, t = 0)$ be the initial state to be evolved under the action of a unitary operator constructed from H_{qp} . The initial state to be evolved under the action of H_{3D} be denoted by $\psi_{3D}(x, t = 0)$. If these initial states are related by

$$\psi_{3D}(x, t = 0) = \psi_{\text{qp}}(x_1, t = 0) \prod_{i=2}^3 \delta(x_i), \quad (114)$$

then both the systems will display the same dynamics. Physically, quasi-periodic system is equivalent to the evolution of a wave in a three dimensional space originating as a pulse from a plane source and the observations are performed perpendicular to the emitter [404,405]. With this understanding, the dynamics displayed by both the systems are identical,

and in particular, classical chaotic dynamics exists in both the systems [404]. The initial state (Eq. (114)) is delocalized along all conjugate momenta except p_1 . Thus, studying transport properties along p_1 direction is equivalent to measuring the momentum distribution $|\psi_{qp}(p, t)|^2$ of QPKR.

9.1. Classical dynamics of quasi-periodic rotor

By integrating the Hamilton's equations of motion, the dynamics of H_{3D} can be reduced to the map:

$$\begin{aligned} p_{1n+1} &= p_{1n} + K \sin x_{1n} (1 + \varepsilon \cos x_{2n} \cos x_{3n}), \\ p_{2n+1} &= p_{2n} + K \varepsilon \cos x_{1n} \sin x_{2n} \cos x_{3n}, \\ p_{3n+1} &= p_{3n} + K \varepsilon \cos x_{1n} \cos x_{2n} \sin x_{3n}, \\ x_{1n+1} &= x_{1n} + p_{1n+1}, \\ x_{2n+1} &= x_{2n} + \omega_2, \\ x_{3n+1} &= x_{3n} + \omega_3. \end{aligned} \quad (115)$$

This relates phase space variables at time $n+1$ to those at time n . To compute the diffusion coefficient, say, along p_3 axis, the starting point is to look at momentum evolution along this direction and it is given by,

$$p_{3n+1} = p_{30} + K \varepsilon \sum_{j=1}^n \cos x_{1j} \cos(x_{20} + \omega_2 j) \sin(x_{30} + \omega_3 j) \quad (116)$$

With three directions, the diffusion coefficient is defined as

$$D_{ij} = \lim_{n \rightarrow \infty} \frac{\langle p_{in} p_{jn} \rangle}{n} \quad (117)$$

where the $\langle \cdot \rangle$ represents an average over the initial conditions. As an example, $\langle p_3^2 \rangle$ can be written as

$$\begin{aligned} \langle p_{3n}^2 \rangle &= K^2 \varepsilon^2 \sum_{j,m=1}^{n-1} \langle \cos x_{1j} \cos x_{1m} \rangle_{x_{10}} \times \langle \cos(x_{20} + \omega_2 j) \cos(x_{20} + \omega_2 m) \rangle_{x_{20}} \times \\ &\quad \times \langle \sin(x_{30} + \omega_3 j) \sin(x_{30} + \omega_3 m) \rangle_{x_{30}} \end{aligned} \quad (118)$$

The correlation function $\langle \cos x_{1j} \cos x_{1m} \rangle_{x_{10}}$ decays exponentially in $|j - m|$, as it happens in the case of 1D kicked rotor. The dominant contribution comes from the diagonal elements, for which $j = m$. After averaging over the initial conditions, the final result is

$$\langle p_{3n}^2 \rangle \approx \frac{K^2 \varepsilon^2}{8} \times n. \quad (119)$$

Similar calculation leads to $\langle p^2 \rangle$ along other directions and the diagonal elements are [403]:

$$\begin{aligned} D_{11} &\approx (K^2/2)(1 + \varepsilon^2/4) \\ D_{22} = D_{33} &\approx K^2 \varepsilon^2 / 8 \quad \text{and} \quad D_{i \neq j} \approx 0. \end{aligned} \quad (120)$$

This is a clear indication that the classical dynamics of Hamiltonian in Eq. (113) is diffusive in all the directions. The diffusion is anisotropic – larger along one principal direction, and smaller in other two principal directions.

The classical simulation results are shown in the left panel of Fig. 23 for $K = 10$, $\varepsilon = 0.8$, $\omega_2 = 2\pi\sqrt{5}$ and $\omega_3 = 2\pi\sqrt{13}$. As it shows, the cross-correlations are negligible (lower-most curves) but the “diagonal” correlations show linear evolution (black, green, red solid lines). Further, the slope of $\langle p_1^2 \rangle$ (black line) is much larger than the slopes of $\langle p_2^2 \rangle$ (in red) and $\langle p_3^2 \rangle$ (in green). The momentum distributions along the three directions are also displayed in right panel of Fig. 23 and the anisotropy is clearly visible in this as well. These distributions have been plotted at time $n = 1000$ and their profiles are Gaussian to a good approximation. The “diagonal” diffusion coefficient D_{ii} depends both on K and ε . For strong anisotropy, $\varepsilon \ll 1$, diffusion coefficient $D(K, \varepsilon) \approx D(K)$, and due to residual correlations (beyond the lowest order) of type $\langle \sin x_n \sin x_0 \rangle$, it displays oscillations as a function of K similar to the case of 1D kicked rotor as in Eq. (20). For weak anisotropy, $\varepsilon \sim 1$, the residual oscillation is negligible and the amplitude of these oscillations decreases as K increases [403].

9.2. Quantum quasi-periodic kicked rotor

In view of ease of analysis, especially from the point of view of numerics and experiments, it is instructive to analyze the quasi-periodic Hamiltonian given in Eq. (112). The time evolution operator in this case will itself be time-dependent and will take the form

$$\widehat{U}_{qp}(t; t-1) = e^{iK \cos x[1 + \varepsilon \cos(\phi_2 + \omega_2 t) \cos(\phi_3 + \omega_3 t)]/\hbar_s} e^{-ip^2/2\hbar_s}, \quad (121)$$

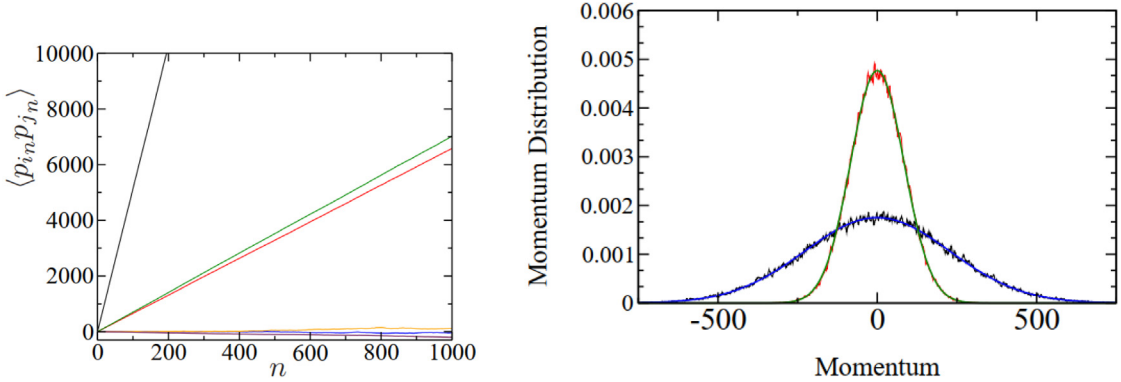


Fig. 23. (left) Classical momentum correlations $\langle p_i p_j \rangle$ as a function of kick number with parameters $K = 10$, $\varepsilon = 0.8$, $\omega_2 = 2\pi\sqrt{5}$ and $\omega_3 = 2\pi\sqrt{13}$. The “non-diagonal” ($i \neq j$) correlations (orange, blue and maroon) are negligible. (right) The momentum distributions at time step $n = 1000$. The anisotropy is visible and the distributions are nearly Gaussian.

Source: Taken from Ref. [403].

where ϕ_2 and ϕ_3 are the phases of the external fields with incommensurate frequencies ω_1 and ω_2 . An initial wavefunction $\Psi(x, 0)$ evolves according to

$$\Psi(x, t) = \prod_{t'=1}^t \hat{U}_{qp}(t; t-1) \Psi(x, 0). \quad (122)$$

In order to see the connection with Anderson model, it must be recalled that the QPKR in Eq. (112) exhibits all the transport properties of the 3D kicked rotor in Eq. (113) [403], through the choice of initial conditions in Eq. (114). The quasi-periodic model has a time-dependent kick strength and cannot be mapped to Anderson model. In contrast, the 3D kicked rotor model can be mapped to Anderson model by a series of steps similar to the one used for 1D kicked rotor (Eqs. (42)–(48)). The eigenvalue problem for the corresponding Floquet operator is $U|\phi_\omega\rangle = \exp(-i\omega)|\phi_\omega\rangle$, where ω are the eigenphases. By using the usual transformation,

$$W(x_1, x_2, x_3) = \tan[K \cos x_1 (1 + \varepsilon \cos x_2 \cos x_3) / 2\hbar_s,] \quad (123)$$

the 3D kicked rotor recast as 3D Anderson model is given by,

$$T_{\mathbf{m}} \Phi_{\mathbf{m}} + \sum_{\mathbf{r} \neq 0} W_{\mathbf{r}} \Phi_{\mathbf{m}-\mathbf{r}} = -W_0 \Phi_{\mathbf{m}}, \quad (124)$$

where $\mathbf{m} \equiv (m_1, m_2, m_3)$ and \mathbf{r} label sites in a cubic lattice in momentum space. This equation has the same form as the standard 3D Anderson model. In this, $T_{\mathbf{m}}$ is the onsite energy and is given by

$$T_{\mathbf{m}} = \tan \left\{ \frac{1}{2} \left[\omega - \left(\frac{\hbar_s m_1^2}{2} + \omega_2 m_2 + \omega_3 m_3 \right) \right] \right\}, \quad (125)$$

while the hopping matrix elements in momentum space $W_{\mathbf{r}}$ are

$$W_{\mathbf{r}} = \iiint_0^{2\pi} \frac{dx_1 dx_2 dx_3}{(2\pi)^3} e^{-i(r_1 x_1 + r_2 x_2 + r_3 x_3)} W(x_1, x_2, x_3). \quad (126)$$

This mapping to 3D Anderson model (for 3D kicked rotor) implies that the dynamics of quasi-periodic kicked rotor should also display similar dynamical features. The on-site energies $T_{\mathbf{m}}$ are pseudo-random and are devoid of long-range correlations. A critical transition, similar to the 3D Anderson model, can be expected in 3D QPKR model as well.

In anticipation of a metal–insulator transition, the mean energy growth obtained by numerically evolving an initial state using Eq. (122) is shown in Fig. 24 for two different kick strengths, $K = 4$ and 8 , at the same value of $\varepsilon = 0.5$. The other parameters are $\omega_2 = 2\pi\sqrt{5}$, $\omega_3 = 2\pi\sqrt{13}$ and $\hbar_s = 1$. If $K = 4$, the localized dynamics in momentum space is observed. The momentum density shown as inset reveals an exponential profile (in Fig. 24(a)). However, when $K = 8$ the quantum dynamics has become diffusive in the long time limit and the momentum density (shown in the inset) is Gaussian. It is then reasonable to expect a critical transition from localization to delocalization in the range $4 \ll K \ll 8$. The transition can be accurately located through finite size scaling introduced earlier.

If a critical transition is indeed taking place, as discussed in Sections 8.4–8.5 and in the spirit of the analogy with 3D Anderson model, finite size scaling theory should be applicable as well. In the Anderson scenario, scaling is sought with respect to finite length L of the system whereas theoretically scaling is expected in the limit of $L \rightarrow \infty$. Applied to

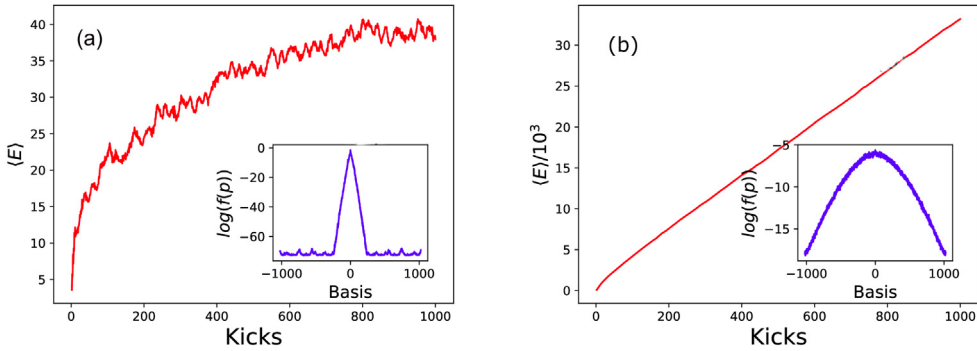


Fig. 24. The evolution of quantum mean energy $\langle E \rangle$ with time for QPKR in Eq. (112) with (a) $K = 4$, and (b) $K = 8$, $\varepsilon = 0.5$. The insets show the momentum distribution after 1000 kicks.

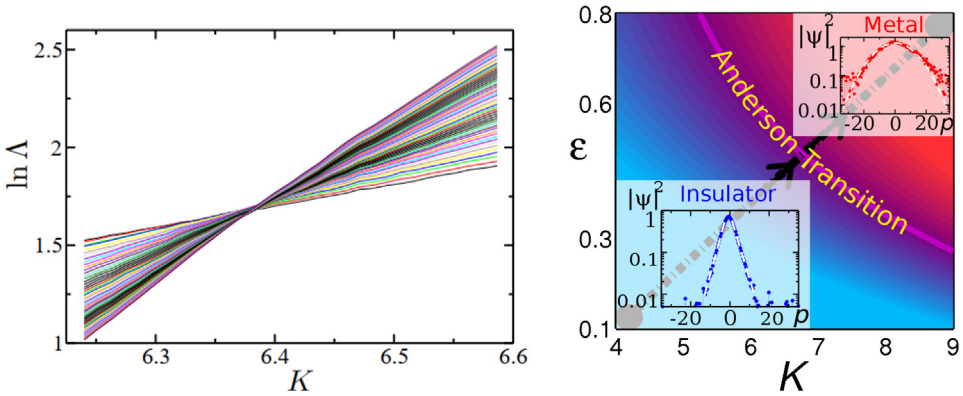


Fig. 25. (left) Dynamics of the quasi-periodic kicked rotor in the vicinity of critical transition. The $\ln \Lambda(K, t)$ is plotted as a function of K for various times ranging from $t = 30$ to $t = 40000$. All the curves meeting at a common point $K = K_c \simeq 6.4$, $\ln \Lambda_c \simeq 1.6$ indicates the transition. Taken from Ref. [404]. (right) Phase diagram for QPKR in the $(\varepsilon - K)$ -plane. Taken from Ref. [406].

the present case, as proposed in Ref. [404,406], it will be a finite time analysis, since both localization and diffusion are defined in the long time limit. A general finite size scaling can be written down in the form

$$\langle p^2 \rangle = t^{\mu_1} \mathcal{F}[(K - K_c) t^{\mu_2}], \quad (127)$$

where μ_1 and μ_2 are scaling exponents, and $\mathcal{F}(.)$ is the scaling function, all of which have to be determined from either experimental or simulated data. This is the programme carried out in Ref. [403,404,406] with remarkable results using data from both these sources. It is useful to examine the various scenarios for $\langle p^2 \rangle$. As Fig. 24 tells us, for $K < K_c$ and as $t \rightarrow \infty$, localization is observed $\langle p^2 \rangle \sim L_m$, where L_m is the localization length. However if $K > K_c$, the dynamics is diffusive and $\langle p^2 \rangle \sim Dt$, and D is the diffusion constant. When $K \sim K_c$ in the vicinity of the critical transition, diffusion rate $D \sim (K - K_c)^s$ vanishes and the localization length

$$L_m \sim (K_c - K)^{-\nu} \quad (128)$$

diverges where s and ν are the critical exponents. The two exponents μ_1 and μ_2 in the scaling hypothesis Eq. (127) can be evaluated using Wegner's scaling law [407], which implies $s = \nu$ in three dimensions [408], and this leads to $\mu_1 = 2/3$ and $\mu_2 = 1/3\nu$ [409].

Based on the foregoing arguments and the exponents, the scaling can be inferred using $\Lambda = \langle (p/\hbar_s)^2 \rangle t^{-2/3}$, a function of time and stochastic parameter K . The transition point can be determined from this equation by realizing that at $K = K_c$, $\Lambda t^{2/3} = \mathcal{F}(0)$, a constant irrespective of time and other parameters. This is demonstrated using data from numerical simulations displayed in Fig. 25. From this, critical transition is seen to occur at $K = K_c \simeq 6.4$. The big picture of the critical transition story can be seen in the simulated phase diagram in the right panel of Fig. 25 showing the critical transition line dividing the localized and delocalized phases. From this, it can be recognized that if transition occurs at $K_c = 6.4$, then the corresponding value of coupling strength is approximately $\varepsilon \approx 0.45$.

The critical exponent ν , obtained from the simulation data of QPKR, was estimated to be $\nu = 1.59 \pm 0.01$ [403]. An accurate estimation of this kind requires corrections to be applied to account for systematic deviations from scaling theory. We shall skip these details here in order to follow the main thread of our discussion, but an interested reader should

consult chapter 3 of Ref. [410] for a general discussion on such deviations, and for kicked rotor specific discussions see Ref. [403]. The critical exponent ν is expected to be universal for a class of systems irrespective of the finer microscopic details. In the context of Anderson model and the quasiperiodic kicked rotor, disregarding any discrete symmetries, the relevant ones are the standard Wigner–Dyson symmetry class, namely, the orthogonal, unitary and symplectic class. These classes correspond, respectively, to systems symmetric under rotation and time-reversal, symmetric under rotation but not under time reversal, systems with spin-1/2 invariant under time reversal but not rotations. The standard Anderson model (Eq. (124)) and quasiperiodic kicked rotor (Eq. (112)) fall in the orthogonal class. Indeed, the estimated $\nu = 1.59$ for QPKR is in good agreement with $\nu = 1.571$ found for the 3D Anderson model [411,412]. Recently, massive parallel computing was used to simulate 3D Anderson model with up to $L = 64$ sites and the mean exponent is $\nu = 1.572$ [413] in good agreement with QPKR as well. Thus, the transition in QPKR and 3D Anderson model belongs to the same orthogonal universality class. Is the exponent ν for QPKR independent of system details? This was indeed tested experimentally by quasiperiodically driving a cloud of cold atoms. In this experiment, nine sets of parameters that govern the microscopic dynamics were used and no major deviation was observed from the value estimated earlier [414]. A somewhat different exercise of using various noise distribution in 3D Anderson model also confirms that ν does not depend on these details [412].

It is worth noting that if the structure of kicked rotor is changed, critical transition properties change drastically. For instance, a double kicked rotor (two closely spaced kicks in a time period) is reported to have different critical statistics with critical exponent being $\nu \approx 0.75$ [415]. The fact that QPKR is a system that exhibits deterministic chaos and not a truly disordered lattice model shows up in the resonance effects [416,417]. As discussed in Section 5.3, quantum resonances can be expected in the standard kicked rotor if the effective Planck's constant is $\hbar_s = 4\pi(l/l')$, where l and l' are co-primes. In the QPKR in d -dimensions ($d - 1$ incommensurate driving frequencies apart from kick period) with $\hbar_s = 4\pi(l/l')$, a richer variety of dynamics and phase transitions can be encountered depending on the value of l' [416,417]. Apart from the localized and metallic phases and transitions between them, the existence of a “super-metallic” phase in low dimensions such as $d = 2$ has been predicted. A metal to super-metal phase transition in $d > 3$ is a possibility depending on the choice of l' . In the super-metal phase, the mean energy of QPKR increases quadratically with time, and this emerges on timescales dependent of kick strength K [417].

9.3. Multifractality of wavefunctions at critical transition

It is known for long that the critical transition in the 3D Anderson model is associated with anomalous scaling of the moments of the particle probability density function $|\psi|^2$ [418]. Physically, this is an evidence for the possibility of large fluctuations in the components or in the spatial correlations of the associated eigenfunction. Due to this, near the critical transition, the associated eigenfunctions are multifractal in nature, *i.e.*, the moments of the probability distribution scale with system size L and display not one but a spectrum of scaling exponents. To appreciate this point, it must be contrasted with eigenstates away from criticality that are compliant with the random matrix type fluctuations in eigenfunctions [202]. In this case, the eigenfunctions are ergodic and the fluctuations are at best short range correlated, and there is just one scaling exponent dependent on the dimensionality of the system (for localized states, the exponent is zero). At criticality, the long-range correlated nature of fluctuations shows up in its multifractal character.

To begin with, we briefly recollect the idea of multifractality [419,420]. See also Ref. [421] for an engaging article on multifractal measures. Let x_i be some variable recorded at discrete values of an independent parameter labeled by i . For instance, the independent parameter could be rescaled time or some other quantity such as the index of a basis state in Hilbert space. In either case, if $F_q(s) \geq 0$ represents a fluctuation function over a scale s , then x_i displays multifractality if

$$F_q(s) \sim s^{-\tau_q}, \quad (129)$$

where τ_q are the exponents and q is a real number. In the standard multifractal formalism F_q is typically the partition function $Z_q(s) = \sum_j [\mu_j(s)]^q$. In this, μ is a suitable measure dependent on s , and j runs over number of boxes of size s required to cover the sequence x_i . In the multifractal detrended fluctuation analysis formalism F_q is taken to be a variance-like quantity in boxes of size s [422], in which case τ_q is replaced by the generalized Hurst exponent h_q . These two exponents are indeed related as $\tau_q = qh_q - 1$ [422]. If $q = 2$, then h_2 is the standard Hurst exponent and its value indicates if the sequence x_i is correlated, uncorrelated or anti-correlated. If h_q (estimated from x_i) depends on q , then x_i is multifractal in nature. Multifractals are characterized by existence of an infinite scaling exponents τ_q , while monofractal (or, just fractal) has one exponent for all q . When dealing with normalized wavefunction $\psi(\mathbf{r})$ in which \mathbf{r} is a d -dimensional vector, a suitable quantity that could act as a “fluctuation function” is the generalized inverse participation ratio (GIPR) defined as

$$P_q = \int_{L^d} dr_1 dr_2 \dots dr_d |\psi(\mathbf{r})|^{2q}, \quad (130)$$

where L is the linear dimension in each direction. If GIPR is averaged over the eigenstates of the system, the averaged GIPR is

$$\bar{P}_q \propto L^{-\tau(q)}. \quad (131)$$

Equivalently, using the relation $\tau(q) = D_q(q - 1)$, it is also possible to employ the multifractal dimension D_q as the characterizer. In practice, box-counting or wavelet transform methods can be used to numerically compute the multifractal spectrum for a wavefunction [423], though any other methods used in timeseries analysis such as detrended fluctuation analysis [422] should work as well. Generally, the GIPR distribution (after appropriate rescaling) is expected to be independent of size L at the transition point as $L \rightarrow \infty$ [424]. This is also observed in the power-law random *banded* matrix models [425], which serves as a random matrix based model for Anderson critical transitions.

In analogy with the 3D Anderson case, the quasiperiodic kicked rotor in Eq. (121) displays multifractal eigenstates at critical transition. While the standard multifractal analysis will be able to reveal this multifractality, though this method will not be particularly useful in the context of cold atoms experiments of kicked rotor. Recently, it was shown that multifractality, especially D_2 , can be inferred from the time evolving wave packet in momentum space through the appearance of a macroscopic peak at zero momentum [426]. This peak becomes more prominent as $t \rightarrow \infty$. Quite interestingly, one-dimensional kicked rotors that have singularity in their potential [323] also display multifractal wavefunctions. For instance, a one dimension kicked rotor with singular potential of the form $V(q) = v_0$ if $q \in [-a, a]$ and $V(q) = 0$ for $|q| > a$, has a singularity at $q = \pm a$. The distribution of level spacings s in this case has the intermediate semi-Poisson distribution $P(s) = 4se^{-s}$, with $P(s) \approx s$ near $s = 0$ and it is dominated by exponential decay for $s \gg 1$. The quantum eigenstates of this system shown to be multifractal, and the averaged multifractal dimension $D(q) \propto 1/q$ [427]. The averaging is performed over the eigenstates and many realizations of the Floquet operator, the latter is possible since the operator depends on a continuous parameter. Other kicked rotor variants such as the kicked rotor in a finite and infinite potentials [317,428] show direct or indirect signatures of multifractal statistics. However if the parity symmetry of the standard kicked rotor with smooth potential is broken then it leads to critical transition and multifractal states [429]. An entire class of quantum maps that display level spacing statistics intermediate between classically integrable and chaotic limits also have fractal wavefunctions [423,430], and so do certain open quantum maps [431]. Experimental realization of multifractality as well as a deeper understanding of the phenomenology of multifractal eigenstates continues to remain as challenges.

It must be noted that fractal characteristics also appear in a one-dimensional system, the open kicked rotor, though in a different form. Using the Floquet operator for the kicked rotor, \widehat{U} (Eq. (28)), a open kicked rotor can be constructed by projecting the evolved state over some set of states. Then, the time evolution is given by,

$$\psi(t+1) = \widehat{P} |\Psi(t)\rangle = \widehat{P} \widehat{U} \psi(t), \quad (132)$$

where \widehat{P} is the projection operator that projects $|\widehat{U} \psi(t)\rangle$ over some set of states. This amounts to absorption of the part of $|\Psi(t)\rangle$ that falls outside these set of states. The conductance fluctuations in mesoscopic systems are known to be related to classical decay of survival probability [432]. If this decay is algebraic, the quantum conductance fluctuations in the *semiclassical* limit is a fractal. In this backdrop, it is surprising to note that a similar relation between the conductance fluctuations and the quantum survival probability should exist in the quantum regime. The purely quantum effects, tunneling and localization, in the open kicked rotor induces an algebraic decay of quantum survival probability [433] with exponent $\mu = -1$. If this condition is met, in analogy with the conductance fluctuations, the quantum survival probability fluctuations in a open kicked rotor turns out to display fractal character [434], and more generally, multifractal properties [435]. Though it was predicted to be observable in experiments [436], there has been no report of its direct observations as yet. Open kicked systems can in general be expected have algebraic decay of survival probability and a fractal character for the survival probability fluctuations. These features can be observed in the kicked Rydberg atom because of the transitions to the continuum which acts as an absorber [437].

9.4. Experimental realization of Anderson transition in quasi-periodic rotor

There are few experimental results for Anderson transition in solid state systems [267,438–442], as bulk of the experiments are from cold atomic matter waves [443]. The stringent requirement of true randomness in on-site energy is generally impossible to attain, and consequently conditions for “clean” Anderson localization in crystalline materials are rarely met. Secondly, while bulk properties could be measured, density profile of the electrons is not easy to access. For these reasons, cold atomic clouds kicked by optical lattices are better suited to experimentally study the physics of disordered condensed matter systems (for recent reviews, see Refs. [444–446]). The reason being the ability to precisely control the atomic interactions, weak absorption in the medium and weak or no coupling with external thermal bath.

The first experimental observation of Anderson transition in 3D kicked rotor was in 2008 [406], and the details relating to its experimental set-up are described in Ref. [447,448]. The basic approach is as follows – cold atoms are prepared in a magneto-optical trap with temperature of about 3–5 μK. The atoms interact with the optical potential created by the standing wave. The main kicking field is a sequence of pulses of finite width w at a pulse period $T \gg w$ (and this sets the value of effective Planck’s constant in the experiment). Additional waves are superposed on this to create a quasiperiodic, off-resonant standing wave. More importantly, after kick sequence is administered, the final evolved quantum state density can be imaged. Atomic velocity distribution is measured using Raman transitions. Decoherence inducing processes such as spontaneous emission are suppressed in the course of the experiment.

The results of this experiment are shown in Fig. 26. Instead of measuring the momentum distribution, it is convenient and relatively easy to measure its proxy, the population in the zero $\Pi_0(t)$ momentum class. As kicks are imparted and

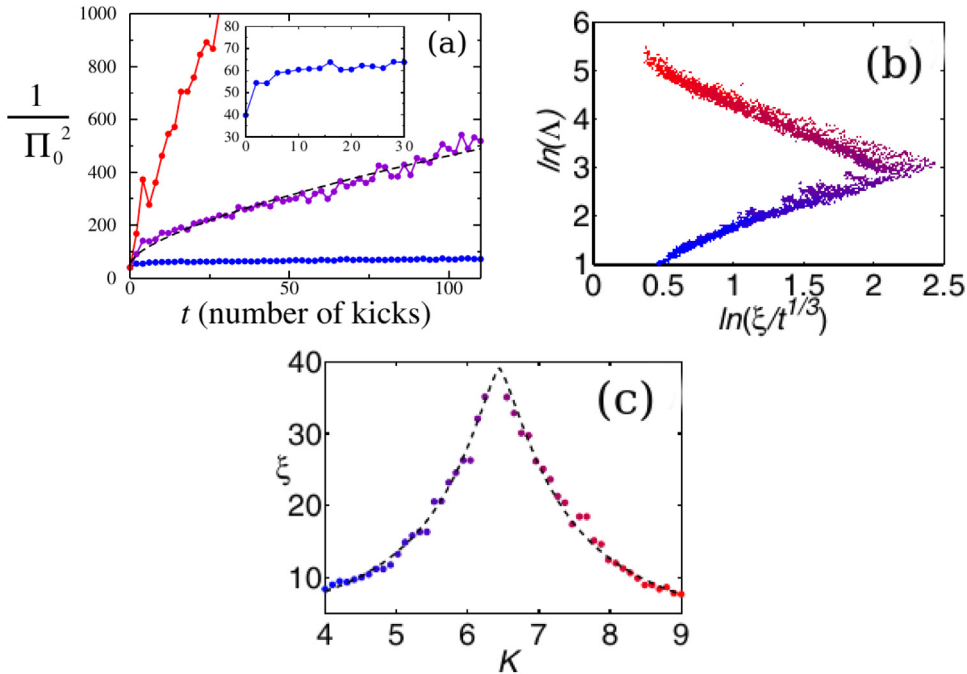


Fig. 26. (a) The time evolution of (inverse square of) zero momentum class, $\Pi_0^{-2}(t)$. Symbols represent experimental data. The population ($\Pi_0^{-2}(t)$) is proportional to average energy ($\langle p^2(t) \rangle$). For $K < K_c$ ($K = 4.0$, blue curve), the dynamics is clearly localized, and it increases linearly with time in the diffusive regime ($K = 9.0$, red curve). Close to the critical point ($K = K_c \approx 6.4$, purple curve), it displays anomalous diffusion $\Pi_0^{-2}(t) \approx t^{2/3}$ as expected from theoretical arguments [409]. The inset shows an enlarged part of the localized dynamics (shown in blue in the main figure). (b) $\ln \Lambda$ as a function of $\ln(\xi/t^{1/3})$. The collapse of data points from different K values demonstrates the existence of scaling. (c) Divergence of localization length $\xi(K)$ in the vicinity of the critical parameter $K = K_c$.

Source: Taken from Ref. [406].

if diffusion takes place, the population in the zero state will decay. In localized regime, beyond the break-time, the population will reach a steady state value. Hence, $(\Pi_0(t))^{-2} \propto p^2(t)$. Fig. 26(a) shows $(\Pi_0(t))^{-2}$ as a function of time. Localized and diffusive regimes (two lower-most curves) are clearly seen. Also shown is $\Pi_0^2(t)$ for the case of critical transition (upper-most curve), which is well fitted by a power-law form in time, $p(t)^2 = A + Bt^{2/3}$, and displays a good agreement with one of the predictions of the scaling theory. The detailed procedure to apply finite size scaling via Eq. (127) to the experimental data is given in Ref. [404]. Fig. 26(b) showing $\log \Lambda$ as a function of $\log(\xi/t^{1/3})$ and the resulting collapse of all the data for various values of K into a single curve with two branches is a proof for the validity of single parameter scaling. The upper branch in Fig. 26(b) is for the diffusive regime and the lower branch is for the localized regime. In both the branches, as $K \rightarrow K_c$, the localization length $\xi(K)$ diverges as indicated in Eq. (128). Far from K_c , as seen in Fig. 26(b), the behavior of scaling function obtained from experimental data for the lower (localized) and upper (diffusive) branch is, respectively, given by

$$\Lambda(K, t) \propto t^{-2/3} \quad \text{and} \quad \Lambda(K, t) \propto t^{1/3}. \quad (133)$$

The data collapse of curves for different kick strengths K is an excellent demonstration of the single parameter scaling in QPKR system. The divergence of the localization length $\xi(K)$ near $K \approx K_c$ is shown in Fig. 26(c). In practice, decoherence induced in the experiment and finite phase coherence times together smooth out the expected divergence. Based on the analysis of experimental data (for details see Ref. [404]), the critical parameter is $K_c = 6.4$, and $\nu = 1.4 \pm 0.3$. Both these numbers are in good agreement with that obtained from theoretically expected value for QPKR system 9.2.

9.5. Other quasiperiodic systems: Aubry–André model and more

In general, quasiperiodic systems (other than kicked rotor) have been immensely useful in shedding new light on localization problems in condensed matter physics. Popular among them is the Aubry–André model [449] for electronic transport in quasiperiodic lattices. In this model, unlike the kicked rotor in which quasiperiodicity is embedded in the kick sequences, it is the lattice potential that is a superposition of two incommensurate length scales. The Hamiltonian of the system is

$$\hat{H} = -J \sum_{\langle i,j \rangle} \hat{b}_i \hat{b}_j^\dagger + \Delta \sum_j \cos(2\pi \beta j) \hat{n}_i + U \sum_i \hat{n}_i (\hat{n}_i - 1), \quad (134)$$

where β is incommensurate with the underlying lattice and is the source of quasiperiodicity in the model. Further, U is strength of interactions, $\hat{b}^\dagger(\hat{b})$ is the creation (annihilation) operator at i th site, J is strength of hopping, $\hat{n}_i = \hat{b}_i^\dagger \hat{b}_i$ is the number operator and Δ is the strength of quasi-disordered potential. A physical model could be the ultracold Bose gas confined to a quasiperiodic potential created by optical lattices. Though a one-dimensional system, Eq. (134) supports transition to localization from a delocalized phase. If hopping is allowed only on nearest-neighbor sites, and if β is incommensurate, then transition takes place at $\Delta/J = 2$. For integral values of β , transition is not observed. Experiments with optical lattices have confirmed the localization transition in this system [450]. Recent theoretical [451] and experiments with optical lattices [452] have confirmed the existence of a mobility edge in a bi-chromatic incommensurate optical lattice potential but also argued that in the limit of large potential depths the mobility edge vanishes and description in terms of Aubry–Andre model becomes appropriate. When kicks at a periodicity of T are applied to the Aubry–Andre model, in the limit of high frequency of kicks, the localization transition still happens though at the rescaled critical value of Δ/JT [453]. Even if the kicks are not exactly periodic but noisy, localization is persistent for rather long times if kicking is periodic in the average sense [454,455], i.e., an average of one kick per cycle is delivered. The localization in the kicked Aubry–Andre model remains robust for long enough time and can be tuned by characteristics of noise [455].

A rather unusual case is that of the one-dimensional quasi-periodically driven spin-1/2 kicked rotor [358,456]. It exhibits infinite topological phases, and transitions between these phases take place upon variation of dimensionless Planck's constant \hbar . There are no external magnetic fields to be applied and yet, quite surprisingly, the transitions between these phases is similar to the case of integer quantum Hall effect [457]. An infinite sequence of critical phase transitions take place as $1/\hbar$ is varied. At the critical values, the kicked rotor shows universal metallic property irrespective of the details of the system and for other values it behaves as an insulator characterized by integer quantum numbers.

10. Quantum correlations and chaos

10.1. Coupled kicked rotors

Until this point in our discussions all the variants of kicked rotors that were encountered can be thought of, in classical terms, as the dynamics of a single particle in a kicked nonlinear potential. The standard kicked rotor is a single particle system, whose dynamics is analogous to a single particle Anderson model in 1D. In the last few years, the effect of interactions on Anderson localization is being vigorously studied and several of them considered various versions of interacting kicked rotors. Needless to say that there is no one unique interacting kicked rotor, but rather a class of interacting kicked rotors with a variety in phenomenology. In the context of interacting kicked rotor as a dynamical system, the core question of interest revolves around the interplay between chaos, localization and interactions. The primary question will be if the interactions sustain or destroy localization. It is tempting to suggest that the localized states might not exist, especially if the interactions are such that the well separated momentum states are coupled together. As against such expectations, some recent results also suggest that the localized states can be extremely long-lived [458]. It is clear that the question of asymptotic fate of localization will require a definite answer in the presence of interactions. Further, since the ultracold atoms based experiments are able to tune the interactions, experiments will be able to evaluate the effects of chaos and interactions, to provide insights for the models of condensed matter physics.

The *linear* kicked rotor is an exactly solvable, integrable model [459], first introduced in Ref. [160], and corresponds physically to a particle moving freely on a ring at a constant speed $2\pi\alpha$ between successive kicks, α being the rotation number between kicks. Though rotor is nonlinear, in this case, the “kinetic energy” type term in the Hamiltonian, $2\pi\alpha p$, is linear in momentum p (as opposed to the usual quadratic dependence) and hence it is referred to as the linear kicked rotor. This also serves to distinguish this from the standard kicked rotor of Eq. (6). Depending on whether α is rational or irrational, the linear rotor can display, respectively, localized or extended states [160,459]. This was a novelty then because the system could be tuned to show one of these phases which was not possible in the 1D kicked rotor or Anderson model, except by going to three- or higher dimensions. Recently this model was extended into a many-body system with N linear kicked rotors coupled together on a ring lattice. A significant result is that despite the interactions, many-body localization is preserved due to integrability of the system [460]. This is one rare instance of an exactly solvable system with interactions and with a well-defined classical limit. Over the years, there had been other efforts to study rotors with different types of interactions [461–464]. In rest of this section, the focus will be on the case of non-linear interactions. The coupled kicked rotors can also be experimentally realized by placing atoms in pulsed, incommensurate optical lattices [465], and these are within the reach of the current experimental efforts.

The dynamics of N kicked rotors with nonlinear coupling is described by the following Hamiltonian [390,466–468]:

$$\hat{H}(t) = \hat{H}_0(\mathbf{p}) + \hat{V}(\mathbf{x}) \sum_{n=-\infty}^{+\infty} \delta(t - n), \quad (135)$$

where $\mathbf{p} = (p_1, p_2, \dots, p_N)$, $\mathbf{x} = (x_1, x_2, \dots, x_N)$ are the momentum and position coordinates. The other terms are

$$\hat{H}_0(\mathbf{p}) = \sum_{j=1}^N \frac{\hat{p}_j^2}{2}, \quad \hat{V}(\mathbf{x}) = \sum_{j=1}^N [K_j \cos \hat{x}_j] + \left[\sum_{j=1}^{N-1} \xi_{j,j+1} \cos (\hat{x}_j - \hat{x}_{j+1}) \right]. \quad (136)$$

Physically, this model describes the dynamics of a collection of single quantum rotors subjected to periodic kicks. At instants of time when kicks are imparted, interaction of strength $\xi = \xi_{j,j+1}$ comes into play and couples the neighboring rotors. Each rotor is also kicked by a sinusoidal potential of strength K_i . The interaction term is in the kicking potential, $V(\mathbf{x})$, which is diagonal angle representation, while $\hat{H}_0(\mathbf{p})$ is diagonal in the angular momentum representation. The form of coupling considered here $\cos(x_j - x_{j+1})$ is non-linear and ensures non-integrability in the system. This type of nearest-neighbor coupling can be interpreted as connecting the rotors through a “spring”. Though less popular, it is also possible to consider global coupling of kicked rotors, i.e., each rotor coupled to all the others. Recently, the globally coupled model was mapped to an infinite-range coupled interacting bosonic model [469].

The classical dynamics of Eq. (135) with $N = 2$ will be considered briefly here, mainly to point out that these are models that display chaotic dynamics. In principle, the result is extendable to all N rotors in general. For the case of $N = 2$ coupled rotors with two kick strengths K_1 and K_2 and one coupling constant ξ_{12} , by solving the Hamilton's equations of motion, the dynamics can be reduced to a 4D map (4 difference equations in this case):

$$\begin{aligned} p_1^{[n+1]} &= p_1^{[n]} + K_1 \sin x_1^{[n]} + \xi_{12} \sin \left(x_1^{[n]} - x_2^{[n]} \right), \\ p_2^{[n+1]} &= p_2^{[n]} + K_2 \sin x_2^{[n]} - \xi_{12} \sin \left(x_1^{[n]} - x_2^{[n]} \right), \\ x_1^{[n+1]} &= x_1^{[n]} + p_1^{[n+1]}, \\ x_2^{[n+1]} &= x_2^{[n]} + p_2^{[n+1]}. \end{aligned} \quad (137)$$

In this, n represents time in units of kick period. It is straightforward to generalize this to the case of general N as explicitly shown in Ref. [391]. For $N = 2$ and with periodic boundary conditions, a similar map is obtained in Ref. [392]. An equivalent standard map in 4D shows the effects in the dynamics arising due to higher dimensionality – Arnold diffusion along the resonance channels, lower dimensional invariant tori affecting the higher dimensional tori and bifurcations in the latter take place without the need to vary parameters [470], one-dimensional tori as a backbone for the organization of higher dimensional tori [393].

If the perturbations which breaks the integrability, namely the periodic driving, are small, then the system persists on quasi-periodic trajectories for exponentially long times. Nevertheless, for strong kick strengths and coupling, the dynamics becomes chaotic and the system starts evolving diffusively in the phase space. In this limit, The mean energy growth can be obtained as,

$$\begin{aligned} \langle p_1^2/2 \rangle &= D_1 t, \\ \langle p_2^2/2 \rangle &= D_2 t, \end{aligned} \quad (138)$$

in which the diffusion coefficients in the quasi-linear approximation are

$$\begin{aligned} D_1^0 &= \left(\frac{1}{2\pi} \right)^2 \iint_0^{2\pi} \left(p_1^{[n+1]} - p_1^{[n]} \right)^2 dx_1^{[n]} dx_2^{[n]} = \frac{(\xi_{12})^2}{2} + \frac{K_1^2}{2}, \\ D_2^0 &= \left(\frac{1}{2\pi} \right)^2 \iint_0^{2\pi} \left(p_2^{[n+1]} - p_2^{[n]} \right)^2 dx_1^{[n]} dx_2^{[n]} = \frac{(\xi_{12})^2}{2} + \frac{K_2^2}{2}. \end{aligned} \quad (139)$$

The diffusion coefficients depend both on the kick strengths and the coupling constants. Though not shown here, the results obtained by numerically iterating Eq. (137) agree with this analytical estimate. Even in the chaotic regime of strong non-integrability and interactions, the N dimensional system still supports stable periodic orbits and accelerator modes that give rise to ballistic motion in phase space [391].

Unless specified otherwise, the quantum dynamics will be studied in a regime in which classical chaos is dominant in the coupled system. The unitary time evolution operator for the 2D coupled kicked rotor is

$$U = (U_1 \otimes U_2) U_{12} \quad (140)$$

where,

$$\begin{aligned} U_j &= \exp \left(-i \frac{p_j^2}{2\hbar_s} \right) \exp \left(-i \frac{K_j}{\hbar_s} \cos(x_j) \right), \quad j = 1, 2 \\ U_{12} &= \exp \left(-i \frac{\xi_{12}}{\hbar_s} \cos(x_1 - x_2) \right), \end{aligned} \quad (141)$$

such that, starting from the initial state $|\Psi(0)\rangle$, the time evolved state is $|\Psi(t)\rangle = U^t |\Psi(0)\rangle$. The initial state is taken to be a product state of the form $|\Psi(0)\rangle = |\psi_1(0)\rangle \otimes |\psi_2(0)\rangle$ where $|\psi_j(0)\rangle$ is a coherent state of the j th rotor. The mean energy of the first rotor in state $\Psi(t)$ is calculated as $\langle p_1^2/2 \rangle$ and the corresponding momentum distribution is $f(p_1) = |\langle \Psi | p_1 \rangle|^2$.

Both $\langle E_1 \rangle$ and $f(p_1)$ are shown in Fig. 27. A significant feature is the emergence of two timescales, the break-time t_b (shown in orange color) and another time scale t^* (indicated in blue) such that for $t > t^*$ normal diffusion takes over. An

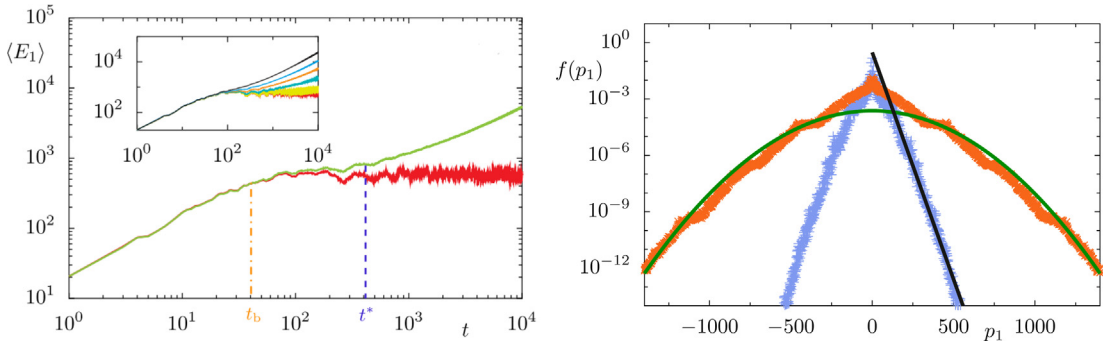


Fig. 27. (left) Mean energy growth $\langle E_1 \rangle$ of the first kicked rotor as a function of kick number. The orange dash-dotted line indicates the break time t_b . IDL state is realized in the timescale $t_b \lesssim t \lesssim t^*$. Inset shows $\langle E_1 \rangle$ for different coupling strengths, $\xi_{12} = 0.0, 0.01, 0.03, 0.05, 0.07, 0.1$, from bottom to top. (right) Momentum distributions at two different times, $t = 150$ (blue symbols) and $t = 10000$ (orange symbols). Plots are for $K_1 = 9.0$, $K_2 = 10.0$, $\xi_{12} = 0.05$ (for green solid line), and $\hbar_s = 1.0$.

Source: Taken from Ref. [471].

transitory state called intermediate dynamical localized (IDL) state is observed for $t_b \leq t \leq t^*$. The timescale t^* during which IDL state is realized diverges as $\xi_{12} \rightarrow 0$, and it can be estimated as [471]

$$t^* = \frac{\hbar_s^2}{3\xi_{12}^2} \left[2 + \frac{1}{\mathcal{G}(\xi_{12}, D_q)} + \mathcal{G}(\xi_{12}, D_q) \right], \quad (142)$$

where, in terms of quantum diffusion coefficient D_q ,

$$\mathcal{G}(\xi_{12}, D_q) = \left[-1 + \frac{27}{8\pi} \frac{\xi_{12}}{D_q} + \frac{3^{3/2} \xi_{12}}{2} \sqrt{\frac{-1}{\pi D_q} + \frac{27}{16\pi^2} \frac{\xi_{12}^2}{D_q^2}} \right]^{\frac{1}{3}}. \quad (143)$$

The leading term in the expression for t^* (Eq. (142)) has similar form as Eq. (81) for the case noisy kicked rotor. As coupling strength ξ_{12} increases, the IDL state could become hard to detect. Physically, this could be understood as arising due to one rotor taking on the role of “environment” and effectively destroying the quantum correlations [471]. It is also clear that in the semiclassical limit of $\hbar \rightarrow 0$, the transient timescale t^* vanishes due to the decay of quantum correlations.

As shown in Ref. [390], the N -coupled kicked rotor in Eq. (135) can be mapped to the N -dimensional Anderson model. Applied naively to the $N = 2$ case, this should guarantee the existence of localized states in the 2D system. At first sight, this result might appear to contradict the existence of IDL state and asymptotic diffusion in Fig. 27. On closer scrutiny, the problem can be traced back to the presence of long range hopping in the 2D Anderson model obtained by transforming Eqs. (140)–(141) (not shown here). The long range hopping, induced by the interaction term, effectively destroys localization in the momentum representation [390,471,472]. The coupling term in Eq. (136) only modifies the hopping term in the mapped 2D Anderson model since the on-site energy term is independent of the coupling and kicking strengths. In fact, it is shown that non-linearity in the off-diagonal terms in the 2D Anderson model leads to sub-diffusive wave-packet spreading, indicating that localization is not always guaranteed [471].

An earlier work had predicted the two coupled kicked rotors (Eq. (136)) to essentially work like a classical system in the semiclassical limit [473]. This numerical result is based quantum dynamics performed with small \hbar and this explains the absence of IDL state in these simulations. Another interesting coupling scheme is that of hard-core interactions in which two kicked rotors are coupled through an interaction of the form $H_{int} = \lambda \delta(\theta_1 - \theta_2)$, where λ is the strength of interaction. Through a coordinate transformation this system splits into two problems – one for the center of mass and one for the relative coordinates. This is a case of non-analytic, contact interaction and large relative momenta are excited that decay slowly in momentum basis. On the other hand, the center of mass decays faster than exponential in the same basis during the course of time evolution. The localization of center of mass is robust even in the presence of interactions but the localization is destroyed in the relative momentum direction [339], and if the kick period is close to its resonance value, then a crossover from a short-time resonant increase in energy to a localized state is observed [474]. Mention must be made of a related work on the classical dynamics of a coupled chain of kicked rotors whose Hamiltonian is same as Eq. (136) with $K_i = 0$ for all i and $\xi_{j,j+1} = \xi$ for all j , and $\xi < 0$. This system displays a long lived steady state before thermalization kicks in and the lifetime of this state is exponential in $1/\xi$ [475]. The steady state itself is well described by a generalized Gibbs ensemble characterized by the temperature associated with the state.

In general, asymptotic delocalization might emerge in N coupled kicked rotor in which the interactions are analytic and arise from coupling of positions of the neighboring rotors as in Eq. (135), though by tuning the coupling strength it might be possible to extend the timescale for which localization survives. The ultimate destruction of localization can be seen as arising from each rotor seeing itself in the ‘noisy environment’ created by other rotors. However, there is at least one

known coupling scenario for two the rotors in which the localization does not survive even as a transient, as demonstrated through an experiment [465]. If the two rotors are driven by two tailored incommensurate optical lattices (such that one lattice does not affect the other) and the interactions between rotors arise during the kinetic evolution phase, then delocalization and consequent quantum-to-classical transition takes place in this closed system. As an emerging area, the question of localization and delocalization in N -body kicked systems with interactions will be vigorously investigated in the years to come.

10.2. Chaos and entanglement in coupled kicked rotors

At one level, the questions investigated under the banner of quantum chaos, in the final analysis, often relate to the connections between the quantum and classical dynamical features. Dynamical localization is a purely quantum effect, unlike others such as quantum scarring whose origins can be traced back to the existence of certain kinds of classical periodic orbits. In a similar manner, several signature properties had been identified, for instance, spectral properties of quantum operators [148], scarring [44] and hypersensitivity to perturbation [476]. All these signify the influence of underlying chaos on the quantum dynamics. However, in the last two decades, an interest in identifying the signatures from a completely different perspective, namely, through the nature of entanglement production, has seen an explosive growth fueled by the advances in quantum information theory and quantum computation. This perspective becomes necessary as entanglement plays a crucial role in the development of quantum information processing [477,478]. Since the core elements of a large quantum computer will be many qubits working in tandem, or essentially a many-body system, it becomes necessary to understand how the effects of chaos play out in the dynamics of entanglement. At first sight, this should sound counter-intuitive since entanglement, or in general the quantum correlations, are purely nonlocal quantum features without any classical analogue. However, the research in the last two decades has given us enough evidence to believe that quantum correlations, though devoid of classical analogue, are impacted by classical dynamics including chaos.

Entanglement [479] is a fundamental phenomenon in quantum physics. For quantum systems made up of several sub-systems, entanglement represents quantum correlations that could be stronger than the classical correlations. These correlations are such that the one subsystem cannot be described disregarding the other subsystems. It is also an important resource, like the energy, for quantum processes such as quantum computation and in other emerging areas of quantum technology. A pure quantum state $|\Psi\rangle$ of a composite system is said to be entangled if it cannot be written as a direct product of states of subsystem:

$$|\Psi\rangle_{\text{entangled}} \neq |\phi_1\rangle \otimes |\phi_2\rangle \otimes |\phi_3\rangle \dots \otimes |\phi_n\rangle \quad (144)$$

It is convenient to consider a bipartite system with Hilbert space dimensions M_1 and $M_2 \geq M_1$. The composite system will have the dimension $M_1 M_2$. Let $|\psi\rangle$ represent the state of the bipartite system with the density matrix $\rho = |\psi\rangle\langle\psi|$. In this case, a reduced density matrix (RDM) can be obtained by tracing over one of the parts of the system. Then, the RDMs will be, $\rho_1 = \text{Tr}_2|\psi\rangle\langle\psi|$ and $\rho_2 = \text{Tr}_1|\psi\rangle\langle\psi|$, where Tr_l indicates that the trace operation will apply on the l th part of the system. If $|\phi_i\rangle_{(1)}$, $i = 1, \dots, M_1$ and $|\phi_j\rangle_{(2)}$, $j = 1, \dots, M_2$ are the eigenvectors of the RDMs ρ_1 and ρ_2 respectively, then the composite state $|\psi\rangle$ can be written in Schmidt decomposed form as

$$|\psi\rangle = \sum_{i=1}^{M_1} \sqrt{\lambda_i} |\phi_i\rangle_{(1)} |\phi_i\rangle_{(2)}, \quad (145)$$

where $\lambda_i > 0$ are the eigenvalues of either ρ_1 or ρ_2 . Note that the non-zero eigenvalues of ρ_2 are identical to λ_i and the rest $M_2 - M_1$ eigenvalues are zero. Then, entanglement of a pure state is measured in terms of the von Neumann entropy given by,

$$S_{\text{vN}} = -\text{Tr}(\rho_l \ln \rho_l) = -\sum_{i=1}^{M_1} \lambda_i \ln \lambda_i, \quad l = 1 \text{ or } 2. \quad (146)$$

Note that since λ_i are the eigenvalues of a density matrix, $\sum_i \lambda_i = 1$. If the subsystems are not entangled, then $|\psi\rangle$ is a product state with only one eigenvalue being unity, i.e., $\lambda_1 = 1$ and $\lambda_i = 0$ for $i = 2, 3, \dots, M_1$. Then, the entanglement entropy is $S_{\text{vN}} = 0$. If the subsystems are entangled, $\lambda_i < 1$ for all i , and $S_{\text{vN}} > 0$. It is worth mentioning that von Neumann entropy is a special case of more general entropies such as the Rényi entropy [480] and Tsallis entropy [481].

One natural question to probe is whether the underlying nature of classical dynamics has any influence, if at all, on the dynamics of quantum entanglement. This question is of particular interest in the context of chaotic systems. This was first addressed in a study of inverted harmonic oscillator (an unstable but not properly chaotic system) weakly coupled to a thermal bath [482], in which von Neumann entropy displays linear temporal growth with the rate given by the Lyapunov exponent. This scenario exists in chaotic systems as well. The rate of entropy growth now corresponds the averaged Lyapunov exponent, the average taken over the points in phase space occupied by a quantum coherent state at initial time. This was numerically verified in the chaotic coupled kicked tops but *without* coupling the tops to an external thermal bath [483]. In this case too, the rate of production of entanglement, characterized by the von Neumann entropy,

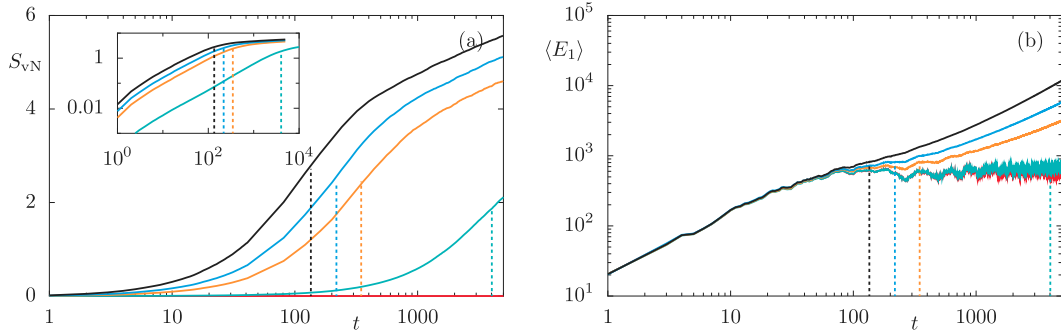


Fig. 28. (a) Linear-log plot of S_{VN} for the system in Eqs. (140)–(141) as a function of time for various coupling strengths ξ_{12} . Inset shows the same data as a log-log plot. (b) Quantum mean energy growth of first kicked rotor is plotted as a function of time for various ξ_{12} . From bottom to top $\xi_{12} = 0, 0.01, 0.05, 0.07, 0.1$. Other parameters are $K_1 = 9.0, K_2 = 10.0, \hbar_s = 1.0$. The dashed vertical lines in both graphs indicate theoretically estimated t^* from Eq. (142).

equals the sum of the positive Lyapunov exponents [483]. Thus, a study of entanglement dynamics does not necessarily require coupling the system of interest to a thermal bath. From the standpoint of chaotic systems, we would like to understand the relation between local exponential instability in classical phase space and quantum entanglement. For this, it is sufficient to have a chaotic system with at least two “parts”.

The discussions below will focus on the coupled kicked rotor in Eq. (135) with $N = 2$, in particular, the system whose unitary operators are given in Eqs. (140)–(141). The two rotors form the two parts of the composite system, and the entanglement between these two rotors is explored. Fig. 28(a) displays growth of S_{VN} as a function of time. The product states at initial time $t = 0$ are entangled by the unitary operators during the course of time evolution. Both the rotors with kick strength $K_1 = 9.0$ and $K_2 = 10.0$ are chaotic. This figure shows that initially S_{VN} grows approximately linear in time until $t \sim t^*$, and is succeeded for $t \gtrsim t^*$ by an asymptotic logarithmic growth. The linear growth rate depends on the coupling strength ξ_{12} rather than on the kick strengths K_j of the two rotors. The asymptotic growth phase is a consequence of the infinite dimensional Hilbert space of the problem. The entropy growth for $t > t^*$ is $S_{VN} = (1/2)\ln t + S_{VN}(t^*)$. To intuitively understand these two distinct entanglement growth profiles, we note the direct correspondence with energy growth shown in Fig. 28(b). The linear growth of S_{VN} dominates in the regime of $t < t^*$ when quantum coherences builds up, and hence transient localization (arrest of energy growth), is sustained. The slower logarithmic growth begins for $t > t^*$, when the system displays classical-like diffusion and the quantum coherences are destroyed. This can also be seen as a faster decay of decoherence until $t = t^*$, and a much slower decay beyond this timescale [471].

The initial linear increase in $S_{VN}(t)$ is not kicked rotor specific, but a generic feature when two chaotic systems are coupled and the initial state at $t = 0$ is taken to be a product (unentangled) state. This has been demonstrated in many examples with coupled kicked tops [483–485]. Entanglement in a kicked top can also be seen as arising from interaction among qubits or spins representing just one top, implying that coupling two different tops is optional. The initial linear growth of S_{VN} is closely tied to the placement of the unentangled initial state in the classical phase space. Typically, if the classical phase space is at least locally chaotic, the initial linear growth of entanglement can be expected [486]. In general, the connection with the underlying classical system, if we might call it that, appears in the form of dependence on where the initial state $|\Psi(0)\rangle$ is located in the classical phase space [487,488]. One possible way to infer the location of an arbitrary state $|\Psi(0)\rangle$ in phase space is by examining its Husimi distribution ρ_H [489]. For N degree of freedom case, it reads

$$\rho_H(\mathbf{p}, \mathbf{q}) = (4\pi^2\hbar)^{-1} |\langle \phi_{\mathbf{p}, \mathbf{q}} | \Psi(0) \rangle|^2, \quad (147)$$

where $\phi_{\mathbf{p}, \mathbf{q}}$ is a minimum uncertainty state located at (\mathbf{p}, \mathbf{q}) in phase space. In general, if $|\Psi(0)\rangle$ is placed in a chaotic region of phase space, then entanglement displays an approximate linear growth phase initially, the growth rate being proportional to the sum of positive Lyapunov exponents [483,490]. If $|\Psi(0)\rangle$ is placed in a region dominated by elliptic islands, then the entanglement production and linear growth phase still exist but is somewhat subdued. These behaviors are also observed in the experimental realizations of kicked top [491,492] and is related to generation of pseudo-random states in the composite Hilbert space of the system [493]. These features of entanglement production interestingly survive even if the quantum kicked rotor interacts with an environment modeled as a collection of harmonic oscillators. In these models of open kicked rotors too, a linear increase in entanglement is observed at initial time and the rate of entanglement production is proportional to the sum of positive Lyapunov exponents [494,495].

In the kicked rotor, the boundary conditions make a significant difference in the asymptotic evolution of entanglement. The asymptotic logarithmic growth of entanglement discussed above is relevant only when the coupled rotors are defined on a cylinder. If the coupled kicked rotor is considered in a topology of a torus, then as $t \rightarrow \infty$, the entanglement saturates to a constant $\langle S_{VN} \rangle$ [496,497]. Physically, this arises because of complete delocalization of the evolving state over the Hilbert space. Such delocalization is also a feature of the eigenstates of the Floquet operator of the coupled

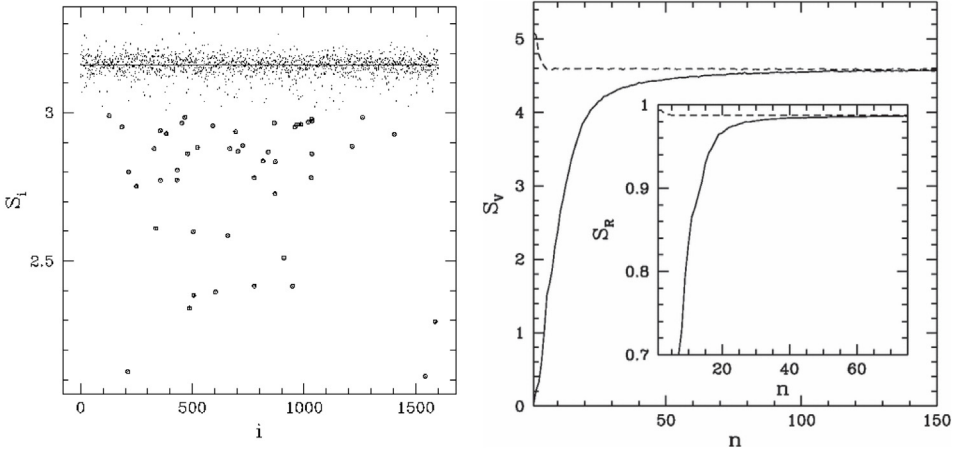


Fig. 29. (left) Entanglement entropy of 1600 eigenstates for the coupled kicked rotor (on a torus) in the chaotic regime. The computations used 40 one-dimensional basis states. (see Ref. [496] for the form of coupled kicked rotor and for the values of parameters). The horizontal solid line is $\langle S_{VN} \rangle \sim 0.6N$. Taken from Ref. [496]. (right) Time evolution of entanglement for coupled kicked top, with unentangled state as initial state. Note the saturation of entanglement as the system evolves. In both the figures, the saturated value $\langle S_{VN} \rangle$ is consistent with the result in Eq. (149). Taken from Ref. [499].

system under conditions of strong coupling between the two subsystems [496]. Hence, for all the delocalized states of a coupled system with finite dimension of Hilbert space, we should expect mean entanglement to saturate at $\langle S_{VN} \rangle$ and this value will depend only on the dimensions of the Hilbert space subsystems, and not on other details of the system. In the parametric regime in which either the evolving state or eigenstate is delocalized, $\langle S_{VN} \rangle$ can be evaluated as an average of $S_{VN} = -\sum_{i=1}^{M_1} \lambda_i \ln \lambda_i$ (in Eq. (146)) taken over the distribution of eigenvalues. The distribution relevant in this case is

$$f(\lambda) = \frac{M_1 Q}{2\pi} \frac{\sqrt{(\lambda_+ - \lambda)(\lambda - \lambda_-)}}{\lambda}, \quad \text{where} \quad \lambda_{\pm} = \frac{1}{M_1} \left(1 + \frac{1}{Q} \pm \frac{2}{\sqrt{Q}} \right). \quad (148)$$

This is obtained for the Laguerre ensemble of random matrix theory [206,498]. The Laguerre ensemble, relevant for the case of reduced density matrices, is a collection of rectangular matrices X of order $M_1 \times M_2$ with i.i.d random numbers with zero mean and finite variance, and $f(\lambda)$ gives the distribution of singular values of X in the limit $M_1, M_2 \rightarrow \infty$ and $Q = M_2/M_1$. Note that the singular values of X are the non-zero eigenvalues of $Y = XX^T$ or $Y = X^TX$. Then, using the random matrix based result in Eq. (148), the mean entanglement is [499]

$$\langle S_{VN} \rangle \sim - \int_{\lambda_-}^{\lambda_+} f(\lambda) (\lambda \ln \lambda) d\lambda = \ln(\gamma M_1), \quad (149)$$

where γ is a constant dependent on Q :

$$\gamma = \frac{Q}{1+Q} \exp \left[\frac{Q}{2(1+Q)^2} {}_3F_2 \left(1, 1, \frac{3}{2}; 2, 3; \frac{4Q}{(1+Q)^2} \right) \right], \quad (150)$$

where ${}_3F_2(\cdot)$ is the generalized Hypergeometric function. For a bipartite quantum system whose subsystem (Hilbert space) dimensions are equal, $M_1 = M_2$, and $Q = 1$. This gives $\gamma \approx 0.6$ and $\langle S_{VN} \rangle \approx \ln(0.6M_1)$ [499].

In Fig. 29(a), entanglement of eigenstates of unitary operator corresponding to the coupled kicked rotor is shown. The parameter choices correspond to strong coupling between the rotors, and as anticipated the entanglement of nearly all the states are maximal and approximately equal to $\ln(\gamma M_1)$, and with $M_1 = 40$, $\langle S_{VN} \rangle \approx 3.178$ in agreement with the cloud of points surrounding the horizontal line in this figure. A few states that deviate from this estimate are localized states that violate the random matrix based assumptions that underlie Eq. (149). Further, Fig. 29(b) also displays the time evolution of entanglement starting from an unentangled initial state for a coupled kicked top system, in which each top forms a subsystem. The successive application of unitary operators entangles the initial state and as $t \rightarrow \infty$ saturates to $\langle S_{VN} \rangle \approx 4.601$ since $M_1 = 166$. The inset in this figure shows linear entropy, which is an easily computable measure than entanglement but carries the same information as the former. Such results have also been noted in a variety of coupled oscillators [500,501] which are infinite Hilbert space dimensional systems, though Eq. (149) would apply if a suitable effective dimensionality is identified [500] using such measures as inverse participation ratio.

Even more remarkable is the fact that, not just the chaos or the absence of it, entanglement is also sensitive to trends in the classical phase space structures. It is by now well established that entanglement reaches extremum, or at least close to an extremum, in the vicinity of a bifurcation. This has been discussed in the context of a variety of chaotic systems [500,502,503]. In particular, if the bifurcation involves local loss of stability such as in case of a pitchfork

bifurcation, then it is conceivable that upon variation of a parameter, elliptic fixed point in phase space suddenly becomes hyperbolic fixed point. The accompanying local instability plays a definite role in the maximization of entanglement in the vicinity of bifurcation for those pure states that localize in this part of the phase space. Indeed, it is generally observed that quantum correlation measures are affected by the classical bifurcations and other phase space features [502].

10.3. Entanglement transition

Given the imprint of classical chaos on quantum entanglement and estimates for entanglement based on random matrix assumptions, it is reasonable to suspect that results of a general nature should be possible. For entanglement in coupled kicked systems, disregarding the specifics of kicking potential, such general results can indeed be obtained (see Ref. [504] for such a universality bounds on entanglement for local Hamiltonians). Stated in less general form, how does entanglement evolve when two chaotic rotors interact with one another? This was answered recently within the random matrix framework [505,506]. The general Hamiltonian of the coupled kicked rotor defined on a torus is

$$H = \frac{p_1^2}{2} + \frac{p_2^2}{2} + [V_1(x_1) + V_2(x_2) + b V(x_1, x_2)] \sum_n \delta(t - n), \quad (151)$$

and the dimension of Hilbert space is M^2 . The interaction of strength b between the two rotors is given by the potential $V(x_1, x_2)$ and breaks the dynamical symmetry for $b > 0$. The quantum evolution of this system is in Eq. (140). Note that if the two chaotic kicked rotors on a torus are coupled together, the spectral fluctuations of the composite system will display Poisson distribution. Even though the individual rotors are chaotic and COE type fluctuations must be expected, it is known that superposition of levels from COE type statistics leads to Poisson fluctuations. Hence, for $b = 0$, the spectral fluctuations are Poisson distributed. On the other hand, as coupling gets stronger, a transition ensues and finally the system is well described by random matrix fluctuations consistent with circular ensembles. This situation can be modeled using a random matrix ensemble, to be called transition random matrix ensemble. This ensemble is the random matrix counterpart for Eq. (140) and is modeled as

$$\mathcal{U} = (\mathcal{F}_1 \otimes \mathcal{F}_2) \mathcal{F}(\epsilon), \quad (152)$$

where $\mathcal{F}_j, j = 1, 2$ are independent matrices drawn from circular unitary ensemble (CUE) of random matrix theory. The interaction matrix is drawn from a diagonal ensemble, $\mathcal{F}_{mn}(\epsilon) = \delta_{mn} \exp(2\pi i \epsilon \xi_{mn})$, where $0 \leq \epsilon \leq 1$ plays the role of interaction strength in this RMT model and ξ_{mn} are random numbers taken from a uniform distribution in the interval $[-1/2, 1/2]$, and δ_{mn} is the Kronecker delta. If there is no coupling, then $\epsilon = 0$, and maximal coupling corresponds to $\epsilon = 1$. In Refs. [505,506], this transition random matrix ensemble is constructed, and an effective parameter Λ , the ratio of mean square interaction matrix element and the mean level density, is identified as

$$\Lambda_{KR}(b) = \frac{M^4 b^2}{32\pi}, \quad \text{and} \quad \Lambda_{RMT}(\epsilon) = \frac{M^2 \epsilon^2}{12}, \quad (153)$$

respectively, for the coupled kicked rotor and the transition random matrix ensemble in the limit of weak coupling – $Mb \ll 1$ and $\epsilon \ll 1$. The parameter $\Lambda_{RMT}(\epsilon)$ governs the universal transition of spectral fluctuations of two interacting circular unitary ensemble (CUE) matrices each of which display Poissonian to random-matrix like fluctuations with increasing interaction strength [506]. An equivalent parameter $\Lambda_{KR}(b)$ is the scaled parameter for the kicked rotor case. The entanglement $\langle S_{VN} \rangle$ also makes a transition and in terms of Λ , which could be either $\Lambda_{KR}(b)$ or $\Lambda_{RMT}(\epsilon)$, is obtained as [506]

$$\langle S_{VN}(\Lambda) \rangle = \left[1 - \exp\left(-\frac{\pi^{3/2}}{\langle S_{VN}^\infty \rangle} \sqrt{\Lambda}\right) \right] \langle S_{VN}^\infty \rangle, \quad (154)$$

where $\langle S_{VN}^\infty \rangle = \ln N - \frac{1}{2}$. Eq. (154) reveals an exponential dependence of $\langle S_{VN}(\Lambda) \rangle$ on Λ and reaches its asymptotic value at $\Lambda = \Lambda_c$, where $\Lambda_c = (\langle S_{VN}^\infty \rangle / \pi^{3/2})^2$. Fig. 30 shows an excellent agreement of the analytical result in Eq. (154) with the numerically computed values of $\langle S_{VN}(\Lambda) \rangle$ for both the coupled kicked rotor and transition random matrix ensemble. However, for smaller values of b , by expanding the exponential, the linear dependence on b as seen in the inset can also be observed. This reported transition (details in Ref. [507]) of entanglement in kicked rotors due to increasing strength of interactions is universal in the sense that it does not depend on the details of the system and its dynamical features until the subsystems are predominantly chaotic. A recent work that demonstrates the validity of entanglement transition for the kicked top adds further strength to the universality of this result [508].

10.4. Out-of-time-ordered correlator and kicked rotor

Among the many measures of quantum chaos in the literature, the out-of-time-ordered correlator (OTOC) is probably the latest entrant with the additional virtue that it carries information about what is called the quantum Lyapunov exponent. The OTOC is defined as

$$\mathcal{O}(t) = \langle [A(t), B(0)]^2 \rangle \quad (155)$$

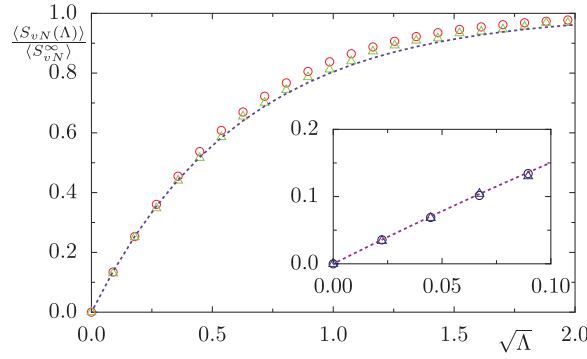


Fig. 30. S_{vN} averaged over all the eigenstates are plotted for coupled kicked rotor (red circles) and CUE matrices (green triangles) with $N = 50$. The x -axis is obtained from the effective parameter Λ given in Eq. (153). Blue dashed line is plotted using Eq. (154) for coupled kicked rotor with $K_1 = 9.0$ and $K_2 = 10.0$. The inset displays the initial linear growth of entanglement entropy.

where $A(t)$ and $B(t)$ are quantum operators at time t in the Heisenberg picture and $\langle \cdot \rangle$ indicates thermal average at temperature T . The equivalence is clearly visible if we consider A and B as position and momentum operators. The commutator $[x(t), p(0)]^2$ in the semi-classical limit is equivalent to the classical Poisson bracket, and hence

$$\hbar^2 \{x(t), p(0)\}^2 = \hbar^2 \left(\frac{\partial x(t)}{\partial x(0)} \right)^2 = \hbar^2 e^{2\lambda t} \quad (156)$$

where λ is the so-called quantum Lyapunov exponent. The last form can be written in the limit of classical chaos in which any small deviation in the initial condition grows exponentially with time t . In the quantum regime, this exponential growth of OTOC can only last until the Ehrenfest time (see at the end of Section 5.4), the timescale over which an initial wavepacket can be well described by classical Liouville evolution. In the quantum chaos context, the hope is that λ would be analogous to the classical Lyapunov exponent and thereby providing a diagnostic measure for quantum chaos. The interest in OTOC, originally introduced in the context of superconductivity [509], surged after a suggestion that quantum Lyapunov exponent has an upper bound $\lambda \leq 2\pi k_B T / \hbar$ [510], where k_B is the Boltzmann constant and T is the temperature, in which λ can be obtained by evaluating OTOC. This bound itself was originally proposed in the specific context of information around black holes [510], though in the last few years OTOC has taken a life of its own in many areas such as quantum chaos and condensed matter physics. In the one-body problems encountered in quantum chaos, including the kicked rotor, this result might not apply since temperature cannot be defined in these cases. The OTOC has also been measured experimentally through nuclear magnetic resonance based techniques [511–514]. Intuitively, the OTOC can be thought of as a measure of information scrambling, a process of local information spreading out into the quantum correlations distributed throughout the system. Consequently, in a scrambled system, local information is not accessible through local measurements. Though scrambling is often taken to be an indicator of chaos, a cautionary note is that scrambling (and hence the exponential growth of OTOC) can be observed even in the absence of chaos, for instance, in the neighborhood of isolated saddle points [515]. Scrambling was experimentally demonstrated in ion-trap quantum simulator using OTOC as the diagnostic measure [516].

The kicked rotor $H = p^2/2 + K \cos x \sum_n \delta(t - n)$ defined on a cylinder is subjected to analysis in terms of OTOC [517]. For a single kicked rotor, thermal averaging is not applicable. To proceed further, the form of OTOC for this problem uses momentum operators and is defined as

$$C(t) = \hbar^2 \langle [p(t), p(0)]^2 \rangle = \hbar^2 \left\langle \left(\frac{\partial p(t)}{\partial x(0)} \right)^2 \right\rangle, \quad (157)$$

in which expectation value is evaluated in the initial state $|\psi(0)\rangle$. Thus, an exponential growth (as in Eq. (156)) with rate $\tilde{\lambda}_q$ must be associated with $C(t)$. The time evolution of $p(t)$ is calculated in the Heisenberg picture as $p(t) = (U^\dagger)^t p(0) U^t$, where U is the time evolution operator for the kicked rotor. The initial state is a Gaussian wavepacket in the momentum representation,

$$|\psi(0)\rangle = \sum_n a_n(0) |n\rangle \quad (158)$$

where $p|n\rangle = \hbar_s n |n\rangle$ and $a_n(0) \approx \exp\left(-\frac{\hbar_s^2(n-n_0)^2}{2\sigma^2}\right)$ is a Gaussian with mean n_0 and variance σ . A classical version of $C(t)$, denoted by $C_{cl}(t)$, can be obtained as

$$C_{cl}(t) = \hbar_s^2 \langle \{p(t), p(0)\} \rangle = \hbar_s^2 \overline{\left(\frac{\Delta p(t)}{\Delta x(0)} \right)} = \exp(2\tilde{\lambda}_{cl} t), \quad (159)$$

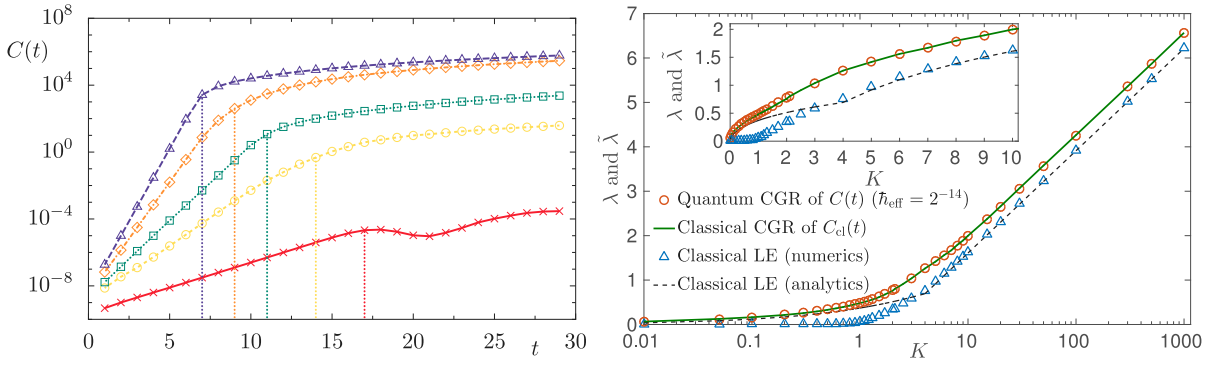


Fig. 31. (left) Growth of OTOC $C(t)$ for several values of the kicking strengths, (bottom to top) $K = 0.5, 2.0, 3.0, 6.0, 10.0$ and for $\hbar_s = 2^{-14}$, $N = 10^{23}$. The vertical lines represent the Ehrenfest time. The initial state is taken as Gaussian with $p_0 = 0$ and $\sigma = 4$. (right) The growth rate of $C(t)$, its classical version $\tilde{\lambda}$, and Lyapunov exponent λ are plotted as a function of K . Orange circles represent quantum growth rate λ_q with $\hbar = 2^{-14}$, and green solid line is classical growth rate λ_{cl} . Blue triangle (dashed line) represents numerically (analytically) computed Lyapunov exponents. The inset shows the same data as in the main plot in linear scales.

Source: Taken from Ref. [517].

where the over-bar denotes phase space average and $\tilde{\lambda}$ is the growth rate. The time evolution of OTOC for different kick strengths K is shown in left panel of Fig. 31. A clear exponential growth phase is seen that lasts until the Ehrenfest time $t_E \sim |\ln \hbar| / \ln(K/2)$ for $K \gg 1$. As K increases, t_E decreases implying that under conditions of strong chaos, the regime of quantum-classical correspondence does not last long. While this adds strength to the validity of Eq. (156), an interesting question is to evaluate if the growth rate of OTOC $\tilde{\lambda}$ is identical to the classical Lyapunov exponent λ or not. To perform this comparison, it is useful to recall the expression for Lyapunov exponent λ for $K \gg 1$ given in Eq. (14), and for $K > 4$ it is well approximated by $\lambda \approx \ln(K/2)$. To see the main results, all these numbers assembled together are shown in Fig. 31 (right panel). In this figure, the classical and quantum growth rates, $\tilde{\lambda}_{cl}$ and $\tilde{\lambda}_q$, display a good agreement with one another for extremely large values of K . What comes as a surprise is that the classical Lyapunov exponent is not in agreement with the classical and quantum rates. In particular, for $K > 8$, the difference between the (classical, quantum) growth rates and Lyapunov exponent λ is approximately $\ln \sqrt{2}$. The behavior of these growth rates around $K \lesssim 1$ makes it unreliable to distinguish between qualitatively distinct dynamics, regular or chaotic. Though the growth rate of $C(t)$ differs from the classical Lyapunov exponent, it might still be useful as a sensitive local probe of dynamical complexity in mixed phase space regime. For $t < t_E$, the growth rates, $(2t)^{-1} \ln C(t)$ and $(2t)^{-1} \ln C_{cl}(t)$, are time-independent and show an excellent agreement with one another. At $t = t_E$, $C(t)$ deviates sharply from $C_{cl}(t)$ and its temporal growth slows down to a power law attributed to weak localization effect [518]. The decay of $C(t)$ until the Ehrenfest time is strongly influenced by the Lyapunov exponent λ and is related to the stretching and folding mechanism of chaos generation in phase space. Another characteristic of chaotic systems is the mixing property, which also leads to exponential decay of classical correlations with a rate governed by Ruelle-Pollicott resonances. The decay of OTOC beyond $t = t_E$ is governed by the Ruelle-Pollicott resonances [519], as demonstrated in the case of a finite Hilbert space dimension system, namely, the perturbed cat map [520].

In two-dimensional weakly interacting kicked rotor a rather surprising development unfolds. It turns out that well beyond the Ehrenfest timescale, a universal regime of OTOC growth emerges induced by the interactions [521]. The growth rate in this regime is governed by an effective parameter that depends on the dimension of Hilbert space and strength of interaction. The Hamiltonian relevant for this discussion is the coupled kicked rotors defined on a torus (finite Hilbert space dimension) in Eq. (151), with

$$V_i(x_i) = \frac{1}{4\pi^2} K_i \cos(2\pi x_i) \sum_n \delta(t - n), \quad i = 1, 2, \quad \text{and} \quad bV(x_1, x_2) = \frac{b}{4\pi^2} \cos(2\pi(x_1 + x_2)) \sum_n \delta(t - n), \quad (160)$$

where b is strength of interaction, and K_1 and K_2 are the kick strengths of the rotors. Since thermal averages cannot be performed for the kicked rotor model, we will work with OTOC $C(t)$ defined without the thermal averaging process. In this limit, by expanding the expression for $C(t)$ in Eq. (155), the commutator can be expressed in terms of two-point and four-point correlators as

$$C(t) = C_2(t) - C_4(t), \quad \text{where,} \quad C_2(t) = \text{Tr}[A(t)^2 B(0)^2] \quad \text{and} \quad C_4(t) = \text{Tr}[A(t)B(0)A(t)B(0)]. \quad (161)$$

Now, if both the operators A and B are defined on the same rotor of the coupled system, then $C(t)$ is denoted by $C_{AA}(t)$, otherwise by $C_{AB}(t)$ if defined on two different rotors. The kick strengths of each rotor is assumed large enough, $K_1 = 9.0$ and $K_2 = 10.0$, for them to be chaotic but interaction between them is in the weak limit, $b \ll 1$. Fig. 32(a) shows the growth of $C_{AA}(t)$ and $C_{AB}(t)$, both display the anticipated Lyapunov growth regime. This exponential growth is maintained

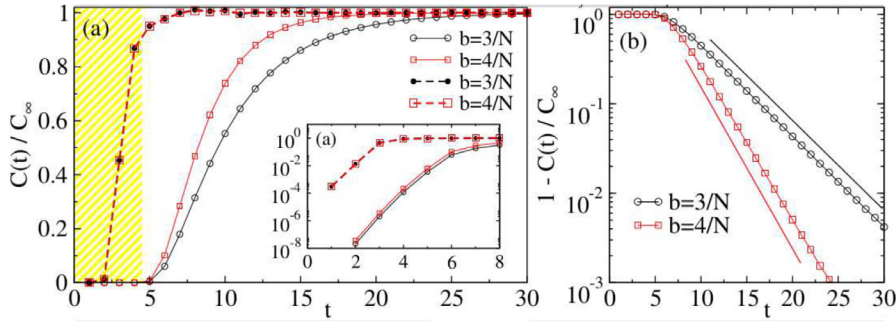


Fig. 32. OTOC growth with time is shown for various cases. The kick parameters are $K_1 = 9$, $K_2 = 10$ for both (a) and (b). (a) Normalized OTOC $C(t)/C_\infty$ for two cases, operators in different subspace (solid lines) and in same subspace (dashed lines). Inset shows the exponential growth till Ehrenfest time in the initial growth (log-linear scale), this is the Lyapunov phase with intra-subsystem scrambling. (b) $(1 - C(t)/C_\infty)$ (log-linear scale) for operators in different subspace. The solid lines represent the rate given in Eq. (5), and illustrate the RMT phase with inter-subsystem scrambling.

Source: Taken from Ref. [521].

until the Ehrenfest time $t_E = |\ln \hbar_s / \ln(K_2/2)| = \ln N / \lambda$, where $\hbar_s \sim 1/N$, $\lambda \approx \ln(K_2/2)$ and N is the dimension of the Hilbert space for each of the rotors.

In this regime, the growth rate of C_{AB} is nearly the same as that for C_{AA} and is independent of the interaction strength b . Note that $C_{AA}(t)$ is calculated for a single rotor. Thus, it can be inferred that the exponential growth until t_E is purely a manifestation of the intra-subsystem chaos. The prefactor of $C_{AB}(t)$ depends on the interaction strength and is expressed as $C_{AB}(t) \approx \gamma b^2 \exp(2\tilde{\lambda}_q t)$. This prefactor is also the same as that calculated from the classical Poisson bracket $\{\cos(2\pi x_1(t)), \cos(2\pi x_2(0))\}^2 \sim b^2 \exp(2\tilde{\lambda}_{cl} t)$. In this case also, it is observed that $\tilde{\lambda}_q = \tilde{\lambda}_{cl} > \lambda$, i.e. the classical Lyapunov exponent is consistent with the result for a single kicked rotor discussed above [517].

A new regime emerges beyond the Ehrenfest time. Unlike the single kicked rotor where $C(t)$ grows as power-law after t_E , the coupled kicked rotors show an exponential relaxation for $t > t_E$. As Fig. 32(b) reveals, the growth rate strongly depends on the interaction strength b but has weak dependence on the kicking strengths of each rotors. Thus, the post-Ehrenfest growth phase can be expressed as

$$C_{AB}(t) = C_\infty - \gamma_2(b) \exp[-2\mu(b)(t - t_E)], \quad t > t_E, \quad (162)$$

where, C_∞ and $\gamma_2(b)$ are independent of time and $\mu(b)$ is the relaxation rate. The fact that individual rotors are chaotic and the exponent μ depends only on the interaction strength and eventually leads to random states motivates random matrix modeling of the OTOC dynamics based on the transition RMT ensemble discussed in Section 10.3 for the entanglement entropy. The model is constructed by considering circular unitary ensemble (CUE) for the Floquet matrix of each rotor while that for interaction is modeled by a diagonal matrix with random elements. Thus, the transition RMT model can be expressed as in Eq. (152): $\mathcal{U} = (\mathcal{F}_1 \otimes \mathcal{F}_1) \mathcal{F}(\epsilon)$. The time evolution of the RMT matrix \mathcal{U}^t is represented as

$$\mathcal{U}^t = \prod_{j=1}^t (\mathcal{F}_{1j} \otimes \mathcal{F}_{2j}) \mathcal{F}_j(\epsilon) \quad (163)$$

where $\mathcal{F}_j(\epsilon)$, \mathcal{F}_{1j} and \mathcal{F}_{2j} are independent realizations at each time steps. To evaluate the RMT average of $C_{AB}(t)$ in Eq. (161), both $C_4(t)$ and $C_2(t)$ are necessary. In the limit $\epsilon \ll 1$, both these can evaluated to give [521]

$$C(t) = \mathcal{C} (1 - \text{sinc}^{4(t-1)}(\pi\epsilon)), \quad t \gg 1, \quad (164)$$

in which \mathcal{C} is a time-independent constant. Thus, for large times an exponential relaxation takes place with rate $\mu(\epsilon) = -4 \ln |\text{sinc}(\pi\epsilon)| \approx 2\pi^2 \epsilon^2 / 3$. Now, for coupled kicked rotors, by replacing $\mathcal{U}(\epsilon)$ by $U(b)$, and by assuming x_j to be random variable and averaging over, the rate $\mu(b)$ after unit time is [521]

$$\mu(b) \approx \frac{N^2 b^2}{4\pi^2}. \quad (165)$$

As $\mu(b)$ is independent of $K_{1,2}$, scrambling in this regime is between the two subsystems. This is verified in Fig. 32(b), for $C_{AB}(t)$ for two different interaction strengths. This is the dynamics of OTOC in the post-Ehrenfest regime and the growth rates (appears as a decay in this figure because $1 - C_{AB}(t)/C_\infty$ is plotted as a function of t) depend on b , as seen from the solid lines which represent Eq. (165). Fig. 33 shows the rate μ numerically computed from the coupled kicked rotor model, and the analytical estimates $\mu(\epsilon)$ (from transition RMT model) and $\mu(b)$ (from coupled kicked rotor). Even for relatively large interaction strength, i.e. $b = 3/N$, the analytical estimates are in good agreement with that rates computed for coupled kicked rotor.

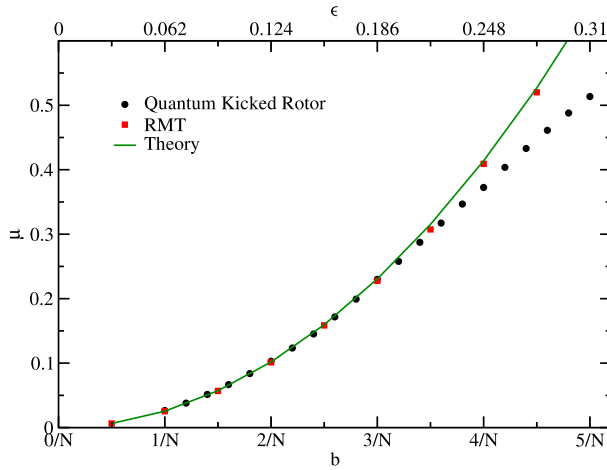


Fig. 33. Dependence of the rate of exponential growth μ of OTOC with interaction strength b is plotted. Black circles show $\mu(b)$ and red squares represent the rate, $\mu(\epsilon)$ for the RMT model. The parameters b and ϵ are scaled according to $\epsilon = \sqrt{3/8(Nb)/\pi^2}$. The solid line corresponds to Eq. (165) with $N = 64$.

Source: Taken from Ref. [521].

11. Applications

11.1. Quantum ratchets

Ratchets are devices that allow motion only in one direction and restricts it in the reverse direction. In physics, the term ratchet is generally used to imply extraction useful work from ambient thermal noise. Richard Feynman, in his *Lectures on Physics* [522], introduced a thought experiment for achieving unidirectional transport in the absence of a biasing force [523]. The experiment consists of two vanes attached to the two ends of a shaft. One of the vanes is attached to a device which allows motion only in one direction. The other vane is bombarded by the air molecules due to random molecular motion. The motivation is to cause the vane to move only in one direction or effectively work as a ratchet. The second law of thermodynamics prohibits the ratchet effect if both the vanes are maintained in thermal equilibrium. However, if they are out of equilibrium and relevant symmetries are broken, the ratchet effect is shown to be possible signifying the rectification of thermal noise to obtain a directed transport. Devices that can extract useful work out of thermal environment in nonequilibrium situations are called the thermal ratchets. Quite interestingly, Feynman ratchet was experimentally realized through a colloidal particle in a one-dimensional optical trap [524], though its efficiency was somewhat low (see also a discussion in Ref. [525]). Thus, Feynman's ratchet is no more a thought experiment. The subject of ratchets and its applications is vast, and for a review of thermal ratchets, the reader is referred to Ref. [526–528].

If thermal noise is replaced by sufficiently strong deterministic chaos, then chaos can play the role of fluctuating “environment” and it might be possible to realize “clean” deterministic ratchets. Further, all the techniques of deterministic dynamical systems can be applied for analysis. Hamiltonian systems are potential candidates to create this class of noise-free ratchets. Kicked rotor being a Hamiltonian system, displays regular, mixed and chaotic dynamical features serving as a quintessential model to study ratchet effect. In the subsequent subsections, discussions will primarily focus on how kicked rotor can be modified to display both classical and quantum ratchet effects. Let us consider the classical motion of a particle in a periodic potential $V(x, t)$. Generally, to qualify as a ratchet mechanism, it is necessary for the force on the particle, averaged over space and time, to be zero i.e., $\int dt \int dx V'(x, t) = 0$, where the integral is carried out over the periodicity of space and time. In order to generate directed motion in the average sense, it is required to break the spatial and temporal reflection symmetries [528,529]. Introducing dissipation in such a system strongly attenuates the momentum variance so that the ratchet effect does not suffer dilution [530,531]. The presence of dissipation automatically breaks temporal symmetry, and it is necessary to break the spatial symmetry to observe non-zero directed current [530].

For instance, the kicked rotor is both symmetric under time reversal and spatial reflection. It follows that the classical map in Eq. (9) cannot generate ratchet current. Over the years, much of the work built around kicked rotor have attempted to generate directed current by inventing different ways of breaking spatio-temporal symmetries. Another motivation is to carry over the ratchet mechanism to the quantum regime, in which there have been several experimental demonstrations [532]. Typically, to generate ratchet current in a kicked rotor system such as the one in Eq. (7), often the potential is made asymmetric through an additional spatial symmetry breaking term, and the kick sequence is manipulated to include more than one kick to break the temporal symmetry. This is not the only way to achieve ratchet current. Further, it must be pointed out that the notion of ratchet in chaotic Hamiltonian systems is not easily defined, partly due to many trivial ways in which this can be realized. Ideally, mean non-zero value for current should be realized

asymptotically in the absence of mean bias and, for this to be meaningful, the second moment should not increase with time.

In this pursuit, Dittrich et al. [533] describe a mechanism for generating ratchet effect in Hamiltonian system, $H = T(p) + V(x, t)$, where the force is periodic in both space and time $V'(x+1, t) = V'(x, t+1) = V'(x, t)$ so that the net force is zero, $\int_0^1 dt \int_0^1 dx V'(x, t) = 0$. To observe ratchet effect in this system, it is argued that mixed phase space is a necessary condition. A mixed phase space can be viewed as a made up several invariant sets, regular islands embedded in a chaotic sea. Typically, ratchet effect is inferred from non-zero current, i.e., mean velocity $\langle v \rangle \neq 0$. However, in this work, current is replaced by transport τ_M defined on an invariant set M . An important virtue of τ_M is that it is an additive quantity. For any invariant set M , the ballistic transport is defined as the product of phase volumes and the average velocity can be expressed as

$$\tau_M = \int_0^1 dt \int_0^1 dx \int_{-\infty}^{\infty} dp \chi_M(x, p, t) \frac{\partial H}{\partial p}, \quad (166)$$

where χ_M is the characteristic function of M . In Eq. (166) the transport is defined on a spatiotemporal unit cell $x, t \in [0, 1]$. For several disjunct invariant sets, a sum rule is obtained [533]:

$$\tau_M = \sum_i \tau_{M_i}. \quad (167)$$

In this, τ_{M_i} represents transport of the set M_i . To understand the working principle of this sum rule in Eq. (167), consider a system with mixed phase space and bounded from above and below by two KAM tori enclosing a chaotic layers and stable islands. The KAM tori are $p_{a,b}(x, t)$, where the index a and b refers to “above” and “below”. This region between these tori is treated as the global invariant set M . Then, $\tau_M = \langle T_a \rangle - \langle T_b \rangle$, where $\langle T \rangle_{a,b} = \int_0^1 dt \int_0^1 dx T(p_{a,b}(x, t))$, denoting averages of the kinetic energy over the tori. For a chaotic sea, $\tau_{ch} = A_{ch}v_{ch}$, where A_{ch} is the area of the chaotic region. If there are several islands indexed by i , and if w_i and A_i are, respectively, the winding number (time-averaged velocity) of the fixed point at the center (time-averaged velocity) and area of i th invariant set, then $\tau_i = A_i w_i$. Now, applying the sum rule gives

$$A_{ch}v_{ch} = \langle T_a \rangle - \langle T_b \rangle - \sum_i A_i w_i. \quad (168)$$

This implies that distinct layers in phase space will have different velocities. If spatio-temporal symmetries are not broken, then $\langle T_a \rangle - \langle T_b \rangle = 0$, and in the elliptic islands every trajectory has a counter-propagating trajectory that cancels one another, and the transport in the chaotic layer vanishes. One corollary of these arguments is that mixed phase space is necessary for directed chaotic transport. An interesting illustration is provided by the dissipative kicked rotor in Ref. [534]. In the Hamiltonian limit, this system does not support ratchet current due to presence of time reversal symmetry. However, with mild dissipation, time reversal symmetry is broken and large currents are generated due to the presence of tiny embedded islands in the chaotic sea. Though the sum rule is strictly not applicable, this provides a good illustration of regular regions in a chaotic sea being the source of ratchet current in a Hamiltonian system in the regime of weak dissipation. This is the central idea for ratchet transport governed by the sum rule in Eq. (167). There can be interesting violation of the classical sum rule as shown in a ratchet accelerator with kicked Harper model [535].

This can be extended to the quantum regime as well. In this case, the stationary states of the floquet operator plays the role of invariant sets. Stationary states corresponding to regular island and chaotic sea are identified based on the presence or absence of avoided crossings in the band spectrum. A band that appears to be a straight line corresponds to regular island. On the other hand, the band spectrum for the chaotic case shows oscillation and avoided crossings. A spectrum dominated by avoided crossings is known to be indicative of quantum chaos. Velocity is defined using the generalization of Hellmann–Feynman theorem as [533,536], $\bar{v}_{\alpha,k} = \frac{d\epsilon_{\alpha}(k)}{dk}$, where $\epsilon_{\alpha} \in [0, 1]$ is the quasi-energy of floquet state α and k is the quasi-momentum, $k \in [0, 1]$. Due to change of character near avoided crossings, the winding number \bar{w} or the average slope of the bands in the Brillouin zone vanish. Going through careful arguments [537] results in a quantum version of the sum rule given by

$$\sum_{\alpha} \bar{w}_{\alpha}^{ch} + \sum_{\alpha} \bar{w}_{\alpha}^{reg} = 0, \quad (169)$$

where the first term represents summation of winding number averaged over all chaotic Floquet states and second term over the regular states. The validity of this rule was confirmed in Ref. [533] (though not in a kicked sinusoidal potential) in the semiclassical limit in which regular bands can be sharply associated with the states localizing on regular regions in phase space.

The ratchet current mechanism discussed above is predicated on the existence of a mixed phase space along with broken spatio-temporal symmetry though nothing in it precludes other mechanisms from achieving directed currents in chaotic phase space. Further, the requirement of bounded motion implied that either the phase-space contains KAM tori or periodic boundary condition is applied on the momentum space. In both these scenarios, net transport of the global phase space is zero. Can there be a ratchet effect in a chaotic system with unbounded motion? In Ref. [538,539], a kicked

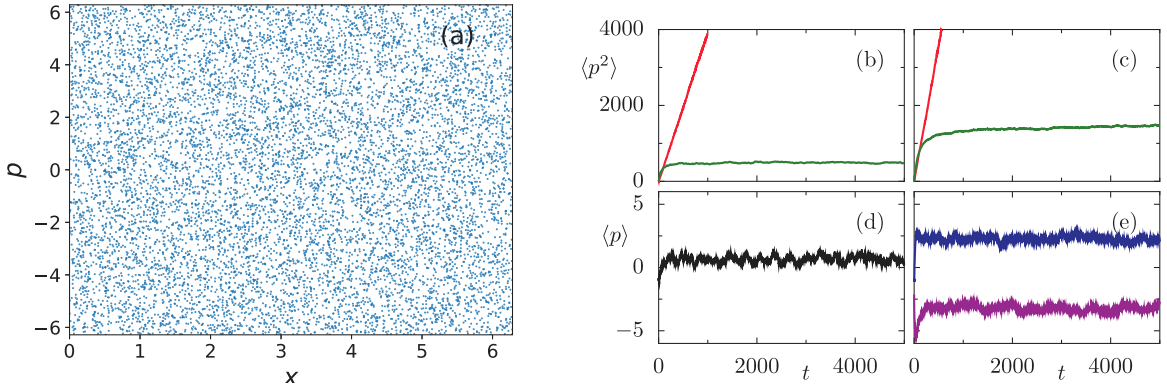


Fig. 34. (a) Stroboscopic section of the modified kicked rotor in Eq. (170) after $t = 500$. In this plot 10^4 initial conditions were taken randomly from $x \in [0, 2\pi]$ and $p \in [-2\pi, 2\pi]$. Other parameters are $N = 3$, $K = 2$, $b = 0.1$ and $a = 0.5$. (b,d) Quantum mean energy (green), classical energy (red), mean momentum (black) for $b = 0$ (one kick per cycle), (c,e) Quantum mean energy (green), classical energy (red), mean momentum (blue and magenta) for $b = 0.1$ (three kicks per cycle).

rotor with unbounded motion was considered that shows ratchet effect despite a largely chaotic phase-space. It effectively discards the need for any specific feature of the phase space for generating directed current.

The Hamiltonian of a kicked rotor modified to achieve a chaotic ratchet is

$$H = \frac{p^2}{2} + K V(x) \sum_{n,i} \delta(t - nT_i), \quad V(x) = [\sin(x) + a \sin(2x + \phi)], \quad (170)$$

in which $V(x)$ represents a double well potential and ϕ breaks the spatial symmetry, while multiple kicks in a period T breaks the temporal symmetry. In this scheme, kicks occur at $T_i = 1 - jb, 1 - (j-1)b, \dots, 1 + jb$, where b is the small time increment and $j > 0$ is integer. If N kicks are applied per cycle, then the total time-period is $T = \sum_{i=1}^N T_i$ such that $\langle T_i \rangle = 1$. This system is defined on a cylinder and is unbounded in momentum direction. The ratchet mechanism is based on the fact that, in the system in Eq. (170) and in the chaotic regime, the diffusion rates for particles with positive and negative momenta are different until t_r , the so-called ratchet timescale. This diffusion asymmetry, that arises due to short time momentum correlations that depend on b [539], builds up only until t_r , and the mean current $\langle p \rangle$ saturates at this time. However, $\langle p^2 \rangle$ continues to display quasi-linear diffusion with rate D . This feature spoils the classical directed current. However, quantum mechanically dynamical localization comes to the rescue and arrests the unbounded increase of $\langle p^2 \rangle$. Hence, quantum ratchet current is best realized if the quantum-classical break-time matches the ratchet timescale, i.e., $t_b \sim t_r$. The ratchet time can be estimated to be $t_r \sim 1/(b^2 D)$, and the break-time is $t_b \sim D/\hbar^2$. Equating the two, the condition for ratchet current with minimal uncertainty associated with $\langle p \rangle$ is $Db/\hbar \sim 1$. To obtain the quantum dynamics, the Floquet operator is $U_i = \exp(-iV(x)/\hbar) \exp(-i\hbar T_i(p + \beta)^2/2)$, where β is the quasi-momentum, is used to evolve an initial state and the required averages are computed. The results are illustrated in Fig. 34 for the case of $N = 3$ kicks in a cycle, with other parameters, $K = 2$, $b = 0.1$ and $a = 0.5$, chosen to break the spatio-temporal symmetries. The stroboscopic section in Fig. 34 reveals a largely chaotic phase space. This figure (right panel) also displays the numerically computed quantum mean energy and momentum. Firstly, if $b = 0$ (one kick per cycle, temporal symmetry not broken), then $\langle p \rangle = 0$ and no ratchet current is realized. However, if $b = 0.1$, depending on the value of phase ϕ , large directed current is realized. Notice also that quantum energy $\langle p^2 \rangle$ is saturated for $t > t_b$ and the growth of uncertainty is arrested as well. These results do not depend on specific choice of initial states. This can be regarded as a possible ratchet mechanism and was experimentally demonstrated in a cold-atoms test bed [540], though the experimental system was slightly different from Eq. (170).

11.2. Resonance ratchets

As pointed out in Section 5.3, quantum resonances in the kicked rotor are uniquely quantum phenomena without a classical analogue. If the kick period is set to half the Talbot time, the ballistic growth of energy is a clear indication of quantum resonances. The ratchet mechanism discussed until now have both the classical and quantum versions, and in the semiclassical limit it should be possible to recover the classical directed currents. It turns out that resonance ratchets [541], like the quantum resonance itself, is a purely quantum phenomenon. Hence, purely quantum ratchets can be achieved through the resonance route. Even more remarkable is the initial state dependence of the state evolution at quantum resonance since this property obviates the need for breaking of spatio-temporal symmetries to realize ratchet current. Experiments using Bose-Einstein condensates in optical lattices have realized resonance ratchets [541–543] and it continues to be an active and fertile area of research for potential applications.

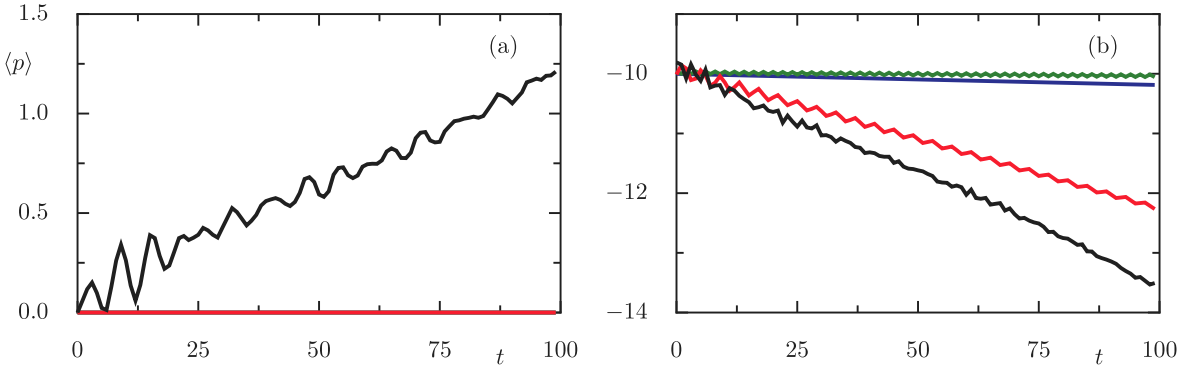


Fig. 35. Ratchet current quantified by mean momentum $\langle k \rangle$ is plotted as a function of time for different resonance conditions: $\hbar_s = 4\pi$ (blue), $\hbar_s = 2\pi$ (green), $\hbar_s = \pi$ (red) and $\hbar_s = \pi/2$ (black). (a) A homogeneous initial state $\psi(0) = \frac{1}{\sqrt{2\pi}}$ is considered. Blue, green and red lines with symbols are overlapped. (b) A coherent state with $\langle k \rangle = -10$ is taken as an initial state. Kick strength for both the plots is $\frac{K}{\hbar_s} = 0.5$.

Let us consider the kicked rotor Hamiltonian with saw-tooth potential given by

$$H = \frac{p^2}{2} + K v(x) \sum_n \delta(t - n), \quad v(x) = \sin(x) + \alpha \sin(2x), \quad (171)$$

where α is the asymmetry parameter and K is the usual kick strength. The time evolution is effected by applying the Floquet operator $U = e^{-i\hbar_s k^2/2} e^{-i\frac{K}{\hbar_s}v(x)}$ on an initial state $|\psi(0)\rangle$. In this, $p = k\hbar_s$ and spatial periodicity restricts k to only integer values. For the quantum resonance at $\hbar_s = 4q\pi$, where q is an integer, the Floquet operator reduces to $U = e^{-i\frac{K}{\hbar_s}v(x)}$ as the free evolution operator is $e^{-i\hbar_s k^2/2} = e^{-i2\pi k^2} = 1$ for all integer values of k . Then, the time evolved state is

$$\psi(x, t) = e^{-it\frac{K}{\hbar_s}v(x)} \psi(x, 0) \quad (172)$$

and the mean momentum is

$$\langle k \rangle = -\frac{tK}{\hbar_s} \int dx v'(x) |\psi(x, 0)|^2. \quad (173)$$

This expression clearly reveals that if the initial state is a plane wave or a zero momentum state, then the net current is zero because $v'(x)$ is a symmetric function. This is observed in Fig. 35(a). On the other hand, if there is any inhomogeneity in the initial state then it will get amplified over time giving rise to a linear growth of ratchet current as indicated by blue line with symbol in Fig. 35(b). This analysis can be repeated for the resonance condition $\hbar_s = 2q\pi$, where q is an odd integer, and similar conclusion results on the dependence on the initial state. The simulation results for this case are displayed in Fig. 35(a) and (b), for the homogeneous and inhomogeneous initial states. The former generates zero current while the latter generates linearly increasing current. If this calculation is repeated for $\hbar_s = \pi/2$, the evolved state turns out to be,

$$\begin{aligned} \psi(x, t+1) = & \frac{1}{2} \left[e^{-i\pi/4} e^{-i\frac{K}{\hbar_s}v(x)} \psi(x, t) + e^{-i\frac{K}{\hbar_s}v(x+\pi/2)} \psi(x+\pi/2, t) \right. \\ & \left. - e^{-i\pi/4} e^{-i\frac{K}{\hbar_s}v(x+\pi)} \psi(x+\pi, t) + e^{-i\frac{K}{\hbar_s}v(x+3\pi/2)} \psi(x+3\pi/2, t) \right], \end{aligned} \quad (174)$$

and it can be shown that $|\langle k \rangle|$ grows with time irrespective of the initial state. This is observed in Fig. 35).

If an asymmetric initial state is prepared and evolved, the spatial symmetry need not be broken. In fact, it can be exactly shown that the necessary condition to generate ratchet current under conditions of quantum resonance is that either asymmetry in the initial state or an asymmetric kick potential is required [544]. This is a necessary, but not sufficient, condition since in some cases it is possible to have one of these conditions satisfied and yet the current can be zero. This can be illustrated by going back to the Hamiltonian in Eq. (171) with $v(x) = \cos(2k_L x)$, where k_L is the wave number. Firstly, notice that with $v(x)$ as defined now, it is simply the standard kicked rotor with spatio-temporal symmetries preserved. If zero momentum state $|0\hbar k\rangle$ is used as the initial state, then no ratchet current will be observed. However, if the initial state is given by

$$|\psi(0)\rangle = \frac{1}{\sqrt{2}} (|0\hbar k\rangle - ie^{i\phi} |-2\hbar k\rangle), \quad (175)$$

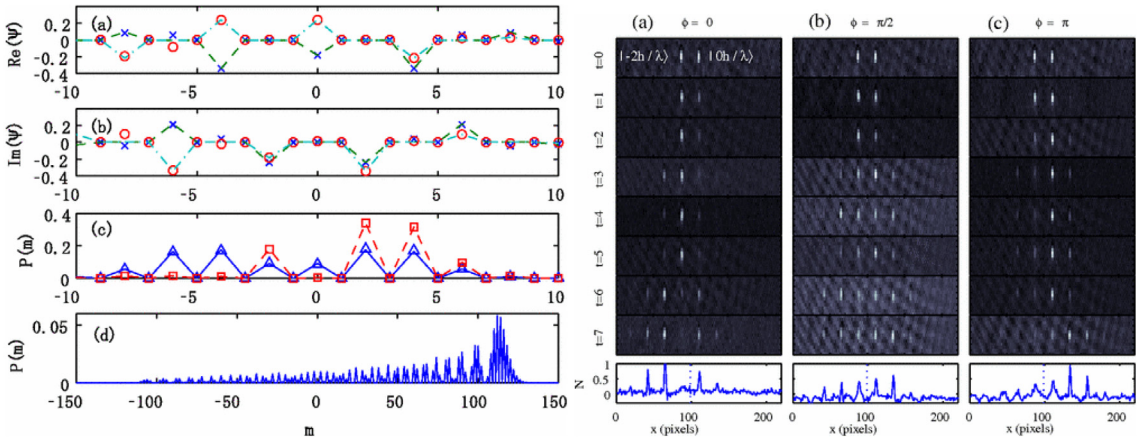


Fig. 36. (left) (a,b) show the evolved function after 5 kicks with phase $\phi = \pi$. The evolution of each of the terms in Eq. (176) is shown separately. The evolved part arising from $|0\hbar k\rangle$ is shown as crosses, and that from $|-2\hbar k\rangle$ is shown as circles, both obtained through simulations. The broken lines are the analytical result from Eq. (177). (c) Probability density for $\phi = \pi$ (squares), and for $\phi = \pi/2$ (triangles) obtained from simulations (symbols) and theory (broken lines). Note the asymmetry in the case of $\phi = \pi$ and symmetry about $|\hbar k\rangle$ for $\phi = \pi/2$. (d) Large asymmetry in the evolved probability density at time $t = 100$. (right) Absorption images of the ratchet BEC experiment as a function of time up to $t = 7$. The initial state superposition state is shown at the top for $t = 0$. The evolution of density for all the cases shows asymmetry, as also evident in the row-integrated intensity for $t = 7$ shown at the bottom as blue colored line plot. This gives the distribution of atoms over the position space.

Source: Taken from Ref. [542].

where ϕ is the phase, is used at quantum resonance $\hbar = 4\pi$, then the time evolved state and momentum distributions, respectively, are

$$\langle m | \psi(t) \rangle = \frac{e^{im\pi/2}}{\sqrt{2}} [J_m(Kt) - e^{i\phi} J_{m+1}(Kt)], \quad \text{and} \quad (176)$$

$$P(m) = |\psi(m, t)|^2 = \frac{1}{2} [J_m^2(Kt) + J_{m+1}^2(Kt) - 2 \cos(\phi) J_m(Kt) J_{m+1}(Kt)]. \quad (177)$$

For arbitrary value of the phase ϕ the momentum distribution $|\psi(m, t)|^2$ would display an asymmetric temporal growth, and hence induce a non-zero mean momentum or ratchet current. It is interesting that the asymmetry itself arises because of interference between the diffraction orders (the last term in Eq. (177) of the two terms of the initial state in Eq. (175)). These features can be seen in the simulation results shown in the left panel of Fig. 36. In particular, the evolved asymmetry after 5 kicks must be noted, and also that the two parts of the initial wavefunction, $|0\hbar k\rangle$ and $|-2\hbar k\rangle$, interfere constructively for $m > 0$ and destructively for $m < 0$. An experiment with BEC in optical standing wave was performed [542], and the absorption images show a clear and remarkable evidence of the asymmetric growth of initial state. In the experiment too, the initial state was prepared as in Eq. (175) through use of Bragg $\pi/2$ pulse and a phase of free evolution. If ϕ is changed from 0 to π , a reversal in the direction is evident leading to reversal of ratchet current. In fact, this is a general feature that allows control over the direction of current by manipulating the phase. As demonstrated in another experiment, by creating an initial state made up of larger superpositions (it was superposition of two momentum states in Eq. (175)), the ratchet current can be maximized [545]. Thus, the resonance ratchet effect arises purely from quintessential quantum effects, namely, the quantum interferences that induce asymmetry in the time evolved states.

There are other interesting extensions that include larger ratchet currents generated due to higher order resonances [186] compared to the low order resonances [546], quantum ratchets coupled to an environment in which the ratchet current is transient [547], and quantum ratchet accelerator based on classical accelerator modes [548,549]. A ratchet accelerator can display net current that accelerates with time, with a steady non-zero acceleration. In Ref. [548], a kicked rotor devoid of spatio-temporal symmetries becomes a ratchet accelerator if parameters are chosen to be in the regime of classical accelerator modes (see Section 4.2).

11.3. Atom interferometry with kicked rotor

Two or more coherent wave forms that have propagated along separate paths and accumulated different phases can, in principle, be superposed to produce an interference pattern. This is the working principle behind interferometers. Depending on the accumulated phase difference, they can interfere either constructively or destructively. The optical interferometers, such as Michelson or Fabry–Perot interferometer, either bright or dark fringes are produced. On the other hand, atom based interferometers exploit the fact that matter can exhibit wave-like properties similar to light to

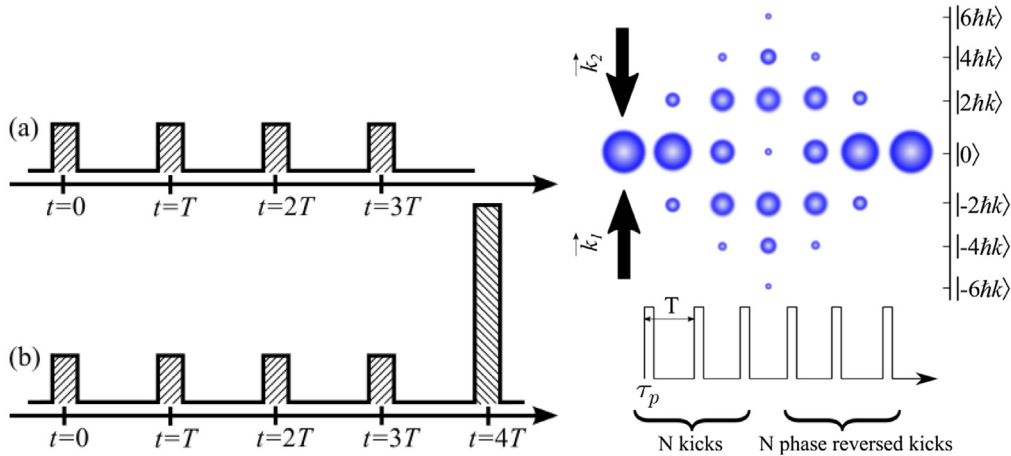


Fig. 37. (left) (a) kicked rotor sequence with kick period T , (b) modified sequence for fidelity measurement. Note the last kick with larger kick strength and phase changed. Taken from Ref. [556]. (right) Kick sequence in which first N kicks and the next N kicks have opposite phases. Blue circles show a schematic of the evolution of atomic cloud under the action of this sequence. The size of the circle represents the population in that state. Taken from Ref. [557].

produce interference effect. Atom interferometers have led to high precision measurement of fundamental constants such as the gravitational constant [550,551] and the fine structure constant α [552,553]. In particular, fine structure constant has been measured to an accuracy of 2×10^{-10} [553] using an atom interferometer.

The role of kicked rotor in interferometry is based on the fact that the energy absorption of the rotor is strongly enhanced at a quantum resonance, while away from a resonance the energy absorption is arrested due to dynamical localization. At resonance kicked rotor acts as a beam-splitter as wave propagates diffusively in both positive and negative momentum states and they are made to interfere. This creates an interferometer out of kicked rotor. Since quantum resonances happen when the kicking period is $T = (l/m)\tau_T$, where l and m are integers, and τ_T is the characteristic Talbot time, it is possible tune for these resonances. The decay of energy absorption in the vicinity of resonances, or, in general the width of the resonance peaks is a sensitive measure of how accurately two distinct frequencies can be distinguished. Theoretical treatments based on semiclassics [188] had earlier predicted the width to scale as $1/N^2$, where N is the number of kicks imparted. Quantum system, or for that matter any system, in a regime of linear response is limited by the standard Fourier scaling, which states that resonance widths are inversely related to the measurement time. The violation of this scaling limit by resonant quantum kicked rotor is related to the nonlinear response of the system, and specifically to the avoided crossings between Floquet states [554]. Such sub-Fourier scaling was in fact observed in an experiment reported in Ref. [555].

As it turns out, quantum kicked rotor can achieve sub-Fourier scaling down to $1/N^3$. To appreciate this, recollect that kicked rotors work like a beam-splitter to evolve them on two paths – positive and negative momentum states. The key is to create large momentum difference with smallest number of kicks. One way to achieve this is by performing a fidelity measurement through a modified pulse sequence shown in Fig. 37. The modified pulse sequence will have $(N-1)$ standard kicked rotor pulses of strength K and N th pulse will have opposite phase with respect to all the other N -pulses and its strength is NK . If the initial state is a zero momentum state $|p=0\rangle$, then the cloud of atoms is diffracted by the kicked rotor pulse sequence. Normally mean energy is inferred from the measured atomic cloud. One alternative is to measure the proportion of this initial cloud that returns back to the state $|p=0\rangle$ under the effect of the last phase shifted pulse of larger strength [556]. The time-dependent potential for this scenario is [556]

$$V(t) = K \cos(2kx) \sum_{n=0}^{N-1} \delta(t - nT) - NK \cos(2kx) \delta(t - NT), \quad (178)$$

where T is the kick period, K is the kick strength and k is the wave number of the external field. Fidelity would be given by the overlap of the initial state with the final state, and it can be written down as

$$F(\epsilon, p_0) = \left| \langle p_0 | \left(e^{iNK \cos(2kx)} e^{-i(p^2/2M\hbar)(\tau_T + \epsilon)} e^{iK \cos(2kx)} \right)^N | p_0 \rangle \right|^2, \quad (179)$$

where $\epsilon = T - \tau_T$ and $|p_0\rangle$ is the initial momentum state. Compared to energy measurements through time-of-flight, $F(\epsilon, p_0)$ will be sensitive to phase deviations from the value of phase at resonance since it crucially depends on the relative phases between the basis states. An approximate expression for the fidelity $F(\epsilon, p_0 = 0)$ of zero momentum state

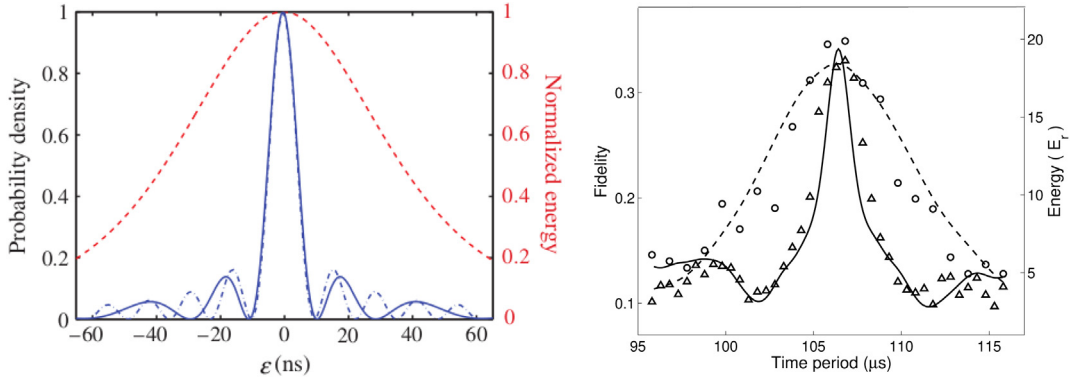


Fig. 38. (left) Red dashed line shows energy of the atomic cloud as a function of $T - \tau_T$. Solid (blue) line shows numerical simulation of Eq. (179). Dashed (blue) line shows the approximate result in Eq. (180). Taken from Ref. [556]. (right) Atom optics experimental realization of fidelity measurement at resonance shown as circles. Note the narrow width of the fidelity resonance peak compared to the energy resonance peak shown as triangles. Taken from Ref. [190].

gives the following result:

$$F(\epsilon, p_0 = 0) \approx J_0^2 \left(\frac{\hbar k^2}{3M} N^3 K^2 \epsilon \right). \quad (180)$$

This gives a scaling of $1/N^3$ for the width of fidelity peak. The left panel of Fig. 38 shows fidelity as a function of $\epsilon = T - \tau_T$. At Talbot time, corresponding to $\epsilon = 0$, a sharp peak or a revival can be observed in fidelity [558], whereas the energy displays a broader resonance width. In practice, for initial states with finite width such as Gaussian states the decay of fidelity width deviates from $1/N^3$ scaling for $N > 20$. This result can be compared with an experiment which implemented this kicking protocol [190] in 2010 and a snapshot of the result is shown in the right panel of Fig. 38. As seen in this figure, the experimental result also shows, in the vicinity of resonance, a narrow width for the fidelity (circles) in contrast to the broader profile of the energy curve (triangles). While the anticipated scaling of fidelity width with N is $1/N^3$, this experiment reports a scaling of $1/N^\alpha$, $\alpha = 2.73 \pm 0.19$. Despite these minor differences, it is a clear demonstration of strong sub-Fourier characteristics of the behavior around resonance for the kicked rotor with modified kick sequence.

There is another approach to achieving the same $1/N^3$ scaling but without using the high order diffraction pulse. This could help achieving the same level of dispersion in momentum without requiring high power laser pulses in an experiment. In this theoretical proposal [191], the kick sequence is modified such that after N kicks, the next N kicks are imparted with a π -pulse applied to them. The net effect is that the waves propagating in both the momentum directions for the first N kicks, change direction and superimpose to produce an interference pattern. A schematic is shown in the right panel of Fig. 37. The Hamiltonian for this kicking scheme is

$$H = \frac{p^2}{2m} + \hbar\phi_d \cos(\kappa x) \left(\sum_{n=0}^{N-1} \delta(t - nT) - \sum_{n=N}^{2N-1} \delta(t - nT) \right). \quad (181)$$

During the first N kicks, the Floquet operator is $U = \exp(-i\frac{p^2}{2m\hbar}T) \exp(-i\phi_d \cos(\kappa x))$ and acts to diffuse the atomic cloud. From N to $2N - 1$ kicks the dynamics is governed by $V = \exp(-i\frac{p^2}{2m\hbar}T) \exp(i\phi_d \cos(\kappa x))$, the atomic cloud diffusing in the reverse direction (as shown in Fig. 37). The output of the interferometer can be evaluated by measuring the number of atoms that return to their initial state and the final result shows $1/N^3$ scaling [191]:

$$I(\epsilon, p_0) = |\langle p_0 | V^N U^N | p_0 \rangle|^2 \propto \frac{1}{N^3}, \quad (182)$$

where the last form is the asymptotic result for the leading term in the limit of $\epsilon \rightarrow 0$. Recent experiment using BEC in standing waves has realized this kick sequence and has reported pronounced dependence on finite pulse width (as opposed to ideal zero widths considered in theory) and strong deviations from $1/N^3$ scaling [557]. In general, this area can be expected to witness major developments especially in the context of emerging trends in quantum technologies.

11.4. Control of decoherence

For any system, sustaining quantum effects such as localization depends on the ability to maintain the system shielded from the decohering influence of the environment. Strictly, this is never possible. The states of a quantum system would invariably get entangled with the environment degrees of freedom, and in the process lose its quantumness.

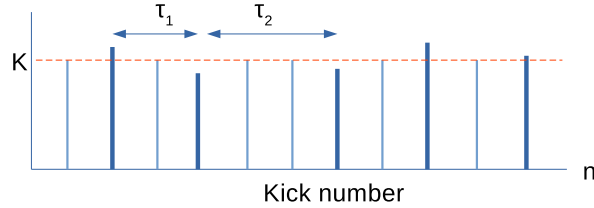


Fig. 39. Schematic diagram of the kicking sequence with a unit time-period. Kick amplitude is plotted as a function of kick number. τ_1 and τ_2 are two of the waiting times between successive amplitude noise events indicated by thick blue lines. The waiting time between the noise events τ_i are taken from Lévy distribution.

This is typically a rapid and nearly most of the time irreversible loss that leads from quantum to classical transition. The decoherence theory, whose recent developments are reviewed in Ref. [559], was initiated almost five decades ago and provides a description of the regime in the boundary between quantum and classical physics. Typically, the rate of coherence loss is exponential in nature with a form $D(t) \sim \exp(-t/t_c)$, where t_c is the mean coherence time. For example, for a diffusing point particle, the coherence time is $t_c = 1/[mk(\Delta x)^2]$ and depends on the mass m of the particle, the coupling strength with the environment κ , and the spatial separation Δx of the interfering states [560,561]. The exponential coherence decay is considered as one of the main impediments in building large scale quantum devices such as quantum computers. It is crucial then to at least slow down decoherence process even if it cannot be entirely eliminated. Several theoretical and experimental works exist in this regard Ref. [559], and this section will only focus on contributions arising from kicked rotor as the test bed. The kicked rotor system is a suitable candidate for the study of decoherence for the reason that its classical and quantum dynamical behaviors, diffusion versus localization, are unambiguous and have quite distinct dynamical features (see Fig. 7(a)). The effect of environment enters the system dynamics in the form of noise added to either the time-period, kick strength or phase of the system. Noisy events lead the quasienergy states of the rotor to couple and induce transitions between them. As a result, dynamical localization is suppressed and quantum diffusion takes place. Decoherence in kicked rotors as a problem of interplay of noise with the localized states has been studied by many authors in the past both in theory and through experiments, and some of them are briefly discussed in Section 7.1.

Given that decoherence cannot be entirely suppressed, the next best thing is to attempt to slow down decoherence, in particular, from its putative exponential form to anything slower than exponential. Most of theoretical proposals and experimental demonstrations attempt to extend mean coherence time τ_c within the framework of exponential coherence decay. In contrast, in Ref. [298,562], it was shown that amplitude noise applied to kick strengths at time intervals drawn from Levy distribution can change the form of coherence decay from exponential to a power-law form. A schematic of this kick sequence is shown in Fig. 39. Position of red dot indicates the noisy kicks while other kicks remain unaffected. The interval between the occurrence of noisy kicks (the red dots) is random and taken from a Lévy waiting time distribution $w(t)$ that asymptotically behaves as power-law $w(t) \propto t^{-1-\alpha}$ for $t \gg 1$, where α is the Lévy exponent [563]. It is important to recognize that the mean waiting time is $\tau = \alpha/(\alpha - 1)$ for $\alpha > 1$ and diverges in the regime $\alpha < 1$ [564].

Approximate expressions of the decoherence function for different α regimes can be obtained analytically [298], where approximations enter through random phase approximation and averaging is performed over waiting times. For $\alpha > 1$ and within a time interval $[t', t'']$, the decoherence function takes the form $D(t', t'') \simeq \exp((t'' - t')/\tau t_c)$, where τ is the mean of the Lévy distribution, t_c is the coherence time and the product τt_c is the effective coherence time. Note that the decoherence function for $\alpha > 1$ does not hold for $\alpha \leq 1$ because the effective coherence time is ill-defined due to diverging τ . A different functional form of decoherence factor is expected for $\alpha \leq 1$. The mathematical expression of the decoherence factor that holds for $\alpha \leq 1$ is $D(t, 0) \simeq E_\alpha(t^\alpha/(\Gamma(-\alpha)c t_c))$, where $E(z) = \sum_{n=0}^{\infty} z^n/\Gamma(\alpha n + 1)$ is the Mittag-Leffler function [565] and $c = \alpha \Gamma(\alpha + 1)$. Now, because of $E(z)$, the initial decay of $D(t, 0)$ is a stretched exponential $D(t, 0) \simeq \exp(t^\alpha/(\Gamma(-\alpha)c t_c))$, while for large times $D(t, 0)$ changes its form to a power-law $D(t, 0) \simeq (c t_c/\alpha)t^{-\alpha}$. Thus, the decoherence factor for $\alpha \leq 1$ is no longer an exponential function but rather a power-law implying slower decoherence. This leads to controllable decoherence governed by the exponent α .

The experimental demonstration of decoherence suppression used a different kicking scheme [299] which does not require amplitude noise but missing of kicks. The Hamiltonian in this case is

$$H = \frac{p^2}{2} + K \cos x \sum_n (1 - g_n) \delta(t - n) \quad (183)$$

where, g_n take values either 0 or 1. If $g_n = 1$, then there is a missing of kick otherwise a kick occurs. The waiting time between the successive occurrences of 0 are taken from $w(t)$. Interestingly, for this system also the functional forms of decoherence factor are different for two distinct regimes of α . For $\alpha \leq 1$, the decoherence factor within the time interval $(t, 0)$ is expressed as [299]

$$D(t, 0) \sim e^{-(1-q^2)t} E_\alpha \left((1 - q^2)t^\alpha \frac{\sin \pi \alpha}{\pi \alpha} \right), \quad (184)$$

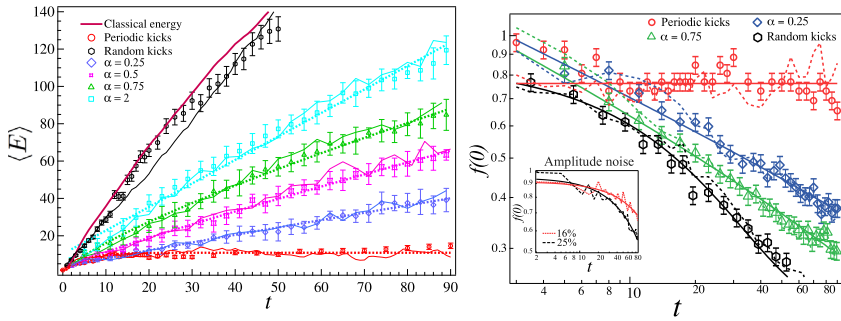


Fig. 40. (left) The mean energy $E(t)$ as a function of time for different values of Lévy exponent α . Symbols with error bars are from the experimental data, solid lines are from simulations, and analytical predictions are represented by dashed lines. Parameters are kick strength $K = 5.8$ and $\hbar_s \approx 2.0$. The lowest curve (red) corresponds to noise-free, periodic kicks and localization is observed. (right) Log-log plot of occupation probability of zero momentum state $f(p = 0)$ as a function of time. Symbols and dashed lines are from experimental and simulation data respectively. Black color corresponds to the case of stationary amplitude noise applied to the kicks (as reported in Ref. [294]), and show exponential decay. Blue and green curves are for the Lévy kicked rotor of Eq. (183), which display a power-law decay. All the solid lines (black, green, blue, red) are to guide the eye.

Source: Taken from Ref. [299].

where the function $q(K'_t/\hbar_s)$ is given by

$$q(K'_t/\hbar_s) = 1 - \frac{K'^2}{2\hbar_s^2} \overline{\cos^2 x} + \frac{K'^4}{4!\hbar_s^4} \overline{\cos^4 x} + \dots \quad (185)$$

In this, $K' = Kg_n$ and $E_\alpha(\cdot)$ is the Mittag-Leffler function. The mean energy growth at $t \gg 1$ is calculated analytically and is expressed as $E(t) = A_0 t + A_1 t^\alpha$ [299], where A_0 and A_1 are time-independent and can be analytically calculated. Fig. 40 shows the $E(t)$ calculated analytically, numerically and experimentally for different values of α . All the three results are in good agreement with one another. The left panel of Fig. 40 shows that for periodic kicks (red symbols), the system shows localization, but as α increases a controlled progression towards quasi-linear diffusion (black symbols) can be observed. This must be contrasted with stationary uniform distributed noise applied to the kick amplitudes as reported in Ref. [294]. In this case the decoherence is exponential. This contrast can be inferred in the right panel of Fig. 40, which shows population in the zero momentum state as a proxy for decoherence factor which was not directly accessible in this experiment. The amplitude noise case of Ref. [294] displays exponential decay of population, while the Levy noise case (of the Hamiltonian in Eq. (183)) displays a much slower non-exponential decay. This is an indirect evidence for slower convergence towards classical states.

However, for $\alpha > 1$ exponential decay of coherence is restored. The decoherence factor is $\mathcal{D}(t, 0) = \exp(-(1-q^2)(1-1/\tau)t)$, and for $t \gg 1$ the diffusive energy growth $E \sim Dt$ is also restored. The diffusion coefficient for $\alpha > 1$ is [566]

$$D = \frac{K^2}{2} \left(-\frac{1}{\alpha} + \frac{1}{1-\alpha/r} \right), \quad \text{where} \quad r = (q^2 - 1)t^*, \quad (186)$$

and t^* is the break time. Fig. 40 (left panel) clearly shows the expected diffusive quantum energy growth for $\alpha = 2$ and it closely matches the classical energy growth. Note that D in Eq. (186) has a nonlinear dependence on both K and the Lévy parameter α . Surprisingly, the dependence on α is non-monotonic which implies that with increase in α , diffusion rate is a maxima at [566]

$$\alpha = \alpha_c = \frac{1 + \sqrt{(1-q^2)t^*}}{1 - \frac{1}{(1-q^2)t^*}}. \quad (187)$$

Thus, as demonstrated in cold-atoms based experiments [566] tuning the value of α allows to optimize the diffusion rate in the kicked rotor system.

11.5. Quantum computing the kicked rotor

In the seminal article [567], Richard Feynman proposed that quantum computer is needed to simulate nature because nature is based on laws of quantum physics. In this context, it is natural to ask if kicked rotor can be simulated by a quantum computer. With the availability of quantum computer hardware with about 100 to a few 1000 qubits (depending on which kind of quantum computer one is interested in), it is a question of interest to evaluate to what extent quantum properties can be simulated on a quantum hardware. As the focus is on the quantum kicked rotor system, the quantum properties of interest are the dynamical localization, diffusion and metal-insulator transition in higher dimensional kicked

rotor. A kicked rotor defined with N momentum states (or levels) can be simulated exponentially faster than on a classical computer. In particular, if N is taken to be the quantity that measures the size of the problem, the time complexity of the quantum algorithm presented in Ref. [568] is $O((\log_2 N)^3)$, while that of a classical algorithm is $O(N \log_2 N)$. This can be seen as follows; for the classical algorithm, the standard way to numerically simulate the kicked rotor is by iteratively operating the unitary operators U_{free} and U_{kick} on an initial state, say, the zero momentum state $|0\rangle$. Note that if the initial state is in momentum representation, then one Fourier transform is required before operation by U_{kick} , and one inverse Fourier transform is also needed before operating by U_{free} . The Fourier transform conveniently uses Fast Fourier Transform (FFT) algorithm of complexity $O(N \log_2 N)$, and in each time a diagonal matrix multiplication of $O(N)$. Hence, to leading order, the time complexity of classical algorithm is $O(N \log_2 N)$. To attain exponential speedup, the FFT part is replaced by quantum Fourier transform algorithm [477]. In addition, certain ancillary qubits need to be created and measurements performed. Taking all this into account (for details see Ref. [568,569]), time complexity of $O((\log_2 N)^3)$ is attained. This, however, does not solve all the problems, and earlier other problems due to imperfections were expected to spoil the quantum coherences and destroy localization [570]. Repeated state measurements can in principle weaken dynamical localization and lead to diffusive dynamics. It turns out that, at least in theory, dynamical localization is sufficiently protected in spite of repeated measurements [571]. This machinery can be used to probe the Anderson transition in a quasiperiodic kicked rotor [572]. Not just the kicked rotor, it is also shown that a quantum computer with a few qubits can simulate dynamical localization in the quantum sawtooth map [573,574].

12. Outlook

One of the prime motivations for the introduction of the kicked rotor nearly 50 years ago was to clarify the ideas of instability of motion in nonlinear Hamiltonian systems. At the heart of kicked rotor is of course the pendulum. Boris Chirikov, as a prelude to introducing a set of problems leading up to the kicked rotor [81], states that the “oscillations of a pendulum give us one of the oldest examples of oscillations, in general, and, in particular, nonlinear oscillations. The centuries-old history of studying this apparently simple system has shown a surprising diversity of its motions”. Indeed, today it is possible to state that an apparently simple system (at first sight) like the kicked rotor has shown surprisingly rich dynamics in the classical and quantum regimes. Five decades ago, from the time when there were hardly any experimental realizations, we have now progressed to many experimental results based on quantum kicked rotor. What we have surveyed are some of the major results obtained over the last five decades, that not only clarified the complex dynamics of kicked rotor, but indeed of the field of classical and quantum chaos itself, and now venturing even beyond into other areas such as condensed matter physics and quantum information and computation. Indeed, solving the initial set of problems has opened up newer questions straddling many areas of physics.

Even four decades after its introduction, quantum kicked rotor continues to surprise us with newer types of dynamical phenomena. One such recent example is what is dubbed as the quantum boomerang effect [575], first explored in the case of the Anderson model [576]. In this, the wavepackets with skewed momentum distribution, after some initial drift, exhibit a tendency to return to its starting point and stay localized at this point. This requires wavepackets to have non-zero average initial velocity. The initial results appear to suggest it might be a general phenomenon in wave propagation in random media, including in interacting systems [577]. A recent pre-print reports an experimental observation of boomerang effect [578]. It also reports that just as dynamical localization is destroyed by noise, so is the boomerang effect.

While such novel phenomena open up newer vistas and renews our interest in kicked rotor, much of the current interest is now beginning to be focussed on the N -dimensional coupled kicked rotors, especially for $N = 3$ and higher dimensions [390,391,469,579]. A general and deeper understanding of the interplay between chaos, localization and interactions is missing. In Section 8.2, interacting kicked rotors and its mapping to Anderson model were discussed. Taking into account all the available results, it is clear that the last word on this question has not yet been pronounced. It appears that localization is destroyed for the interacting kicked rotors in the mean-field limit [336], the results outside of this limit remains unclear with some model predicting persistence of localized phase for long times [580]. It would be interesting to obtain an understanding of how different kinds of interactions (hard-core or other analytic types) and qualitative dynamics might affect many-body localization and thermalization [581]. In recent years, considerable interest has grown around the idea of many-body scars [55]. It was triggered by the experimental observation of scarred states in many-body Rydberg atom based quantum simulator in which interactions are tunable through excitations into Rydberg states [582]. The original ideas of quantum scarring arose from the study of chaotic stadium billiard by McDonald [43] and a theoretical explanation due to Eric Heller [44]. Scarred states are known to arise due to disproportionate influence of certain least unstable classical periodic orbits on the quantum eigenstates. Exploration of scarred modes would be insightful if the many-body models have a classical limit. With coupled many-body kicked rotors, one has a model with a definite classical limit in contrast to some of the models in condensed matter physics. This would help to explore the semiclassical implications in terms of classical phase space structures. It would in general help understand quantum-classical correspondence beyond few body systems that have dominated the quantum chaos research in the last half a century. We had already noted some of the interesting connections between quantum correlation measures such as entanglement and underlying classical dynamics. This needs to be carried over to many-body systems, especially the exploration of how multi-partite measures of quantum correlations are modulated by classical dynamics. In general, an

exploration of Hamiltonian chaos in many-body systems must be embarked upon and in this journey N -body kicked rotor and insights obtained from a single kicked rotor will play an important role.

Two other aspects of quantum kicked rotor have not received sufficient attention. First of them is the class of non-KAM kicked rotor whose phase space features are different from the standard rotor. There are interesting questions on the interplay of spatial and temporal scales in such systems. For instance, in the kicked rotor in a square well potential [316,317] non-KAM features arise when commensurability of spatial scales is violated. A broader understanding must be obtained about how non-KAM dynamical features arise in terms of spatial and temporal scales in the system. Even in experimental test-beds, non-KAM kicked rotor models have not received much attention as yet. A wide spectrum of phenomena ranging from quantum resonances to localized modes remain unexplored. Secondly, in the last few years several papers have been published on the question of kicked rotor with a spin-1/2 degree of freedom. More refined models based on this are able to display phenomenon similar to the integer quantum Hall effect and this appears to be promising in that it might tie in more closely with condensed matter physics models and might even provide a relatively easier route to building quantum simulators based on kicked rotor. This line of research requires deeper exploration.

Finally, we might point out that another promising avenue is the connections between quantum walks [583,584] and kicked rotor [196,585,586]. This potentially has many applications in the context of quantum computing, and in the form novel quantum search and other quantum algorithms to quantum ratchet. Some initial works have begun but this clearly is in its infancy. There is another approach to quantum walks that directly exploits quantum chaos. The standard quantum walks are based on a “coin” operator that decides if the walker moves left or right. Coin operators can be replaced by a unitary operator corresponding to a chaotic system (such as kicked rotor or Harper model [587]). In a sense, in these types of quantum walks, the randomness of the quantum walk has its origins in chaotic quantum systems. In the context of the emerging interests in quantum algorithms and quantum machine learning problems [588], this might turn out to be one possible approach to design as well as implement them using atom-optics test bed. Models and techniques based on kicked rotor might play a significant role in some of these emerging areas at the intersection of dynamical systems, condensed matter physics and quantum information and computation.

Declaration of competing interest

The authors declare the following financial interests/personal relationships which may be considered as potential competing interests: M. S. Santhanam reports financial support was provided by Science and Engineering Research Board – India.

Acknowledgments

MSS acknowledges the MATRICS grant MTR/2019/001111 from Science and Engineering Research Board, Govt. of India. JBK would like to acknowledge the partial funding from IISER Pune, India and from the QuEST programme of DST, Govt. of India during the course of this work. All the authors would like to acknowledge National Supercomputing Mission for the use of Param-Brahma Cluster Computer at IISER Pune for computational purposes.

References

- [1] A. Aaboe, *Saros Cycle Dates and Related Babylonian Astronomical Texts*, vol. 81, American Philosophical Society, 1991.
- [2] J. Kepler, W. Donahue, *Astronomia Nova*, Green Lion Press, 2015, URL <https://books.google.co.in/books?id=hqMvijgEACAAJ>.
- [3] I. Newton, *The Principia: Mathematical Principles Of Natural Philosophy*, www.snowballpublishing.com, 2011, URL <https://books.google.co.in/books?id=z-d5XwAACAAJ>.
- [4] P.S. Laplace, *Théorie Analytique Des Probabilités*, Madame Veuve Courcier, (Paris), 1820.
- [5] R. Montgomery, The three-body problem, *Sci. Am.* 321 (2019) 66, <http://dx.doi.org/10.1038/scientificamerican0819-66>.
- [6] G.S. Krishnaswami, H. Senapati, An introduction to the classical three-body problem, *Resonance* 19 (2019) 87, <http://dx.doi.org/10.1007/s12045-019-0760-1>.
- [7] K. Sundman, Mémoire sur le problème des trois corps, *Acta Math.* 36 (1912) 105.
- [8] Q. Wang, The global solution of the n -body problem, *Celestial Mech.* 50 (1991) 73.
- [9] F. Diacu, The solution of the n -body problem, *Math. Intell.* 18 (1996) 66.
- [10] H. Poincaré, *New Methods Of Celestial Mechanics*, 3 vol., Springer Science & Business Media, 2004, (English Transl.).
- [11] M. Lighthill, The recently recognized failure of predictability in Newtonian dynamics, *Proc. R. Soc. Lond. Ser. A Math. Phys. Eng. Sci.* 407 (1986) 35, <http://dx.doi.org/10.1098/rspa.1986.0082>.
- [12] I.R. Epstein, J.A. Pojman, *An Introduction To Nonlinear Chemical Dynamics: Oscillations, Waves, Patterns, And Chaos*, Oxford University Press, New York, 1998.
- [13] J.P. Gollub, H.L. Swinney, Onset of turbulence in a rotating fluid, *Phys. Rev. Lett.* 35 (1975) 927–930, <http://dx.doi.org/10.1103/PhysRevLett.35.927>.
- [14] H.L. Swinney, J.P. Gollub, The transition to turbulence, *Phys. Today* 31 (8) (1978) 41, <http://dx.doi.org/10.1063/1.2995142?ver=pdfcov>.
- [15] J. Laskar, P. Robutel, The chaotic obliquity of the planets, *Nature* 361 (1993) 608–612, <http://dx.doi.org/10.1038/361608a0>.
- [16] B. Chirikov, *ReSearch Concerning the Theory of Nonlinear Resonance and Stochasticity*, Technical Report N-267, Institute of Nuclear Physics, Novosibirsk, 1969.
- [17] A.J. Lichtenberg, M.A. Lieberman, *Regular And Stochastic Motion*, in: *Applied Mathematical Sciences*, vol. 38, Springer Science & Business Media, 2013.
- [18] E. Ott, *Chaos In Dynamical Systems*, second ed., Cambridge University Press, 2002, <http://dx.doi.org/10.1017/CBO9780511803260>.
- [19] S. Smale, *Differentiable dynamical systems*, *Bull. Am. Math. Soc.* 73 (6) (1967) 747–817.

- [20] S. Wiggins, *Introduction to Applied Nonlinear Dynamical Systems and Chaos*, Springer, 2003.
- [21] M. Tabor, *Chaos And Integrability In Nonlinear Dynamics*, John Wiley, New York, 1988.
- [22] R. Brown, L.O. Chua, Clarifying chaos: examples and counterexamples, *Int. J. Bifurc. Chaos* 06 (02) (1996) 219–249, <http://dx.doi.org/10.1142/S0218127496000023>.
- [23] M.W. Hirsch, S. Smale, R.L. Devaney, *Differential Equations, Dynamical Systems, And An Introduction To Chaos*, Academic Press, 2012.
- [24] J. Hadamard, Les surfaces a courbures opposées et leurs lignes géodésiques, *J. De Math. Pures Appl.* 4 (1898) 27–74.
- [25] N. Balazs, A. Voros, Chaos on the pseudosphere, *Phys. Rep.* 143 (3) (1986) 109–240, [http://dx.doi.org/10.1016/0370-1573\(86\)90159-6](http://dx.doi.org/10.1016/0370-1573(86)90159-6), URL <http://www.sciencedirect.com/science/article/pii/0370157398010596>.
- [26] V.I. Oseledec, A multiplicative ergodic theorem. Liapunov characteristic number for dynamical systems, *Trans. Moscow Math. Soc.* 19 (1968) 197–231, URL <https://ci.nii.ac.jp/naid/10004591080/en/>.
- [27] A.M. Lyapunov, *Ann. Math. Studies*, 17 (1907) 1947.
- [28] G. Benettin, L. Galgani, A. Giorgilli, J.-M. Strelcyn, Lyapunov characteristic exponents for smooth dynamical systems and for Hamiltonian systems; a method for computing all of them. Part 1: Theory, *Meccanica* 15 (1) (1980) 9–20.
- [29] G. Benettin, L. Galgani, A. Giorgilli, J.-M. Strelcyn, Lyapunov characteristic exponents for smooth dynamical systems and for Hamiltonian systems; a method for computing all of them. Part 2: Numerical application, *Meccanica* 15 (1) (1980) 21–30.
- [30] Y.B. Pesin, Characteristic Lyapunov exponents and smooth ergodic theory, *Russian Math. Surveys* 32 (4) (1977) 55–114, <http://dx.doi.org/10.1070/rm1977v03n04abeh001639>.
- [31] G.S. Krishnaswami, H. Senapati, Classical three rotor problem: Periodic solutions, stability and chaos, *Chaos* 29 (12) (2019) 123121, <http://dx.doi.org/10.1063/1.5110032>.
- [32] G. Cristadoro, R. Ketzmerick, Universality of algebraic decays in Hamiltonian systems, *Phys. Rev. Lett.* 100 (2008) 184101, <http://dx.doi.org/10.1103/PhysRevLett.100.184101>.
- [33] E.G. Altmann, A.E. Motter, H. Kantz, Stickiness in Hamiltonian systems: From sharply divided to hierarchical phase space, *Phys. Rev. E* 73 (2006) 026207, <http://dx.doi.org/10.1103/PhysRevE.73.026207>, URL <https://link.aps.org/doi/10.1103/PhysRevE.73.026207>.
- [34] G. Casati, I. Guarneri, G. Maspero, Fractal survival probability fluctuations, *Phys. Rev. Lett.* 84 (2000) 63–66, <http://dx.doi.org/10.1103/PhysRevLett.84.63>.
- [35] M.C. Gutzwiller, *Chaos In Classical And Quantum Mechanics*, vol. 1, Springer Science & Business Media, 2013.
- [36] J.P. Bird, *Electron Transport In Quantum Dots*, Springer Science & Business Media, 2013.
- [37] S. Shinohara, T. Hayayama, T. Fukushima, M. Hentschel, T. Sasaki, E.E. Narimanov, Chaos-assisted directional light emission from microcavity lasers, *Phys. Rev. Lett.* 104 (2010) 163902, <http://dx.doi.org/10.1103/PhysRevLett.104.163902>, URL <https://link.aps.org/doi/10.1103/PhysRevLett.104.163902>.
- [38] C. Gmachl, F. Capasso, E.E. Narimanov, J.U. Nöckel, A.D. Stone, J. Faist, D.L. Sivco, A.Y. Cho, High-power directional emission from microlasers with chaotic resonators, *Science* 280 (5369) (1998) 1556–1564, <http://dx.doi.org/10.1126/science.280.5369.1556>, URL <https://science.sciencemag.org/content/280/5369/1556>.
- [39] L.A. Bunimovich, On the ergodic properties of nowhere dispersing billiards, *Commun. Math. Phys.* 65 (3) (1979) 295–312.
- [40] Y.G. Sinai, Dynamical systems with elastic reflections, *Russian Math. Surveys* 25 (2) (1970) 137.
- [41] A. Bäcker, Numerical aspects of eigenvalue and eigenfunction computations for chaotic quantum systems, in: M.D. Esposti, S. Graffi (Eds.), *The Mathematical Aspects Of Quantum Maps*, Springer Berlin Heidelberg, Berlin, Heidelberg, 2003, pp. 91–144.
- [42] M.V. Berry, Regular and irregular semiclassical wavefunctions, *J. Phys. A: Math. Gen.* 10 (12) (1977) 2083–2091, <http://dx.doi.org/10.1088/0305-4470/10/12/016>.
- [43] S.W. McDonald, Wave Dynamics of Regular and Chaotic Rays, Technical Report LBL-14837, University of California, Berkeley, and Lawrence Berkeley Laboratory, 1983, <http://dx.doi.org/10.2172/5373229>, URL <https://www.osti.gov/biblio/5373229>.
- [44] E.J. Heller, Bound-state eigenfunctions of classically chaotic Hamiltonian systems:nearly linear Scars of periodic orbits, *Phys. Rev. Lett.* 53 (1984) 1515–1518, <http://dx.doi.org/10.1103/PhysRevLett.53.1515>, URL <https://link.aps.org/doi/10.1103/PhysRevLett.53.1515>.
- [45] A. Bäcker, R. Schubert, Autocorrelation function of eigenstates in chaotic and mixed systems, *J. Phys. A: Math. Gen.* 35 (3) (2002) 539–564, <http://dx.doi.org/10.1088/0305-4470/35/3/307>.
- [46] L. Kaplan, Wave function intensity statistics from unstable periodic orbits, *Phys. Rev. Lett.* 80 (1998) 2582–2585, <http://dx.doi.org/10.1103/PhysRevLett.80.2582>, URL <https://link.aps.org/doi/10.1103/PhysRevLett.80.2582>.
- [47] L. Kaplan, Scars in quantum chaotic wavefunctions, *Nonlinearity* 12 (2) (1999) R1–R40, <http://dx.doi.org/10.1088/0951-7715/12/2/009>.
- [48] L. Kaplan, E. Heller, Linear and nonlinear theory of eigenfunction scars, *Ann. Phys.* 264 (2) (1998) 171–206, <http://dx.doi.org/10.1006/aphy.1997.5773>, URL <http://www.sciencedirect.com/science/article/pii/S0003491697957730>.
- [49] S. Sridhar, Experimental observation of scarred eigenfunctions of chaotic microwave cavities, *Phys. Rev. Lett.* 67 (1991) 785–788, <http://dx.doi.org/10.1103/PhysRevLett.67.785>, URL <https://link.aps.org/doi/10.1103/PhysRevLett.67.785>.
- [50] J. Stein, H.-J. Stöckmann, Experimental determination of billiard wave functions, *Phys. Rev. Lett.* 68 (1992) 2867–2870, <http://dx.doi.org/10.1103/PhysRevLett.68.2867>, URL <https://link.aps.org/doi/10.1103/PhysRevLett.68.2867>.
- [51] M.S. Santhanam, V.B. Sheorey, A. Lakshminarayan, Chaos and exponentially localized eigenstates in smooth Hamiltonian systems, *Phys. Rev. E* 57 (1998) 345–349, <http://dx.doi.org/10.1103/PhysRevE.57.345>, URL <https://link.aps.org/doi/10.1103/PhysRevE.57.345>.
- [52] M.S. Santhanam, V.B. Sheorey, A. Lakshminarayan, Chaos and localization in coupled quartic oscillators, *Pramana J. Phys.* 48 (2) (1997) 439–457, URL <https://www.ias.ac.in/describe/article/pram/048/02/0439-0457>.
- [53] K. Müller, D. Wintgen, Scars in wavefunctions of the diamagnetic Kepler problem, *J. Phys. B: At. Mol. Opt. Phys.* 27 (13) (1994) 2693–2718, <http://dx.doi.org/10.1088/0953-4075/27/13/003>.
- [54] E. Bogomolny, Smoothed wave functions of chaotic quantum systems, *Physica D* 31 (2) (1988) 169–189, [http://dx.doi.org/10.1016/0167-2789\(88\)90075-9](http://dx.doi.org/10.1016/0167-2789(88)90075-9), URL <http://www.sciencedirect.com/science/article/pii/0167278988900759>.
- [55] C.J. Turner, A.A. Michailidis, D.A. Abanin, M. Serbyn, Z. Papić, Weak ergodicity breaking from quantum many-body scars, *Nat. Phys.* 14 (2018) 745–749, <http://dx.doi.org/10.1038/s41567-018-0137-5>.
- [56] H. Zhao, J. Vovrosh, F. Mintert, J. Knolle, Quantum many-body scars in optical lattices, *Phys. Rev. Lett.* 124 (2020) 160604, <http://dx.doi.org/10.1103/PhysRevLett.124.160604>, URL <https://link.aps.org/doi/10.1103/PhysRevLett.124.160604>.
- [57] C.-J. Lin, O.I. Motrunich, Exact quantum many-body scar states in the Rydberg-blockaded atom chain, *Phys. Rev. Lett.* 122 (2019) 173401, <http://dx.doi.org/10.1103/PhysRevLett.122.173401>, URL <https://link.aps.org/doi/10.1103/PhysRevLett.122.173401>.
- [58] A.M. Alhambra, A. Anshu, H. Wilming, Revivals imply quantum many-body scars, *Phys. Rev. B* 101 (2020) 205107, <http://dx.doi.org/10.1103/PhysRevB.101.205107>, URL <https://link.aps.org/doi/10.1103/PhysRevB.101.205107>.
- [59] M. Hénon, C. Heiles, The applicability of the third integral of motion: some numerical experiments, *Astron. J.* 69 (1964) 73.
- [60] O. Bohigas, S. Tomsovic, D. Ullmo, Manifestations of classical phase space structures in quantum mechanics, *Phys. Rep.* 223 (2) (1993) 43–133, [http://dx.doi.org/10.1016/0370-1573\(93\)90109-Q](http://dx.doi.org/10.1016/0370-1573(93)90109-Q), URL <http://www.sciencedirect.com/science/article/pii/037015739390109Q>.
- [61] H. Friedrich, D. Wintgen, The hydrogen atom in a uniform magnetic field – an example of chaos, *Phys. Rep.* 183 (2) (1989) 37–79, [http://dx.doi.org/10.1016/0370-1573\(89\)90121-X](http://dx.doi.org/10.1016/0370-1573(89)90121-X).

- [62] M. Gutzwiller, The semi-classical quantization of chaotic Hamiltonian systems, in: M.-J. Giannoni, A. Voros, J. Zinn-Justin (Eds.), *Chaos And Quantum Physics*, Les Houches Session LII, North-Holland, 1989, p. 201.
- [63] A. Einstein, Zum quantensatz von sommerfeld und epstein, *Verhandlungen Der Deutschen Physikalischen Gesellschaft* 19 (1917) 82.
- [64] A.D. Stone, Einstein's unknown insight and the problem of quantizing chaos, *Phys. Today* 58 (8) (2005) 37.
- [65] J.B. Keller, Corrected bohr-sommerfeld quantum conditions for nonseparable systems, *Ann. Physics* 4 (1958) 180–188, [http://dx.doi.org/10.1016/0003-4916\(58\)90032-0](http://dx.doi.org/10.1016/0003-4916(58)90032-0).
- [66] M.C. Gutzwiller, Phase-integral approximation in momentum space and the bound states of an atom, *J. Math. Phys.* 8 (10) (1967) 1979–2000.
- [67] M.C. Gutzwiller, Phase-integral approximation in momentum space and the bound states of an atom. II, *J. Math. Phys.* 10 (6) (1969) 1004–1020.
- [68] M.C. Gutzwiller, Energy spectrum according to classical mechanics, *J. Math. Phys.* 11 (6) (1970) 1791–1806.
- [69] M.C. Gutzwiller, Periodic orbits and classical quantization conditions, *J. Math. Phys.* 12 (3) (1971) 343–358.
- [70] A. Holle, J. Main, G. Wiebusch, H. Rrottke, K.H. Welge, Quasi-Landau spectrum of the chaotic diamagnetic hydrogen atom, *Phys. Rev. Lett.* 61 (1988) 161–164, <http://dx.doi.org/10.1103/PhysRevLett.61.161>, URL <https://link.aps.org/doi/10.1103/PhysRevLett.61.161>.
- [71] E.N. Lorenz, Deterministic nonperiodic flow, *J. Atmos. Sci.* 20 (2) (1963) 130–141, [http://dx.doi.org/10.1175/1520-0469\(1963\)020](http://dx.doi.org/10.1175/1520-0469(1963)020).
- [72] R.M. May, Simple mathematical models with very complicated dynamics, *Nature* 261 (1976) 459–467, <http://dx.doi.org/10.1038/261459a0>.
- [73] R. Hilborn, *Chaos and Nonlinear Dynamics: An Introduction For Scientists and Engineers*, second ed., Oxford University Press, 2000, <http://dx.doi.org/10.1093/acprof:oso/9780198507239.001.0001>.
- [74] S. Strogatz, *Nonlinear Dynamics And Chaos: With Applications To Physics, Biology, Chemistry, And Engineering*, in: *Studies in Nonlinearity*, Avalon Publishing, 2014, URL <https://books.google.co.in/books?id=jDQCAwAAQBAJ>.
- [75] T. Tél, M. Gruiz, *Chaotic Dynamics: An Introduction Based On Classical Mechanics*, Cambridge University Press, 2006, <http://dx.doi.org/10.1017/CBO9780511803277>.
- [76] F. Borgonovi, I. Guarneri, D.L. Shepelyansky, Statistics of quantum lifetimes in a classically chaotic system, *Phys. Rev. A* 43 (1991) 4517–4520, <http://dx.doi.org/10.1103/PhysRevA.43.4517>, URL <https://link.aps.org/doi/10.1103/PhysRevA.43.4517>.
- [77] G. Casati, G. Maspero, D.L. Shepelyansky, Quantum fractal eigenstates, *Physica D* 131 (1) (1999) 311–316, [http://dx.doi.org/10.1016/S0167-2789\(98\)00265-6](http://dx.doi.org/10.1016/S0167-2789(98)00265-6), Classical Chaos and its Quantum Manifestations, URL <http://www.sciencedirect.com/science/article/pii/S0167278998002656>.
- [78] M. Kopp, H. Schomerus, Fractal weyl laws for quantum decay in dynamical systems with a mixed phase space, *Phys. Rev. E* 81 (2010) 026208, <http://dx.doi.org/10.1103/PhysRevE.81.026208>, URL <https://link.aps.org/doi/10.1103/PhysRevE.81.026208>.
- [79] L. Reichl, *The Transition To Chaos: Conservative Classical Systems And Quantum Manifestations*, Springer, 2004.
- [80] G.M. Zaslavsky, *The Physics Of Chaos In Hamiltonian Systems*, World Scientific, 2007.
- [81] B. Chirikov, A universal instability of many-dimensional oscillator systems, *Phys. Rep.* 52 (1979) 263–379, [http://dx.doi.org/10.1016/0370-1573\(79\)90023-1](http://dx.doi.org/10.1016/0370-1573(79)90023-1).
- [82] F. Izrailev, Nearly linear mappings and their applications, *Physica D* 1 (3) (1980) 243–266, [http://dx.doi.org/10.1016/0167-2789\(80\)90025-1](http://dx.doi.org/10.1016/0167-2789(80)90025-1), URL <http://www.sciencedirect.com/science/article/pii/0167278980900251>.
- [83] T. Petrosky, Chaos and cometary clouds in the solar system, *Phys. Lett. A* 117 (7) (1986) 328–332, [http://dx.doi.org/10.1016/0375-9601\(86\)90673-0](http://dx.doi.org/10.1016/0375-9601(86)90673-0), URL <http://www.sciencedirect.com/science/article/pii/0375960186906730>.
- [84] R.V. Chirikov, V.V. Vecheslavov, Chaotic dynamics of Comet Halley, *Astron. Astrophys.* 221 (1) (1989) 146–154, URL <https://ui.adsabs.harvard.edu/abs/1989A&A...221..146C>.
- [85] T.C.N. Boekholt, F.I. Pelupessy, D.C. Heggie, S.F. Portegies Zwart, The origin of chaos in the orbit of comet 1P/Halley, *Mon. Not. R. Astron. Soc.* 461 (4) (2016) 3576–3584, <http://dx.doi.org/10.1093/mnras/stw1504>.
- [86] G. Casati, I. Guarneri, D.L. Shepelyansky, Hydrogen atom in monochromatic field: chaos and dynamical photonic localization, *IEEE J. Quantum Electron.* 24 (7) (1988) 1420–1444.
- [87] G. Casati, B.V. Chirikov, D.L. Shepelyansky, I. Guarneri, Relevance of classical chaos in quantum mechanics: The hydrogen atom in a monochromatic field, *Phys. Rep.* 154 (2) (1987) 77–123, [http://dx.doi.org/10.1016/0370-1573\(87\)90009-3](http://dx.doi.org/10.1016/0370-1573(87)90009-3), URL <http://www.sciencedirect.com/science/article/pii/0370157387900093>.
- [88] D.L. Shepelyansky, A.D. Stone, Chaotic Landau level mixing in classical and quantum wells, *Phys. Rev. Lett.* 74 (1995) 2098–2101, <http://dx.doi.org/10.1103/PhysRevLett.74.2098>, URL <https://link.aps.org/doi/10.1103/PhysRevLett.74.2098>.
- [89] B.V. Chirikov, A universal instability of many-dimensional oscillator systems, *Phys. Rep.* 52 (5) (1979) 263–379, [http://dx.doi.org/10.1016/0370-1573\(79\)90023-1](http://dx.doi.org/10.1016/0370-1573(79)90023-1), URL <https://www.sciencedirect.com/science/article/pii/037015737379900231>.
- [90] A. Kolmogorov, On the conservation of conditionally periodic motions under small perturbation of the Hamiltonian, in: *Dokl. Akad. Nauk. SSR*, 98, (527) 1954, pp. 2–3.
- [91] A. Moser, On invariant curves of area-preserving mappings on an annulus, *Nachr. Akad. Wiss. Goettingen Math. Phys. K1* (1962) 1.
- [92] V.I. Arnol'd, Proof of a theorem of AN Kolmogorov on the invariance of quasi-periodic motions under small perturbations of the Hamiltonian, *Russian Math. Surveys* 18 (5) (1963) 9.
- [93] J. Poschel, A lecture on the classical KAM theorem, in: *Proc. Symp. Pure Math.*, vol. 69, 2001, pp. 707–732.
- [94] H. Rüssmann, "Über invariante Kurven differenzierbarer Abbildungen eines Kreisringes, *Nachr. Akad. Wiss. Goettingen Math. Phys. K1* (II) (1970) 67–105.
- [95] M. Herman, Sur les courbes invariantes par les difféomorphismes de l'anneau, *Soc. Math. Fr.* 1 (1983) 103–104.
- [96] J.M. Greene, A method for determining a stochastic transition, *J. Math. Phys.* 20 (6) (1979) 1183–1201, <http://dx.doi.org/10.1063/1.524170>.
- [97] R. MacKay, A renormalization approach to invariant circles in area-preserving maps, *Physica D* 7 (1) (1983) 283–300, [http://dx.doi.org/10.1016/0167-2789\(83\)90131-8](http://dx.doi.org/10.1016/0167-2789(83)90131-8), URL <http://www.sciencedirect.com/science/article/pii/0167278983901318>.
- [98] S.J. Shenker, L.P. Kadanoff, Critical behavior of a KAM surface: I. Empirical results, *J. Stat. Phys.* 27 (1982) 631–656, <http://dx.doi.org/10.1007/BF01013439>, URL <https://link.springer.com/article/10.1007/BF01013439>.
- [99] R.S. MacKay, I.C. Percival, Converse KAM: theory and practice, *Comm. Math. Phys.* 98 (4) (1985) 469–512, URL <https://projecteuclid.org:443/euclid.cmp/1103942538>.
- [100] D. Escande, Stochasticity in classical Hamiltonian systems: Universal aspects, *Phys. Rep.* 121 (3) (1985) 165–261, [http://dx.doi.org/10.1016/0370-1573\(85\)90019-5](http://dx.doi.org/10.1016/0370-1573(85)90019-5), URL <http://www.sciencedirect.com/science/article/pii/0370157385900195>.
- [101] G. Berman, G. Zaslavsky, Theory of quantum nonlinear resonance, *Phys. Lett. A* 61 (5) (1977) 295–296, [http://dx.doi.org/10.1016/0375-9601\(77\)90618-1](http://dx.doi.org/10.1016/0375-9601(77)90618-1), URL [https://link.aps.org/doi/10.1016/0375-9601\(77\)90618-1](https://link.aps.org/doi/10.1016/0375-9601(77)90618-1).
- [102] G. Berman, A. Kolovsky, Structure and stability of the quasi-energy spectrum of two interacting quantum nonlinear resonances, *Phys. Lett. A* 95 (1) (1983) 15–18, [http://dx.doi.org/10.1016/0375-9601\(83\)90768-5](http://dx.doi.org/10.1016/0375-9601(83)90768-5), URL [https://link.aps.org/doi/10.1016/0375-9601\(83\)90768-5](https://link.aps.org/doi/10.1016/0375-9601(83)90768-5).
- [103] G. Berman, A. Kolovsky, Renormalization method for the quantum system of interacting resonances, *Phys. Lett. A* 125 (4) (1987) 188–192, [http://dx.doi.org/10.1016/0375-9601\(87\)90095-8](http://dx.doi.org/10.1016/0375-9601(87)90095-8), URL [https://link.aps.org/doi/10.1016/0375-9601\(87\)90095-8](https://link.aps.org/doi/10.1016/0375-9601(87)90095-8).
- [104] L.E. Reichl, W.A. Lin, Exact quantum model of field-induced resonance overlap, *Phys. Rev. A* 33 (1986) 3598–3601, <http://dx.doi.org/10.1103/PhysRevA.33.3598>, URL <https://link.aps.org/doi/10.1103/PhysRevA.33.3598>.

- [105] W.A. Lin, L.E. Reichl, Spectral analysis of quantum-resonance zones, quantum Kolmogorov-Arnold-Moser theorem, and quantum-resonance overlap, Phys. Rev. A 37 (1988) 3972–3985, <http://dx.doi.org/10.1103/PhysRevA.37.3972>, URL <https://link.aps.org/doi/10.1103/PhysRevA.37.3972>.
- [106] L.E. Reichl, Mechanism for extension of the wave function in quantum dynamics, Phys. Rev. A 39 (1989) 4817–4827, <http://dx.doi.org/10.1103/PhysRevA.39.4817>, URL <https://link.aps.org/doi/10.1103/PhysRevA.39.4817>.
- [107] M. Burns, L.E. Reichl, Nonlinear resonance in the hydrogen atom, Phys. Rev. A 45 (1992) 333–341, <http://dx.doi.org/10.1103/PhysRevA.45.333>, URL <https://link.aps.org/doi/10.1103/PhysRevA.45.333>.
- [108] J.D. Meiss, Thirty years of turnstiles and transport, Chaos 25 (9) (2015) 097602, <http://dx.doi.org/10.1063/1.4915831>.
- [109] S. Aubry, The new concept of transitions by breaking of analyticity in a crystallographic model, in: A.R. Bishop, T. Schneider (Eds.), *Solitons And Condensed Matter Physics*, Springer-Verlag, New York, 1989, p. 264.
- [110] I. Percival, Variational principles for invariant tori and cantori, in: M. Month, J.C. Herrera (Eds.), AIP Conf. Proc. 57 (1980) 302–310, <http://dx.doi.org/10.1063/1.32113>.
- [111] R.S. MacKay, J.D. Meiss, I.C. Percival, Stochasticity and transport in Hamiltonian systems, Phys. Rev. Lett. 52 (1984) 697–700, <http://dx.doi.org/10.1103/PhysRevLett.52.697>, URL <https://link.aps.org/doi/10.1103/PhysRevLett.52.697>.
- [112] R. Mackay, J. Meiss, I. Percival, Transport in Hamiltonian systems, Physica D 13 (1) (1984) 55–81, [http://dx.doi.org/10.1016/0167-2789\(84\)90270-7](http://dx.doi.org/10.1016/0167-2789(84)90270-7), URL <http://www.sciencedirect.com/science/article/pii/0167278984902707>.
- [113] J.D. Meiss, Visual explorations of dynamics: The standard map, Pramana 70 (6) (2008) 965.
- [114] E.G. Altmann, A.E. Motter, H. Kantz, Stickiness in Hamiltonian systems: From sharply divided to hierarchical phase space, Phys. Rev. E 73 (2006) 026207, <http://dx.doi.org/10.1103/PhysRevE.73.026207>, URL <https://link.aps.org/doi/10.1103/PhysRevE.73.026207>.
- [115] G. Cristadoro, R. Ketzmerick, Universality of algebraic decays in Hamiltonian systems, Phys. Rev. Lett. 100 (2008) 184101, <http://dx.doi.org/10.1103/PhysRevLett.100.184101>.
- [116] D.L. Shepelyansky, Poincaré recurrences in Hamiltonian systems with a few degrees of freedom, Phys. Rev. E 82 (2010) 055202, <http://dx.doi.org/10.1103/PhysRevE.82.055202>, URL <https://link.aps.org/doi/10.1103/PhysRevE.82.055202>.
- [117] W. Li, P. Bak, Fractal dimension of cantori, Phys. Rev. Lett. 57 (1986) 655–658, <http://dx.doi.org/10.1103/PhysRevLett.57.655>, URL <https://link.aps.org/doi/10.1103/PhysRevLett.57.655>.
- [118] T. Geisel, G. Radons, J. Rubner, Kolmogorov-Arnol'd-Moser barriers in the quantum dynamics of chaotic systems, Phys. Rev. Lett. 57 (1986) 2883–2886, <http://dx.doi.org/10.1103/PhysRevLett.57.2883>, URL <https://link.aps.org/doi/10.1103/PhysRevLett.57.2883>.
- [119] T. Geisel, G. Radons, Nonlinear phenomena associated with cantori in classical and quantum systems, Phys. Scr. 40 (3) (1989) 340–345, <http://dx.doi.org/10.1088/0031-8949/40/3/015>.
- [120] K. Vant, G. Ball, H. Ammann, N. Christensen, Experimental evidence for the role of cantori as barriers in a quantum system, Phys. Rev. E 59 (1999) 2846–2852, <http://dx.doi.org/10.1103/PhysRevE.59.2846>, URL <https://link.aps.org/doi/10.1103/PhysRevE.59.2846>.
- [121] M. Michler, A. Bäcker, R. Ketzmerick, H.-J. Stöckmann, S. Tomsovic, Universal quantum localizing transition of a partial barrier in a chaotic sea, Phys. Rev. Lett. 109 (2012) 234101, <http://dx.doi.org/10.1103/PhysRevLett.109.234101>, URL <https://link.aps.org/doi/10.1103/PhysRevLett.109.234101>.
- [122] M.J. Körber, A. Bäcker, R. Ketzmerick, Localization of chaotic resonance states due to a partial transport barrier, Phys. Rev. Lett. 115 (2015) 254101, <http://dx.doi.org/10.1103/PhysRevLett.115.254101>, URL <https://link.aps.org/doi/10.1103/PhysRevLett.115.254101>.
- [123] B. Chirikov, Research concerning the theory of nonlinear resonance and stochasticity, Preprint N 267, Institute Of Nuclear Physics, Novosibirsk (1969) (Engl. Trans., CERN Trans. 71-40 (1971)) (1971) URL <https://cds.cern.ch/record/325497?ln=en>.
- [124] F.M. Izrailev, Simple models of quantum chaos: Spectrum and eigenfunctions, Phys. Rep. 196 (5) (1990) 299–392, [http://dx.doi.org/10.1016/0370-1573\(90\)90067-C](http://dx.doi.org/10.1016/0370-1573(90)90067-C), URL <http://www.sciencedirect.com/science/article/pii/03701573900067C>.
- [125] A.B. Rechester, R.B. White, Calculation of turbulent diffusion for the Chirikov-Taylor model, Phys. Rev. Lett. 44 (1980) 1586–1589, <http://dx.doi.org/10.1103/PhysRevLett.44.1586>, URL <https://link.aps.org/doi/10.1103/PhysRevLett.44.1586>.
- [126] A.B. Rechester, M.N. Rosenbluth, R.B. White, Fourier-space paths applied to the calculation of diffusion for the Chirikov-Taylor model, Phys. Rev. A 23 (1981) 2664–2672, <http://dx.doi.org/10.1103/PhysRevA.23.2664>, URL <https://link.aps.org/doi/10.1103/PhysRevA.23.2664>.
- [127] T. Manos, M. Robnik, Survey on the role of accelerator modes for anomalous diffusion: The case of the standard map, Phys. Rev. E 89 (2014) 022905, <http://dx.doi.org/10.1103/PhysRevE.89.022905>, URL <https://link.aps.org/doi/10.1103/PhysRevE.89.022905>.
- [128] C.F. Karney, A.B. Rechester, R.B. White, Effect of noise on the standard mapping, Physica D 4 (3) (1982) 425–438, [http://dx.doi.org/10.1016/0167-2789\(82\)90045-8](http://dx.doi.org/10.1016/0167-2789(82)90045-8), URL <https://www.sciencedirect.com/science/article/pii/0167278982900458>.
- [129] Y.H. Ichikawa, T. Kamimura, T. Hatori, Stochastic diffusion in the standard map, Physica D 29 (1) (1987) 247–255, [http://dx.doi.org/10.1016/0167-2789\(87\)90060-1](http://dx.doi.org/10.1016/0167-2789(87)90060-1), URL <https://www.sciencedirect.com/science/article/pii/0167278987900601>.
- [130] R. Ishizaki, T. Horita, T. Kobayashi, H. Mori, Anomalous diffusion due to accelerator modes in the standard map, Progr. Theoret. Phys. 85 (5) (1991) 1013–1022, <http://dx.doi.org/10.1143/ptp/85.5.1013>, arXiv:<https://academic.oup.com/ptp/article-pdf/85/5/1013/5454457/85-5-1013.pdf>.
- [131] R.S. MacKay, J.D. Meiss, *Hamiltonian Dynamical Systems*, Adam Hilger, Bristol, 1987.
- [132] J.D. Meiss, J.R. Cary, C. Grebogi, J.D. Crawford, A.N. Kaufman, H.D. Abarbanel, Correlations of periodic, area-preserving maps, Physica D 6 (3) (1983) 375–384, [http://dx.doi.org/10.1016/0167-2789\(83\)90019-2](http://dx.doi.org/10.1016/0167-2789(83)90019-2), URL <https://www.sciencedirect.com/science/article/pii/016727893900192>.
- [133] M. Harsoula, G. Contopoulos, Global and local diffusion in the standard map, Phys. Rev. E 97 (2018) 022215, <http://dx.doi.org/10.1103/PhysRevE.97.022215>, URL <https://link.aps.org/doi/10.1103/PhysRevE.97.022215>.
- [134] R. Ishizaki, T. Horita, T. Kobayashi, H. Mori, Anomalous diffusion due to accelerator modes in the standard map, Progr. Theoret. Phys. 85 (5) (1991) 1013–1022, <http://dx.doi.org/10.1143/ptp/85.5.1013>.
- [135] G. Zaslavsky, Chaos, fractional kinetics, and anomalous transport, Phys. Rep. 371 (6) (2002) 461–580, [http://dx.doi.org/10.1016/S0370-1573\(02\)00331-9](http://dx.doi.org/10.1016/S0370-1573(02)00331-9), URL <http://www.sciencedirect.com/science/article/pii/S0370157302003319>.
- [136] A.V. Chechkin, R. Metzler, J. Klafter, V.Y. Gonchar, Introduction to the theory of Lévy flights, in: *Anomalous Transport*, John Wiley and Sons, Ltd, 2008, pp. 129–162, <http://dx.doi.org/10.1002/9783527622979.ch5>, URL <https://onlinelibrary.wiley.com/doi/abs/10.1002/9783527622979.ch5>.
- [137] E.G. Altmann, H. Kantz, Anomalous transport in Hamiltonian systems, in: *Anomalous Transport*, John Wiley and Sons, Ltd, 2008, pp. 269–291, <http://dx.doi.org/10.1002/9783527622979.ch9>, URL <https://onlinelibrary.wiley.com/doi/abs/10.1002/9783527622979.ch9>.
- [138] B.G. Klappauf, W.H. Oskay, D.A. Steck, M.G. Raizen, Experimental study of quantum dynamics in a regime of classical anomalous diffusion, Phys. Rev. Lett. 81 (1998) 4044–4047, <http://dx.doi.org/10.1103/PhysRevLett.81.4044>, URL <https://link.aps.org/doi/10.1103/PhysRevLett.81.4044>.
- [139] M.K. Oberthaler, R.M. Godun, M.B. d'Arcy, G.S. Summy, K. Burnett, Observation of quantum accelerator modes, Phys. Rev. Lett. 83 (1999) 4447–4451, <http://dx.doi.org/10.1103/PhysRevLett.83.4447>, URL <https://link.aps.org/doi/10.1103/PhysRevLett.83.4447>.
- [140] M.B. d'Arcy, G.S. Summy, S. Fishman, I. Guarneri, Novel quantum chaotic dynamics in cold atoms, Phys. Scr. 69 (6) (2004) C25–C31, <http://dx.doi.org/10.1238/physica.regular.069a00c25>.
- [141] N. Korabel, R. Klages, A.V. Chechkin, I.M. Sokolov, V.Y. Gonchar, Fractal properties of anomalous diffusion in intermittent maps, Phys. Rev. E 75 (2007) 036213, <http://dx.doi.org/10.1103/PhysRevE.75.036213>, URL <https://link.aps.org/doi/10.1103/PhysRevE.75.036213>.
- [142] R. Klages, *From deterministic chaos to anomalous diffusion*, in: H. Schuster (Ed.), *Reviews Of Non-Linear Dynamics And Complexity*, vol. 3, Wiley-VCH Verlag, 2010, pp. 169–227.

- [143] F. Cagnetta, G. Gonnella, A. Mossa, S. Ruffo, Strong anomalous diffusion of the phase of a chaotic pendulum, *Europhys. Lett.* 111 (1) (2015) 10002, <http://dx.doi.org/10.1209/0295-5075/111/10002>.
- [144] J.D. Meiss, N. Miguel, C. Simó, A. Vieiro, Accelerator modes and anomalous diffusion in 3D volume-preserving maps, *Nonlinearity* 31 (12) (2018) 5615–5642, <http://dx.doi.org/10.1088/1361-6544/aae69f>.
- [145] E.G. Altmann, H. Kantz, Hypothesis of strong chaos and anomalous diffusion in coupled symplectic maps, *Europhys. Lett.* 78 (1) (2007) 10008, <http://dx.doi.org/10.1209/0295-5075/78/10008>.
- [146] Y. Sato, R. Klages, Anomalous diffusion in random dynamical systems, *Phys. Rev. Lett.* 122 (2019) 174101, <http://dx.doi.org/10.1103/PhysRevLett.122.174101>, URL <https://link.aps.org/doi/10.1103/PhysRevLett.122.174101>.
- [147] G. Casati, B.V. Chirikov, F.M. Izrailev, J. Ford, Stochastic behavior of a quantum pendulum under a periodic perturbation, in: G. Casati, J. Ford (Eds.), *Stochastic Behavior In Classical And Quantum Hamiltonian Systems*, Springer Berlin Heidelberg, Berlin, Heidelberg, 1979, pp. 334–352.
- [148] F. Haake, *Quantum Signatures Of Chaos*, Springer-Verlag, Berlin, 2010.
- [149] B.V. Chirikov, F. Izrailev, D. Shepelyansky, Dynamical stochasticity in classical and quantum mechanics, *Sov. Sci. Rev. C* 2 (4) (1981) 209–267.
- [150] D. Shepelyansky, Some statistical properties of simple classically stochastic quantum systems, *Physica D* 8 (1983) 208–222.
- [151] P. Ehrenfest, Bemerkung über die angenäherte Gültigkeit der klassischen Mechanik innerhalb der Quantenmechanik, *Zeitschrift FÜR Physik* 45 (7–8) (1927) 455–457.
- [152] G. Berman, G. Zaslavsky, Condition of stochasticity in quantum nonlinear systems, *Phys. A* 91 (3) (1978) 450–460, [http://dx.doi.org/10.1016/0378-4371\(78\)90190-5](http://dx.doi.org/10.1016/0378-4371(78)90190-5), URL <https://www.sciencedirect.com/science/article/pii/0378437178901905>.
- [153] B. Chirikov, F. Izrailev, D. Shepelyansky, Quantum chaos: Localization vs. ergodicity, *Physica D* 33 (1) (1988) 77–88, [http://dx.doi.org/10.1016/S0167-2789\(98\)90011-2](http://dx.doi.org/10.1016/S0167-2789(98)90011-2), URL <https://www.sciencedirect.com/science/article/pii/S0167278998900112>.
- [154] B. Chirikov, Time-dependent quantum systems, in: M.-J. Giannoni, A. Voros, J. Zinn-Justin (Eds.), *Chaos And Quantum Physics*, Les Houches Session LII, North-Holland, Amsterdam, 1989, p. 443.
- [155] G. Casati, B.V. Chirikov, The legacy of chaos in quantum mechanics, in: G. Casati, B.V. Chirikov (Eds.), *Quantum Chaos : Between Order And Chaos*, North-Holland, Amsterdam, 1989, p. 3.
- [156] D.L. Shepelyansky, Localization of quasienergy eigenfunctions in action space, *Phys. Rev. Lett.* 56 (1986) 677–680, <http://dx.doi.org/10.1103/PhysRevLett.56.677>, URL <https://link.aps.org/doi/10.1103/PhysRevLett.56.677>.
- [157] R. Artuso, M. Rusconi, Asymptotic quantum behavior of classically anomalous maps, *Phys. Rev. E* 64 (2001) 015204, <http://dx.doi.org/10.1103/PhysRevE.64.015204>, URL <https://link.aps.org/doi/10.1103/PhysRevE.64.015204>.
- [158] P. Lloyd, Exactly solvable model of electronic states in a three-dimensional disordered Hamiltonian: non-existence of localized states, *J. Phys. C: Solid State Phys.* 2 (10) (1969) 1717–1725, <http://dx.doi.org/10.1088/0022-3719/2/10/303>.
- [159] P.W. Anderson, Absence of diffusion in certain random lattices, *Phys. Rev.* 109 (1958) 1492–1505, <http://dx.doi.org/10.1103/PhysRev.109.1492>, URL <https://link.aps.org/doi/10.1103/PhysRev.109.1492>.
- [160] D.R. Grempel, S. Fishman, R.E. Prange, Localization in an incommensurate potential: An exactly solvable model, *Phys. Rev. Lett.* 49 (1982) 833–836, <http://dx.doi.org/10.1103/PhysRevLett.49.833>, URL <https://link.aps.org/doi/10.1103/PhysRevLett.49.833>.
- [161] M. Feingold, S. Fishman, Statistics of quasienergies in chaotic and random systems, *Physica D* 25 (1–3) (1987) 181–195.
- [162] M. Griniasy, S. Fishman, Localization by pseudorandom potentials in one dimension, *Phys. Rev. Lett.* 60 (1988) 1334–1337, <http://dx.doi.org/10.1103/PhysRevLett.60.1334>, URL <https://link.aps.org/doi/10.1103/PhysRevLett.60.1334>.
- [163] N. Mott, W. Twose, The theory of impurity conduction, *Adv. Phys.* 10 (38) (1961) 107–163, <http://dx.doi.org/10.1080/00018736100101271>.
- [164] H. Furstenberg, Noncommuting random products, *Trans. Am. Math. Soc.* 108 (3) (1963) 377–428.
- [165] H. Kunz, B. Souillard, On the spectral properties of random finite difference operators, *Commun. Math. Phys.* 78 (2) (1980) 201–246.
- [166] T. Spencer, Mathematical aspects of Anderson localization, in: 50 Years Of Anderson Localization, World Scientific, 2010, pp. 327–345, http://dx.doi.org/10.1142/9789814299084_0015, arXiv:https://www.worldscientific.com/doi/pdf/10.1142/9789814299084_0015, URL https://www.worldscientific.com/doi/abs/10.1142/9789814299084_0015.
- [167] G. Casati, L. Molinari, “Quantum chaos” with time-periodic Hamiltonians, *Progr. Theoret. Phys. Supplement* 98 (1989) 287–322, <http://dx.doi.org/10.1143/PTPS.98.287>, arXiv:<https://academic.oup.com/ptps/article-pdf/doi/10.1143/PTPS.98.287/5368384/98-287.pdf>.
- [168] A.D. Mirlin, Y.V. Fyodorov, F.-M. Dittes, J. Quezada, T.H. Seligman, Transition from localized to extended eigenstates in the ensemble of power-law random banded matrices, *Phys. Rev. E* 54 (1996) 3221–3230, <http://dx.doi.org/10.1103/PhysRevE.54.3221>, URL <https://link.aps.org/doi/10.1103/PhysRevE.54.3221>.
- [169] Y.V. Fyodorov, A.D. Mirlin, Scaling properties of localization in random band matrices: A σ -model approach, *Phys. Rev. Lett.* 67 (1991) 2405–2409, <http://dx.doi.org/10.1103/PhysRevLett.67.2405>, URL <https://link.aps.org/doi/10.1103/PhysRevLett.67.2405>.
- [170] I. Guarneri, G. Casati, V. Karle, Classical dynamical localization, *Phys. Rev. Lett.* 113 (2014) 174101, <http://dx.doi.org/10.1103/PhysRevLett.113.174101>, URL <https://link.aps.org/doi/10.1103/PhysRevLett.113.174101>.
- [171] D.J. Thouless, A relation between the density of states and range of localization for one dimensional random systems, *J. Phys. C: Solid State Phys.* 5 (1) (1972) 77–81, <http://dx.doi.org/10.1088/0022-3719/5/1/010>.
- [172] K. Ishii, Localization of eigenstates and transport phenomena in the one-dimensional disordered system, *Progr. Theoret. Phys. Supplement* 53 (1973) 77–138, <http://dx.doi.org/10.1143/PTPS.53.77>.
- [173] R. Johnston, H. Kunz, A method for calculating the localisation length, with an analysis of the Lloyd model, *J. Phys. C: Solid State Phys.* 16 (23) (1983) 4565–4580, <http://dx.doi.org/10.1088/0022-3719/16/23/018>.
- [174] F. Saif, Classical and quantum chaos in atom optics, *Phys. Rep.* 419 (6) (2005) 207–258, <http://dx.doi.org/10.1016/j.physrep.2005.07.002>, URL <http://www.sciencedirect.com/science/article/pii/S0370157305003005>.
- [175] F. Haake, M. Kuš, R. Scharf, Classical and quantum chaos for a kicked top, *Zeitschrift FÜR Physik B Condensed Matter* 65 (3) (1987) 381–395.
- [176] F. Haake, D.L. Shepelyansky, The Kicked Rotator as a Limit of the kicked top, 5(8) (1988) 671–676, <http://dx.doi.org/10.1209/0295-5075/5/8/001>.
- [177] F. Izrailev, D. Shepelyanski, Quantum resonance for a rotator in a nonlinear periodic field, *Sov. Phys. Dokl.* 24 (1979) 996.
- [178] F. Izrailev, D. Shepelyanski, Quantum resonance for a rotator in a nonlinear periodic field, *Theoret. Math. Phys.* 43 (1980) 553–561, <http://dx.doi.org/10.1007/BF01029131>, URL <https://link.springer.com/article/10.1007/BF01029131>.
- [179] B. Dorizzi, B. Grammaticos, Y. Pomeau, The periodically kicked rotator: Recurrence and/or energy growth, *J. Stat. Phys.* 37 (1) (1984) 93–108.
- [180] G. Casati, J. Ford, I. Guarneri, F. Vivaldi, Search for randomness in the kicked quantum rotator, *Phys. Rev. A* 34 (1986) 1413–1419, <http://dx.doi.org/10.1103/PhysRevA.34.1413>, URL <https://link.aps.org/doi/10.1103/PhysRevA.34.1413>.
- [181] A. Ullah, S. Ruddell, J. Curriev, M. Hoogerland, Quantum resonant effects in the delta-kicked rotor revisited, *Eur. Phys. J. D* 66 (12) (2012) 315.
- [182] M. Saunders, P.L. Halkyard, K.J. Challis, S.A. Gardiner, Manifestation of quantum resonances and antiresonances in a finite-temperature dilute atomic gas, *Phys. Rev. A* 76 (2007) 043415, <http://dx.doi.org/10.1103/PhysRevA.76.043415>, URL <https://link.aps.org/doi/10.1103/PhysRevA.76.043415>.
- [183] H. Talbot, LXXVI. Facts relating to optical science. No. IV, Lond. Edinb. Dublin Philos. Mag. J. Sci. 9 (56) (1836) 401–407, <http://dx.doi.org/10.1080/14786443608649032>.

- [184] M.B. d'Arcy, R.M. Godun, M.K. Oberthaler, D. Cassettari, G.S. Summy, Quantum enhancement of momentum diffusion in the delta-kicked rotor, Phys. Rev. Lett. 87 (2001) 074102, <http://dx.doi.org/10.1103/PhysRevLett.87.074102>, URL <https://link.aps.org/doi/10.1103/PhysRevLett.87.074102>.
- [185] C. Ryu, M.F. Andersen, A. Vaziri, M.B. d'Arcy, J.M. Grossman, K. Helmerson, W.D. Phillips, High-order quantum resonances observed in a periodically kicked Bose-Einstein condensate, Phys. Rev. Lett. 96 (2006) 160403, <http://dx.doi.org/10.1103/PhysRevLett.96.160403>, URL <https://link.aps.org/doi/10.1103/PhysRevLett.96.160403>.
- [186] J.F. Kanem, S. Maneshi, M. Partlow, M. Spanner, A.M. Steinberg, Observation of high-order quantum resonances in the kicked rotor, Phys. Rev. Lett. 98 (2007) 083004, <http://dx.doi.org/10.1103/PhysRevLett.98.083004>, URL <https://link.aps.org/doi/10.1103/PhysRevLett.98.083004>.
- [187] V. Ramareddy, G. Behniaein, I. Talukdar, P. Ahmadi, G.S. Summy, High-order resonances of the quantum δ -kicked accelerator, Europhys. Lett. 89 (3) (2010) 33001, <http://dx.doi.org/10.1209/0295-5075/89/33001>.
- [188] S. Wimberger, I. Guarneri, S. Fishman, Quantum resonances and decoherence for δ -kicked atoms, Nonlinearity 16 (4) (2003) 1381, <http://dx.doi.org/10.1088/0951-7715/16/4/312>.
- [189] M. Lepers, V. Zehnlé, J.C. Garreau, Kicked-rotor quantum resonances in position space, Phys. Rev. A 77 (2008) 043628, <http://dx.doi.org/10.1103/PhysRevA.77.043628>, URL <https://link.aps.org/doi/10.1103/PhysRevA.77.043628>.
- [190] I. Talukdar, R. Shrestha, G.S. Summy, Sub-Fourier characteristics of a δ -kicked-rotor resonance, Phys. Rev. Lett. 105 (2010) 054103, <http://dx.doi.org/10.1103/PhysRevLett.105.054103>, URL <https://link.aps.org/doi/10.1103/PhysRevLett.105.054103>.
- [191] B. Daszuta, M.F. Andersen, Atom interferometry using δ -kicked and finite-duration pulse sequences, Phys. Rev. A 86 (2012) 043604, <http://dx.doi.org/10.1103/PhysRevA.86.043604>, URL <https://link.aps.org/doi/10.1103/PhysRevA.86.043604>.
- [192] S. Wimberger, I. Guarneri, S. Fishman, Classical scaling theory of quantum resonances, Phys. Rev. Lett. 92 (2004) 084102, <http://dx.doi.org/10.1103/PhysRevLett.92.084102>, URL <https://link.aps.org/doi/10.1103/PhysRevLett.92.084102>.
- [193] M.B. d'Arcy, R.M. Godun, M.K. Oberthaler, G.S. Summy, K. Burnett, S.A. Gardiner, Approaching classicality in quantum accelerator modes through decoherence, Phys. Rev. E 64 (2001) 056233, <http://dx.doi.org/10.1103/PhysRevE.64.056233>, URL <https://link.aps.org/doi/10.1103/PhysRevE.64.056233>.
- [194] S. Fishman, I. Guarneri, L. Rebbuzzini, Stable quantum resonances in atom optics, Phys. Rev. Lett. 89 (2002) 084101, <http://dx.doi.org/10.1103/PhysRevLett.89.084101>, URL <https://link.aps.org/doi/10.1103/PhysRevLett.89.084101>.
- [195] G. Berman, A. Kolovsky, F. Izrailev, Quantum chaos and peculiarities of diffusion in Wigner representation, Phys. A 152 (1) (1988) 273–286, [http://dx.doi.org/10.1016/0378-4378\(88\)90077-5](http://dx.doi.org/10.1016/0378-4378(88)90077-5), URL <https://www.sciencedirect.com/science/article/pii/0378437188900775>.
- [196] M. Weiß, C. Groiseau, W.K. Lam, R. Burioni, A. Vezzani, G.S. Summy, S. Wimberger, Steering random walks with kicked ultracold atoms, Phys. Rev. A 92 (2015) 033606, <http://dx.doi.org/10.1103/PhysRevA.92.033606>, URL <https://link.aps.org/doi/10.1103/PhysRevA.92.033606>.
- [197] S. Dadras, A. Gresch, C. Groiseau, S. Wimberger, G.S. Summy, Experimental realization of a momentum-space quantum walk, Phys. Rev. A 99 (2019) 043617, <http://dx.doi.org/10.1103/PhysRevA.99.043617>, URL <https://link.aps.org/doi/10.1103/PhysRevA.99.043617>.
- [198] M. Delvecchio, F. Petrioli, S. Wimberger, Resonant quantum kicked rotor as a continuous-time quantum walk, Condensed Matter 5 (1) (2020) <http://dx.doi.org/10.3390/condmat5010004>, URL <https://www.mdpi.com/2410-3896/5/1/4>.
- [199] E. Wigner, Proceedings of the conference on neutron physics by time-of-flight, Gatlinburg, Tennessee, 1956.
- [200] E.P. Wigner, Random matrices in physics, SIAM Rev. 9 (1) (1967) 1–23, <http://dx.doi.org/10.1137/1009001>.
- [201] M. Mehta, *Random Matrices*, Elsevier, 2004.
- [202] T.A. Brody, J. Flores, J.B. French, P.A. Pandey, S.S.M. Wong, Random-matrix physics: spectrum and strength fluctuations, Rev. Modern Phys. 53 (1981) 385–479, <http://dx.doi.org/10.1103/RevModPhys.53.385>, URL <https://link.aps.org/doi/10.1103/RevModPhys.53.385>.
- [203] F.J. Dyson, The threefold way. Algebraic structure of symmetry groups and ensembles in quantum mechanics, J. Math. Phys. 3 (6) (1962) 1199–1215, <http://dx.doi.org/10.1063/1.1703863>.
- [204] T. Guhr, A. Müller-Groeling, H.A. Weidenmüller, Random-matrix theories in quantum physics: common concepts, Phys. Rep. 299 (4) (1998) 189–425, [http://dx.doi.org/10.1016/S0370-1573\(97\)00088-4](http://dx.doi.org/10.1016/S0370-1573(97)00088-4), URL <http://www.sciencedirect.com/science/article/pii/S0370157397000884>.
- [205] G. Akemann, J. Baik, P. Di Francesco, *The Oxford Handbook Of Random Matrix Theory*, Oxford University Press, 2011.
- [206] G. Livan, M. Novaes, P. Vivo, *Introduction To Random Matrices: Theory And Practice*, vol. 26, Springer, 2018.
- [207] M. Zirnbauer, Symmetry classes in random matrix theory, in: J.-P.F. coise, G.L. Naber, T.S. Tsun (Eds.), *Encyclopedia Of Mathematical Physics*, Academic Press, Oxford, 2006, pp. 204–212, <http://dx.doi.org/10.1016/B0-12-512666-2/00069-9>, URL <https://www.sciencedirect.com/science/article/pii/B0125126662000699>.
- [208] G. Casati, F. Valz-Gris, I. Guarneri, On the connection between quantization of nonintegrable systems and statistical theory of spectra, Lett. Nuovo Cimento 28 (8) (1980) 279–282.
- [209] M. Berry, Quantizing a classically ergodic system: Sinai's billiard and the KKR method, Ann. Phys. 131 (1) (1981) 163–216, [http://dx.doi.org/10.1016/0003-4916\(81\)90189-5](http://dx.doi.org/10.1016/0003-4916(81)90189-5), URL <https://www.sciencedirect.com/science/article/pii/0003491681901895>.
- [210] L.A. Bunimovich, On ergodic properties of certain billiards, Funct. Anal. Appl. 8 (3) (1974) 254–255.
- [211] O. Bohigas, M.J. Giannoni, C. Schmit, Characterization of chaotic quantum spectra and universality of level fluctuation laws, Phys. Rev. Lett. 52 (1984) 1–4, <http://dx.doi.org/10.1103/PhysRevLett.52.1>, URL <https://link.aps.org/doi/10.1103/PhysRevLett.52.1>.
- [212] N.S. Krylov, J.S. Migdal, *Works On The Foundations Of Statistical Physics*, Princeton University Press, Princeton, 2014.
- [213] A.N. Kolmogorov, Entropy per unit time as a metric invariant of automorphisms, in: Dokl. Akad. Nauk SSSR, 124 (4) (1959) 754–755.
- [214] Y.G. Sinai, Classical dynamic systems with countably-multiple lebesgue spectrum. II, Izvestiya Rossiiskoi Akademii Nauk. Seriya Matematicheskaya 30 (1) (1966) 15–68.
- [215] M.V. Berry, Semiclassical theory of spectral rigidity, Proc. R. Soc. Lond. A Math. Phys. Sci. 400 (1819) (1985) 229–251, <http://dx.doi.org/10.1098/rspa.1985.0078>, URL <https://royalsocietypublishing.org/doi/abs/10.1098/rspa.1985.0078>.
- [216] M. Sieber, K. Richter, Correlations between periodic orbits and their R?le in spectral statistics, Phys. Scr. T90 (1) (2001) 128, <http://dx.doi.org/10.1238/physica.topical.090a00128>.
- [217] S. Müller, S. Heusler, P. Braun, F. Haake, A. Altland, Semiclassical foundation of universality in quantum chaos, Phys. Rev. Lett. 93 (2004) 014103, <http://dx.doi.org/10.1103/PhysRevLett.93.014103>, URL <https://link.aps.org/doi/10.1103/PhysRevLett.93.014103>.
- [218] S. Müller, M. Novaes, Semiclassical calculation of spectral correlation functions of chaotic systems, Phys. Rev. E 98 (2018) 052207, <http://dx.doi.org/10.1103/PhysRevE.98.052207>, URL <https://link.aps.org/doi/10.1103/PhysRevE.98.052207>.
- [219] V.K.B. Kota, *Embedded Random Matrix Ensembles In Quantum Physics*, vol. 3, Springer, 2014.
- [220] J. Gómez, K. Kar, V. Kota, R. Molina, A.R. no, J. Retamosa, Many-body quantum chaos: Recent developments and applications to nuclei, Phys. Rep. 499 (4) (2011) 103–226, <http://dx.doi.org/10.1016/j.physrep.2010.11.003>, URL <https://www.sciencedirect.com/science/article/pii/S0370157310003091>.
- [221] U. Klein, What is the limit $\hbar \rightarrow 0$ of quantum theory? Am. J. Phys. 80 (11) (2012) 1009–1016, <http://dx.doi.org/10.1119/1.4751274>.
- [222] M. Berry, Some quantum-to-classical asymptotics, in: M.-J. Giannoni, A. Voros, J. Zinn-Justin (Eds.), *Chaos And Quantum Physics*, Les Houches Session LII, North-Holland, 1989, p. 251.
- [223] F.J. Dyson, Statistical theory of the energy levels of complex systems. I, J. Math. Phys. 3 (1) (1962) 140–156, <http://dx.doi.org/10.1063/1.1703773>.

- [224] F.J. Dyson, Statistical theory of the energy levels of complex systems. II, *J. Math. Phys.* 3 (1) (1962) 157–165, <http://dx.doi.org/10.1063/1.1703774>.
- [225] F. Izrailev, Distribution of quasienergy level spacings for classically chaotic quantum systems, Preprint 84-63, Institute Of Nuclear Physics, Novosibirsk, (1984).
- [226] M.V. Berry, M. Tabor, Level clustering in the regular spectrum, *Proc. R. Soc. Lond. A Math. Phys. Sci.* 356 (1686) (1977) 375–394, <http://dx.doi.org/10.1098/rspa.1977.0140>, URL <https://royalsocietypublishing.org/doi/abs/10.1098/rspa.1977.0140>.
- [227] M. Feingold, S. Fishman, D.R. Grempel, R.E. Prange, Statistics of quasi-energy separations in chaotic systems, *Phys. Rev. B* 31 (1985) 6852–6855, <http://dx.doi.org/10.1103/PhysRevB.31.6852>, URL <https://link.aps.org/doi/10.1103/PhysRevB.31.6852>.
- [228] S. Molčanov, The local structure of the spectrum of the one-dimensional Schrödinger operator, *Commun. Math. Phys.* 78 (3) (1981) 429–446.
- [229] F.M. Izrailev, Limiting quasienergy statistics for simple quantum systems, *Phys. Rev. Lett.* 56 (1986) 541–544, <http://dx.doi.org/10.1103/PhysRevLett.56.541>, URL <https://link.aps.org/doi/10.1103/PhysRevLett.56.541>.
- [230] F. Izrailev, Chaotic stucture of eigenfunctions in systems with maximal quantum chaos, *Phys. Lett. A* 125 (5) (1987) 250–252, [http://dx.doi.org/10.1016/0375-9601\(87\)90203-9](http://dx.doi.org/10.1016/0375-9601(87)90203-9), URL <https://www.sciencedirect.com/science/article/pii/0375960187902039>.
- [231] F.M. Izrailev, Intermediate statistics of the quasi-energy spectrum and quantum localisation of classical chaos, *J. Phys. A: Math. Gen.* 22 (7) (1989) 865–878, <http://dx.doi.org/10.1088/0305-4470/22/7/017>.
- [232] S. Wimberger, Nonlinear Dynamics And Quantum Chaos: An Introduction, Springer International Publishing, 2014, <http://dx.doi.org/10.1007/978-3-319-06343-0>.
- [233] H. Frahm, H.J. Mikeska, Quantum suppression of irregularity in the spectral properties of the kicked rotator, *Phys. Rev. Lett.* 60 (1988) 3–6, <http://dx.doi.org/10.1103/PhysRevLett.60.3>, URL <https://link.aps.org/doi/10.1103/PhysRevLett.60.3>.
- [234] M. Feingold, S. Fishman, D.R. Grempel, R.E. Prange, Comment on “quantum suppression of irregularity in the spectral properties of the kicked rotator”, *Phys. Rev. Lett.* 61 (1988) 377, <http://dx.doi.org/10.1103/PhysRevLett.61.377>, URL <https://link.aps.org/doi/10.1103/PhysRevLett.61.377>.
- [235] F. Izrailev, Quantum localization and statistics of quasienergy spectrum in a classically chaotic system, *Phys. Lett. A* 134 (1) (1988) 13–18, [http://dx.doi.org/10.1016/0375-9601\(88\)90538-5](http://dx.doi.org/10.1016/0375-9601(88)90538-5), URL <https://www.sciencedirect.com/science/article/pii/0375960188905385>.
- [236] B. Batistić, T. Manos, M. Robnik, The intermediate level statistics in dynamically localized chaotic eigenstates, *Europhys. Lett.* 102 (5) (2013) 50008, <http://dx.doi.org/10.1209/0295-5075/102/50008>.
- [237] T. Brody, A statistical measure for the repulsion of energy levels, *Lettore Al Nuovo Cimento (1971-1985)* 7 (12) (1973) 482–484.
- [238] M.V. Berry, M. Robnik, Semiclassical level spacings when regular and chaotic orbits coexist, 17(12) (1984) 2413–2421, <http://dx.doi.org/10.1088/0305-4470/17/12/013>.
- [239] V. Oganesyan, D.A. Huse, Localization of interacting fermions at high temperature, *Phys. Rev. B* 75 (2007) 155111, <http://dx.doi.org/10.1103/PhysRevB.75.155111>, URL <https://link.aps.org/doi/10.1103/PhysRevB.75.155111>.
- [240] Y.Y. Atas, E. Bogomolny, O. Giraud, G. Roux, Distribution of the ratio of consecutive level spacings in random matrix ensembles, *Phys. Rev. Lett.* 110 (2013) 084101, <http://dx.doi.org/10.1103/PhysRevLett.110.084101>, URL <https://link.aps.org/doi/10.1103/PhysRevLett.110.084101>.
- [241] S.H. Tekur, U.T. Bhosale, M.S. Santhanam, Higher-order spacing ratios in random matrix theory and complex quantum systems, *Phys. Rev. B* 98 (2018) 104305, <http://dx.doi.org/10.1103/PhysRevB.98.104305>, URL <https://link.aps.org/doi/10.1103/PhysRevB.98.104305>.
- [242] S.H. Tekur, M.S. Santhanam, Symmetry deduction from spectral fluctuations in complex quantum systems, *Phys. Rev. Res.* 2 (2020) 032063, <http://dx.doi.org/10.1103/PhysRevResearch.2.032063>, URL <https://link.aps.org/doi/10.1103/PhysRevResearch.2.032063>.
- [243] P. Sierant, J. Zakrzewski, Level statistics across the many-body localization transition, *Phys. Rev. B* 99 (2019) 104205, <http://dx.doi.org/10.1103/PhysRevB.99.104205>, URL <https://link.aps.org/doi/10.1103/PhysRevB.99.104205>.
- [244] J. Šuntajs, J. Bonča, T. Prosen, L. Vidmar, Ergodicity breaking transition in finite disordered spin chains, *Phys. Rev. B* 102 (2020) 064207, <http://dx.doi.org/10.1103/PhysRevB.102.064207>, URL <https://link.aps.org/doi/10.1103/PhysRevB.102.064207>.
- [245] A. Samanta, K. Damle, R. Sensarma, Tracking the many-body localized to ergodic transition via extremal statistics of entanglement eigenvalues, *Phys. Rev. B* 102 (2020) 104201, <http://dx.doi.org/10.1103/PhysRevB.102.104201>, URL <https://link.aps.org/doi/10.1103/PhysRevB.102.104201>.
- [246] W.-J. Rao, Critical level statistics at the many-body localization transition region, *J. Phys. A* 54 (10) (2021) 105001.
- [247] B. Eckhardt, Quantum mechanics of classically non-integrable systems, *Phys. Rep.* 163 (4) (1988) 205–297, [http://dx.doi.org/10.1016/0370-1573\(88\)90130-5](http://dx.doi.org/10.1016/0370-1573(88)90130-5), URL <https://www.sciencedirect.com/science/article/pii/0370157388901305>.
- [248] K.R.W. Jones, Entropy of random quantum states, 23 (23) (1990) L1247–L1251, <http://dx.doi.org/10.1088/0305-4470/23/23/011>.
- [249] G. Casati, I. Guarneri, F. Izrailev, R. Scharf, Scaling behavior of localization in quantum chaos, *Phys. Rev. Lett.* 64 (1990) 5–8, <http://dx.doi.org/10.1103/PhysRevLett.64.5>, URL <https://link.aps.org/doi/10.1103/PhysRevLett.64.5>.
- [250] J. Pichard, The one-dimensional Anderson model: scaling and resonances revisited, *J. Phys. C: Solid State Phys.* 19 (10) (1986) 1519.
- [251] P.A. Lee, T.V. Ramakrishnan, Disordered electronic systems, *Rev. Modern Phys.* 57 (1985) 287–337, <http://dx.doi.org/10.1103/RevModPhys.57.287>, URL <https://link.aps.org/doi/10.1103/RevModPhys.57.287>.
- [252] P. Bourgade, Random band matrices, in: Proceedings Of The International Congress Of Mathematicians (ICM 2018), World Scientific, 2018, pp. 2759–2783, http://dx.doi.org/10.1142/9789813272880_0159, arXiv:https://www.worldscientific.com/doi/pdf/10.1142/9789813272880_0159, URL https://www.worldscientific.com/doi/abs/10.1142/9789813272880_0159.
- [253] T. Spencer, Random banded and sparse matrices, in: The Oxford Handbook Of Random Matrix Theory, Oxford University Press, 2015, <http://dx.doi.org/10.1093/oxfordhb/9780198744191.013.23>.
- [254] V.V. Flambaum, A.A. Gribakina, G.F. Gribakin, M.G. Kozlov, Structure of compound states in the chaotic spectrum of the Ce atom: Localization properties, matrix elements, and enhancement of weak perturbations, *Phys. Rev. A* 50 (1994) 267–296, <http://dx.doi.org/10.1103/PhysRevA.50.267>, URL <https://link.aps.org/doi/10.1103/PhysRevA.50.267>.
- [255] T.H. Seligman, J.J.M. Verbaarschot, M.R. Zirnbauer, Spectral fluctuation properties of Hamiltonian systems: the transition region between order and chaos, *J. Phys. A: Math. Gen.* 18 (14) (1985) 2751–2770, <http://dx.doi.org/10.1088/0305-4470/18/14/026>.
- [256] E.P. Wigner, Characteristic vectors of bordered matrices with infinite dimensions, *Ann. Math.* 62 (3) (1955) 548–564, URL <http://www.jstor.org/stable/1970079>.
- [257] G. Casati, L. Molinari, F. Izrailev, Scaling properties of band random matrices, *Phys. Rev. Lett.* 64 (1990) 1851–1854, <http://dx.doi.org/10.1103/PhysRevLett.64.1851>, URL <https://link.aps.org/doi/10.1103/PhysRevLett.64.1851>.
- [258] A.D. Fyodorov, Statistical properties of random banded matrices: Analytical results, in: M. Fannes, A. Maes (Eds.), On Three Levels: Micro-, Meso-, And Macro-Approaches In Physics, Springer USA, Boston, MA, 1994, pp. 289–293, http://dx.doi.org/10.1007/978-1-4615-2460-1_33.
- [259] F.J. Dyson, A Brownian-motion model for the eigenvalues of a random matrix, *J. Math. Phys.* 3 (6) (1962) 1191–1198, <http://dx.doi.org/10.1063/1.1703862>.
- [260] A. Pandey, A. Kumar, S. Puri, Finite-range Coulomb gas models. I. Some analytical results, *Phys. Rev. E* 101 (2020) 022217, <http://dx.doi.org/10.1103/PhysRevE.101.022217>, URL <https://link.aps.org/doi/10.1103/PhysRevE.101.022217>.
- [261] A. Pandey, A. Kumar, S. Puri, Finite-range Coulomb gas models of banded random matrices and quantum kicked rotors, *Phys. Rev. E* 96 (2017) 052211, <http://dx.doi.org/10.1103/PhysRevE.96.052211>, URL <https://link.aps.org/doi/10.1103/PhysRevE.96.052211>.
- [262] A. Kumar, A. Pandey, S. Puri, Finite-range Coulomb gas models. II. Applications to quantum kicked rotors and banded random matrices, *Phys. Rev. E* 101 (2020) 022218, <http://dx.doi.org/10.1103/PhysRevE.101.022218>, URL <https://link.aps.org/doi/10.1103/PhysRevE.101.022218>.

- [263] E.B. Bogomolny, U. Gerland, C. Schmit, Models of intermediate spectral statistics, Phys. Rev. E 59 (1999) R1315–R1318, <http://dx.doi.org/10.1103/PhysRevE.59.R1315>, URL <https://link.aps.org/doi/10.1103/PhysRevE.59.R1315>.
- [264] E. Fermi, On the origin of the cosmic radiation, Phys. Rev. 75 (1949) 1169–1174, <http://dx.doi.org/10.1103/PhysRev.75.1169>, URL <https://link.aps.org/doi/10.1103/PhysRev.75.1169>.
- [265] I. Varga, D. Braun, Critical statistics in a power-law random-banded matrix ensemble, Phys. Rev. B 61 (2000) R11859–R11862, <http://dx.doi.org/10.1103/PhysRevB.61.R11859>, URL <https://link.aps.org/doi/10.1103/PhysRevB.61.R11859>.
- [266] M.L. Ndawana, V.E. Kravtsov, Energy level statistics of a critical random matrix ensemble, J. Phys. A: Math. Gen. 36 (12) (2003) 3639–3645, <http://dx.doi.org/10.1088/0305-4470/36/12/344>.
- [267] F. Evers, A.D. Mirlin, Anderson transitions, Rev. Modern Phys. 80 (2008) 1355–1417, <http://dx.doi.org/10.1103/RevModPhys.80.1355>, URL <https://link.aps.org/doi/10.1103/RevModPhys.80.1355>.
- [268] M. Wright, R. Weaver, *New Directions In Linear Acoustics And Vibration: Quantum Chaos, Random Matrix Theory And Complexity*, Cambridge University Press, 2010.
- [269] K.C. Hegewisch, S. Tomsovic, Random matrix theory for underwater sound propagation, Europhys. Lett. 97 (3) (2012) 34002, <http://dx.doi.org/10.1209/0295-5075/97/34002>.
- [270] J.A. Méndez-Bermúdez, G.F. de Arruda, F.A. Rodrigues, Y. Moreno, Diluted banded random matrices: scaling behavior of eigenfunction and spectral properties, J. Phys. A 50 (49) (2017) 495205, <http://dx.doi.org/10.1088/1751-8121/aa9509>.
- [271] J.E. Bayfield, P.M. Koch, Multiphoton ionization of highly excited hydrogen atoms, Phys. Rev. Lett. 33 (1974) 258–261, <http://dx.doi.org/10.1103/PhysRevLett.33.258>, URL <https://link.aps.org/doi/10.1103/PhysRevLett.33.258>.
- [272] R. Blümel, W.P. Reinhardt, Chaos In Atomic Physics, in: Cambridge Monographs on Atomic, Molecular and Chemical Physics, Cambridge University Press, 1997, <http://dx.doi.org/10.1017/CBO9780511524509>.
- [273] J.G. Leopold, I.C. Percival, Microwave ionization and excitation of rydberg atoms, Phys. Rev. Lett. 41 (1978) 944–947, <http://dx.doi.org/10.1103/PhysRevLett.41.944>, URL <https://link.aps.org/doi/10.1103/PhysRevLett.41.944>.
- [274] P.M. Koch, Microwave “ionization” of excited hydrogen atoms: How nonclassical local stability brought about by scarred separatrix states is affected by broadband noise and by varying the pulse envelope, Physica D 83 (1) (1995) 178–205, [http://dx.doi.org/10.1016/0167-2789\(94\)00261-N](http://dx.doi.org/10.1016/0167-2789(94)00261-N). Quantum Complexity in Mesoscopic Systems, URL <http://www.sciencedirect.com/science/article/pii/016727899400261N>.
- [275] P.M. Koch, L. Moorman, B.E. Sauer, E.J. Galvez, K.A.H. van Leeuwen, D. Richards, Experiments in quantum chaos: Microwave ionization of hydrogen atoms, Phys. Scr. T26 (1989) 51–58, <http://dx.doi.org/10.1088/0031-8949/1989/t26/008>.
- [276] P. Koch, K. van Leeuwen, The importance of resonances in microwave “ionization” of excited hydrogen atoms, Phys. Rep. 255 (5) (1995) 289–403, [http://dx.doi.org/10.1016/0370-1573\(94\)00093-I](http://dx.doi.org/10.1016/0370-1573(94)00093-I), URL <http://www.sciencedirect.com/science/article/pii/037015739400093I>.
- [277] G. Casati, I. Guarneri, D.L. Shepelyansky, Exponential photonic localization for the hydrogen atom in a monochromatic field, Phys. Rev. A 36 (1987) 3501–3504, <http://dx.doi.org/10.1103/PhysRevA.36.3501>, URL <https://link.aps.org/doi/10.1103/PhysRevA.36.3501>.
- [278] H.J. Stöckmann, *Quantum Chaos: An Introduction*, Cambridge University Press, Cambridge, 1999.
- [279] A. Krug, A. Buchleitner, Chaotic ionization of nonhydrogenic alkali rydberg states, Phys. Rev. Lett. 86 (2001) 3538–3541, <http://dx.doi.org/10.1103/PhysRevLett.86.3538>, URL <https://link.aps.org/doi/10.1103/PhysRevLett.86.3538>.
- [280] R.V. Jensen, S.M. Susskind, M.M. Sanders, Chaotic ionization of highly excited hydrogen atoms: Comparison of classical and quantum theory with experiment, Phys. Rep. 201 (1) (1991) 1–56, [http://dx.doi.org/10.1016/0370-1573\(91\)90113-Z](http://dx.doi.org/10.1016/0370-1573(91)90113-Z), URL <http://www.sciencedirect.com/science/article/pii/037015739190113Z>.
- [281] H. Maeda, T.F. Gallagher, Quantum suppression of microwave ionization of rydberg atoms at high scaled frequency, Phys. Rev. Lett. 93 (2004) 193002, <http://dx.doi.org/10.1103/PhysRevLett.93.193002>, URL <https://link.aps.org/doi/10.1103/PhysRevLett.93.193002>.
- [282] A. Schelle, D. Delande, A. Buchleitner, Microwave-driven atoms: From Anderson localization to Einstein’s photoeffect, Phys. Rev. Lett. 102 (2009) 183001, <http://dx.doi.org/10.1103/PhysRevLett.102.183001>, URL <https://link.aps.org/doi/10.1103/PhysRevLett.102.183001>.
- [283] M.G. Raizen, Quantum chaos with cold atoms, in: B. Bederson, H. Walther (Eds.), in: Advances In Atomic, Molecular, and Optical Physics, vol. 41, Academic Press, 1999, pp. 43–81, [http://dx.doi.org/10.1016/S1049-250X\(98\)60218-9](http://dx.doi.org/10.1016/S1049-250X(98)60218-9), URL <http://www.sciencedirect.com/science/article/pii/S1049250X08602189>.
- [284] W.K. Hensinger, N.R. Heckenberg, G.J. Milburn, H. Rubinsztein-Dunlop, Experimental tests of quantum nonlinear dynamics in atom optics, J. Opt. B: Quantum Semiclassical Opt. 5 (2) (2003) R83–R120, <http://dx.doi.org/10.1088/1464-4266/5/2/202>.
- [285] R. Graham, M. Schlautmann, P. Zoller, Dynamical localization of atomic-beam deflection by a modulated standing light wave, Phys. Rev. A 45 (1992) R19–R22, <http://dx.doi.org/10.1103/PhysRevA.45.R19>, URL <https://link.aps.org/doi/10.1103/PhysRevA.45.R19>.
- [286] F.L. Moore, J.C. Robinson, C. Bharucha, P.E. Williams, M.G. Raizen, Observation of dynamical localization in atomic momentum transfer: A new testing ground for quantum chaos, Phys. Rev. Lett. 73 (1994) 2974–2977, <http://dx.doi.org/10.1103/PhysRevLett.73.2974>, URL <https://link.aps.org/doi/10.1103/PhysRevLett.73.2974>.
- [287] F.L. Moore, J.C. Robinson, C.F. Bharucha, B. Sundaram, M.G. Raizen, Atom optics realization of the quantum δ-kicked rotor, Phys. Rev. Lett. 75 (1995) 4598–4601, <http://dx.doi.org/10.1103/PhysRevLett.75.4598>, URL <https://link.aps.org/doi/10.1103/PhysRevLett.75.4598>.
- [288] H. Ammann, R. Gray, I. Shvarchuck, N. Christensen, Quantum delta-kicked rotor: Experimental observation of decoherence, Phys. Rev. Lett. 80 (1998) 4111–4115, <http://dx.doi.org/10.1103/PhysRevLett.80.4111>, URL <https://link.aps.org/doi/10.1103/PhysRevLett.80.4111>.
- [289] B. Fischer, A. Rosen, A. Bekker, S. Fishman, Experimental observation of localization in the spatial frequency domain of a kicked optical system, Phys. Rev. E 61 (2000) R4694–R4697, <http://dx.doi.org/10.1103/PhysRevE.61.R4694>, URL <https://link.aps.org/doi/10.1103/PhysRevE.61.R4694>.
- [290] B. Fischer, B. Vodonos, S. Atkins, A. Bekker, Experimental demonstration of localization in the frequency domain of mode-locked lasers with dispersion, Opt. Lett. 27 (12) (2002) 1061–1063, <http://dx.doi.org/10.1364/OL.27.001061>, URL <http://ol.osa.org/abstract.cfm?URI=ol-27-12-1061>.
- [291] E. Ott, T.M. Antonsen, J.D. Hanson, Effect of noise on time-dependent quantum chaos, Phys. Rev. Lett. 53 (1984) 2187–2190, <http://dx.doi.org/10.1103/PhysRevLett.53.2187>, URL <https://link.aps.org/doi/10.1103/PhysRevLett.53.2187>.
- [292] D. Cohen, Quantum chaos, dynamical correlations, and the effect of noise on localization, Phys. Rev. A 44 (1991) 2292–2313, <http://dx.doi.org/10.1103/PhysRevA.44.2292>, URL <https://link.aps.org/doi/10.1103/PhysRevA.44.2292>.
- [293] D. Cohen, Localization, dynamical correlations, and the effect of colored noise on coherence, Phys. Rev. Lett. 67 (1991) 1945–1948, <http://dx.doi.org/10.1103/PhysRevLett.67.1945>, URL <https://link.aps.org/doi/10.1103/PhysRevLett.67.1945>.
- [294] B.G. Klappauf, W.H. Oskay, D.A. Steck, M.G. Raizen, Observation of noise and dissipation effects on dynamical localization, Phys. Rev. Lett. 81 (1998) 1203–1206, <http://dx.doi.org/10.1103/PhysRevLett.81.1203>, URL <https://link.aps.org/doi/10.1103/PhysRevLett.81.1203>.
- [295] W.H. Oskay, D.A. Steck, M.G. Raizen, Timing noise effects on dynamical localization, Chaos Solitons Fractals 16 (3) (2003) 409–416, [http://dx.doi.org/10.1016/S0960-0779\(02\)00302-8](http://dx.doi.org/10.1016/S0960-0779(02)00302-8), URL <http://www.sciencedirect.com/science/article/pii/S0960077902003028>.
- [296] D.A. Steck, V. Milner, W.H. Oskay, M.G. Raizen, Quantitative study of amplitude noise effects on dynamical localization, Phys. Rev. E 62 (2000) 3461–3475, <http://dx.doi.org/10.1103/PhysRevE.62.3461>, URL <https://link.aps.org/doi/10.1103/PhysRevE.62.3461>.
- [297] D.H. White, S.K. Ruddell, M.D. Hoogerland, Phase noise in the delta kicked rotor: from quantum to classical, New J. Phys. 16 (11) (2014) 113039, <http://dx.doi.org/10.1088/1367-2630/16/11/113039>.
- [298] H. Schomerus, E. Lutz, Nonexponential decoherence and momentum subdiffusion in a quantum Lévy kicked rotator, Phys. Rev. Lett. 98 (2007) 260401, <http://dx.doi.org/10.1103/PhysRevLett.98.260401>, URL <https://link.aps.org/doi/10.1103/PhysRevLett.98.260401>.

- [299] S. Sarkar, S. Paul, C. Vishwakarma, S. Kumar, G. Verma, M. Sainath, U.D. Rapol, M.S. Santhanam, Nonexponential decoherence and subdiffusion in atom-optics kicked rotor, Phys. Rev. Lett. 118 (2017) 174101, <http://dx.doi.org/10.1103/PhysRevLett.118.174101>, URL <https://link.aps.org/doi/10.1103/PhysRevLett.118.174101>.
- [300] A. Boumemoura, S. Fischer, The classical KAM theorem for Hamiltonian systems via rational approximations, Regul. Chaotic Dyn. 19 (2) (2014) 251–265.
- [301] G.P. Brandino, J.-S. Caux, R.M. Konik, Glimmers of a quantum KAM theorem: Insights from quantum quenches in one-dimensional bose gases, Phys. Rev. X 5 (2015) 041043, <http://dx.doi.org/10.1103/PhysRevX.5.041043>, URL <https://link.aps.org/doi/10.1103/PhysRevX.5.041043>.
- [302] G. Zaslavskii, Regular and stochastic dynamics of particles in the field of a wave packet, ZhETF 88 (1985) 1984–1995.
- [303] G. Zaslavsky, *Hamiltonian Chaos And Fractional Dynamics*, Oxford University Press, 2008.
- [304] I. Dana, Kicked harper models and kicked charge in a magnetic field, Phys. Lett. A 197 (5) (1995) 413–416, [http://dx.doi.org/10.1016/0375-9601\(94\)01007-H](http://dx.doi.org/10.1016/0375-9601(94)01007-H), URL <http://www.sciencedirect.com/science/article/pii/037596019401007H>.
- [305] D. Shepelyansky, C. Sire, Quantum evolution in a dynamical quasi-crystal, Europhys. Lett. 20 (2) (1992) 95–100, <http://dx.doi.org/10.1209/0295-5075/20/2/001>.
- [306] I. Dana, Quantum suppression of diffusion on stochastic webs, Phys. Rev. Lett. 73 (1994) 1609–1612, <http://dx.doi.org/10.1103/PhysRevLett.73.1609>, URL <https://link.aps.org/doi/10.1103/PhysRevLett.73.1609>.
- [307] R. Artuso, G. Casati, D. Shepelyansky, Fractal spectrum and anomalous diffusion in the kicked harper model, Phys. Rev. Lett. 68 (1992) 3826–3829, <http://dx.doi.org/10.1103/PhysRevLett.68.3826>, URL <https://link.aps.org/doi/10.1103/PhysRevLett.68.3826>.
- [308] G.A. Kells, J. Twamley, D.M. Heffernan, Dynamical properties of the delta-kicked harmonic oscillator, Phys. Rev. E 70 (2004) 015203, <http://dx.doi.org/10.1103/PhysRevE.70.015203>, URL <https://link.aps.org/doi/10.1103/PhysRevE.70.015203>.
- [309] T.P. Billam, S.A. Gardiner, Quantum resonances in an atom-optical δ -kicked harmonic oscillator, Phys. Rev. A 80 (2009) 023414, <http://dx.doi.org/10.1103/PhysRevA.80.023414>, URL <https://link.aps.org/doi/10.1103/PhysRevA.80.023414>.
- [310] R. Lima, D. Shepelyansky, Fast delocalization in a model of quantum kicked rotator, Phys. Rev. Lett. 67 (1991) 1377–1380, <http://dx.doi.org/10.1103/PhysRevLett.67.1377>, URL <https://link.aps.org/doi/10.1103/PhysRevLett.67.1377>.
- [311] A.R.R. Carvalho, A. Buchleitner, Web-assisted tunneling in the kicked harmonic oscillator, Phys. Rev. Lett. 93 (2004) 204101, <http://dx.doi.org/10.1103/PhysRevLett.93.204101>, URL <https://link.aps.org/doi/10.1103/PhysRevLett.93.204101>.
- [312] T. Fromhold, A. Patane, S. Bujkiewicz, P. Wilkinson, D. Fowler, D. Sherwood, S. Stapleton, A. Krokhin, L. Eaves, M. Henini, et al., Chaotic electron diffusion through stochastic webs enhances current flow in superlattices, Nature 428 (6984) (2004) 726–730, <http://dx.doi.org/10.1038/nature02445>.
- [313] S.M. Soskin, I.A. Khovanov, P.V.E. McClintock, Mechanism of resonant enhancement of electron drift in nanometer semiconductor superlattices subjected to electric and inclined magnetic fields, Phys. Rev. B 100 (2019) 235203, <http://dx.doi.org/10.1103/PhysRevB.100.235203>, URL <https://link.aps.org/doi/10.1103/PhysRevB.100.235203>.
- [314] G.B. Lemos, R.M. Gomes, S.P. Walborn, P.H.S. Ribeiro, F. Toscano, Experimental observation of quantum chaos in a beam of light, Nature Commun. 3 (1) (2012) 1–7, <http://dx.doi.org/10.1038/ncomms2214>.
- [315] S.A. Gardiner, J.I. Cirac, P. Zoller, Quantum chaos in an ion trap: The delta-kicked harmonic oscillator, Phys. Rev. Lett. 79 (1997) 4790–4793, <http://dx.doi.org/10.1103/PhysRevLett.79.4790>, URL <https://link.aps.org/doi/10.1103/PhysRevLett.79.4790>.
- [316] R. Sankaranarayanan, A. Lakshminarayanan, V.B. Sheorey, Quantum chaos of a particle in a square well: Competing length scales and dynamical localization, Phys. Rev. E 64 (2001) 046210, <http://dx.doi.org/10.1103/PhysRevE.64.046210>, URL <https://link.aps.org/doi/10.1103/PhysRevE.64.046210>.
- [317] B. Hu, B. Li, J. Liu, Y. Gu, Quantum chaos of a kicked particle in an infinite potential well, Phys. Rev. Lett. 82 (1999) 4224–4227, <http://dx.doi.org/10.1103/PhysRevLett.82.4224>, URL <https://link.aps.org/doi/10.1103/PhysRevLett.82.4224>.
- [318] R. Sankaranarayanan, A. Lakshminarayanan, V. Sheorey, Chaos in a well: effects of competing length scales, Phys. Lett. A 279 (5) (2001) 313–320, [http://dx.doi.org/10.1016/S0375-9601\(01\)00019-6](http://dx.doi.org/10.1016/S0375-9601(01)00019-6), URL <http://www.sciencedirect.com/science/article/pii/S0375960101000196>.
- [319] S. Paul, H. Pal, M.S. Santhanam, Barrier-induced chaos in a kicked rotor: Classical subdiffusion and quantum localization, Phys. Rev. E 93 (2016) 060203, <http://dx.doi.org/10.1103/PhysRevE.93.060203>, URL <https://link.aps.org/doi/10.1103/PhysRevE.93.060203>.
- [320] H. Pal, M.S. Santhanam, Dynamics of kicked particles in a double-barrier structure, Phys. Rev. E 82 (2010) 056212, <http://dx.doi.org/10.1103/PhysRevE.82.056212>, URL <https://link.aps.org/doi/10.1103/PhysRevE.82.056212>.
- [321] H. Pal, M. Santhanam, Classically induced suppression of energy growth in a chaotic quantum system, Pramana 77 (5) (2011) 793–802.
- [322] S. Paul, M.S. Santhanam, Floquet states of a kicked particle in a singular potential: Exponential and power-law profiles, Phys. Rev. E 97 (2018) 032217, <http://dx.doi.org/10.1103/PhysRevE.97.032217>, URL <https://link.aps.org/doi/10.1103/PhysRevE.97.032217>.
- [323] A.M. García-García, J. Wang, Anderson transition in quantum chaos, Phys. Rev. Lett. 94 (2005) 244102, <http://dx.doi.org/10.1103/PhysRevLett.94.244102>, URL <https://link.aps.org/doi/10.1103/PhysRevLett.94.244102>.
- [324] A.M. García-García, J. Wang, Anderson localization in quantum chaos: Scaling and universality, Acta Phys. Polon. A 112 (2007) 635, <http://dx.doi.org/10.12693/APhysPolA.112.635>.
- [325] F. Dalfovo, S. Giorgini, L.P. Pitaevskii, S. Stringari, Theory of Bose-Einstein condensation in trapped gases, Rev. Modern Phys. 71 (1999) 463–512, <http://dx.doi.org/10.1103/RevModPhys.71.463>, URL <https://link.aps.org/doi/10.1103/RevModPhys.71.463>.
- [326] C. Zhang, J. Liu, M.G. Raizen, Q. Niu, Transition to instability in a kicked Bose-Einstein condensate, Phys. Rev. Lett. 92 (2004) 054101, <http://dx.doi.org/10.1103/PhysRevLett.92.054101>, URL <https://link.aps.org/doi/10.1103/PhysRevLett.92.054101>.
- [327] P. Nozières, D. Pines, *The Theory Of Quantum Liquids*, Addison-Wesley, 1990.
- [328] Y. Castin, R. Dum, Instability and depletion of an excited Bose-Einstein condensate in a trap, Phys. Rev. Lett. 79 (1997) 3553–3556, <http://dx.doi.org/10.1103/PhysRevLett.79.3553>, URL <https://link.aps.org/doi/10.1103/PhysRevLett.79.3553>.
- [329] J. Reslen, C.E. Creffield, T.S. Monteiro, Dynamical instability in kicked Bose-Einstein condensates, Phys. Rev. A 77 (2008) 043621, <http://dx.doi.org/10.1103/PhysRevA.77.043621>, URL <https://link.aps.org/doi/10.1103/PhysRevA.77.043621>.
- [330] B. Mieck, R. Graham, Bose-Einstein condensate of kicked rotators, J. Phys. A: Math. Gen. 37 (44) (2004) L581–L588, <http://dx.doi.org/10.1088/0305-4470/37/44/016>.
- [331] B. Mieck, R. Graham, Bose-Einstein condensate of kicked rotators with time-dependent interaction, J. Phys. A: Math. Gen. 38 (7) (2005) L139–L144, <http://dx.doi.org/10.1088/0305-4470/38/7/016>.
- [332] T.P. Billam, S.A. Gardiner, Coherence and instability in a driven Bose-Einstein condensate: a fully dynamical number-conserving approach, New J. Phys. 14 (1) (2012) 013038, <http://dx.doi.org/10.1088/1367-2630/14/1/013038>.
- [333] T.P. Billam, P. Mason, S.A. Gardiner, Second-order number-conserving description of nonequilibrium dynamics in finite-temperature Bose-Einstein condensates, Phys. Rev. A 87 (2013) 033628, <http://dx.doi.org/10.1103/PhysRevA.87.033628>, URL <https://link.aps.org/doi/10.1103/PhysRevA.87.033628>.
- [334] G.J. Duffy, A.S. Mellish, K.J. Challis, A.C. Wilson, Nonlinear atom-optical δ -kicked harmonic oscillator using a Bose-Einstein condensate, Phys. Rev. A 70 (2004) 041602, <http://dx.doi.org/10.1103/PhysRevA.70.041602>, URL <https://link.aps.org/doi/10.1103/PhysRevA.70.041602>.
- [335] D.L. Shepelyansky, Delocalization of quantum chaos by weak nonlinearity, Phys. Rev. Lett. 70 (1993) 1787–1790, <http://dx.doi.org/10.1103/PhysRevLett.70.1787>, URL <https://link.aps.org/doi/10.1103/PhysRevLett.70.1787>.

- [336] S. Lellouch, A. Rançon, S. De Bièvre, D. Delande, J.C. Garreau, Dynamics of the mean-field-interacting quantum kicked rotor, Phys. Rev. A 101 (2020) 043624, <http://dx.doi.org/10.1103/PhysRevA.101.043624>, URL <https://link.aps.org/doi/10.1103/PhysRevA.101.043624>.
- [337] T.V. Laptjeva, J.D. Bodyfelt, D.O. Krimer, C. Skokos, S. Flach, The crossover from strong to weak chaos for nonlinear waves in disordered systems, Europhys. Lett. 91 (3) (2010) 30001, <http://dx.doi.org/10.1209/0295-5075/91/30001>.
- [338] L. Ermann, D.L. Shepelyansky, Destruction of Anderson localization by nonlinearity in kicked rotator at different effective dimensions, J. Phys. A 47 (33) (2014) 335101, <http://dx.doi.org/10.1088/1751-8113/47/33/335101>.
- [339] P. Qin, A. Andreanov, H.C. Park, S. Flach, Interacting ultracold atomic kicked rotors: loss of dynamical localization, Sci. Rep. 7 (2017) 41139, <http://dx.doi.org/10.1038/srep41139>.
- [340] I. García-Mata, D.L. Shepelyansky, Delocalization induced by nonlinearity in systems with disorder, Phys. Rev. E 79 (2009) 026205, <http://dx.doi.org/10.1103/PhysRevE.79.026205>, URL <https://link.aps.org/doi/10.1103/PhysRevE.79.026205>.
- [341] C. Skokos, I. Gkolias, S. Flach, Nonequilibrium chaos of disordered nonlinear waves, Phys. Rev. Lett. 111 (2013) 064101, <http://dx.doi.org/10.1103/PhysRevLett.111.064101>, URL <https://link.aps.org/doi/10.1103/PhysRevLett.111.064101>.
- [342] B. Vermersch, D. Delande, J.C. Garreau, Bogoliubov excitations in the quasiperiodic kicked rotor: Stability of a kicked condensate and the quasi-insulator-to-metal transition, Phys. Rev. A 101 (2020) 053625, <http://dx.doi.org/10.1103/PhysRevA.101.053625>, URL <https://link.aps.org/doi/10.1103/PhysRevA.101.053625>.
- [343] S. Wimberger, R. Mannella, O. Morsch, E. Arimondo, Resonant nonlinear quantum transport for a periodically kicked Bose condensate, Phys. Rev. Lett. 94 (2005) 130404, <http://dx.doi.org/10.1103/PhysRevLett.94.130404>, URL <https://link.aps.org/doi/10.1103/PhysRevLett.94.130404>.
- [344] L. Rebuzzini, S. Wimberger, R. Artuso, Delocalized and resonant quantum transport in nonlinear generalizations of the kicked rotor model, Phys. Rev. E 71 (2005) 036220, <http://dx.doi.org/10.1103/PhysRevE.71.036220>, URL <https://link.aps.org/doi/10.1103/PhysRevE.71.036220>.
- [345] R. Blümel, S. Fishman, U. Smilansky, Excitation of molecular rotation by periodic microwave pulses. A testing ground for Anderson localization, J. Chem. Phys. 84 (5) (1986) 2604–2614, <http://dx.doi.org/10.1063/1.450330>.
- [346] J. Floß, S. Fishman, I.S. Averbukh, Anderson localization in laser-kicked molecules, Phys. Rev. A 88 (2013) 023426, <http://dx.doi.org/10.1103/PhysRevA.88.023426>, URL <https://link.aps.org/doi/10.1103/PhysRevA.88.023426>.
- [347] J. Floß, I.S. Averbukh, Quantum resonance, Anderson localization, and selective manipulations in molecular mixtures by ultrashort laser pulses, Phys. Rev. A 86 (2012) 021401, <http://dx.doi.org/10.1103/PhysRevA.86.021401>, URL <https://link.aps.org/doi/10.1103/PhysRevA.86.021401>.
- [348] M. Bitter, V. Milner, Experimental observation of dynamical localization in laser-kicked molecular rotors, Phys. Rev. Lett. 117 (2016) 144104, <http://dx.doi.org/10.1103/PhysRevLett.117.144104>, URL <https://link.aps.org/doi/10.1103/PhysRevLett.117.144104>.
- [349] S. Zhdanovich, C. Bloomquist, J. Floß, I.S. Averbukh, J.W. Hepburn, V. Milner, Quantum resonances in selective rotational excitation of molecules with a sequence of ultrashort laser pulses, Phys. Rev. Lett. 109 (2012) 043003, <http://dx.doi.org/10.1103/PhysRevLett.109.043003>, URL <https://link.aps.org/doi/10.1103/PhysRevLett.109.043003>.
- [350] J. Floß, A. Kamalov, I.S. Averbukh, P.H. Bucksbaum, Observation of Bloch oscillations in molecular rotation, Phys. Rev. Lett. 115 (2015) 203002, <http://dx.doi.org/10.1103/PhysRevLett.115.203002>, URL <https://link.aps.org/doi/10.1103/PhysRevLett.115.203002>.
- [351] J. Floß, I.S. Averbukh, Edge states of periodically kicked quantum rotors, Phys. Rev. E 91 (2015) 052911, <http://dx.doi.org/10.1103/PhysRevE.91.052911>, URL <https://link.aps.org/doi/10.1103/PhysRevE.91.052911>.
- [352] A. Bakman, H. Veksler, S. Fishman, Edge states of a three dimensional kicked rotor, Eur. Phys. J. B 92 (10) (2019) 236, <http://dx.doi.org/10.1140/epjb/e2019-100174-8>.
- [353] R. Scharf, Kicked rotator for a spin-1/2 particle, J. Phys. A: Math. Gen. 22 (19) (1989) 4223–4242, <http://dx.doi.org/10.1088/0305-4470/22/19/016>.
- [354] D. Mašović, A. Tancić, The tight-binding model corresponding to the quantum kicked rotor for a spin-12 particle in the magnetic field, Phys. Lett. A 191 (5) (1994) 384–388, [http://dx.doi.org/10.1016/0375-9601\(94\)90790-0](http://dx.doi.org/10.1016/0375-9601(94)90790-0), URL <http://www.sciencedirect.com/science/article/pii/0375960194907900>.
- [355] M. Thaha, R. Blümel, U. Smilansky, Symmetry breaking and localization in quantum chaotic systems, Phys. Rev. E 48 (1993) 1764–1781, <http://dx.doi.org/10.1103/PhysRevE.48.1764>, URL <https://link.aps.org/doi/10.1103/PhysRevE.48.1764>.
- [356] C. Hainaut, I. Manai, J.-F. Clément, J.C. Garreau, P. Szriftgiser, G. Lemarié, N. Cheroret, D. Delande, R. Chicireanu, Controlling symmetry and localization with an artificial gauge field in a disordered quantum system, Nature Commun. 9 (1) (2018) 1–9, <http://dx.doi.org/10.1038/s41467-018-03481-9>.
- [357] J.P. Dahlhaus, J.M. Edge, J. Tworzydł o, C.W.J. Beenakker, Quantum Hall effect in a one-dimensional dynamical system, Phys. Rev. B 84 (2011) 115133, <http://dx.doi.org/10.1103/PhysRevB.84.115133>, URL <https://link.aps.org/doi/10.1103/PhysRevB.84.115133>.
- [358] C. Tian, Y. Chen, J. Wang, Emergence of integer quantum Hall effect from chaos, Phys. Rev. B 93 (2016) 075403, <http://dx.doi.org/10.1103/PhysRevB.93.075403>, URL <https://link.aps.org/doi/10.1103/PhysRevB.93.075403>.
- [359] L. Zhou, J. Gong, Floquet topological phases in a spin-1/2 double kicked rotor, Phys. Rev. A 97 (2018) 063603, <http://dx.doi.org/10.1103/PhysRevA.97.063603>, URL <https://link.aps.org/doi/10.1103/PhysRevA.97.063603>.
- [360] I. Dana, K. Kubo, Floquet systems with Hall effect: Topological properties and phase transitions, Phys. Rev. B 100 (2019) 045107, <http://dx.doi.org/10.1103/PhysRevB.100.045107>, URL <https://link.aps.org/doi/10.1103/PhysRevB.100.045107>.
- [361] M. Ben-Harush, I. Dana, Generic superweak chaos induced by Hall effect, Phys. Rev. E 93 (2016) 052207, <http://dx.doi.org/10.1103/PhysRevE.93.052207>, URL <https://link.aps.org/doi/10.1103/PhysRevE.93.052207>.
- [362] V. Arnold, Instability of dynamical systems with several degrees of freedom, Russ. Math. Dokl. 5 (1964) 581–585.
- [363] P.J. Holmes, J.E. Marsden, Melnikov's method and arnold diffusion for perturbations of integrable Hamiltonian systems, J. Math. Phys. 23 (4) (1982) 669–675, <http://dx.doi.org/10.1063/1.525415>.
- [364] V.I. Arnol'd, Instability of dynamical systems with several degrees of freedom, in: Hamiltonian Dynamical Systems, CRC Press, 2020, pp. 633–637.
- [365] P.M. Cincotta, Arnold diffusion: an overview through dynamical astronomy, New Astron. Rev. 46 (1) (2002) 13–39, [http://dx.doi.org/10.1016/S1387-6473\(01\)00153-1](http://dx.doi.org/10.1016/S1387-6473(01)00153-1), URL <https://www.sciencedirect.com/science/article/pii/S1387647301001531>.
- [366] B.V. Chirikov, J. Ford, F. Vivaldi, Some numerical studies of arnold diffusion in a simple model, AIP Conf. Proc. 57 (1) (1980) 323–340, <http://dx.doi.org/10.1063/1.32115>, arXiv:<https://aip.scitation.org/doi/pdf/10.1063/1.32115>, URL <https://aip.scitation.org/doi/abs/10.1063/1.32115>.
- [367] C. Froeschlé, Numerical study of a four-dimensional mapping, Astronom. Astrophys. 16 (1972) 172.
- [368] N.N. Nekhoroshev, An exponential estimate of the time of stability of nearly-integrable Hamiltonian systems, Uspekhi Matematicheskikh Nauk 32 (6) (1977) 5–66.
- [369] S. Karmakar, S. Keshavamurthy, Intramolecular vibrational energy redistribution and the quantum ergodicity transition: a phase space perspective, Phys. Chem. Chem. Phys. 22 (2020) 11139–11173, <http://dx.doi.org/10.1039/D0CP01413C>, URL <http://dx.doi.org/10.1039/D0CP01413C>.
- [370] K. Kaneko, R.J. Bagley, Arnold diffusion, ergodicity and intermittency in a coupled standard mapping, Phys. Lett. A 110 (1985) 435–440, [http://dx.doi.org/10.1016/0375-9601\(85\)90548-1](http://dx.doi.org/10.1016/0375-9601(85)90548-1).
- [371] G. Wang, B. Hu, S. Chen, Arnold diffusion in a four-dimensional standard map, Phys. Lett. A 151 (1) (1990) 37–42, [http://dx.doi.org/10.1016/0375-9601\(90\)90843-D](http://dx.doi.org/10.1016/0375-9601(90)90843-D), URL <http://www.sciencedirect.com/science/article/pii/037596019090843D>.

- [372] B.P. Wood, A.J. Lichtenberg, M.A. Lieberman, Arnold diffusion in weakly coupled standard maps, Phys. Rev. A 42 (1990) 5885–5893, <http://dx.doi.org/10.1103/PhysRevA.42.5885>, URL <https://link.aps.org/doi/10.1103/PhysRevA.42.5885>.
- [373] C. Froeschlé, M. Guzzo, E. Lega, First numerical evidence of global Arnold diffusion in quasi-integrable systems, Discrete Contin. Dyn. Syst. Ser. B 5 (2005) 687, <http://dx.doi.org/10.3934/dcdsb.2005.5.687>, URL <http://aimscescences.org/article/id/1442087a-0b10-4953-b5d7-2d2b5adff1e4>.
- [374] J. von Milczewski, G.H.F. Diercksen, T. Uzer, Computation of the Arnol'd web for the hydrogen atom in crossed electric and magnetic fields, Phys. Rev. Lett. 76 (1996) 2890–2893, <http://dx.doi.org/10.1103/PhysRevLett.76.2890>, URL <https://link.aps.org/doi/10.1103/PhysRevLett.76.2890>.
- [375] V.Y. Demikhovskii, F.M. Izrailev, A.I. Malyshev, Manifestation of Arnol'd diffusion in quantum systems, Phys. Rev. Lett. 88 (2002) 154101, <http://dx.doi.org/10.1103/PhysRevLett.88.154101>, URL <https://link.aps.org/doi/10.1103/PhysRevLett.88.154101>.
- [376] V.Y. Demikhovskii, F.M. Izrailev, A.I. Malyshev, Quantum Arnol'd diffusion in a simple nonlinear system, Phys. Rev. E 66 (2002) 036211, <http://dx.doi.org/10.1103/PhysRevE.66.036211>, URL <https://link.aps.org/doi/10.1103/PhysRevE.66.036211>.
- [377] A. Malyshev, L. Chizhova, Arnol'd diffusion in a system with 2.5 degrees of freedom: Classical and quantum mechanical approaches, J. Exp. Theor. Phys. 110 (5) (2010) 837–844.
- [378] K. Nakamura, T. Harayama, *Quantum Chaos And Quantum Dots*, vol. 3, Oxford University Press on Demand, 2004.
- [379] Y. Boretz, L.E. Reichl, Arnold diffusion in a driven optical lattice, Phys. Rev. E 93 (2016) 032214, <http://dx.doi.org/10.1103/PhysRevE.93.032214>, URL <https://link.aps.org/doi/10.1103/PhysRevE.93.032214>.
- [380] P.M. Cincotta, C. Efthymiopoulos, C.M. Giordano, M. n F. Mestre, Chirikov and Nekhoroshev diffusion estimates: Bridging the two sides of the river, Physica D 266 (2014) 49–64, <http://dx.doi.org/10.1016/j.physd.2013.10.005>, URL <http://www.sciencedirect.com/science/article/pii/S0167278913002819>.
- [381] C. Efthymiopoulos, M. Harsoula, The speed of Arnold diffusion, Physica D 251 (2013) 19–38, <http://dx.doi.org/10.1016/j.physd.2013.01.016>, URL <http://www.sciencedirect.com/science/article/pii/S0167278913000420>.
- [382] L. Reichl, Arnol'd diffusion, in: *The Transition To Chaos: Conservative Classical And Quantum Systems*, Springer International Publishing, 2021, pp. 133–153, http://dx.doi.org/10.1007/978-3-030-63534-3_5.
- [383] S. Karmakar, S. Keshavamurthy, Relevance of the resonance junctions on the Arnold web to dynamical tunneling and eigenstate delocalization, J. Phys. Chem. A 122 (43) (2018) 8636–8649, <http://dx.doi.org/10.1021/acs.jpca.8b08626>.
- [384] D.M. Leitner, P.G. Wolynes, Quantization of the stochastic pump model of arnold diffusion, Phys. Rev. Lett. 79 (1997) 55–58, <http://dx.doi.org/10.1103/PhysRevLett.79.55>, URL <https://link.aps.org/doi/10.1103/PhysRevLett.79.55>.
- [385] V. Demikhovskii, F. Izrailev, A. Malyshev, Quantum Arnol'd diffusion in a rippled waveguide, Phys. Lett. A 352 (6) (2006) 491–495, <http://dx.doi.org/10.1016/j.physleta.2005.10.110>, URL <https://link.aps.org/science/article/pii/S0375960105019225>.
- [386] D. Basko, Weak chaos in the disordered nonlinear Schrödinger chain: Destruction of Anderson localization by Arnold diffusion, Ann. Phys. 326 (7) (2011) 1577–1655, <http://dx.doi.org/10.1016/j.aop.2011.02.004>, July 2011 Special Issue, URL <http://www.sciencedirect.com/science/article/pii/S003491611000339>.
- [387] S. Lange, A. Bäcker, R. Ketzmerick, What is the mechanism of power-law distributed Poincaré recurrences in higher-dimensional systems? Europhys. Lett. 116 (3) (2016) 30002, <http://dx.doi.org/10.1209/0295-5075/116/30002>.
- [388] E. Doron, S. Fishman, Anderson localization for a two-dimensional rotor, Phys. Rev. Lett. 60 (1988) 867–870, <http://dx.doi.org/10.1103/PhysRevLett.60.867>, URL <https://link.aps.org/doi/10.1103/PhysRevLett.60.867>.
- [389] J. Wang, A.M. Garcí a, Anderson transition in a three-dimensional kicked rotor, Phys. Rev. E 79 (2009) 036206, <http://dx.doi.org/10.1103/PhysRevE.79.036206>, URL <https://link.aps.org/doi/10.1103/PhysRevE.79.036206>.
- [390] S. Notarnicola, F. Iemini, D. Rossini, R. Fazio, A. Silva, A. Russomanno, From localization to anomalous diffusion in the dynamics of coupled kicked rotors, Phys. Rev. E 97 (2018) 022202, <http://dx.doi.org/10.1103/PhysRevE.97.022202>, URL <https://link.aps.org/doi/10.1103/PhysRevE.97.022202>.
- [391] A. Rajak, I. Dana, Stability, isolated chaos, and superdiffusion in nonequilibrium many-body interacting systems, Phys. Rev. E 102 (2020) 062120, <http://dx.doi.org/10.1103/PhysRevE.102.062120>, URL <https://link.aps.org/doi/10.1103/PhysRevE.102.062120>.
- [392] M. Richter, S. Lange, A. Bäcker, R. Ketzmerick, Visualization and comparison of classical structures and quantum states of four-dimensional maps, Phys. Rev. E 89 (2014) 022902, <http://dx.doi.org/10.1103/PhysRevE.89.022902>, URL <https://link.aps.org/doi/10.1103/PhysRevE.89.022902>.
- [393] S. Lange, M. Richter, F. Onken, A. Bäcker, R. Ketzmerick, Global structure of regular tori in a generic 4D symplectic map, Chaos 24 (2) (2014) 024409, <http://dx.doi.org/10.1063/1.4882163>.
- [394] E. Abrahams, P.W. Anderson, D.C. Licciardello, T.V. Ramakrishnan, Scaling theory of localization: Absence of quantum diffusion in two dimensions, Phys. Rev. Lett. 42 (1979) 673–676, <http://dx.doi.org/10.1103/PhysRevLett.42.673>, URL <https://link.aps.org/doi/10.1103/PhysRevLett.42.673>.
- [395] I. Manai, J.-F. Clément, R. Chicireanu, C. Hainaut, J.C. Garreau, P. Sriftgiser, D. Delande, Experimental observation of two-dimensional Anderson localization with the atomic kicked rotor, Phys. Rev. Lett. 115 (2015) 240603, <http://dx.doi.org/10.1103/PhysRevLett.115.240603>, URL <https://link.aps.org/doi/10.1103/PhysRevLett.115.240603>.
- [396] J. Chabé, H. Lignier, H. Cavalcante, D. Delande, P. Sriftgiser, J.C. Garreau, Quantum scaling laws in the onset of dynamical delocalization, Phys. Rev. Lett. 97 (2006) 264101, <http://dx.doi.org/10.1103/PhysRevLett.97.264101>, URL <https://link.aps.org/doi/10.1103/PhysRevLett.97.264101>.
- [397] E. Cuevas, Critical spectral statistics in two-dimensional interacting disordered systems, Phys. Rev. Lett. 83 (1999) 140–143, <http://dx.doi.org/10.1103/PhysRevLett.83.140>, URL <https://link.aps.org/doi/10.1103/PhysRevLett.83.140>.
- [398] M. Schreiber, H. Grussbach, Multifractal wave functions at the Anderson transition, Phys. Rev. Lett. 67 (1991) 607–610, <http://dx.doi.org/10.1103/PhysRevLett.67.607>, URL <https://link.aps.org/doi/10.1103/PhysRevLett.67.607>.
- [399] M. Schreiber, H. Grussbach, Dimensionality dependence of the metal-insulator transition in the Anderson model of localization, Phys. Rev. Lett. 76 (1996) 1687–1690, <http://dx.doi.org/10.1103/PhysRevLett.76.1687>, URL <https://link.aps.org/doi/10.1103/PhysRevLett.76.1687>.
- [400] A.M. Garcí a, E. Cuevas, Dimensional dependence of the metal-insulator transition, Phys. Rev. B 75 (2007) 174203, <http://dx.doi.org/10.1103/PhysRevB.75.174203>, URL <https://link.aps.org/doi/10.1103/PhysRevB.75.174203>.
- [401] G. Casati, I. Guarneri, D.L. Shepelyansky, Anderson transition in a one-dimensional system with three incommensurate frequencies, Phys. Rev. Lett. 62 (1989) 345–348, <http://dx.doi.org/10.1103/PhysRevLett.62.345>, URL <https://link.aps.org/doi/10.1103/PhysRevLett.62.345>.
- [402] D.M. Basko, M.A. Skvortsov, V.E. Kravtsov, Dynamic localization in quantum dots: Analytical theory, Phys. Rev. Lett. 90 (2003) 096801, <http://dx.doi.org/10.1103/PhysRevLett.90.096801>, URL <https://link.aps.org/doi/10.1103/PhysRevLett.90.096801>.
- [403] G. Lemarié, B. Grémaud, D. Delande, Universality of the Anderson transition with the quasiperiodic kicked rotor, Europhys. Lett. 87 (3) (2009) 37007, <http://dx.doi.org/10.1209/0295-5075/87/37007>.
- [404] G. Lemarié, J. Chabé, P. Sriftgiser, J.C. Garreau, B. Grémaud, D. Delande, Observation of the Anderson metal-insulator transition with atomic matter waves: Theory and experiment, Phys. Rev. A 80 (2009) 043626, <http://dx.doi.org/10.1103/PhysRevA.80.043626>, URL <https://link.aps.org/doi/10.1103/PhysRevA.80.043626>.
- [405] G. Lemarié, D. Delande, J.C. Garreau, P. Sriftgiser, Classical diffusive dynamics for the quasiperiodic kicked rotor, J. Modern Opt. 57 (19) (2010) 1922–1927, <http://dx.doi.org/10.1080/09500340.2010.506009>.

- [406] J. Chabé, G. Lemarié, B. Grémaud, D. Delande, P. Sriftgiser, J.C. Garreau, Experimental observation of the Anderson metal-insulator transition with atomic matter waves, *Phys. Rev. Lett.* 101 (2008) 255702, <http://dx.doi.org/10.1103/PhysRevLett.101.255702>, URL <https://link.aps.org/doi/10.1103/PhysRevLett.101.255702>.
- [407] F. Wegner, Inverse participation ratio in $2+\epsilon$ dimensions, *Zeitschrift Für Physik B Condensed Matter* 36 (3) (1980) 209–214, <http://dx.doi.org/10.1007/BF01325284>.
- [408] J.L. Pichard, G. Sarma, Finite size scaling approach to Anderson localisation, *J. Phys. C: Solid State Phys.* 14 (6) (1981) L127–L132, <http://dx.doi.org/10.1088/0022-3719/14/6/003>.
- [409] T. Ohtsuki, T. Kawarabayashi, Anomalous diffusion at the Anderson transitions, *J. Phys. Soc. Japan* 66 (2) (1997) 314–317, <http://dx.doi.org/10.1143/JPSJ.66.314>.
- [410] J. Cardy, Scaling And Renormalization In Statistical Physics, in: Cambridge Lecture Notes in Physics, Cambridge University Press, 1996, <http://dx.doi.org/10.1017/CBO9781316036440>.
- [411] A. MacKinnon, Critical exponents for the metal-insulator transition, *J. Phys.: Condens. Matter.* 6 (13) (1994) 2511–2518, <http://dx.doi.org/10.1088/0953-8984/6/13/012>.
- [412] K. Slevin, T. Ohtsuki, Critical exponent for the Anderson transition in the three-dimensional orthogonal universality class, *New J. Phys.* 16 (1) (2014) 015012, <http://dx.doi.org/10.1088/1367-2630/16/1/015012>.
- [413] K. Slevin, T. Ohtsuki, Critical exponent of the Anderson transition using massively parallel supercomputing, *J. Phys. Soc. Japan* 87 (9) (2018) 094703, <http://dx.doi.org/10.7566/JPSJ.87.094703>.
- [414] M. Lopez, J.-F. Clément, P. Sriftgiser, J.C. Garreau, D. Delande, Experimental test of universality of the Anderson transition, *Phys. Rev. Lett.* 108 (2012) 095701, <http://dx.doi.org/10.1103/PhysRevLett.108.095701>, URL <https://link.aps.org/doi/10.1103/PhysRevLett.108.095701>.
- [415] C.E. Creffield, G. Hur, T.S. Monteiro, Localization-delocalization transition in a system of quantum kicked rotors, *Phys. Rev. Lett.* 96 (2006) 024103, <http://dx.doi.org/10.1103/PhysRevLett.96.024103>, URL <https://link.aps.org/doi/10.1103/PhysRevLett.96.024103>.
- [416] C. Tian, A. Altland, M. Garst, Theory of the Anderson transition in the quasiperiodic kicked rotor, *Phys. Rev. Lett.* 107 (2011) 074101, <http://dx.doi.org/10.1103/PhysRevLett.107.074101>, URL <https://link.aps.org/doi/10.1103/PhysRevLett.107.074101>.
- [417] J. Wang, C. Tian, A. Altland, Unconventional quantum criticality in the kicked rotor, *Phys. Rev. B* 89 (2014) 195105, <http://dx.doi.org/10.1103/PhysRevB.89.195105>, URL <https://link.aps.org/doi/10.1103/PhysRevB.89.195105>.
- [418] C. Castellani, L. Peliti, Multifractal wavefunction at the localisation threshold, *J. Phys. A: Math. Gen.* 19 (8) (1986) L429–L432, <http://dx.doi.org/10.1088/0305-4470/19/8/004>.
- [419] B.B. Mandelbrot, Intermittent turbulence in self-similar cascades: divergence of high moments and dimension of the carrier, *J. Fluid Mech.* 62 (2) (1974) 331–358, <http://dx.doi.org/10.1017/S0022112074000711>.
- [420] H.E. Stanley, P. Meakin, Multifractal phenomena in physics and chemistry, *Nature* 335 (6189) (1988) 405–409, <http://dx.doi.org/10.1038/335405a0>.
- [421] B.B. Mandelbrot, *Multifractal measures, especially for the geophysicist*, in: *Fractals In Geophysics*, Springer, 1989, pp. 5–42.
- [422] J.W. Kantelhardt, S.A. Zschiegner, E. Koscielny-Bunde, S. Havlin, A. Bunde, H. Stanley, Multifractal detrended fluctuation analysis of nonstationary time series, *Phys. A* 316 (1) (2002) 87–114, [http://dx.doi.org/10.1016/S0378-4371\(02\)01383-3](http://dx.doi.org/10.1016/S0378-4371(02)01383-3), URL <http://www.sciencedirect.com/science/article/pii/S0378437102013833>.
- [423] J. Martin, I. García-Mata, O. Giraud, B. Georgeot, Multifractal wave functions of simple quantum maps, *Phys. Rev. E* 82 (2010) 046206, <http://dx.doi.org/10.1103/PhysRevE.82.046206>, URL <https://link.aps.org/doi/10.1103/PhysRevE.82.046206>.
- [424] V.N. Prigodin, B.L. Altshuler, Long-range spatial correlations of eigenfunctions in quantum disordered systems, *Phys. Rev. Lett.* 80 (1998) 1944–1947, <http://dx.doi.org/10.1103/PhysRevLett.80.1944>, URL <https://link.aps.org/doi/10.1103/PhysRevLett.80.1944>.
- [425] F. Evers, A.D. Mirlin, Fluctuations of the inverse participation ratio at the Anderson transition, *Phys. Rev. Lett.* 84 (2000) 3690–3693, <http://dx.doi.org/10.1103/PhysRevLett.84.3690>, URL <https://link.aps.org/doi/10.1103/PhysRevLett.84.3690>.
- [426] P. Akridas-Morel, N. Cherreton, D. Delande, Multifractality of the kicked rotor at the critical point of the Anderson transition, *Phys. Rev. A* 100 (2019) 043612, <http://dx.doi.org/10.1103/PhysRevA.100.043612>, URL <https://link.aps.org/doi/10.1103/PhysRevA.100.043612>.
- [427] A.M. Garcí a Garcí a, J. Wang, Semi-Poisson statistics in quantum chaos, *Phys. Rev. E* 73 (2006) 036210, <http://dx.doi.org/10.1103/PhysRevE.73.036210>, URL <https://link.aps.org/doi/10.1103/PhysRevE.73.036210>.
- [428] S. Paul, M.S. Santhanam, Floquet states of a kicked particle in a singular potential: Exponential and power-law profiles, *Phys. Rev. E* 97 (2018) 032217, <http://dx.doi.org/10.1103/PhysRevE.97.032217>, URL <https://link.aps.org/doi/10.1103/PhysRevE.97.032217>.
- [429] R. Dutta, P. Shukla, Criticality in the quantum kicked rotor with a smooth potential, *Phys. Rev. E* 78 (2008) 031115, <http://dx.doi.org/10.1103/PhysRevE.78.031115>, URL <https://link.aps.org/doi/10.1103/PhysRevE.78.031115>.
- [430] J. Martin, O. Giraud, B. Georgeot, Multifractality and intermediate statistics in quantum maps, *Phys. Rev. E* 77 (2008) 035201, <http://dx.doi.org/10.1103/PhysRevE.77.035201>, URL <https://link.aps.org/doi/10.1103/PhysRevE.77.035201>.
- [431] A.M. Bilen, I. García-Mata, B. Georgeot, O. Giraud, Multifractality of open quantum systems, *Phys. Rev. E* 100 (2019) 032223, <http://dx.doi.org/10.1103/PhysRevE.100.032223>, URL <https://link.aps.org/doi/10.1103/PhysRevE.100.032223>.
- [432] R. Ketzmerick, Fractal conductance fluctuations in generic chaotic cavities, *Phys. Rev. B* 54 (1996) 10841–10844, <http://dx.doi.org/10.1103/PhysRevB.54.10841>, URL <https://link.aps.org/doi/10.1103/PhysRevB.54.10841>.
- [433] G. Casati, G. Maspero, D.L. Shepelyansky, Quantum Poincaré recurrences, *Phys. Rev. Lett.* 82 (1999) 524–527, <http://dx.doi.org/10.1103/PhysRevLett.82.524>, URL <https://link.aps.org/doi/10.1103/PhysRevLett.82.524>.
- [434] G. Benenti, G. Casati, I. Guarneri, M. Terraneo, Quantum fractal fluctuations, *Phys. Rev. Lett.* 87 (2001) 014101, <http://dx.doi.org/10.1103/PhysRevLett.87.014101>.
- [435] A. Facchini, S. Wimberger, A. Tomadin, Multifractal fluctuations in the survival probability of an open quantum system, *Phys. A* 376 (2007) 266–274, <http://dx.doi.org/10.1016/j.physa.2006.10.012>, URL <http://www.sciencedirect.com/science/article/pii/S0378437106010582>.
- [436] A. Tomadin, R. Mannella, S. Wimberger, Can quantum fractal fluctuations be observed in an atom-optics kicked rotor experiment? *J. Phys. A: Math. Gen.* 39 (10) (2006) 2477–2491, <http://dx.doi.org/10.1088/0305-4470/39/10/015>.
- [437] E. Persson, S. Fürtbauer, S. Wimberger, J. Burgdörfer, Transient localization in the kicked rydberg atom, *Phys. Rev. A* 74 (2006) 053417, <http://dx.doi.org/10.1103/PhysRevA.74.053417>, URL <https://link.aps.org/doi/10.1103/PhysRevA.74.053417>.
- [438] H. Stupp, M. Hornung, M. Lakner, O. Madel, H.v. Löhneysen, Possible solution of the conductivity exponent puzzle for the metal-insulator transition in heavily doped uncompensated semiconductors, *Phys. Rev. Lett.* 71 (1993) 2634–2637, <http://dx.doi.org/10.1103/PhysRevLett.71.2634>, URL <https://link.aps.org/doi/10.1103/PhysRevLett.71.2634>.
- [439] M.E. Gershenson, Y.B. Khavin, A.G. Mikhalchuk, H.M. Bozler, A.L. Bogdanov, Crossover from weak to strong localization in quasi-one-dimensional conductors, *Phys. Rev. Lett.* 79 (1997) 725–728, <http://dx.doi.org/10.1103/PhysRevLett.79.725>, URL <https://link.aps.org/doi/10.1103/PhysRevLett.79.725>.
- [440] S. Waffenschmidt, C. Pfleiderer, H.v. Löhneysen, Critical behavior of the conductivity of Si:P at the metal-insulator transition under uniaxial stress, *Phys. Rev. Lett.* 83 (1999) 3005–3008, <http://dx.doi.org/10.1103/PhysRevLett.83.3005>, URL <https://link.aps.org/doi/10.1103/PhysRevLett.83.3005>.
- [441] A. Lagendijk, B. van Tiggelen, D.S. Wiersma, Fifty years of Anderson localization, *Phys. Today* 62 (2009) 24, <http://dx.doi.org/10.1063/1.3206091>.

- [442] M. Wang, A. Debernardi, W. Zhang, C. Xu, Y. Yuan, Y. Xie, Y. Berencén, S. Prucnal, M. Helm, S. Zhou, Critical behavior of the insulator-to-metal transition in Te-hyperdoped Si, Phys. Rev. B 102 (2020) 085204, <http://dx.doi.org/10.1103/PhysRevB.102.085204>, URL <https://link.aps.org/doi/10.1103/PhysRevB.102.085204>.
- [443] E.J. Meier, F.A. An, A. Dauphin, M. Maffei, P. Massignan, T.L. Hughes, B. Gadway, Observation of the topological Anderson insulator in disordered atomic wires, Science 362 (6417) (2018) 929–933, <http://dx.doi.org/10.1126/science.aat3406>, URL <https://science.scienmag.org/content/362/6417/929>.
- [444] W. Hofstetter, T. Qin, Quantum simulation of strongly correlated condensed matter systems, J. Phys. B: At. Mol. Opt. Phys. 51 (8) (2018) 082001, <http://dx.doi.org/10.1088/1361-6455/aaa31b>.
- [445] J.-C. Garreau, Quantum simulation of disordered systems with cold atoms, Comptes Rendus Physique 18 (1) (2017) 31–46, <http://dx.doi.org/10.1016/j.crhy.2016.09.002>, Prizes of the French Academy of Sciences 2015 / Prix de l’Académie des sciences 2015, URL <http://www.sciencedirect.com/science/article/pii/S1631070516301426>.
- [446] C.-C. Chien, S. Peotta, M. Di Ventra, Quantum transport in ultracold atoms, Nat. Phys. 11 (12) (2015) 998–1004.
- [447] P. Sriftgiser, H. Lignier, J. Ringot, J.C. Garreau, D. Delande, Experimental study of quantum chaos with cold atoms, Commun. Nonlinear Sci. Numer. Simul. 8 (3) (2003) 301–313, [http://dx.doi.org/10.1016/S1007-5704\(03\)00031-5](http://dx.doi.org/10.1016/S1007-5704(03)00031-5), Chaotic transport and compexity in classical and quantum dynamics, URL <http://www.sciencedirect.com/science/article/pii/S1007570403000315>.
- [448] J. Ringot, P. Sriftgiser, J.C. Garreau, Subrecoil Raman spectroscopy of cold cesium atoms, Phys. Rev. A 65 (2001) 013403, <http://dx.doi.org/10.1103/PhysRevA.65.013403>, URL <https://link.aps.org/doi/10.1103/PhysRevA.65.013403>.
- [449] G.A. Domínguez-Castro, R. Paredes, The Aubry–André model as a hobbyhorse for understanding the localization phenomenon, Eur. J. Phys. 40 (4) (2019) 045403, <http://dx.doi.org/10.1088/1361-6404/ab1670>.
- [450] G. Roati, C. D’Errico, L. Fallani, M. Fattori, C. Fort, M. Zaccanti, G. Modugno, M. Modugno, M. Inguscio, Anderson localization of a non-interacting Bose–Einstein condensate, Nature 453 (7197) (2008) 895–898, <http://dx.doi.org/10.1038/nature07071>.
- [451] X. Li, X. Li, S. Das Sarma, Mobility edges in one-dimensional bichromatic incommensurate potentials, Phys. Rev. B 96 (2017) 085119, <http://dx.doi.org/10.1103/PhysRevB.96.085119>, URL <https://link.aps.org/doi/10.1103/PhysRevB.96.085119>.
- [452] H.P. Lüschen, S. Scherg, T. Kohlert, M. Schreiber, P. Bordia, X. Li, S. Das Sarma, I. Bloch, Single-particle mobility edge in a one-dimensional quasiperiodic optical lattice, Phys. Rev. Lett. 120 (2018) 160404, <http://dx.doi.org/10.1103/PhysRevLett.120.160404>, URL <https://link.aps.org/doi/10.1103/PhysRevLett.120.160404>.
- [453] P. Qin, C. Yin, S. Chen, Dynamical Anderson transition in one-dimensional periodically kicked incommensurate lattices, Phys. Rev. B 90 (2014) 054303, <http://dx.doi.org/10.1103/PhysRevB.90.054303>, URL <https://link.aps.org/doi/10.1103/PhysRevB.90.054303>.
- [454] T. Čadež, R. Mondaini, P.D. Sacramento, Dynamical localization and the effects of aperiodicity in Floquet systems, Phys. Rev. B 96 (2017) 144301, <http://dx.doi.org/10.1103/PhysRevB.96.144301>, URL <https://link.aps.org/doi/10.1103/PhysRevB.96.144301>.
- [455] V. Ravindranath, M.S. Santhanam, Dynamical transitions in aperiodically kicked tight-binding models, Phys. Rev. B 103 (2021) 134303, <http://dx.doi.org/10.1103/PhysRevB.103.134303>, URL <https://link.aps.org/doi/10.1103/PhysRevB.103.134303>.
- [456] Y. Chen, C. Tian, Planck’s quantum-driven integer quantum Hall effect in chaos, Phys. Rev. Lett. 113 (2014) 216802, <http://dx.doi.org/10.1103/PhysRevLett.113.216802>, URL <https://link.aps.org/doi/10.1103/PhysRevLett.113.216802>.
- [457] J. Avron, D. Osadchy, R. Seiler, A topological look at the quantum hall effect, Phys. Today 56 (2003) 38, <http://dx.doi.org/10.1063/1.1611351>, URL <https://physicstoday.scitation.org/doi/10.1063/1.1611351>.
- [458] C. Rylands, E.B. Rozenbaum, V. Galitski, R. Konik, Many-body dynamical localization in a kicked Lieb–Liniger gas, Phys. Rev. Lett. 124 (2020) 155302, <http://dx.doi.org/10.1103/PhysRevLett.124.155302>, URL <https://link.aps.org/doi/10.1103/PhysRevLett.124.155302>.
- [459] M. Berry, Incommensurability in an exactly-soluble quantal and classical model for a kicked rotator, Physica D 10 (3) (1984) 369–378, [http://dx.doi.org/10.1016/0167-2789\(84\)90185-4](http://dx.doi.org/10.1016/0167-2789(84)90185-4), URL <http://www.sciencedirect.com/science/article/pii/0167278984901854>.
- [460] A.C. Keser, S. Ganeshan, G. Refael, V. Galitski, Dynamical many-body localization in an integrable model, Phys. Rev. B 94 (2016) 085120, <http://dx.doi.org/10.1103/PhysRevB.94.085120>, URL <https://link.aps.org/doi/10.1103/PhysRevB.94.085120>.
- [461] E.B. Rozenbaum, V. Galitski, Dynamical localization of coupled relativistic kicked rotors, Phys. Rev. B 95 (2017) 064303, <http://dx.doi.org/10.1103/PhysRevB.95.064303>, URL <https://link.aps.org/doi/10.1103/PhysRevB.95.064303>.
- [462] B. Toloui, L.E. Ballentine, Quantum localization for two coupled kicked rotors, 2009, <arXiv:0903.4632>.
- [463] S. Adachi, M. Toda, K. Ikeda, Quantum-classical correspondence in many-dimensional quantum chaos, Phys. Rev. Lett. 61 (1988) 659–661, <http://dx.doi.org/10.1103/PhysRevLett.61.659>, URL <https://link.aps.org/doi/10.1103/PhysRevLett.61.659>.
- [464] S. Nag, G. Ghosh, A. Lahiri, Quantum chaos: Reduced density matrix fluctuations in coupled systems, Physica D 204 (1–2) (2005) 110–121, <http://dx.doi.org/10.1016/j.physd.2005.04.008>, URL <https://ui.adsabs.harvard.edu/abs/2005PhyD..204..110N>.
- [465] B. Gadway, J. Reeves, L. Krinner, D. Schneble, Evidence for a quantum-to-classical transition in a pair of coupled quantum rotors, Phys. Rev. Lett. 110 (2013) 190401, <http://dx.doi.org/10.1103/PhysRevLett.110.190401>, URL <https://link.aps.org/doi/10.1103/PhysRevLett.110.190401>.
- [466] K. Kaneko, T. Konishi, Diffusion in Hamiltonian dynamical systems with many degrees of freedom, Phys. Rev. A 40 (1989) 6130–6133, <http://dx.doi.org/10.1103/PhysRevA.40.6130>, URL <https://link.aps.org/doi/10.1103/PhysRevA.40.6130>.
- [467] T. Konishi, K. Kaneko, Diffusion in Hamiltonian chaos and its size dependence, J. Phys. A: Math. Gen. 23 (15) (1990) L715–L720, <http://dx.doi.org/10.1088/0305-4470/23/15/004>.
- [468] B. Chirikov, V. Vecheslavov, Theory of fast Arnold diffusion in many-frequency systems, J. Stat. Phys. 71 (1) (1993) 243–258, <http://dx.doi.org/10.1007/BF01048098>.
- [469] A. Russomanno, M. Fava, R. Fazio, Chaos and subdiffusion in infinite-range coupled quantum kicked rotors, Phys. Rev. B 103 (2021) 224301, <http://dx.doi.org/10.1103/PhysRevB.103.224301>, URL <https://link.aps.org/doi/10.1103/PhysRevB.103.224301>.
- [470] F. Onken, S. Lange, R. Ketzmerick, A. Bäcker, Bifurcations of families of 1D-tori in 4D symplectic maps, Chaos 26 (6) (2016) 063124, <http://dx.doi.org/10.1063/1.4954024>.
- [471] S. Paul, A. Bäcker, Linear and logarithmic entanglement production in an interacting chaotic system, Phys. Rev. E 102 (2020) 050102, <http://dx.doi.org/10.1103/PhysRevE.102.050102>, URL <https://link.aps.org/doi/10.1103/PhysRevE.102.050102>.
- [472] S. Notaricola, A. Silva, R. Fazio, A. Russomanno, Slow heating in a quantum coupled kicked rotors system, J. Stat. Mech. Theory Exp. 2020 (2) (2020) 024008, <http://dx.doi.org/10.1088/1742-5468/ab6de4>.
- [473] S. Adachi, M. Toda, K. Ikeda, Quantum-classical correspondence in many-dimensional quantum chaos, Phys. Rev. Lett. 61 (1988) 659–661, <http://dx.doi.org/10.1103/PhysRevLett.61.659>, URL <https://link.aps.org/doi/10.1103/PhysRevLett.61.659>.
- [474] A. Marino, G. Torre, R. Citro, Dynamical localization of interacting ultracold atomic kicked rotors, Europhys. Lett. 127 (5) (2019) 50008, <http://dx.doi.org/10.1209/0295-5075/127/50008>.
- [475] A. Rajak, I. Dana, E.G. Dalla Torre, Characterizations of prethermal states in periodically driven many-body systems with unbounded chaotic diffusion, Phys. Rev. B 100 (2019) 100302, <http://dx.doi.org/10.1103/PhysRevB.100.100302>, URL <https://link.aps.org/doi/10.1103/PhysRevB.100.100302>.
- [476] R. Schack, G. D’Ariano, C.M. Caves, Hypersensitivity to perturbation in the quantum kicked top, Phys. Rev. E 50 (1994) 972–987, <http://dx.doi.org/10.1103/PhysRevE.50.972>, URL <https://link.aps.org/doi/10.1103/PhysRevE.50.972>.
- [477] M.A. Nielsen, I.L. Chuang, Quantum Computation And Quantum Information, Cambridge University Press, Cambridge, 2010.

- [478] C.H. Bennett, D.P. DiVincenzo, Quantum information and computation, *Nature* 404 (2000) 247–255, <http://dx.doi.org/10.1038/35005001>.
- [479] R. Horodecki, P. Horodecki, M. Horodecki, K. Horodecki, Quantum entanglement, *Rev. Modern Phys.* 81 (2009) 865–942, <http://dx.doi.org/10.1103/RevModPhys.81.865>, URL <https://link.aps.org/doi/10.1103/RevModPhys.81.865>.
- [480] A. Rényi, On measures of entropy and information, in: *Proceedings Of The Fourth Berkeley Symposium On Mathematical Statistics And Probability, Volume 1: Contributions To The Theory Of Statistics*, University of California Press, 1961, pp. 547–561.
- [481] C. Tsallis, Possible generalization of Boltzmann-Gibbs statistics, *J. Stat. Phys.* 52 (1) (1988) 479–487, <http://dx.doi.org/10.1007/BF01016429>.
- [482] W.H. Zurek, J.P. Paz, Decoherence, chaos, and the second law, *Phys. Rev. Lett.* 72 (1994) 2508–2511, <http://dx.doi.org/10.1103/PhysRevLett.72.2508>, URL <https://link.aps.org/doi/10.1103/PhysRevLett.72.2508>.
- [483] P.A. Miller, S. Sarkar, Signatures of chaos in the entanglement of two coupled quantum kicked tops, *Phys. Rev. E* 60 (1999) 1542–1550, <http://dx.doi.org/10.1103/PhysRevE.60.1542>, URL <https://link.aps.org/doi/10.1103/PhysRevE.60.1542>.
- [484] J.N. Bandyopadhyay, A. Lakshminarayan, Entanglement production in coupled chaotic systems: Case of the kicked tops, *Phys. Rev. E* 69 (2004) 016201, <http://dx.doi.org/10.1103/PhysRevE.69.016201>, URL <https://link.aps.org/doi/10.1103/PhysRevE.69.016201>.
- [485] H. Fujisaki, T. Miyadera, A. Tanaka, Dynamical aspects of quantum entanglement for weakly coupled kicked tops, *Phys. Rev. E* 67 (2003) 066201, <http://dx.doi.org/10.1103/PhysRevE.67.066201>, URL <https://link.aps.org/doi/10.1103/PhysRevE.67.066201>.
- [486] A. Lerose, S. Pappalardi, Bridging entanglement dynamics and chaos in semiclassical systems, *Phys. Rev. A* 102 (2020) 032404, <http://dx.doi.org/10.1103/PhysRevA.102.032404>, URL <https://link.aps.org/doi/10.1103/PhysRevA.102.032404>.
- [487] J.B. Ruebeck, J. Lin, A.K. Pattanayak, Entanglement and its relationship to classical dynamics, *Phys. Rev. E* 95 (2017) 062222, <http://dx.doi.org/10.1103/PhysRevE.95.062222>, URL <https://link.aps.org/doi/10.1103/PhysRevE.95.062222>.
- [488] U.T. Bhosale, M.S. Santhanam, Periodicity of quantum correlations in the quantum kicked top, *Phys. Rev. E* 98 (2018) 052228, <http://dx.doi.org/10.1103/PhysRevE.98.052228>, URL <https://link.aps.org/doi/10.1103/PhysRevE.98.052228>.
- [489] K. Takahashi, Wigner and Husimi functions in quantum mechanics, *J. Phys. Soc. Japan* 55 (3) (1986) 762–779, <http://dx.doi.org/10.1143/JPSJ.55.762>.
- [490] A. Tanaka, H. Fujisaki, T. Miyadera, Saturation of the production of quantum entanglement between weakly coupled mapping systems in a strongly chaotic region, *Phys. Rev. E* 66 (2002) 045201, <http://dx.doi.org/10.1103/PhysRevE.66.045201>, URL <https://link.aps.org/doi/10.1103/PhysRevE.66.045201>.
- [491] C. Neill, P. Roushan, M. Fang, Y. Chen, M. Kolodrubetz, Z. Chen, A. Megrant, R. Barends, B. Campbell, B. Chiaro, et al., Ergodic dynamics and thermalization in an isolated quantum system, *Nat. Phys.* 12 (11) (2016) 1037–1041, <http://dx.doi.org/10.1038/nphys3830>.
- [492] V.R. Krithika, V.S. Anjusha, U.T. Bhosale, T.S. Mahesh, NMR studies of quantum chaos in a two-qubit kicked top, *Phys. Rev. E* 99 (2019) 032219, <http://dx.doi.org/10.1103/PhysRevE.99.032219>, URL <https://link.aps.org/doi/10.1103/PhysRevE.99.032219>.
- [493] V. Madhok, S. Dogra, A. Lakshminarayan, Quantum correlations as probes of chaos and ergodicity, *Opt. Commun.* 420 (2018) 189–193, <http://dx.doi.org/10.1016/j.optcom.2018.03.069>, URL <http://www.sciencedirect.com/science/article/pii/S0030401818302542>.
- [494] P.A. Miller, S. Sarkar, Entropy production, dynamical localization and criteria for quantum chaos in the open quantum kicked rotor, *Nonlinearity* 12 (2) (1999) 419–442, <http://dx.doi.org/10.1088/0951-7715/12/2/016>.
- [495] S. Nag, A. Lahiri, G. Ghosh, Entropy production due to coupling to a heat bath in the kicked rotor problem, *Phys. Lett. A* 292 (1) (2001) 43–48, [http://dx.doi.org/10.1016/S0375-9601\(01\)00746-0](http://dx.doi.org/10.1016/S0375-9601(01)00746-0), URL <http://www.sciencedirect.com/science/article/pii/S0375960101007460>.
- [496] A. Lakshminarayan, Entangling power of quantized chaotic systems, *Phys. Rev. E* 64 (2001) 036207, <http://dx.doi.org/10.1103/PhysRevE.64.036207>, URL <https://link.aps.org/doi/10.1103/PhysRevE.64.036207>.
- [497] H. Fujisaki, A. Tanaka, T. Miyadera, Dynamical aspects of quantum entanglement for coupled mapping systems, *J. Phys. Soc. Japan* 72 (Suppl. C) (2003) 111–114, <http://dx.doi.org/10.1143/JPSJ.72SC.111>.
- [498] A.M. Sengupta, P.P. Mitra, Distributions of singular values for some random matrices, *Phys. Rev. E* 60 (1999) 3389–3392, <http://dx.doi.org/10.1103/PhysRevE.60.3389>, URL <https://link.aps.org/doi/10.1103/PhysRevE.60.3389>.
- [499] J.N. Bandyopadhyay, A. Lakshminarayan, Testing statistical bounds on entanglement using quantum chaos, *Phys. Rev. Lett.* 89 (2002) 060402, <http://dx.doi.org/10.1103/PhysRevLett.89.060402>, URL <https://link.aps.org/doi/10.1103/PhysRevLett.89.060402>.
- [500] M.S. Santhanam, V.B. Sheorey, A. Lakshminarayan, Effect of classical bifurcations on the quantum entanglement of two coupled quartic oscillators, *Phys. Rev. E* 77 (2008) 026213, <http://dx.doi.org/10.1103/PhysRevE.77.026213>, URL <https://link.aps.org/doi/10.1103/PhysRevE.77.026213>.
- [501] N.N. Chung, L.Y. Chew, Dependence of entanglement dynamics on the global classical dynamical regime, *Phys. Rev. E* 80 (2009) 016204, <http://dx.doi.org/10.1103/PhysRevE.80.016204>, URL <https://link.aps.org/doi/10.1103/PhysRevE.80.016204>.
- [502] U.T. Bhosale, M.S. Santhanam, Signatures of bifurcation on quantum correlations: Case of the quantum kicked top, *Phys. Rev. E* 95 (2017) 012216, <http://dx.doi.org/10.1103/PhysRevE.95.012216>, URL <https://link.aps.org/doi/10.1103/PhysRevE.95.012216>.
- [503] G. Stamatou, D.P. Ghikas, Quantum entanglement dependence on bifurcations and scars in non-autonomous systems. The case of quantum kicked top, *Phys. Lett. A* 368 (3) (2007) 206–214, <http://dx.doi.org/10.1016/j.physleta.2007.04.003>, URL <http://www.sciencedirect.com/science/article/pii/S0375960107005166>.
- [504] Y. Huang, Universal eigenstate entanglement of chaotic local Hamiltonians, *Nuclear Phys. B* 938 (2019) 594–604, <http://dx.doi.org/10.1016/j.nuclphysb.2018.09.013>, URL <http://www.sciencedirect.com/science/article/pii/S0550321318302608>.
- [505] S.C.L. Srivastava, S. Tomsovic, A. Lakshminarayan, R. Ketzmerick, A. Bäcker, Universal scaling of spectral fluctuation transitions for interacting chaotic systems, *Phys. Rev. Lett.* 116 (2016) 054101, <http://dx.doi.org/10.1103/PhysRevLett.116.054101>, URL <https://link.aps.org/doi/10.1103/PhysRevLett.116.054101>.
- [506] A. Lakshminarayan, S.C.L. Srivastava, R. Ketzmerick, A. Bäcker, S. Tomsovic, Entanglement and localization transitions in eigenstates of interacting chaotic systems, *Phys. Rev. E* 94 (2016) 010205, <http://dx.doi.org/10.1103/PhysRevE.94.010205>, URL <https://link.aps.org/doi/10.1103/PhysRevE.94.010205>.
- [507] S. Tomsovic, A. Lakshminarayan, S.C.L. Srivastava, A. Bäcker, Eigenstate entanglement between quantum chaotic subsystems: Universal transitions and power laws in the entanglement spectrum, *Phys. Rev. E* 98 (2018) 032209, <http://dx.doi.org/10.1103/PhysRevE.98.032209>, URL <https://link.aps.org/doi/10.1103/PhysRevE.98.032209>.
- [508] T. Herrmann, M.F.I. Kieler, F. Fritzsch, A. Bäcker, Entanglement in coupled kicked tops with chaotic dynamics, *Phys. Rev. E* 101 (2020) 022221, <http://dx.doi.org/10.1103/PhysRevE.101.022221>, URL <https://link.aps.org/doi/10.1103/PhysRevE.101.022221>.
- [509] Y.N.O. A.I. Larkin, Quasiclassical method in the theory of superconductivity, *JETP* 28 (6) (1969) 1200, URL <http://www.jetp.ac.ru/cgi-bin/e/index/e/28/6/p1200?a=list>.
- [510] J. Maldacena, S.H. Shenker, D. Stanford, A bound on chaos, *J. High Energy Phys.* 106 (8) (2016) 1–17, [http://dx.doi.org/10.1007/JHEP08\(2016\)106](http://dx.doi.org/10.1007/JHEP08(2016)106).
- [511] M. Gárttner, J.G. Bohnet, A. Safavi-Naini, M.L. Wall, J.J. Bollinger, A.M. Rey, Measuring out-of-time-order correlations and multiple quantum spectra in a trapped-ion quantum magnet, *Nat. Phys.* 13 (2017) 781–786, <http://dx.doi.org/10.1038/nphys4119>.
- [512] J. Li, R. Fan, H. Wang, B. Ye, B. Zeng, H. Zhai, X. Peng, J. Du, Measuring out-of-time-order correlators on a nuclear magnetic resonance quantum simulator, *Phys. Rev. X* 7 (2017) 031011, <http://dx.doi.org/10.1103/PhysRevX.7.031011>, URL <https://link.aps.org/doi/10.1103/PhysRevX.7.031011>.
- [513] K.X. Wei, C. Ramanathan, P. Cappellaro, Exploring localization in nuclear spin chains, *Phys. Rev. Lett.* 120 (2018) 070501, <http://dx.doi.org/10.1103/PhysRevLett.120.070501>, URL <https://link.aps.org/doi/10.1103/PhysRevLett.120.070501>.

- [514] M. Niknam, L.F. Santos, D.G. Cory, Sensitivity of quantum information to environment perturbations measured with a nonlocal out-of-time-order correlation function, Phys. Rev. Res. 2 (2020) 013200, <http://dx.doi.org/10.1103/PhysRevResearch.2.013200>, URL <https://link.aps.org/doi/10.1103/PhysRevResearch.2.013200>.
- [515] T. Xu, T. Scaffidi, X. Cao, Does scrambling equal chaos? Phys. Rev. Lett. 124 (2020) 140602, <http://dx.doi.org/10.1103/PhysRevLett.124.140602>, URL <https://link.aps.org/doi/10.1103/PhysRevLett.124.140602>.
- [516] M.K. Joshi, A. Elben, B. Vermersch, T. Brydges, C. Maier, P. Zoller, R. Blatt, C.F. Roos, Quantum information scrambling in a trapped-ion quantum simulator with tunable range interactions, Phys. Rev. Lett. 124 (2020) 240505, <http://dx.doi.org/10.1103/PhysRevLett.124.240505>, URL <https://link.aps.org/doi/10.1103/PhysRevLett.124.240505>.
- [517] E.B. Rozenbaum, S. Ganeshan, V. Galitski, Lyapunov exponent and out-of-time-ordered correlator's growth rate in a chaotic system, Phys. Rev. Lett. 118 (2017) 086801, <http://dx.doi.org/10.1103/PhysRevLett.118.086801>, URL <https://link.aps.org/doi/10.1103/PhysRevLett.118.086801>.
- [518] C. Tian, A. Kamenev, A. Larkin, Weak dynamical localization in periodically kicked cold atomic gases, Phys. Rev. Lett. 93 (2004) 124101, <http://dx.doi.org/10.1103/PhysRevLett.93.124101>, URL <https://link.aps.org/doi/10.1103/PhysRevLett.93.124101>.
- [519] I. García-Mata, M. Saraceno, R.A. Jalabert, A.J. Roncaglia, D.A. Wisniacki, Chaos signatures in the short and long time behavior of the out-of-time ordered correlator, Phys. Rev. Lett. 121 (2018) 210601, <http://dx.doi.org/10.1103/PhysRevLett.121.210601>, URL <https://link.aps.org/doi/10.1103/PhysRevLett.121.210601>.
- [520] V.I. Arnold, A. Avez, Ergodic Problems Of Classical Mechanics, in: Advanced book classics, Addison-Wesley, 1989, URL <https://books.google.co.in/books?id=9TxhQgAACAAj>.
- [521] R. Prakash, A. Lakshminarayanan, Scrambling in strongly chaotic weakly coupled bipartite systems: Universality beyond the Ehrenfest timescale, Phys. Rev. B 101 (2020) 121108, <http://dx.doi.org/10.1103/PhysRevB.101.121108>, URL <https://link.aps.org/doi/10.1103/PhysRevB.101.121108>.
- [522] R.P. Feynman, R.B. Leighton, M. Sands, *The feynman lectures on physics; vol. i*, Am. J. Phys. 33 (9) (1965) 750–752.
- [523] R.P. Feynman, R.B. Leighton, M. Sands, *The Feynman Lectures On Physics, Vol. I: The New Millennium Edition: Mainly Mechanics, Radiation, And Heat*, vol. 1, Basic books, 2011.
- [524] J. Bang, R. Pan, T.M. Hoang, J. Ahn, C. Jarzynski, H.T. Quan, T. Li, Experimental realization of Feynman's ratchet, New J. Phys. 20 (10) (2018) 103032, <http://dx.doi.org/10.1088/1367-2630/aae71f>.
- [525] J.M.R. Parrondo, P. Español, Criticism of Feynman's analysis of the ratchet as an engine, Am. J. Phys. 64 (9) (1996) 1125–1130, <http://dx.doi.org/10.1119/1.18393>.
- [526] P. Reimann, Brownian motors: noisy transport far from equilibrium, Phys. Rep. 361 (2) (2002) 57–265, [http://dx.doi.org/10.1016/S0370-1573\(01\)00081-3](http://dx.doi.org/10.1016/S0370-1573(01)00081-3), URL <http://www.sciencedirect.com/science/article/pii/S0370157301000813>.
- [527] P. Hänggi, F. Marchesoni, Artificial Brownian motors: Controlling transport on the nanoscale, Rev. Modern Phys. 81 (2009) 387–442, <http://dx.doi.org/10.1103/RevModPhys.81.387>, URL <https://link.aps.org/doi/10.1103/RevModPhys.81.387>.
- [528] S. Denisov, S. Flach, P. Hänggi, Tunable transport with broken space–time symmetries, Phys. Rep. 538 (3) (2014) 77–120, <http://dx.doi.org/10.1016/j.physrep.2014.01.003>, URL <http://www.sciencedirect.com/science/article/pii/S0370157314000064>.
- [529] S. Flach, O. Yevtushenko, Y. Zolotaryuk, Directed current due to broken time-space symmetry, Phys. Rev. Lett. 84 (2000) 2358–2361, <http://dx.doi.org/10.1103/PhysRevLett.84.2358>, URL <https://link.aps.org/doi/10.1103/PhysRevLett.84.2358>.
- [530] L. Cavallasca, R. Artuso, G. Casati, Directed deterministic classical transport: Symmetry breaking and beyond, Phys. Rev. E 75 (2007) 066213, <http://dx.doi.org/10.1103/PhysRevE.75.066213>, URL <https://link.aps.org/doi/10.1103/PhysRevE.75.066213>.
- [531] G.G. Carlo, G. Benenti, G. Casati, D.L. Shepelyansky, Quantum ratchets in dissipative chaotic systems, Phys. Rev. Lett. 94 (2005) 164101, <http://dx.doi.org/10.1103/PhysRevLett.94.164101>, URL <https://link.aps.org/doi/10.1103/PhysRevLett.94.164101>.
- [532] T. Salger, S. Kling, T. Hecking, C. Geckeler, L. Morales-Molina, M. Weitz, Directed transport of atoms in a Hamiltonian quantum ratchet, Science 326 (5957) (2009) 1241–1243, <http://dx.doi.org/10.1126/science.1179546>, URL <https://science.sciencemag.org/content/326/5957/1241>.
- [533] H. Schanz, M.-F. Otto, R. Ketzmerick, T. Dittrich, Classical and quantum Hamiltonian ratchets, Phys. Rev. Lett. 87 (2001) 070601, <http://dx.doi.org/10.1103/PhysRevLett.87.070601>, URL <https://link.aps.org/doi/10.1103/PhysRevLett.87.070601>.
- [534] L. Wang, G. Benenti, G. Casati, B. Li, Ratchet effect and the transporting islands in the chaotic sea, Phys. Rev. Lett. 99 (2007) 244101, <http://dx.doi.org/10.1103/PhysRevLett.99.244101>, URL <https://link.aps.org/doi/10.1103/PhysRevLett.99.244101>.
- [535] J. Wang, J. Gong, Quantum ratchet accelerator without a bichromatic lattice potential, Phys. Rev. E 78 (2008) 036219, <http://dx.doi.org/10.1103/PhysRevE.78.036219>, URL <https://link.aps.org/doi/10.1103/PhysRevE.78.036219>.
- [536] H. Sambe, Steady states and quasienergies of a quantum-mechanical system in an oscillating field, Phys. Rev. A 7 (1973) 2203–2213, <http://dx.doi.org/10.1103/PhysRevA.7.2203>, URL <https://link.aps.org/doi/10.1103/PhysRevA.7.2203>.
- [537] H. Schanz, T. Dittrich, R. Ketzmerick, Directed chaotic transport in Hamiltonian ratchets, Phys. Rev. E 71 (2005) 026228, <http://dx.doi.org/10.1103/PhysRevE.71.026228>, URL <https://link.aps.org/doi/10.1103/PhysRevE.71.026228>.
- [538] T.S. Monteiro, P.A. Dando, N.A.C. Hutchings, M.R. Isherwood, Proposal for a chaotic ratchet using cold atoms in optical lattices, Phys. Rev. Lett. 89 (2002) 194102, <http://dx.doi.org/10.1103/PhysRevLett.89.194102>, URL <https://link.aps.org/doi/10.1103/PhysRevLett.89.194102>.
- [539] N.A.C. Hutchings, M.R. Isherwood, T. Jonckheere, T.S. Monteiro, Chaotic Hamiltonian ratchets for pulsed periodic double-well potentials: Classical correlations and the ratchet current, Phys. Rev. E 70 (2004) 036205, <http://dx.doi.org/10.1103/PhysRevE.70.036205>, URL <https://link.aps.org/doi/10.1103/PhysRevE.70.036205>.
- [540] P.H. Jones, M. Goonasekera, D.R. Meacher, T. Jonckheere, T.S. Monteiro, Directed motion for delta-kicked atoms with broken symmetries: Comparison between theory and experiment, Phys. Rev. Lett. 98 (2007) 073002, <http://dx.doi.org/10.1103/PhysRevLett.98.073002>, URL <https://link.aps.org/doi/10.1103/PhysRevLett.98.073002>.
- [541] J. Ni, S. Dadras, W.K. Lam, R.K. Shrestha, M. Sadgrove, S. Wimberger, G.S. Summy, Hamiltonian ratchets with ultra-cold atoms, Annalen Der Physik 529 (8) (2017) 1600335, <http://dx.doi.org/10.1002/andp.201600335>, URL <https://onlinelibrary.wiley.com/doi/abs/10.1002/andp.201600335>.
- [542] M. Sadgrove, M. Horikoshi, T. Sekimura, K. Nakagawa, Rectified momentum transport for a kicked Bose-Einstein condensate, Phys. Rev. Lett. 99 (2007) 043002, <http://dx.doi.org/10.1103/PhysRevLett.99.043002>, URL <https://link.aps.org/doi/10.1103/PhysRevLett.99.043002>.
- [543] I. Dana, V. Ramareddy, I. Talukdar, G.S. Summy, Experimental realization of quantum-resonance ratchets at arbitrary quasimomenta, Phys. Rev. Lett. 100 (2008) 024103, <http://dx.doi.org/10.1103/PhysRevLett.100.024103>, URL <https://link.aps.org/doi/10.1103/PhysRevLett.100.024103>.
- [544] D. Poletti, G.G. Carlo, B. Li, Current behavior of a quantum Hamiltonian ratchet in resonance, Phys. Rev. E 75 (2007) 011102, <http://dx.doi.org/10.1103/PhysRevE.75.011102>, URL <https://link.aps.org/doi/10.1103/PhysRevE.75.011102>.
- [545] J. Ni, W.K. Lam, S. Dadras, M.F. Borunda, S. Wimberger, G.S. Summy, Initial-state dependence of a quantum resonance ratchet, Phys. Rev. A 94 (2016) 043620, <http://dx.doi.org/10.1103/PhysRevA.94.043620>, URL <https://link.aps.org/doi/10.1103/PhysRevA.94.043620>.
- [546] A. Kenfack, J. Gong, A.K. Pattanayak, Controlling the Ratchet effect for cold atoms, Phys. Rev. Lett. 100 (2008) 044104, <http://dx.doi.org/10.1103/PhysRevLett.100.044104>, URL <https://link.aps.org/doi/10.1103/PhysRevLett.100.044104>.
- [547] G.G. Carlo, L. Ermann, F. Borondo, R.M. Benito, Environmental stability of quantum chaotic ratchets, Phys. Rev. E 83 (2011) 011103, <http://dx.doi.org/10.1103/PhysRevE.83.011103>, URL <https://link.aps.org/doi/10.1103/PhysRevE.83.011103>.
- [548] J. Gong, P. Brumer, Directed anomalous diffusion without a biased field: A ratchet accelerator, Phys. Rev. E 70 (2004) 016202, <http://dx.doi.org/10.1103/PhysRevE.70.016202>, URL <https://link.aps.org/doi/10.1103/PhysRevE.70.016202>.

- [549] C. Hainaut, A. Rançon, J.-F. Clément, J.C. Garreau, P. Sriftgiser, R. Chicireanu, D. Delande, Ratchet effect in the quantum kicked rotor and its destruction by dynamical localization, Phys. Rev. A 97 (2018) 061601, <http://dx.doi.org/10.1103/PhysRevA.97.061601>, URL <https://link.aps.org/doi/10.1103/PhysRevA.97.061601>.
- [550] J.B. Fixler, G.T. Foster, J.M. McGuirk, M.A. Kasevich, Atom interferometer measurement of the Newtonian constant of gravity, Science 315 (5808) (2007) 74–77, <http://dx.doi.org/10.1126/science.1135459>, URL <https://science.sciencemag.org/content/315/5808/74>.
- [551] G. Rosi, F. Sorrentino, L. Cacciapuoti, M. Prevedelli, G.M. Tino, Precision measurement of the Newtonian gravitational constant using cold atoms, Nature 510 (2014) 518–521, <http://dx.doi.org/10.1038/nature13433>.
- [552] B. Estey, C. Yu, H. Müller, P.-C. Kuan, S.-Y. Lan, High-resolution atom interferometers with suppressed diffraction phases, Phys. Rev. Lett. 115 (2015) 083002, <http://dx.doi.org/10.1103/PhysRevLett.115.083002>, URL <https://link.aps.org/doi/10.1103/PhysRevLett.115.083002>.
- [553] R.H. Parker, C. Yu, W. Zhong, B. Estey, H. Müller, Measurement of the fine-structure constant as a test of the standard model, Science 360 (6385) (2018) 191–195, <http://dx.doi.org/10.1126/science.aap7706>, URL <https://science.sciencemag.org/content/360/6385/191>.
- [554] D. Cubero, G.R.M. Robb, F. Renzoni, Avoided crossing and sub-Fourier-sensitivity in driven quantum systems, Phys. Rev. Lett. 121 (2018) 213904, <http://dx.doi.org/10.1103/PhysRevLett.121.213904>, URL <https://link.aps.org/doi/10.1103/PhysRevLett.121.213904>.
- [555] P. Sriftgiser, J. Ringot, D. Delande, J.C. Garreau, Observation of sub-Fourier resonances in a quantum-chaotic system, Phys. Rev. Lett. 89 (2002) 224101, <http://dx.doi.org/10.1103/PhysRevLett.89.224101>, URL <https://link.aps.org/doi/10.1103/PhysRevLett.89.224101>.
- [556] P. McDowall, A. Hilliard, M. McGovern, T. Grünzweig, M.F. Andersen, A fidelity treatment of near-resonant states in the atom-optics kicked rotor, New J. Phys. 11 (12) (2009) 123021, <http://dx.doi.org/10.1088/1367-2630/11/12/123021>.
- [557] J. Mangaonkar, C. Vishwakarma, S.S. Maurya, S. Sarkar, J.L. MacLennan, P. Dutta, U.D. Rapol, Effects of finite momentum width on the reversal dynamics in a BEC based atom optics δ -kicked rotor, J. Phys. B: At. Mol. Opt. Phys. 53 (23) (2020) 235502, <http://dx.doi.org/10.1088/1361-6455/abbf43>.
- [558] M. Abb, I. Guarneri, S. Wimberger, Pseudoclassical theory for fidelity of nearly resonant quantum rotors, Phys. Rev. E 80 (2009) 035206, <http://dx.doi.org/10.1103/PhysRevE.80.035206>, URL <https://link.aps.org/doi/10.1103/PhysRevE.80.035206>.
- [559] M. Schlosshauer, Quantum decoherence, Phys. Rep. 831 (2019) 1–57, <http://dx.doi.org/10.1016/j.physrep.2019.10.001>, URL <http://www.sciencedirect.com/science/article/pii/S0370157319303084>.
- [560] W.H. Zurek, Decoherence, einselection, and the quantum origins of the classical, Rev. Modern Phys. 75 (2003) 715–775, <http://dx.doi.org/10.1103/RevModPhys.75.715>, URL <https://link.aps.org/doi/10.1103/RevModPhys.75.715>.
- [561] D. Giulini, E. Joos, C. Kiefer, J. Kupsch, I.-O. Stamatescu, H. Zeh, Decoherence and the Appearance of a Classical World in Quantum Theory, Springer, Berlin, 1996.
- [562] H. Schomerus, E. Lutz, Controlled decoherence in a quantum Lévy kicked rotator, Phys. Rev. A 77 (2008) 062113, <http://dx.doi.org/10.1103/PhysRevA.77.062113>, URL <https://link.aps.org/doi/10.1103/PhysRevA.77.062113>.
- [563] M.F. Shlesinger, G.M. Zaslavsky, J. Klafter, Strange kinetics, Nature 363 (1993) 31–37, <http://dx.doi.org/10.1038/363031a0>.
- [564] H.A. Simon, On a class of skew distribution functions, Biometrika 42 (3–4) (1955) 425–440, <http://dx.doi.org/10.1093/biomet/42.3-4.425>.
- [565] A. Erdélyi, Higher Transcendental Functions, vol. 3, McGrawHill, New York, 1955.
- [566] S. Paul, S. Sarkar, C. Vishwakarma, J. Mangaonkar, M.S. Santhanam, U. Rapol, Nonmonotonic diffusion rates in an atom-optics Lévy kicked rotor, Phys. Rev. E 100 (2019) 060201, <http://dx.doi.org/10.1103/PhysRevE.100.060201>, URL <https://link.aps.org/doi/10.1103/PhysRevE.100.060201>.
- [567] R.P. Feynman, Simulating physics with computers, Int. J. Theor. Phys. 21 (6/7) (1982).
- [568] B. Georgeot, D.L. Shepelyansky, Exponential gain in quantum computing of quantum chaos and localization, Phys. Rev. Lett. 86 (13) (2001) 2890, <http://dx.doi.org/10.1103/PhysRevLett.86.2890>.
- [569] B. Lévi, B. Georgeot, D.L. Shepelyansky, Quantum computing of quantum chaos in the kicked rotator model, Phys. Rev. E 67 (2003) 046220, <http://dx.doi.org/10.1103/PhysRevE.67.046220>, URL <https://link.aps.org/doi/10.1103/PhysRevE.67.046220>.
- [570] P.H. Song, D.L. Shepelyansky, Quantum computing of quantum chaos and imperfection effects, Phys. Rev. Lett. 86 (10) (2001) 2162, <http://dx.doi.org/10.1103/PhysRevLett.86.2162>.
- [571] M. Terraneo, D. Shepelyansky, Dynamical localization and repeated measurements in a quantum computation process, Phys. Rev. Lett. 92 (3) (2004) 037902, <http://dx.doi.org/10.1103/PhysRevLett.92.037902>.
- [572] A.A. Pomeransky, D.L. Shepelyansky, Quantum computation of the Anderson transition in the presence of imperfections, Phys. Rev. A 69 (1) (2004) 014302, <http://dx.doi.org/10.1103/PhysRevA.69.014302>.
- [573] G. Benenti, G. Casati, S. Montangero, D.L. Shepelyansky, Dynamical localization simulated on a few-qubit quantum computer, Phys. Rev. A 67 (2003) 052312, <http://dx.doi.org/10.1103/PhysRevA.67.052312>, URL <https://link.aps.org/doi/10.1103/PhysRevA.67.052312>.
- [574] G. Casati, Quantum chaos and quantum computing, J. Phys. Soc. Japan 72 (Suppl.C) (2003) 157–164, <http://dx.doi.org/10.1143/JPSJS.72SC.157>.
- [575] L. Tessieri, Z. Akdeniz, N. Cheroret, D. Delande, P. Vignolo, Quantum boomerang effect: Beyond the standard Anderson model, Phys. Rev. A 103 (2021) 063316, <http://dx.doi.org/10.1103/PhysRevA.103.063316>, URL <https://link.aps.org/doi/10.1103/PhysRevA.103.063316>.
- [576] T. Prat, D. Delande, N. Cheroret, Quantum boomeranglike effect of wave packets in random media, Phys. Rev. A 99 (2019) 023629, <http://dx.doi.org/10.1103/PhysRevA.99.023629>, URL <https://link.aps.org/doi/10.1103/PhysRevA.99.023629>.
- [577] J. Janarek, D. Delande, N. Cheroret, J. Zakrzewski, Quantum boomerang effect for interacting particles, Phys. Rev. A 102 (2020) 013303, <http://dx.doi.org/10.1103/PhysRevA.102.013303>, URL <https://link.aps.org/doi/10.1103/PhysRevA.102.013303>.
- [578] R. Sajjad, J.L. Tanlimco, H. Mas, A. Cao, E. Nolasco-Martinez, E.Q. Simmons, F.L.N. Santos, P. Vignolo, T. Macr, D.M. Weld, Observation of the quantum boomerang effect, Phys. Rev. X (2022) arXiv:2109.00696.
- [579] A. Kundu, A. Rajak, T. Nag, Dynamics of fluctuation correlation in a periodically driven classical system, Phys. Rev. B 104 (2021) 075161, <http://dx.doi.org/10.1103/PhysRevB.104.075161>, URL <https://link.aps.org/doi/10.1103/PhysRevB.104.075161>.
- [580] C. Rylands, E.B. Rozenbaum, V. Galitski, R. Konik, Many-body dynamical localization in a kicked Lieb-Liniger gas, Phys. Rev. Lett. 124 (2020) 155302, <http://dx.doi.org/10.1103/PhysRevLett.124.155302>, URL <https://link.aps.org/doi/10.1103/PhysRevLett.124.155302>.
- [581] F. Borgonovi, F. Izrailev, L. Santos, V. Zelevinsky, Quantum chaos and thermalization in isolated systems of interacting particles, Phys. Rep. 626 (2016) 1–58, <http://dx.doi.org/10.1016/j.physrep.2016.02.005>, Quantum chaos and thermalization in isolated systems of interacting particles, URL <http://www.sciencedirect.com/science/article/pii/S0370157316000831>.
- [582] H. Bernien, S. Schwartz, A. Keesling, H. Levine, A. Omran, H. Pichler, S. Choi, A.S. Zibrov, M. Endres, M. Greiner, V. Vuletić, M.D. Lukin, Probing many-body dynamics on a 51-atom quantum simulator, Nature 551 (7682) (2017) 579–584, <http://dx.doi.org/10.1038/nature24622>.
- [583] S.E. Venegas-Andraca, Quantum walks: a comprehensive review, Quantum Inf. Process. 11 (5) (2012) 1015–1106, <http://dx.doi.org/10.1007/s11128-012-0432-5>.
- [584] W. Zhou, Review on quantum walk algorithm, J. Phys.: Conf. Ser. 1748 (2021) 032022, <http://dx.doi.org/10.1088/1742-6596/1748/3/032022>.
- [585] S. Dadras, A. Gresch, C. Groiseau, S. Wimberger, G.S. Summy, Quantum walk in momentum space with a Bose-Einstein condensate, Phys. Rev. Lett. 121 (2018) 070402, <http://dx.doi.org/10.1103/PhysRevLett.121.070402>, URL <https://link.aps.org/doi/10.1103/PhysRevLett.121.070402>.
- [586] M. Delvecchio, C. Groiseau, F. Petruoli, G.S. Summy, S. Wimberger, Quantum search with a continuous-time quantum walk in momentum space, J. Phys. B: At. Mol. Opt. Phys. 53 (6) (2020) 065301, <http://dx.doi.org/10.1088/1361-6455/ab63ad>.
- [587] S. Omanakuttan, A. Lakshminarayanan, Quantum walks with quantum chaotic coins: Loschmidt echo, classical limit, and thermalization, Phys. Rev. E 103 (2021) 012207, <http://dx.doi.org/10.1103/PhysRevE.103.012207>.
- [588] J. Biamonte, P. Wittek, N. Pancotti, P. Rebentrost, N. Wiebe, S. Lloyd, Quantum machine learning, Nature 549 (7671) (2017) 195–202, <http://dx.doi.org/10.1038/nature23474>.